UNIVERSIDAD DE LA RIOJA

TESIS DOCTORAL
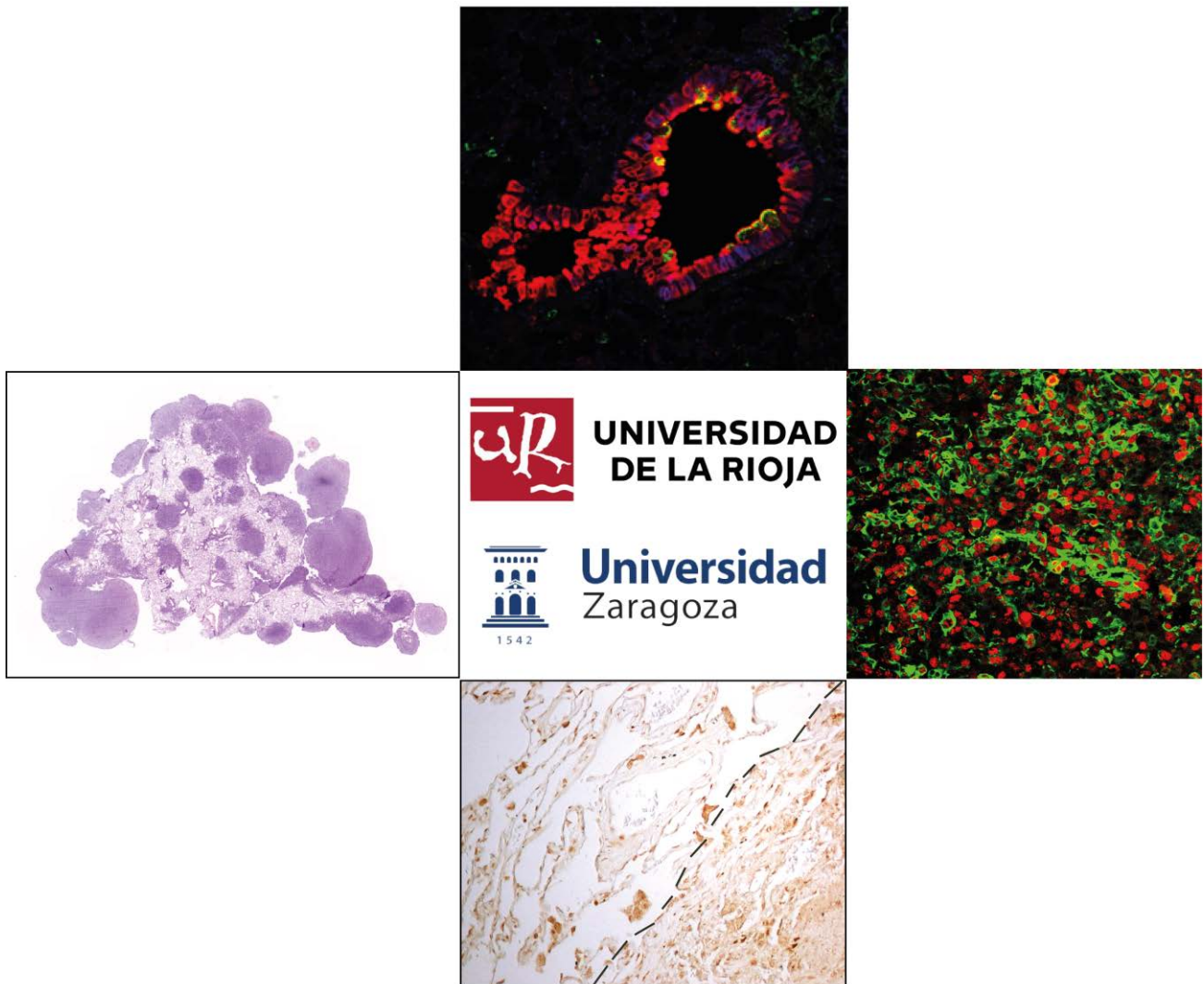
Título
IGF1R as a pharmacological target in allergic asthma and cancer-promoting factor in the lung tumor microenvironment

Autor/es
Elvira Alfaro Arnedo

Director/es
José Manuel García Pichel y Iciar Paula López García

Facultad
Facultad de Ciencia y Tecnología

Titulación

Departamento
Agricultura y Alimentación

Curso Académico

IGF1R AS A PHARMACOLOGICAL TARGET IN ALLERGIC ASTHMA AND CANCER-PROMOTING FACTOR IN THE LUNG TUMOR MICROENVIRONMENT

Thesis for doctoral degree (Ph.D)   **Elvira Alfaro Arnedo**

Fundación Rioja Salud, Center for Biomedical Research of La Rioja (CIBIR)

Lung Cancer and Respiratory Diseases Unit, Logroño, Spain

IGF1R AS A PHARMACOLOGICAL TARGET IN ALLERGIC ASTHMA AND CANCER-PROMOTING FACTOR IN THE LUNG TUMOR MICROENVIRONMENT

Elvira Alfaro Arnedo

Logroño 2021

José Manuel García Pichel, Ph.D. in Biological Sciences and head of the Lung Cancer and Respiratory Diseases Unit from the Center for Biomedical Research of La Rioja, and **Icíar Paula López García**, Ph.D. in Biological Sciences as co-director,

certify that:

The present thesis entitled "*IGF1R as a pharmacological target in allergic asthma and cancer-promoting factor in the lung tumor microenvironment*" undertaken by **Elvira Alfaro Arnedo**, B.Sc. in Pharmacy, meets the conditions of originality and content required to qualify for the doctorate mention from the Universities of La Rioja and Zaragoza.

Logroño, 06 October 2021.

José M. García Pichel, Ph.D.
Email: jgpichel@riojasalud.es

Icíar P. López García, Ph.D.
Email: iplgarcia@riojasalud.es

Elvira Alfaro Arnedo
Email: ealfaro@riojasalud.es

A mi familia y amigos

que siempre están ahí

ACKNOWLEDGEMENTS

LIST OF ABBREVIATIONS

4-OHT	4-hydroxytamoxifen
53BP1	Antigen identified by polyclonal antibody 53BP1
ADC	Adenocarcinoma
AEC1	Alveolar epithelial type 1 cells
AEC2	Alveolar epithelial type 2 cells
AHR	Airway hyperresponsiveness
AKT	AKT serine/threonine kinase 1
ALK	Anaplastic lymphoma kinase
AQP5	Aquaporin 5
ARDS	Acute respiratory distress syndrome
AW	Airway
B16-F10	Melanoma cell line
BADJ	Bronchioalveolar duct junction
BALF	Bronchoalveolar lavage fluid
BASCs	Bronchioalveolar stem cells
BLM	Bleomicine
BM	Bone marrow
bp	Base pairs
BRAF	B-Raf proto-oncogen
C3	Antigen identified by monoclonal antibody Caspase3
CAF	Cancer-associated fibroblasts
CC10	Club cell 10-kDa protein
Ccl2	Chemokine (C-C motif) ligand 2 (gene)
Ccl12	Chemokine (C-C motif) ligand 12 (gene)
CCL5	Chemokine (C-C motif) ligand 5
Ccl11	Chemokine (C-C motif) ligand 11 (gene)
CCL11	C-C motif chemokine ligand 11 (eotaxin-1)
CD31	Antigen identified by polyclonal antibody CD31
CD34	Antigen identified by monoclonal antibody CD34
Cd4	CD4 antigen (gene)
CD4	Antigen identified by monoclonal antibody CD4

CD45	Antigen identified by monoclonal antibody CD45
Cd68	CD68 antigen (gene)
CD68	Antigen identified by monoclonal antibody CD68
Cd8a	CD8a antigen (gene)
Cd80	CD80 antigen (gene)
Cd86	CD86 antigen (gene)
Cd163	CD163 antigen (gene)
Cd274 (PDL-1)	CD274 antigen (gene)
cDNA	Complementary DNA
Cdyn	Dynamic compliance
Cgrp	Péptido relacionado con el gen de la calcitonina
COPD	Chronic obstructive pulmonary disease
COVID-19	Coronavirus-19
CPNM	Cáncer de pulmón no microcítico
Cre	Cre recombinase
CreERT2	UBC-CreERT2; Igf1r$^{\Delta/\Delta}$ mice
Cxcl1	Chemokine (C-X-C motif) ligand 1 (gene)
D	Day
DAB	3,3´-Diaminobenzidine
DAPI	4′,6-diamidino-2-phenylindole
DC	Dendritic cell
Derp1	Derp1 allergen
DMEN	Dulbecco's Modified Eagle Medium
DMSO	Dimetilsulfóxido
DNA	Deoxyribonucleic acid
DTCs	Disseminated tumor cells
ECM	Extracellular matrix
EDTA	Ethylenediaminetetraacetic acid
Egfr	Epidermal growth factor receptor (gene)
EGFR	Epidermal growth factor receptor
ELISA	Enzyme-linked immunosorbent assay
EMT	Epitelial-mesenchymal transition

ERK	Extracellular signal-regulated kinase
EV	Extracellular vesicle
F	Forward
FEV1	Forced expiratory volume
Fl	Flox
Foxm1	Forkhead box M1 (gene)
FOXM1	Forkhead box M1
Foxp3	Forkhead 3 (gene)
FOXP3	Antigen identified by monoclonal antibody FOXP3
FN	Antigen identified by polyclonal antibody Fibronectin
FVC	Forced vital capacity
GH	Growth hormone
GHRH	Growth hormone releasing hormone
GLUTUB	Glu-tubulin
GM-CSF	Granulocyte-macrophage colony-stimulating factor
HDM	House dust mite
H&E	Hematoxylin and eosin
Hif1a	Hypoxia inducible factor 1, alpha subunit (gene)
HIF1α	Hypoxia inducible factor 1, alpha subunit
Hmox1	Heme oxygenase (gene)
HMOX1/HO-1	Heme oxygenase 1
HSP90	Heat shock protein 90
Iba1	Antigen identified by polyclonal antibody Iba1
Ifnγ	Interferon-gamma (gene)
IgE	Immunoglobulin E
IGF-ALS	IGF-Binding Protein Acid Labile Subunit
IGFs	Insulin-like Growth Factors
IGFBPs	IGF-binding proteins
Igfbp2	Insulin-like growth factor binding protein 2 (gene)
Igfbp3	Insulin-like growth factor binding protein 3 (gene)
Igfbp4	Insulin-like growth factor binding protein 4 (gene)
Igfbp5	Insulin-like growth factor binding protein 5 (gene)

Igfbp6	Insulin-like growth factor binding protein 6 (gene)
Igf1	Insulin-like growth factor 1 (gene)
IGF1	Insulin-like growth factor 1
Igf1r	Insulin-like growth factor 1 receptor (gene)
IGF1R	Insulin-like growth factor 1 receptor
IGF2	Insulin-like growth factor 2
IGF2R	Insulin-like growth factor 2 receptor
Il1β	Interleukin 1 beta (gene)
IL1B	Interleukin 1 beta
IL2	Interleukin 2
Il4	Interleukin 4 (gene)
IL4	Interleukin 4
IL6	Interleukin 6
Il10	Interleukin 10 (gene)
IL10	Interleukin 10
Il13	Interleukin 13 (gene)
IL13	Interleukin 13
IL25	Interleukin 25
Il33	Interleukin 33 (gene)
IL33	Interleukin 33
INSR	Insulin receptor
Insr	Insulin receptor (gene)
i.n.	Intranasal
i.p.	Intraperitoneal
i.v.	Intravenous
Ki67	Antigen identified by monoclonal antibody Ki67
loxP	DNA sequence for Cre-mediated recombination
LLC	Lewis lung carcinoma
LR	Lung resistance
MAPKs	Mitogen-activated protein kinases
MAT	Microambiente tumoral
MCh	Methacholine

MDSC	Myeloid-derived suppressor cells
MET	MET proto-oncogene
MGG	May-Grünwald Giemsa
Mmp2	Matrix Metallopeptidase 2 (gene)
Mmp9	Matrix Metallopeptidase 9 (gene)
MMP9	Matrix Metallopeptidase 9
Mpo	Mieloperoxidasa (gene)
mRNA	Messenger ribonucleic acid
Muc5ac	Mucin 5, subtypes A and C (gene)
MUC5AC	Mucin 5AC, oligomeric mucus/gel-forming
NE	Neuroendocrine
NK	Natural killer cell
NKx2.1	NK2 homeobox 1
NSCLC	Non-small-cell lung cancer
NVP	NVP-ADW742
NLRP3	NLR family pyrin domain containing 3 (NLRP3 inflammasome)
NTRK	Neurotrophic tyrosine receptor kinase
P	Peritumoral
p-	Phospho-
p21	Antigen identified by polyclonal antibody p21
PAS	Periodic acid-Schiff
PBS	Phosphate buffered saline
PBS –T	PBS-Triton
PCR	Polymerase chain reaction
Pdcd1 (PD-1)	Programmed cell death protein 1 (gene)
PDCD1	Programmed cell death protein 1
p-ERK1/2	Antigen identified by monoclonal antibody p-ERK1/2
p-IGF1R	Antigen identified by polyclonal antibody p-IGF1R
PI3K	Phosphoinositide-3 kinase
qPCR	Quantitative PCR
R	Reverse
RAS	RAS proto-oncogene

RET	Rearranged during transfection proto-oncogene
RIPA	Radioimmunoprecipitation assay buffer
Rn18s	18S ribosomal RNA (gene)
RPMI	Medio Roswell Park Memorial Institute
ROS1	Proto-oncogene tyrosine-protein kinase ROS
s.c.	Subcutaneous
Scgb1a1	Secretoglobin, family 1A, member 1 (uteroglobin) (gene)
SCGB1A1	Secretoglobin, family 1A, member 1 (uteroglobin)
SCLC	Small-cell lung cancer
Sftpa1	Surfactant associated protein A1 (gene)
Sftpb	Surfactant associated protein B (gene)
Sftpc	Surfactant-associated protein C (gene)
SFTPC	Surfactant-associated protein C
Sftpd	Surfactant-associated protein D (gene)
SM	Smooth muscle
SMA	Smooth muscle actin
SMS	Somatostatin
Sox2	SRY-box transcription factor 2 (gene)
SOX2	Antigen identified by monoclonal antibody SOX2
SOX9	Antigen identified by monoclonal antibody SOX9
Spdef	SAM pointed domain containing ets transcription factor (gene)
SPF	Specific pathogen-free
SQC	Squamous cell carcinoma
STATs	Signal transducers and activators of transcription
T	Tumor
TAMs	Tumor associated maccrophages
TBS	Tris-buffered saline
Tgfβ	Transforming growth factor beta (gene)
TGFβ	Transforming growth factor beta
Th1	T helper type 1 lymphocytes
Th2	T helper type 2 lymphocytes
TILs	Tumor infiltrating lymphocytes

Timp1	Tissue inhibitor matrix metalloproteinase 1 (gene)
Timp2	Tissue inhibitor matrix metalloproteinase 2 (gene)
Timp3	Tissue inhibitor matrix metalloproteinase 3 (gene)
TKI	Tyrosine kinase inhibitor
TME	Tumor microenvironment
TMX	Tamoxifen
Tnf	Tumor necrosis factor (gene)
TNFα	Tumor necrosis factor alpha
Treg	T regulatory cells
TSLP	Thymic stromal lymphopoietin
wt	Wild type
W	Week
wks	Weeks

ABSTRACT

Background: IGF1R (Insulin-like Growth Factor 1 Receptor) is a ubiquitous tyrosine kinase that modulates multiple cellular functions including proliferation, growth, differentiation and survival. Asthma is a chronic lung disease characterized by reversible airflow obstruction, airway hyperresponsiveness (AHR), mucus overproduction and inflammation. Lung cancer is a leading cause of malignant diseases, given the long-term ineffectiveness of current therapies and late-stage diagnoses, and tumor progression is influenced by cancer cell interactions with the tumor microenvironment (TME). Although IGF1R was found to be involved in asthma and reported to affect the TME, pharmacological inhibition of IGF1R in asthma and its role in the lung TME have not previously been investigated.

Methods: C57BL/6J mice were challenged by house dust mite (HDM) extract or PBS for four weeks and therapeutically treated with the IGF1R tyrosine kinase inhibitor (TKI) NVP-ADW742 (NVP) once allergic phenotype was established. The correlation of IGF1R with established clinical biomarkers of allergic asthma was also studied. On the other hand, we assessed IGF1R genomic alterations and expression in non-small-cell lung cancer (NSCLC) patient tissue samples as well as IGF1R serum levels. Moreover, we performed tumor heterotopic transplantation and pulmonary metastases in IGF1R-deficient mice using melanoma and Lewis lung carcinoma (LLC) cells.

Results: Lungs of HDM-challenged mice exhibited a significant increase in phospho-IGF1R levels, incremented AHR, airway remodeling, eosinophilia and allergic inflammation, as well as altered pulmonary surfactant expression, being all of these parameters counteracted by NVP treatment. HDM-challenged lungs also displayed augmented expression of the IGF1R signaling mediator p-ERK1/2, which was greatly reduced upon treatment with NVP. Furthermore, serum IGF1R levels in patients with allergic asthma were significantly increased as compared to healthy subjects and correlated with IgE levels and circulating eosinophils. On the other hand, increased amplification and mRNA expression, as well as increased protein expression (IGF1R/p-IGF1R) and IGF1R levels were found in tumor samples and serum from NSCLC patients, respectively. Moreover, IGF1R deficiency in mice reduced tumor growth, proliferation, inflammation and vascularization, and increased apoptosis after tumor heterotopic transplantation. Following induction of lung metastasis, IGF1R-deficient mice exhibited a decreased presence of leukocytes in bone marrow and BALF, and attenuated IL6 and TNFα serum levels. IGF1R-deficient lungs also demonstrated a reduced tumor burden, and decreased expression of tumor progression markers, p-IGF1R and p-ERK1/2. Additionally, IGF1R-deficient lungs showed increased apoptosis and diminished proliferation, senescence, vascularization, epithelial-mesenchymal transition (EMT) and fibrosis, along with attenuated inflammation and immunosuppression upon induction of lung metastasis.

Conclusions: These findings demonstrate that IGF1R could be considered a potential pharmacological target in murine HDM-induced asthma and that IGF1R promotes metastatic tumor initiation and progression in the lung TME. In addition, IGF1R is suggested to be a candidate biomarker in allergic asthma and in early prediction of drug response and clinical evolution in NSCLC patients.

RESUMEN

IGF1R (receptor del factor de crecimiento similar a la insulina tipo 1) es una tirosina quinasa ubicua que modula múltiples funciones celulares, como la proliferación, el crecimiento, la diferenciación y la supervivencia. El asma es una enfermedad pulmonar crónica caracterizada por obstrucción reversible del flujo de aire, hiperreactividad de las vías respiratorias, sobreproducción de moco e inflamación. El cáncer de pulmón es la causa principal de enfermedades malignas, dada la ineficacia de las terapias actuales a largo plazo y debido a los diagnósticos en etapa tardía. La progresión del tumor está influenciada por las interacciones de las células cancerosas con el microambiente tumoral (MAT). Aunque se sabe que IGF1R está involucrado en el asma y que afecta al MAT, la inhibición farmacológica de IGF1R en asma y su papel en el MAT pulmonar no se ha investigado previamente. Para ello, los ratones C57BL/6J fueron inoculados intranasalmente con extracto de ácaros del polvo doméstico o PBS durante cuatro semanas y tratados terapéuticamente con el inhibidor de la tirosina quinasa IGF1R NVP-ADW742 (NVP) una vez que se estableció el fenotipo alérgico. También se estudió la correlación de IGF1R con marcadores clínicos establecidos para el asma alérgica. Por otro lado, se evaluaron las alteraciones genómicas y la expresión de IGF1R en muestras de tejido de pacientes con cáncer de pulmón no microcítico (CPNM), así como los niveles séricos de IGF1R. Además, usando ratones deficientes de IGF1R se realizaron modelos de trasplante heterotópico de tumores y metástasis pulmonares utilizando células de melanoma y carcinoma de pulmón de Lewis. Los pulmones de los ratones inoculados con ácaros del polvo doméstico exhibieron un aumento significativo en los niveles de fosfo-IGF1R, aumento de hiperreactividad pulmonar, remodelación de las vías respiratorias, eosinofilia e inflamación alérgica, así como expresión alterada de la surfactante pulmonar, estando todos estos parámetros contrarrestados por el tratamiento con NVP. Los pulmones de los ratones inoculados con ácaros del polvo doméstico también mostraron un aumento de la expresión de fosfo-ERK1/2 (mediador de señalización de IGF1R) que se redujo tras el tratamiento con NVP. Además, los niveles séricos de IGF1R en pacientes con asma alérgica aumentaron significativamente en comparación con los sujetos sanos y se encontraron correlacionados con los niveles de IgE y eosinófilos circulantes. Por otro lado, se observó una mayor amplificación y expresión de ARNm, así como una mayor expresión de proteínas (IGF1R/p-IGF1R) y niveles de IGF1R en muestras tumorales y sueros de pacientes con CPNM, respectivamente. Además, la deficiencia de IGF1R en ratones redujo el crecimiento, la proliferación, la inflamación y la vascularización del tumor, y aumentó la apoptosis después del trasplante heterotópico. Tras la inducción de metástasis pulmonar, los ratones deficientes en IGF1R mostraron menor presencia de leucocitos en la médula ósea y lavado bronquioalveolar, y niveles séricos atenuados de IL6 y TNFα. Los pulmones deficientes de IGF1R también mostraron una carga tumoral reducida y una disminución de la expresión de los marcadores de progresión tumoral, fosfo-IGF1R y fosfo-ERK1/2. Además, los pulmones deficientes de IGF1R mostraron un aumento de la apoptosis y una disminución de la proliferación, la senescencia, la vascularización, la transición epitelio-mesénquima y la fibrosis, además de una inflamación e inmunosupresión atenuada tras la inducción de metástasis pulmonar. Estos hallazgos demuestran que IGF1R podría considerarse una diana farmacológica potencial en el asma inducida con ácaros del polvo doméstico en ratones y que IGF1R promueve la iniciación y progresión de la metastásis pulmonar en el MAT. Además, se sugiere que IGF1R es un biomarcador candidato en el asma alérgica y en la predicción temprana de la respuesta famacológica y evolución clínica en pacientes con CPNM.

CONTENTS

1 INTRODUCTION

1.1 The mouse respiratory system

1.1.1 Structure and function

The lower respiratory system is organized in two anatomical regions: a conducting zone and a respiratory zone. The conducting zone consists of airways that transport gases into and out of the lungs and includes the trachea, bronchi, and extends to the terminal bronchioles. The respiratory zone corresponds to the lung parenchyma and includes the respiratory bronchioles, alveolar ducts, alveolar sacs, and alveoli. For the lungs to function properly, the conducting zone must be open to the respiratory zone where gas exchange occurs. In this region, the surface available for gas exchange is maximized by septation into hundreds of millions of alveoli, surrounded by a dense capillary network [Meyerholz *et al.*, 2018; Rock *et al.*, 2010; Rock and Hogan 2011].

Species differences exist in both the gross anatomy and histology of the lower respiratory system, and these may compensate for variations in body size and basal metabolic rate. The basic design of the respiratory system is conserved among vertebrates, but there are important differences between mouse and human lungs. Concerning the gross anatomy, in rodents, the right lung is divided into four lobes, whereas the left lung has one lobe. The four right lung lobes are the cranial, middle, caudal, and accessory. The right lung of humans is divided into upper, middle and lower lobes, by two interlobar fissures, the oblique and the horizontal. In contrast, the left lung is divided into two lobes, upper and lower, by one interlobar fissure, the oblique fissure (**Figure 1 A,B**) [Meyerholz *et al.*, 2018].
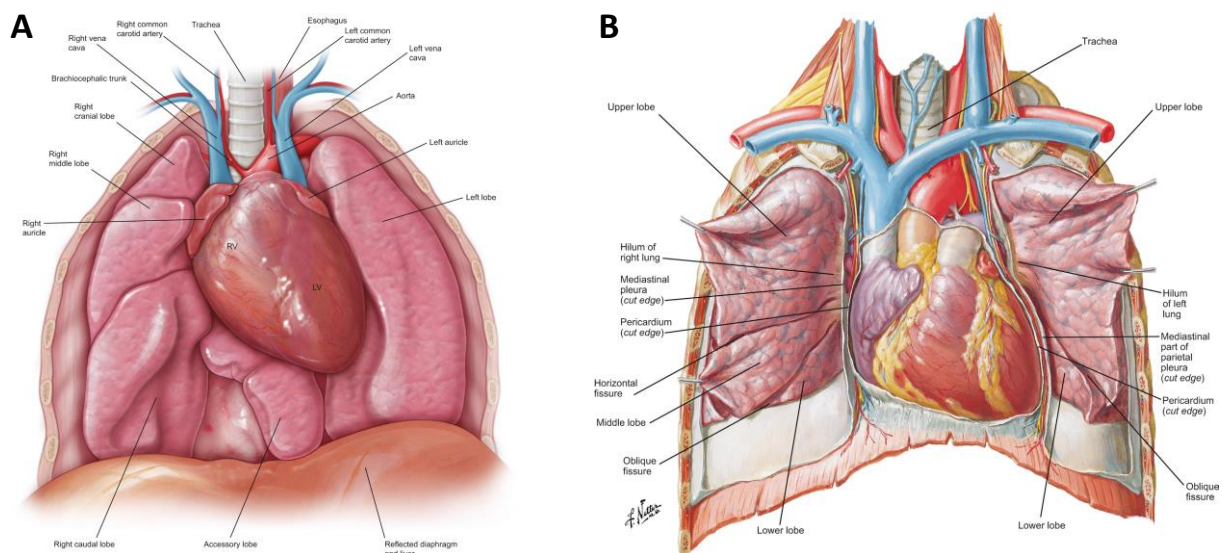
Figure 1. Comparative anatomy of mouse (**A**) and human (**B**) lungs (Meyerholz *et al.*, 2018).

In mice, the largest airway, the trachea, has an internal diameter of ~1.5 mm, equivalent to the diameter of the small peripheral airways in the human lung. Moreover, cartilage rings are only present in the extrapulmonary airways but, in humans, cartilage extends for several bronchial generations into the lung. Submucosal glands, which produce mucins and other factors, are restricted to the proximal lung in

the mouse but penetrate deep into the human lung. In addition, in the human lung there are more generations of intrapulmonary branches than in the mouse (**Figure 2**) [Herriges and Morrisey 2014; Hogan *et al.*, 2014; Rock *et al.*, 2010; Rock and Hogan 2011; Volckaert and De Langhe 2014].
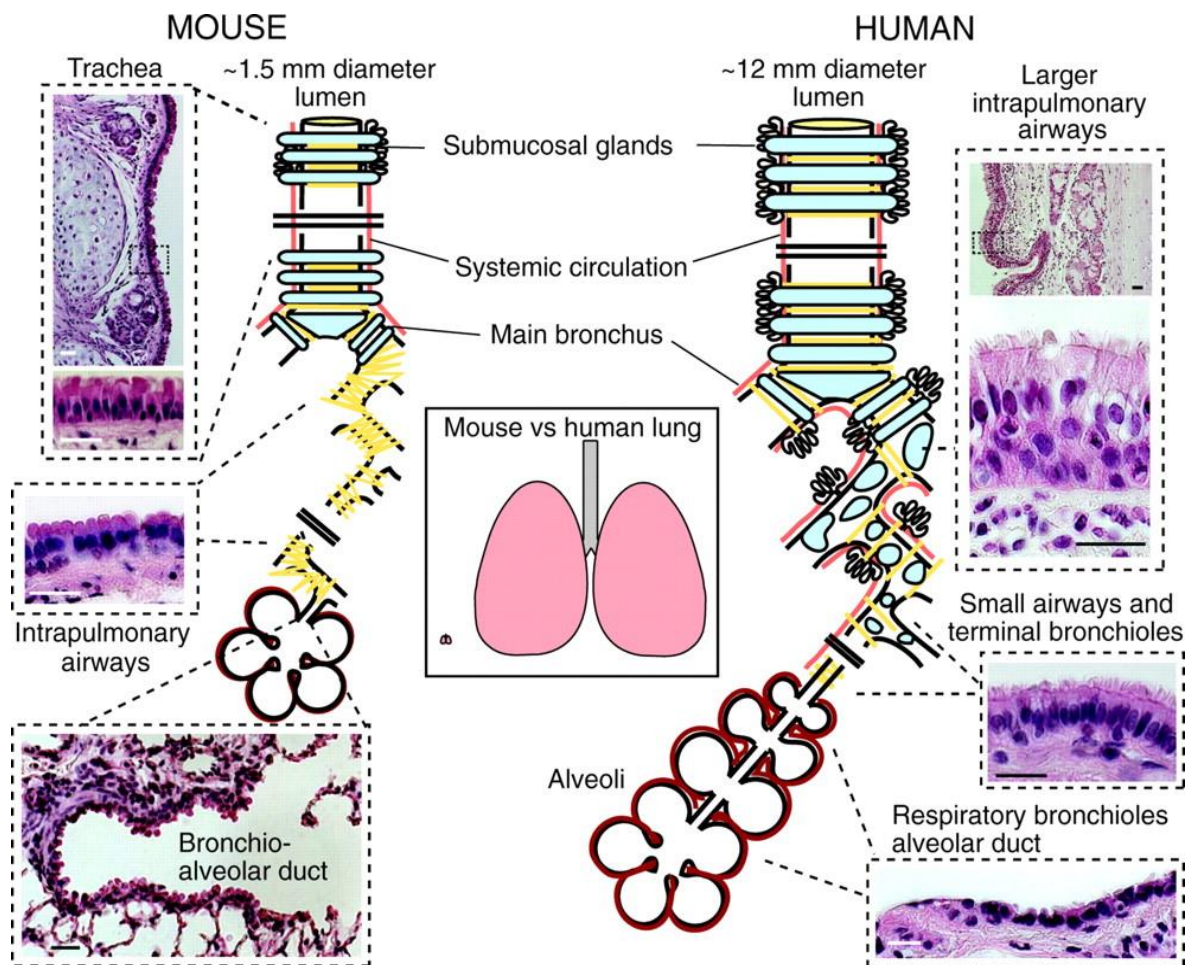
Figure 2. Shematic comparison of the structure of mouse and human lungs (Rock *et al.*, 2010).

1.1.2 Cellular composition

The cellular composition of the lung varies along its proximodistal axis, consisting of different cell types, whose main roles include facilitating gas exchange, balancing fluids in the lung, detoxifying and clearing foreign agents, and the activation of inflammation due to injury [Meyerholz *et al.*, 2018; Herriges and Morrisey 2014; Rock and Hogan 2011; Sullivan *et al.*, 2010].

The adult mouse trachea and primary bronchi are lined by a pseudostratified columnar epithelium containing basal, ciliated and club cells and a small number of neuroendocrine (NE) cells (**Figure 3**). In the intralobar or intrapulmonary bronchioles, the epithelium is simple columnar containing ciliated cells (GLUTUB+), secretory cells including club (SCGB1A1+) and goblet (MUC5AC+) cells and a higher number of NE cells than in the trachea. In this region, club cells predominate over ciliated cells and both ciliated and secretory cells drive mucociliary clearance. The bronchioalveolar duct junction (BADJ) contains a few cells proposed as bronchioalveolar stem cells (BASCs) that coexpress SCGB1A1 and surfactant-associated

2

protein C (SFTPC). In addition, the most distal region of the lung is organized into a complex system of alveoli lined by squamous alveolar epithelial type 1 cells (AEC1) (AQP5$^+$) and cuboidal alveolar epithelial type 2 cells (AEC2). While AEC1 are the primary sites of gas exchange and fluid homeostasis, AEC2 cells are the main source of SFTPC and other components of pulmonary surfactant, a mix of extracellular proteins and lipids that decreases alveolar surface tension and contributes to host defense and alveolar homeostasis (**Figure 3**) [Hogan *et al.*, 2014; Rawlins and Hogan 2006; Rock and Hogan 2011].
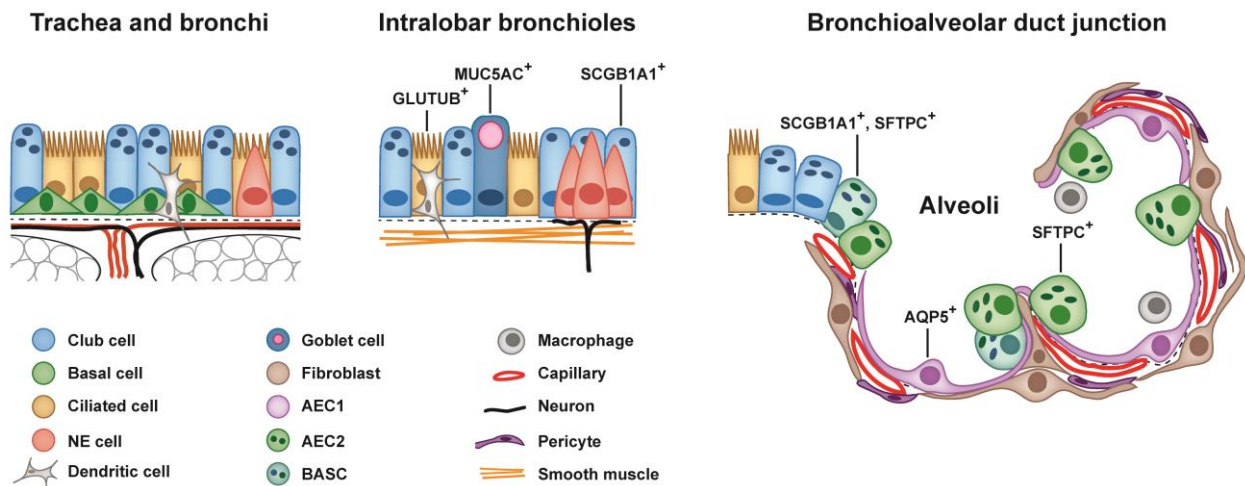
Figure 3. Cellular composition of the adult mouse lung epithelium (Modified from Rock and Hogan 2011).

There are important differences between the human and mouse lung with respect to the cellular composition. These differences are reflected in the construction of the anatomic and cell ontologies for both species. In the human lung, the trachea and proximal conducting airways are lined by a pseudostratified columnar epithelium, while the more peripheral conducting airways are lined by a cuboidal epithelium. The more proximal, intrapulmonary, cartilaginous airways (bronchi) are lined by tall, pseudostratified, columnar epithelia composed of basal, ciliated, club, serous, mucus, intermediate and neuroendocrine cells, and exhibit abundant submucosal glands. In addition, the respiratory bronchioles are lined by cuboidal epithelia, alternating with thin-walled alveoli lined by squamous alveolar type I pneumocytes [Pan *et al.*, 2019]. Respiratory cell types and their lineage differentiaton either during development or after lung injury, as well as respiratory system differences between mice and humans are illustrated in **Figure 4A** and tissue organization of the different cell types in the human respiratory system in **Figure 4B.**
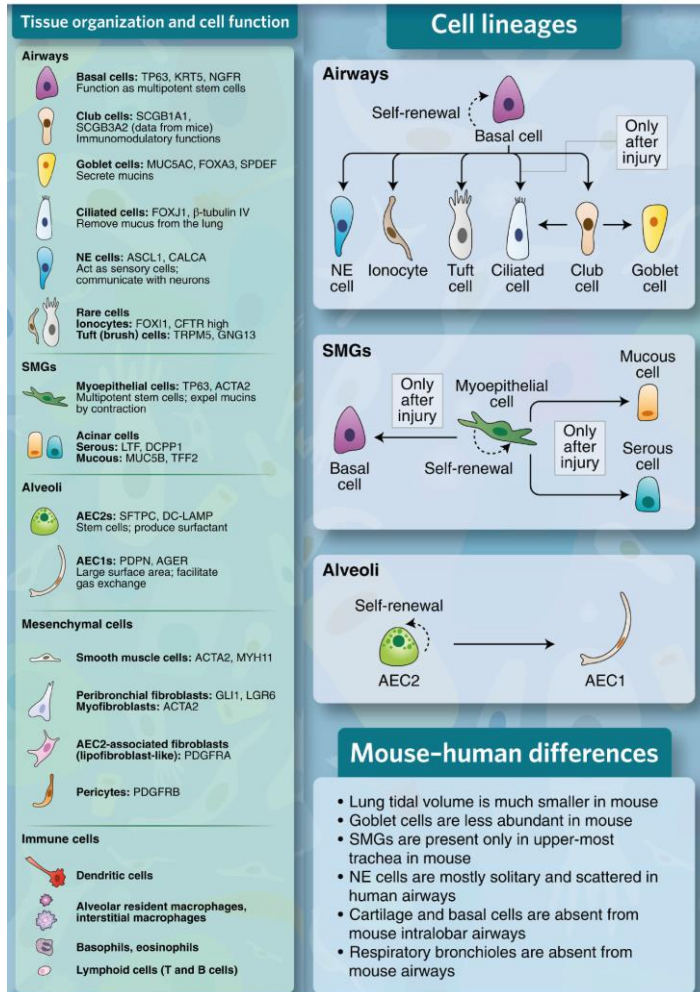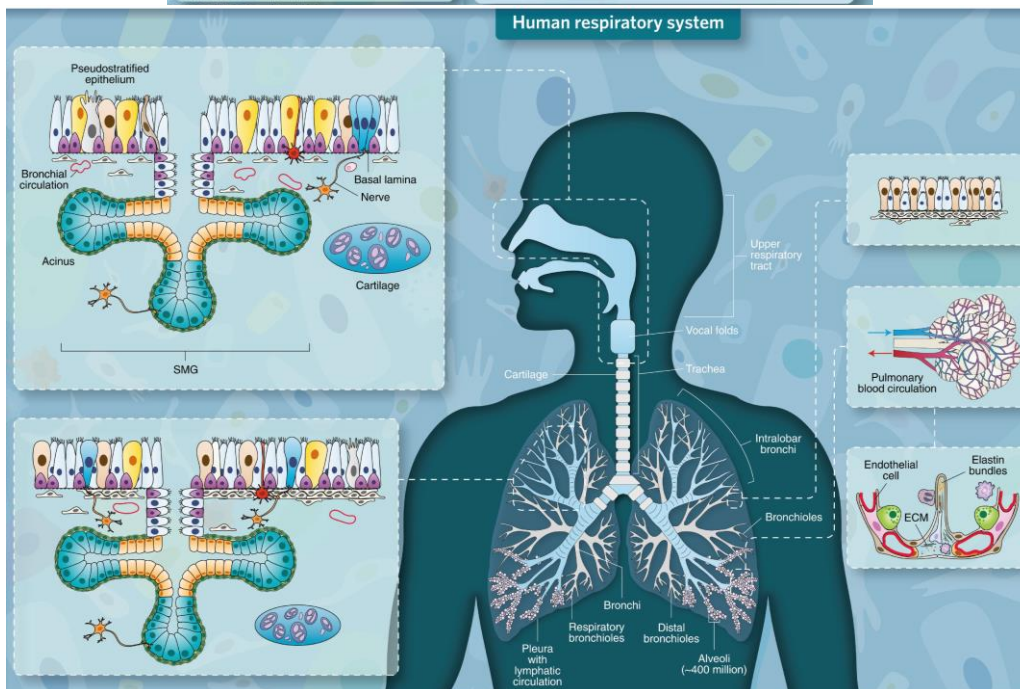
Figure 4. Cellular organization of the respiratory system. (**A**) Respiratory system cell types, cell functions and differences between mice and humans. (**B**) Tissue organization in the human respiratory system (Modified from Hogan and Tata 2019).

1.2 Asthma

1.2.1 Background

Asthma is currently considered as the most common chronic lung pathology. Approximately 339 million people worldwide suffer from asthma and at least 365000 deaths are attributed to the disease each year, which results in a substantial morbidity and annual healthcare expenditure [Fahy 2015; The Global Asthma Report 2018; Lambrecht and Hammad 2012; Lambrecht and Hammad 2015; Masoli *et al.*, 2004].

Asthma is a chronic inflammatory disease of conducting airways characterized by reversible airflow obstruction, bronchial hyperresponsiveness and airway inflammation. Asthma exacerbations lead to repeated periods of shortness of breath, wheezing, cough and sputum production. Exacerbations can range from mild to severe and can result in near-fatal or fatal episodes of respiratory failure. Airway narrowing during asthma exacerbations results not only from concentric smooth muscle contraction but also from mucosal edema and the formation of pathological intraluminal mucus. Airway remodeling in asthma is characterized by increased number of blood vessels and submucosal glands, subepithelial fibrosis and smooth muscle and goblet cell hyperplasia (**Figure 5**).
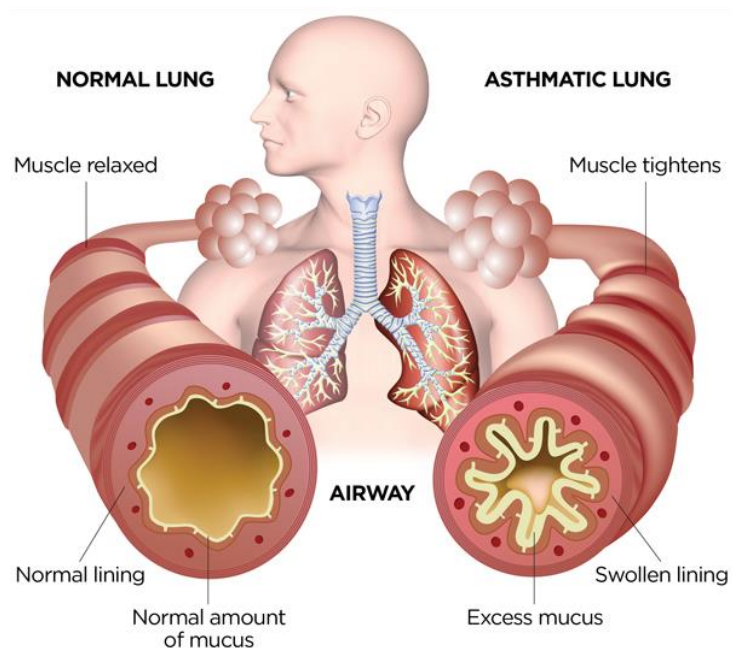
Figure 5. Schematic representation of a normal (left) versus an asthmatic airway (right) (Asthma and Allergy Foundation of America (AAFA) 2019).

1.2.2 House dust mite allergy

The house dust mite (HDM) is globally ubiquitous in human habitats and a significant factor underlying allergic asthma. The majority of allergic asthmatic individuals are sensitive to HDM. Notably, 1% to 2% of the world's population might be affected with HDM allergy, which is equivalent to 65 to 130 million people. The main food staple of HDM is keratin (human skin scales), cellulose (textile fibers), and

chitin (fungal hyphae and mite cuticles), as well as bacteria, pollen, fungal mycelia, and the spores of microorganisms. During digestion, disassociated digestive cells containing allergenic enzymes bind to ingested food, which are then excreted in the HDM fecal pellets. The main source of HDM allergens are *Dermatophagoides pteronyssinus* (Der p) species, whose allergic potential rests with the mites themselves and with their fecal pellets, which contains Derp1 allergens with cysteine protease activity (**Figure 6**). Der p 1 allergens exhibits a complex mixture of molecules including proteases, allergen epitopes, and activators of the innate immune system. Der p 1 allergens serve as adjuvants to disrupt intercellular tight junctions leading to cytokine, chemokine, and growth factor production and cellular influx, as well as airway remodeling and mucus hypersecretion [Buday and Plevkova 2014; Calderón *et al.*, 2015; Gregory and Lloyd 2011; Khweek *et al.*, 2020].
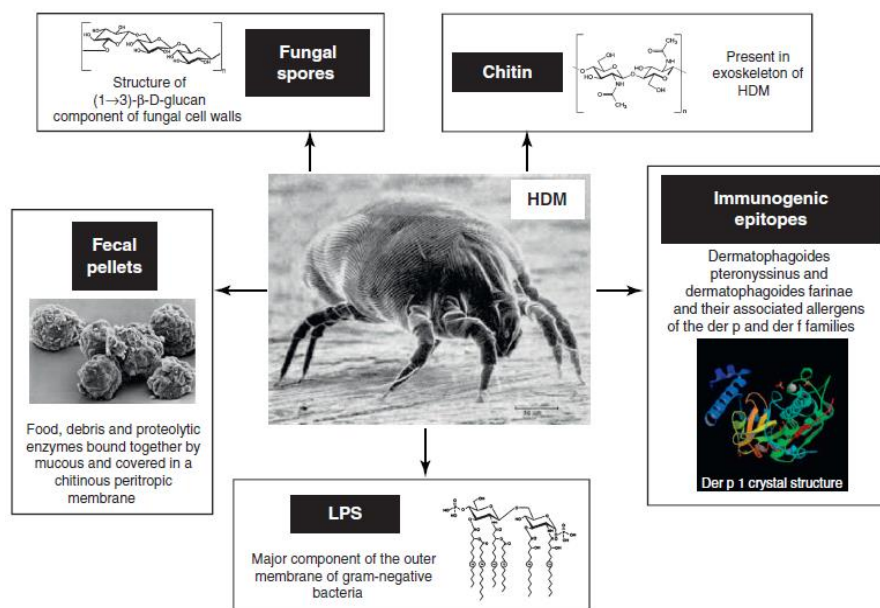
Figure 6. Components of HDM and their associated fecal pellets and dust (Gregory and Lloyd 2011).

1.2.3 Pathogenesis of allergic asthma

The airway epithelium is an essential controller of inflammatory, immune, and regenerative responses in asthma. In response to HDM, airway epithelial cells secrete cytokines and chemokines, activating dendritic cells and bridging innate and adaptive immunity. The allergenic effects of HDM are thought to be orchestrated through two main routes: T-helper-2 (Th2) CD4^{+} T lymphocytes that induce and drive the IgE-dependent allergic response and the innate immune system [Calderón *et al.*, 2015, Lambrecht and Hammad 2012; Whitsett and Alenghat 2015]. When the allergen is inhaled into the airway, it is taken up and processed by dendritic cells, which are stimulated to migrate from the airway mucosa to regional lymph nodes by the epithelial cytokines IL25, IL33, TSLP and GM-CSF. Then, dendritic cells sensitize naïve T cells to the allergen and direct their development into Th2 cells (**Figure 7**). This induces production of inflammatory cytokines IL4 and IL13 and trigger B cells to produce allergen-specific IgE. During their class-switching to IgE-secreting plasma cells, B cells also express membrane-bound IgE,

which assists in antigen processing and signal transduction. Secreted IgE binds to the surface of mast cells and basophils and sensitizes them to the allergen.

Repeated allergen exposure leads to cross-linking of membrane-bound IgE in mast cells and basophils, inducing cellular degranulation and the release of histamine, leukotrienes, and platelet-activating factors. These cytokines affect the early allergic response manifested in edema, vasodilation, and bronchoconstriction. The events induced in the early response lead to the production and release of cytokines and chemokines such as IL3, IL4, IL5, IL13, CCL5, CCL11 and GM-CSF, which recruit inflammatory cells such as neutrophils, eosinophils, basophils, T cells, and macrophages to the site of inflammation. Specifically, once the eosinophils reach the airways through the vasculature, release high inflammatory granule-associated proteins with cytotoxic, immunological, and remodeling properties in the lung. All of these phenomena are known as the late allergic response, characterized by mucus hypersecretion, airway inflammation, hyperresponsiveness, and airway remodeling (**Figure 7**) [Humbert *et al*., 2019; Calderón *et al*., 2015; Erle and Sheppard 2014; Gregory and Lloyd 2011; Hammad and Lambrecht 2008; Lambrecht and Hammad 2015; Lemanske and Busse 2010; Lukacs 2001; Possa *et al*., 2013].
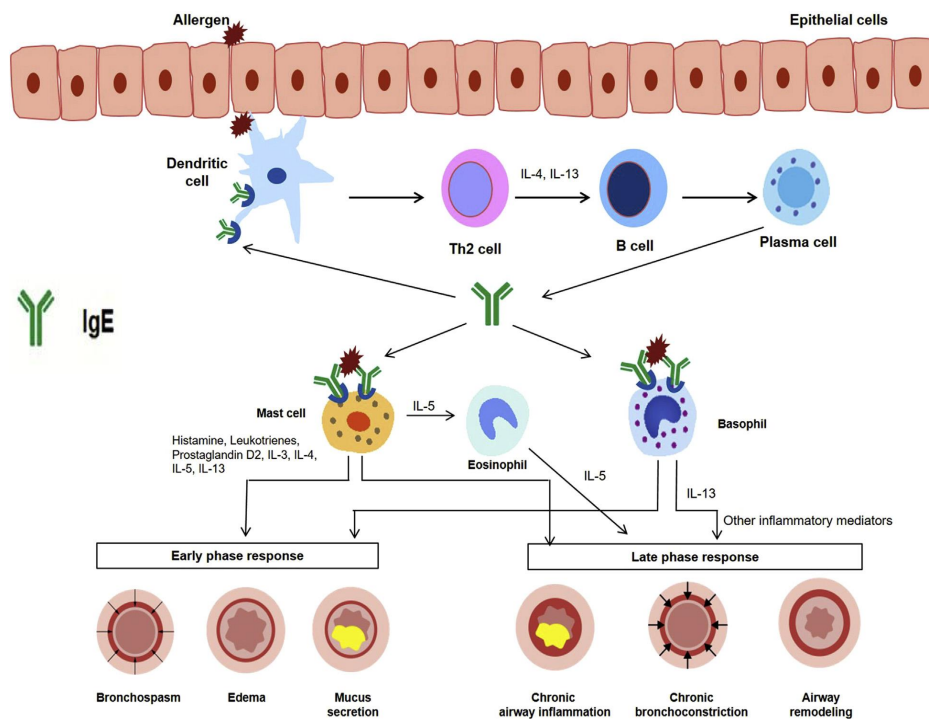
Figure 7. Pathogenesis of allergic asthma (Modified from Humbert *et al*., 2019).

1.2.4 Asthma treatments

Although asthma symptoms are controllable, a cure for asthma has remained elusive. The most effective treatment for allergic asthma includes identifying and avoiding allergens that trigger symptoms. In the pursuit of achieving control in severe asthma, improved knowledge of chronic airway inflammatory pathways has resulted in the development of new targeted therapies mostly to treat a Th2-high asthma. In this sense, the identification of asthma phenotypes, as well as underling Th2-high (eosinophilic) or Th2-

low (noeosinophilic) endotypes, represent a key point for the development of novel therapeutic strategies (**Table 1**) [Kuruvilla *et al.*, 2019; Huang *et al.*, 2019].

Table1. Asthma endotypes: Th2-high (eosinophilic) or Th2-low (noeosinophilic)

Endotypes	T2 High Asthma	T2 Low Asthma
Predominant cell in airways or sputum	Eosinophils	Neutrophils or paucigranulocyte
Predominant cells and cytokines involved		
Epithelium	TSLP, IL-33	IL-8, IL-23
Neutrophils		Proteases, ROS
Eosinophils/mast cells	IL-4, IL-5, IL-9, CRTH2/PGD2	
Th1		IFN-γ, IL-17, IL-22
Th2	IL-4, IL-5, IL-9, L-13, CRTH2/PGD2	
Th17		IL-17, 1L-22, 1L-23, CXCR2
ILC	ILC2-IL-4, IL-5, IL-13, IL-9, Areg	ILC1 & 3, IL-17, IL-22
FeNO	>27 ppb	
Eosinophils: Sputum Peripheral blood eosinophils	>2% in sputum >150 cells/μL	
Therapies	Anticytokines, anti-IgE	

Regarding the treatment of asthma, both inhaled β2-adrenergic receptor agonists and glucocorticoids continue to be the main treatment for individuals with asthma, although leukotriene receptor antagonists and IgE-directed therapies are additional treatment options (**Table 2**). However, some patients including those with eosinophilic asthma, continue to experience symptoms and exacerbations with no effective treatments [Huang *et al.*, 2019; Fahy 2015; Lambrecht and Hammad 2015; Kuo *et al.*, 2017]. A summary of targeted agents for treating Th2-high and Th2-low asthma are listed in **Table 2**.

Table2. Th2-high and Th2-low asthma treatment agents

T2 High Agents		Possible T2 Low Treatment Agents	
Anti-IgE	Omalizumab, ligelizumab (QGE031) Quilizumab (RG7449)	Airway smooth muscle	Bronchial thermoplasty[a]
IL-5	Mepolizumab Reslizumab	Neutrophils Anti-CXCR2 Anti–granulocyte-macrophage colony-stimulating factor (GM CSF)	Macrolides
IL-5Rα	Benralizumab	TNF-α	Adalimumab, Etarnecept
IL-13Rβ	Lebrikizumab	Th17 pathway	Secukinumab, Brodalumab
IL-13	Tralokinumab		
IL-4α	Dupilumab		
GATA3	GATA3 DNAzyme		
TSLP	Tezepelumab		
PDG2-antagonist	Fevipiprant		
ILC2	Anti-CRTH2		

1.3 Lung cancer

1.3.1 Background

Lung cancer is a leading cause of malignant diseases and the most common cause of cancer-related death worldwide with a 5-year survival rate of about 21% [Siegel *et al.*, 2021; American Cancer Society 2021]. The predominant lung cancer subtype, non-small-cell lung cancer (NSCLC), accounts for 80% of lung cancer-associated deaths, and about 70% of patients have locally advanced or metastatic disease at the time of diagnosis. Clinically, NSCLC can be classified into adenocarcinoma (ADC), squamous cell carcinoma (SQC), and large cell carcinoma (**Figure 8**). ADC and SQC constitutes two major subtypes of NSCLC, and there is a trend that incidence of ADC is increasing worldwide, particularly in women. There are many risk factors for the development of lung cancer, with smoking being the most important one responsible for about 80% of lung cancer deaths. Additional risk factors include passive smoking, asbestos exposure, various chemicals, air-pollution, and familial history [Zappa and Mousa 2016].
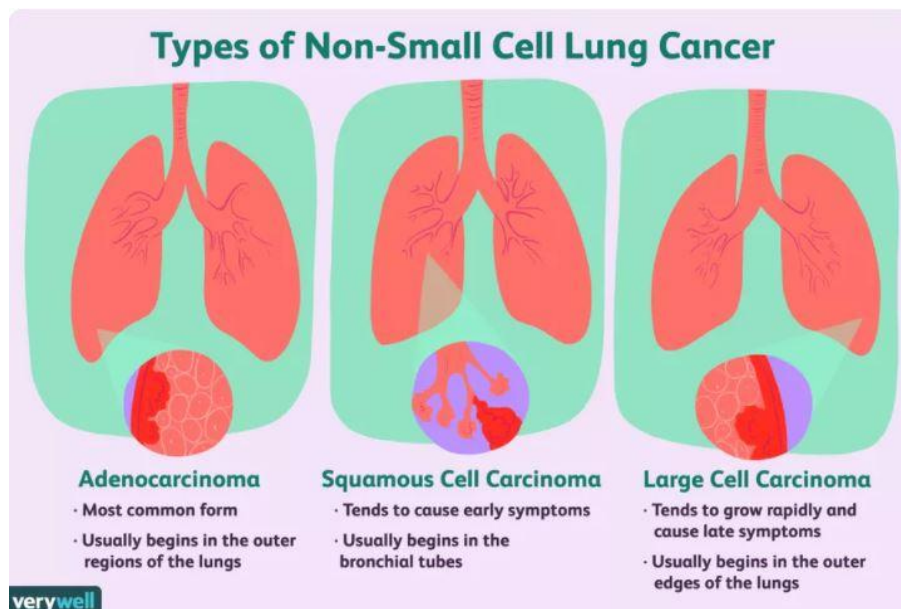
Figure 8. Types of Non-Small Cell Lung Cancer (NSCLC) (Humbert *et al.*, 2019).

Over the past 60 years, the development of systemic therapies for lung cancer has been hampered by disease heterogeneity, patient comorbidities, and a lack of safe, tolerable and effective drug therapies. Notably, chemotherapy, which was used to be the main treatment for NSCLC, has a lower efficacy and more side effects than targeted drugs. Specifically, important advancements in the treatment of NSCLC have been achieved over the past two decades, increasing our understanding of the disease biology and mechanisms of tumor progression, and advancing early detection and multimodal care. The use of small molecule tyrosine kinase inhibitors and immunotherapy has led to unprecedented survival benefits in selected patients (**Figure 9**). However, the overall cure and survival rates for NSCLC remain low, particularly in metastatic disease. Therefore, continued research into new drugs, combination therapies, and a better understanding of mechanisms of resistance are required to expand the clinical benefit to a

broader patient population and to improve outcomes in NSCLC [Herbst *et al.*, 2018; Chaft *et al.*, 2021; Ye *et al.*, 2021].

Molecular testing has become a mandatory component of the NSCLC management. Thus, the detection of EGFR, BRAF and MET mutations as well as the analysis of ALK, ROS1, RET and NTRK translocations have already been incorporated in the NSCLC diagnostic standards, and the inhibitors of these kinases are in routine clinical use. Furthermore, correlating cancer genomic information with the cellular components of the tumor microenvironment (TME) could allow the use of rationally designed combination therapies [Herbst *et al.*, 2018; Imyanitov *et al.*, 2021; König *et al.*, 2021; Majeed *et al.*, 2021].
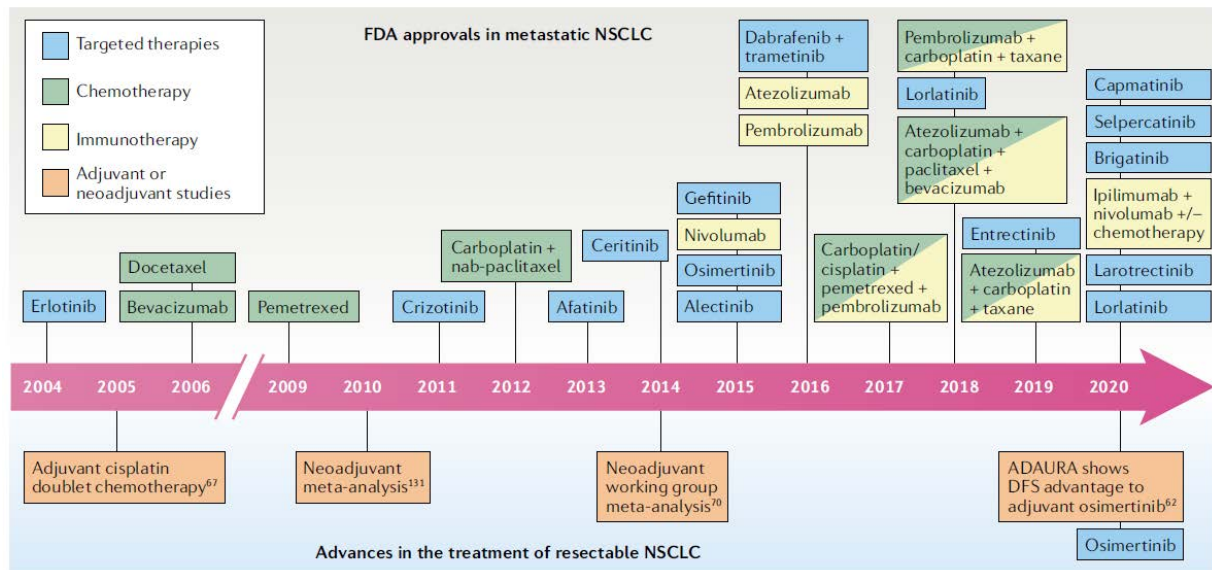
Figure 9. Timeline showing drugs approved or indicated for the treatment of NSCLC as of December 2020 (Chaft *et al.*, 2021).

1.3.2 Tumor Microenvironment

Tumor masses consist of a heterogeneous population of cancer cells and a variety of resident and infiltrating host cells, secreted factors, and extracellular matrix proteins, collectively known as the tumor microenvironment (TME). Specifically, the TME typically comprises immune cells, including T and B lymphocytes, tumor-associated macrophages (TAM), dendritic cells (DC), natural killer (NK) cells, neutrophils, and myeloid-derived suppressor cells (MDSC); stromal cells such as cancer-associated fibroblasts (CAF), pericytes, and mesenchymal stromal cells; the extracellular matrix (ECM) and other secreted molecules, such as growth factors, cytokines, chemokines, and extracellular vesicles (EV); and the blood and lymphatic vascular networks (**Figure 10**). Tumor progression is profoundly influenced by cancer cells interactions with the TME, which ultimately determine whether the primary tumor is eradicated, metastasizes, or establishes dormant micrometastases. Moreover, tumor metastasis requires the development of a pre-metastatic niche suitable for a subpopulation of tumor cells to colonize and develop into metastases with their own TME. Since the TME can also shape therapeutic responses and resistance, a deeper understanding of TME characteristics and function is required for developing new

strategies for targeting its components in patients with primary and metastatic tumors [Bejarano *et al.*, 2021; Hanahan *et al.*, 2011; Peinado *et al.*, 2017; Maru 2015; Kerkar and Restifo 2012].
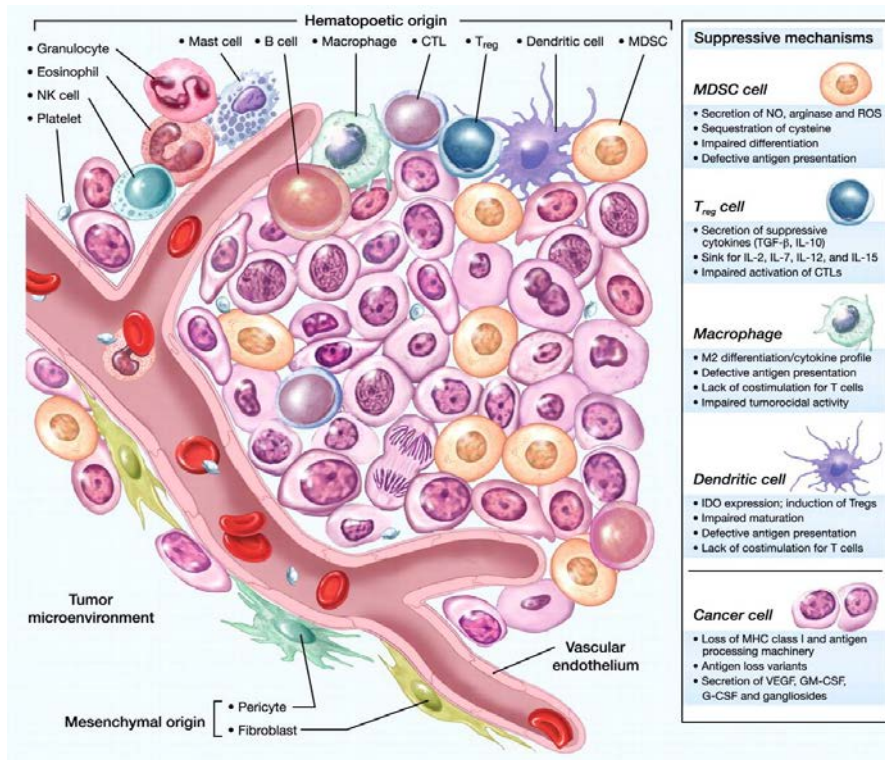
Figure 10. Components of the tumor microenvironment (Modified from Kerkar and Restifo 2012).

1.3.3 Lung metastasis

Metastasis is a term used to describe the spread of tumor cells from primary sites to surrounding structures and distant sites. Specifically, the lung is the second most frequent site of metastatic growth, with pulmonary secondary lesions being detected in 20-54% of cases. It should be noted that distant metastasis is an indicative marker of the aggressive nature of the primary tumor. Metastatic dissemination to the lung changes staging, clinical prognosis and treatment options of the original tumor and severely decreases survival rate [Peinado *et al.*, 2017; Stella *et al.*, 2019; Rangachari *et al.*, 2013; Gerull *et al.*, 2021; Jamil and Kasi 2021].

Tumors spread to the lungs either by hematogenous or lymphatic route or by direct invasion. Primary tumors secrete factors and extracellular vesicles, which systemically reprogram the lung microenvironment to generate pre-metastatic niches, which provide permissive microenvironments that support extravasation, colonization and metastatic outgrowth of disseminated tumor cells (DTCs) (**Figure 11**). Metastatic dissemination to the lung can arise from a variety of extrathoracic malignancies. Common cancers that metastasize to the lung parenchyma include breast, lung and colorectal tumors, uterine leiomyosarcomas, and head/neck squamous cell carcinomas. On the other hand, cancers that spread to the endobronchial tree of lungs include colorectal, renal and lung tumors and lymphomas. Other tumors that can metastasize to the lungs include osteosarcomas, testicular, adrenal and thyroid tumors,

choriocarcinomas and hypernephromas [Altorki *et al.*, 2018; Krishnan *et al.*, 2006; Stella *et al.*, 2019]. Conversely, brain, bone and liver are the three most frequent sites of lung cancer metastasis, and such metastasis lead to a worsened prognosis of patients [Zhu *et al.*, 2020].
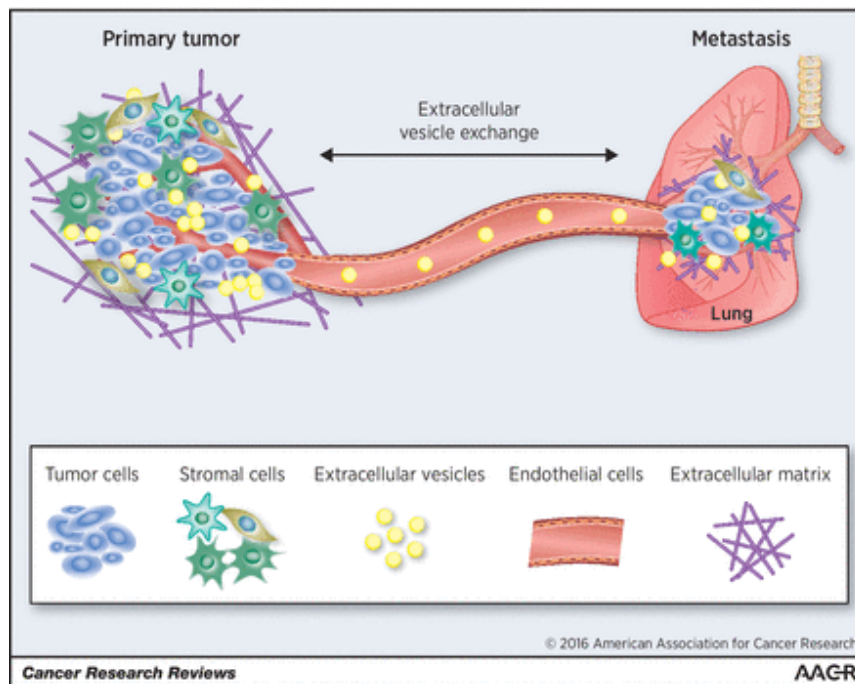
Figure 11. Reciprocal extracellular vesicle (EV)-mediated communication between cells in primary tumors and distant metastases. Different cell types present in heterogeneous tumors, including tumor cells and stromal cells, release EVs that can be taken up by neighboring cells or can be systemically transferred to distant cells present in the pre-metastatic niche. Conversely, cells present in metastases may release EVs that change the behavior of cells in the primary tumor (Zomer and van Rheenen, 2016).

1.3.4 Lewis lung carcinoma and melanoma preclinical models to study lung tumorigenesis and metastasis

Murine models for the study of lung cancer have historically been the backbone of preclinical data to support early human clinical trials. Specifically, the Lewis lung carcinoma (LLC) is a tumor that spontaneously developed as an epidermoid carcinoma in the lung of a C57BL mouse (**Figure 12A**). LLC was discovered in 1951 by Dr. Margaret Lewis and became one of the first transplantable tumors. In adittion, LLC is the only reproducible syngeneic model for NSCLC, which utilizes a transplant that is immunologically compatible. Notably, this model is a useful tool in predicting the clinical benefit of potential anti-tumor agents in preclinical experiments [Rashidi *et al.*, 2000; Kellar *et al.*, 2015; Chen *et al.*, 2018].

The B16 Melanoma cell line was discovered and maintained in the Jackson Laboratories in Maine in 1954 when a tumor developed naturally behind the ear of a C57BL/6 mouse (**Figure 12B**). The cells were resected, transplanted, and maintained *in vivo*. One of his first major studies involving B16 was in 1970, when Dr. Fidler stained B16s for tracking and measurement of the cells in the blood and in different

organs. He ascertained that 99% of the original cell population had perished within a day, and that a cohort of about 400 cells had colonized the lung. Today, B16 melanoma remains indispensable for metastasis studies, being a powerful research tool, and a staple for metastasis studies, and its development as such can be considered a huge benefit to the cancer research community [Teicher and Beverly 2002; Fidler and Isaiah 1970; Martín-Granado *et al.*, 2017; Erpenbeck *et al.*, 2010].
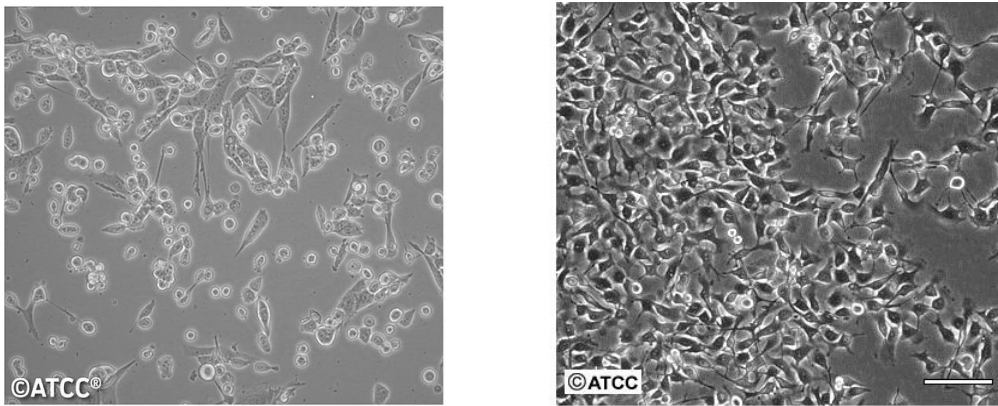
Figure 12. Lewis Lung Carcinoma (LLC1) (**A**) and Melanoma (B16-10) (**B**) cell lines.

LLC can also be used as orthotopic model, by injecting or implanting tumors into the corresponding organ that they originated from. On this basis, orthotopic models are considered to be more physiologically relevant in representing human tumorigenesis [Kellar *et al.*, 2015; Qiu and Su 2013]. In addition, LLC is highly metastatic in immunocompetent mice. Thus, if subcutaneously injected into mice, it is known that LLC cells show avidly to metastasize to the lung (**Figure 13A**). Moreover, several studies reported that LLC predominantly metastasizes into the lungs after tail vein injection (**Figure 13B**) [Anderson *et al.*, 1996; Bugge *et al.*, 1997; Ahmed *et al.*, 2011; Alhakamy *et al.*, 2016; Vandereyken *et al.*, 2017; Zuo *et al.*, 2017].
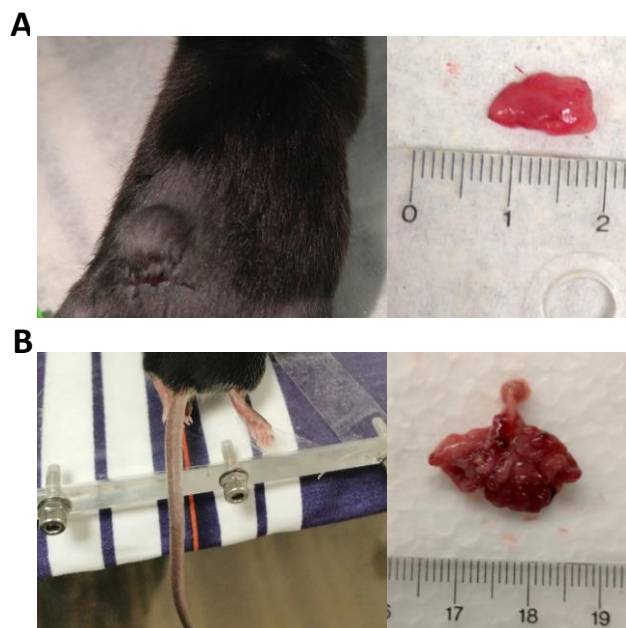
Figure 13. Subcutaneous Lewis tumor transplantation (**A**) and experimental pulmonary metastasis by i.v. tail vein injection of Lewis cells (**B**) in mice.

1.4 Insulin-like growth factors (IGFs)

1.4.1 The IGF/Insulin system: signaling and function in the lung

The insulin-like growth factor 1 receptor (IGF1R) is a ubiquitously expressed membrane-bound tyrosine kinase receptor formed by two β subunits with the intracellular tyrosine kinase signaling domain and two extracellular α subunits that recognize its two major ligands, IGF1 and IGF2 (**Figure 14**). IGF2 also interacts with a second receptor (IGF2R) that reduces IGF2 signaling through lysosomal degradation. Homology between IGF1R and the insulin receptor (INSR) allows IGF signaling through INSR, although with lower affinity; and *vice versa*, insulin (and pro-insulin) can activate IGF1R. Furthermore, IGF1R and INSR can form hybrid receptors, which have a high binding affinity for IGF1, thereby functioning as IGF1R. Noteworthy, IGF activity and availability are modulated by six high-affinity IGF binding proteins (IGFBPs 1-6). Although IGF1R expression has been found in almost all tissues and cell types during pre- and postnatal development and in adults, IGF1R and ligand expression is tightly regulated in a cell type-specific and spatiotemporal manner. Binding of ligands to IGF1R causes activation of various signaling pathways, including mitogen-activated protein kinases (MAPKs), involved in cell proliferation and differentiation, PI3K/Akt, with proven cell survival activity and signal transducers and activators of transcription proteins (STATs). IGF1R function is pleiotropic: it controls cell and body growth and tissue homeostasis of endocrine, paracrine and autocrine action of IGFs, playing important roles in regulation of cell survival, proliferation, differentiation, adhesion, migration, metabolism and senescence. These actions keep lung homeostasis, with implications in lung development and self-renewing and repair after injury (**Figure 14**) [Annunziata *et al.*, 2011; Girnita *et al.*, 2014; Crudden *et al*, 2015; LeRoith and Roberts 2003; Pollak 2008].
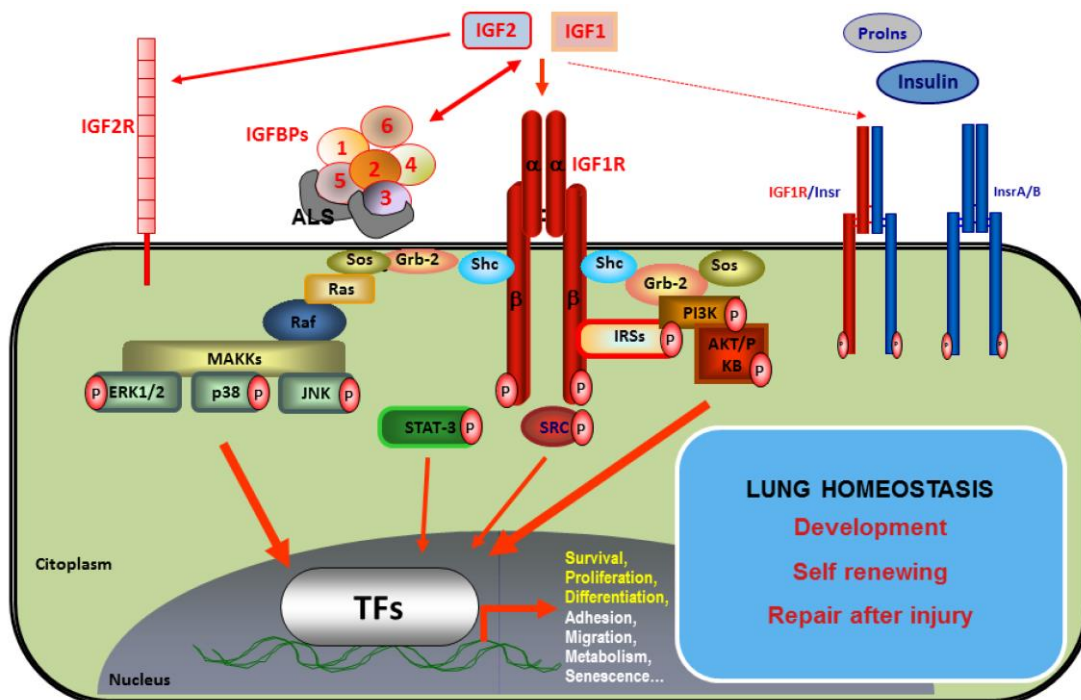
Figure 14. The Insulin-Like Growth Factor (IGF) System: signaling and function in the lung.

1.4.2 Regulation of circulating and tissue levels of IGFs

At the whole organism level, most circulating insulin-like growth factors are produced in the liver, whereas insulin is produced by the pancreatic β cells. In particular, the Growth Hormone (GH), which is produced in the pituitary gland under control of the hypothalamic factors growth hormone releasing hormone (GHRH) and somatostatin (SMS), is a key stimulator of IGF1 production (**Figure 15**).
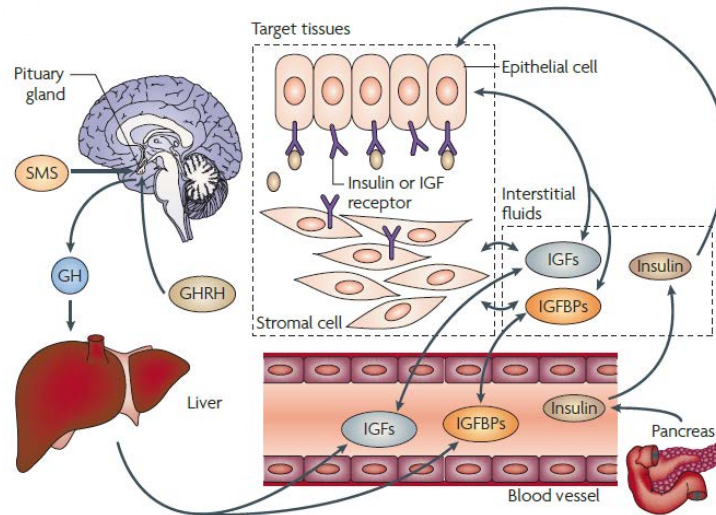
Figure 15. Regulation of circulating and tissue levels of IGFs (Pollak 2008).

Various IGF-binding proteins (IGFBPs) are also produced in the liver. Noteworthy, IGF2 is also expressed both in the liver and in extrahepatic sites, but it is not tightly regulated by GH. In IGF responsive tissues, the ligands IGF1 and IGF2 as well as IGFBPs can be delivered through the circulation from the liver (an 'endocrine' source), but IGFs and IGFBPs can also be locally produced through autocrine or paracrine mechanisms [Pollak *et al.*, 2004; Pollak 2008].

1.4.3 IGFs in human pathology

IGF activity is highly relevant in several chronic lung pathologies, including cancer, ARDS, COPD, pulmonary fibrosis and asthma [Wang *et al.*, 2018; Griffiths *et al.*, 2020; Nurwidya *et al.*, 2016; Agulló-Ortuño *et al.*, 2015; Ahasic *et al.*, 2014; Esnault *et al.*, 2013; Hoshino *et al.*, 1998; Hsu and Feghali-Bostwick 2008; Pala *et al.*, 2001; Ruan and Ying 2010; Veraldi *et al.*, 2009; Ye *et al.*, 2014]. IGF1/IGF1R signaling is implicated in multiple human pathologies, including intrauterine and postnatal growth failure, microcephaly, mental retardation and deafness [Abuzzahab *et al.*, 2003; Raile *et al.*, 2006; Varela-Nieto *et al.*, 2013; Walenkamp *et al.*, 2005; Walenkamp *et al.*, 2008]. Recently, IGF1R was identified as a novel outcome biomarker in critical COVID-19 patients to predict mortality [Fraser *et al.*, 2020]. Of note, IGF1R signaling has been profusely implicated as a critical contributor to cancer cell proliferation, survival, migration, and resistance to anticancer therapies, thus targeting IGF signaling is an attractive therapeutic strategy. In this regard, IGF1R is currently being evaluated as a pharmacological target in clinical trials for oncologic patients, including NSCLC [Iams *et al.*, 2015; Osher *et al.*, 2019; Kellar *et al.*, 2015; Corvaia *et al.*, 2013; Pollak 2008; Werner and Bruchim 2009].

1.4.4 Implication of IGF1R in embryonic lung development

IGF signaling is relevant for lung tissue development, homeostasis and repair. In particular, *Igf1r* knockout embryos exhibit growth retardation and developmental abnormalities, including altered central nervous system, abnormal skin formation, delayed bone development, reduced pancreatic beta-cells, failure of testicular determination, cochlear defects and lung immaturity [Bonnette and Hadsell 2001; Epaud *et al.*, 2012; Liu *et al.*, 1993; Nef *et al.*, 2003; Okano *et al.*, 2011; Scolnick *et al.*, 2008; Withers *et al.*, 1999]. Remarkably, *Igf1r* knockout embryos die at birth as they show lungs with strong hypoplasia, atelectasis, increased cell proliferation and apoptotic rates, vascular abnormalities, and altered alveolar differentiation, as well as decreased body weight (**Figure 16**) [Epaud *et al.*, 2012; Holzenberger *et al.*, 2000; Liu *et al.*, 1993]. Accordingly, prenatal *Igf1$^{-/-}$* mice die shortly after birth due to respiratory failure showing lungs with severe hypoplasia, increased cell proliferation, and altered alveolar differentiation and vasculogenesis [Moreno-Barriuso *et al.*, 2006; Pais *et al.*, 2013]. In this regard, *Igf1r* conditional mutant mice allow the generation of postnatal IGF1R-deficient mice to avoid perinatal mortality and to study IGF1R function at later stages of mouse life.
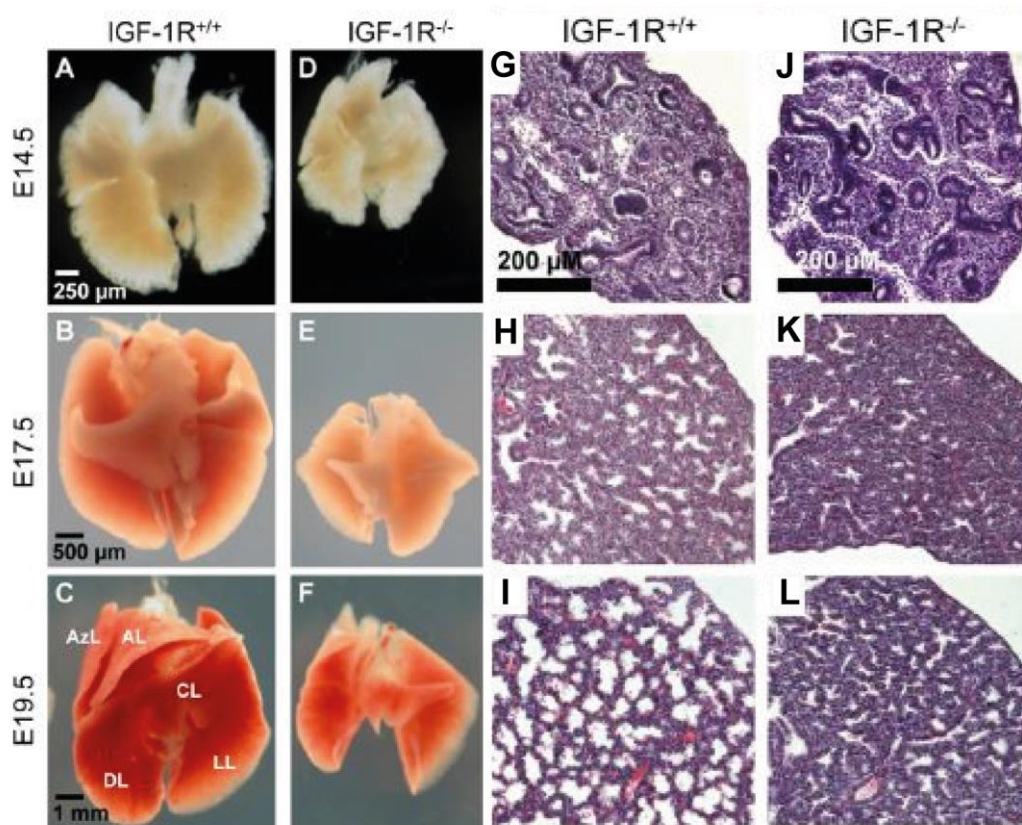
Figure 16. Lung development in late gestation *Igf1r$^{-/-}$* mice. (**A-F**) Ventra view of lungs from *Igf1r$^{+/+}$* and *Igf1r$^{-/-}$* embryos at developmental stages E14.5, E17.5 and E19.5. Abbreviations: AL, apical lobe; AzL, azygous lobe; CL, cardiac lobe; DL, diaphragmatic lobes; E, embryonic; LL, left lobe. (**G-L**) H&E stained lung sections of *Igf1r$^{+/+}$* versus *Igf1r$^{-/-}$* embryos at developmental stages E14.5, E17.5 and E19.5, showing that saccular walls are thicker and acinar buds smaller in *Igf1r$^{-/-}$* embryos as compared with controls of the same stage (Epaud *et al.*, 2012).

1.4.5 Igf1r expression in the adult mouse lung and involvement in airway epithelial regeneration

The adult mouse lung displays the highest level of IGF1R activation of any organ upon challenge with IGF1 [Moody *et al.*, 2014]. Although IGF1R is expressed throughout the entire lung, the highest expression levels were found in epithelial cells, alveolar macrophages, and the smooth muscle (**Figure 17**) [López *et al.*, 2016]. Specifically, IGF1R expression in smooth muscle and endothelial cells of pulmonary blood vessels also indicates a role of this receptor in lung vasculature [Abbas *et al.*, 2011; Engberding *et al.*, 2009].

Regeneration of lung epithelium is crucial for maintaining airway function. Thus, an imbalance between epithelial damage and repair is at the basis of numerous chronic lung diseases [Hogan *et al.*, 2014]. Concerning the role of IGF1R in bronchiolar epithelial regeneration, it was reported that the conditional deletion of *Igf1r* in the murine pulmonary epithelium followed by selective club cell ablation, altered the bronchiolar epithelium homeostasis, causing increased proliferation and delayed differentiation of club and ciliated cells. These findings support the implication of IGF1R in maintaining control of bronchiolar epithelial regeneration after injury [López *et al.*, 2016].
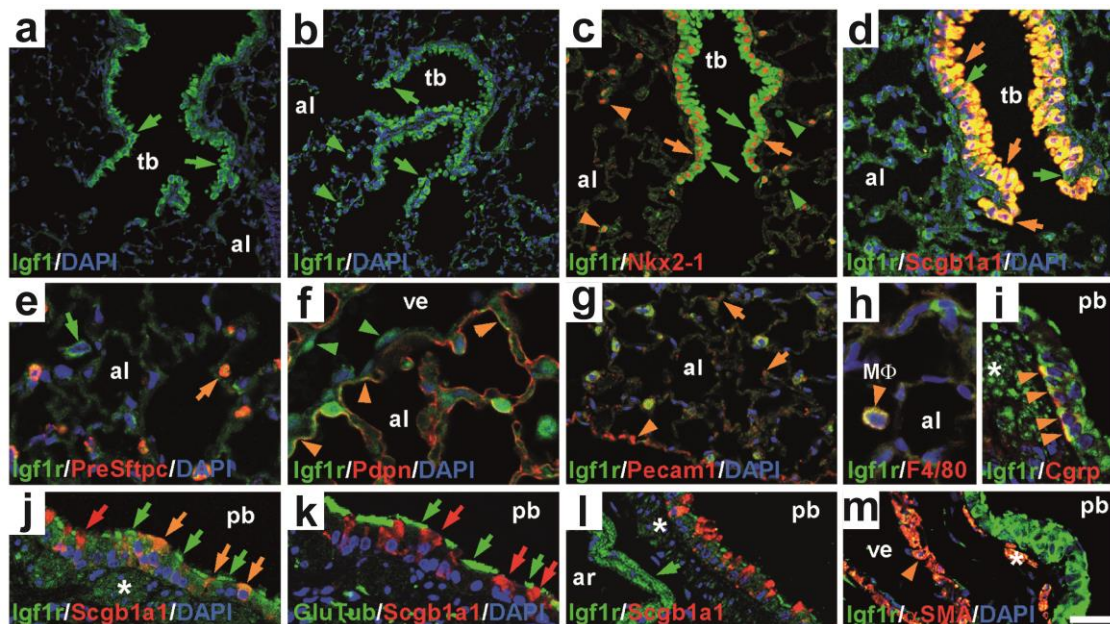
Figure 17. (**A-B**) Immuno-staining for IGF1 (**A**) and IGF1R (**B**) (green labeling) in six-month-old lungs. Distal bronchiolar epithelium showed strong staining for both proteins (green arrows). Note that IGF1R was also found scattered throughout the alveolar parenchyma (green arrowheads in B). (**C-M**) Immuno-staining for IGF1R (green labeling), counterstained in red with lung cell-type specific markers and blue with DAPI to visualize nuclei, in three-month-old lungs. (**C**) All bronchiolar epithelial cells showed co-localization of IGF1R (green arrows) with nuclear Nkx2-1 (orange arrows), and also co-localized with Nkx2-1+ AEC2 cells in the alveoli (orange arrowheads). There were Nkx2-1- alveolar cells that additionally stained for IGF1R (green arrowheads). (**D**) IGF1R strongly stained abundant Scgb1a1+ club cells in terminal bronchioles (orange arrows), and in apical cilia of scarce ciliated cells (green arrows). (**E**) IGF1R stained the cytoplasm of Pre-Sftpc+ AEC2 cells (orange arrows), and additional cells in alveolar spaces (green arrow). (**F**) IGF1R co-stained with Pdpn in areas of the apical membrane in AEC1 cells (orange arrowheads). Note the light staining of IGF1R in vein endothelial cells (green arrowheads). (**G**) IGF1R co-localized

with endothelial Pecam1^{+} cells (orange arrows), more abundantly in capillaries under the pleura (orange arrowhead). (**H**) IGF1R co-localization with the F4/80[+] alveolar macrophage marker in cells located in alveolar spaces (orange arrowhead). (**I**) IGF1R stained Cgrp^{+} neuroendocrine cells (orange arrowheads) in proximal bronchioles. (**J**) IGF1R staining in Scgb1a1[+] proximal bronchiole club cells is faint (orange and red arrows), but strong in apical membranes (cilia) of ciliated cells (green arrows). In an adjacent section (**K**), the Glu-Tubulin (GluTub, a cilium specific marker) stained the same ciliated cells (green arrows) as in K, whereas Scgb1a1 stained club cells (red arrows). (**L**) Pulmonary artery smooth muscle showed strong staining for IGF1R (green arrow), whereas para-bronchiolar smooth muscle stained fainter (asterisk). (**M**) α-SMA[+] smooth muscle cells in veins also co-express IGF1R (orange arrowhead), as does the para-bronchiolar smooth muscle (asterisk). al, alveolus; ar, artery; MΦ, macrophage; pb, proximal bronchiole; tb, terminal bronchiole; ve, vein. Scale bar in **M**: 32 μm in **A**; 50 μm in **B**; 34 μm in **C-D**; 16.6 μm in **E**; 12,5 μm in **F**, **H**, **I**; 18 μm in **J-K**; and 25 μm in **L-M** (Modified form López *et al.*, 2016).

1.5 Generation of *UBC-CreERT2; Igf1r*^fl/fl^ conditional mutant mice to study IGF1R function postnatally

1.5.1 TMX-inducible Cre/lox site-specific recombination system

The Cre/lox site-specific recombination system is an important tool for generating conditional somatic mouse mutants. This method allows gene activity to be controlled in both space and time in almost any mouse tissue. This approach takes advantage of the properties of P1 phage Cre recombinase, a 38 kDa enzyme that recognizes a 34 bp DNA sequence called loxP. The basic strategy for Cre/lox-directed gene knockout experiments is to flank an essential sequence of the gene of interest. Introduction of loxP sites flanking a DNA target sequence enables binding by Cre-recombinase and either inversion or excision of the sequence, thus generating a null allele in all cells where Cre is active (**Figure 18A,B**) [Le and Sauer 2001; Kim *et al.*, 2018].
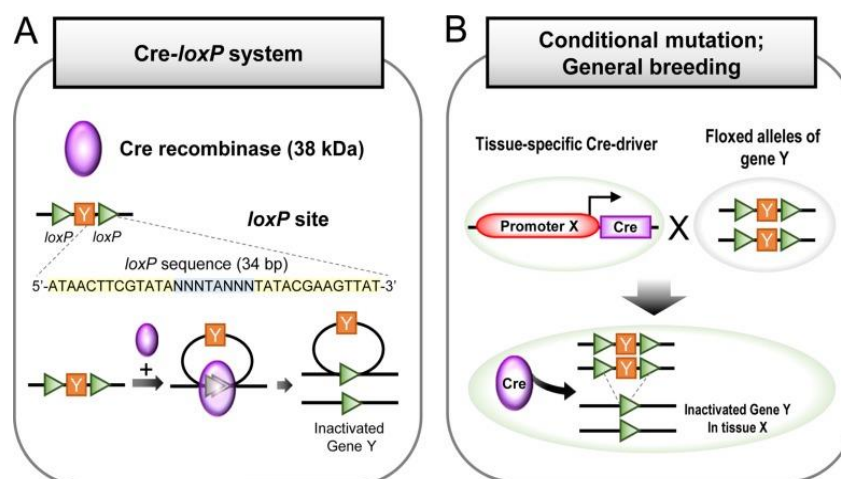
Figure 18. Mechanism of Cre-loxP system. (**A**) An overview of Cre-loxP system. 38 kDa Cre recombinase recognizes the loxP sites of specific 34 bp DNA sequences. (**B**) General breeding strategy for conditional mutation using loxP and Cre driving mouse line. One mouse use to have a tissue-specific or conditionally induced gene driven Cre gene and another mouse the loxP flanked (floxed) alleles of interest gene Y (Kim *et al.*, 2018.).

The *UBC-CreERT2* transgene consist of an Ubiquitin C gene promoter which drives generalized Cre-recombinase expression and the *CreERT2* fusion protein consisting of the Cre recombinase fused to a triple mutant form of the human estrogen receptor with a G400V/M543A/L544A triple mutation, which is selectively activated only in the presence of tamoxifen (TMX), but not to endogenous estrogen (**Figure 19**) (Feil *et al.*, 1997). *CreERT2* functions as a specific receptor for 4-hydroxytamoxifen (4-OHT). TMX acts as a prodrug that requires metabolism to form the pharmacologically active metabolite 4-OHT by cytochrome P450 (CYP2D6)-mediated catalysis [Chang *et al.*, 2012]. In the absence of 4-OHT, *CreERT2* protein is sequestered in the cytoplasm, complexed with the heat shock protein 90 (HSP90) [Mattioni *et al.*, 1994]. Binding to 4-OHT disrupts the interaction with HSP90 and permits the translocation of *CreERT2* to the nucleus wherein it catalyzes loxP-specific recombination events, resulting in deletion of flanked sequences in widespread cells/tissues (**Figure 19**) [Feil *et al.*, 1997; Feil *et al.*, 2007; Feil *et al.*, 2009; Hayashi and McMahon 2002; Metzger and Chambon 2001; Ruzankina *et al.*, 2007].
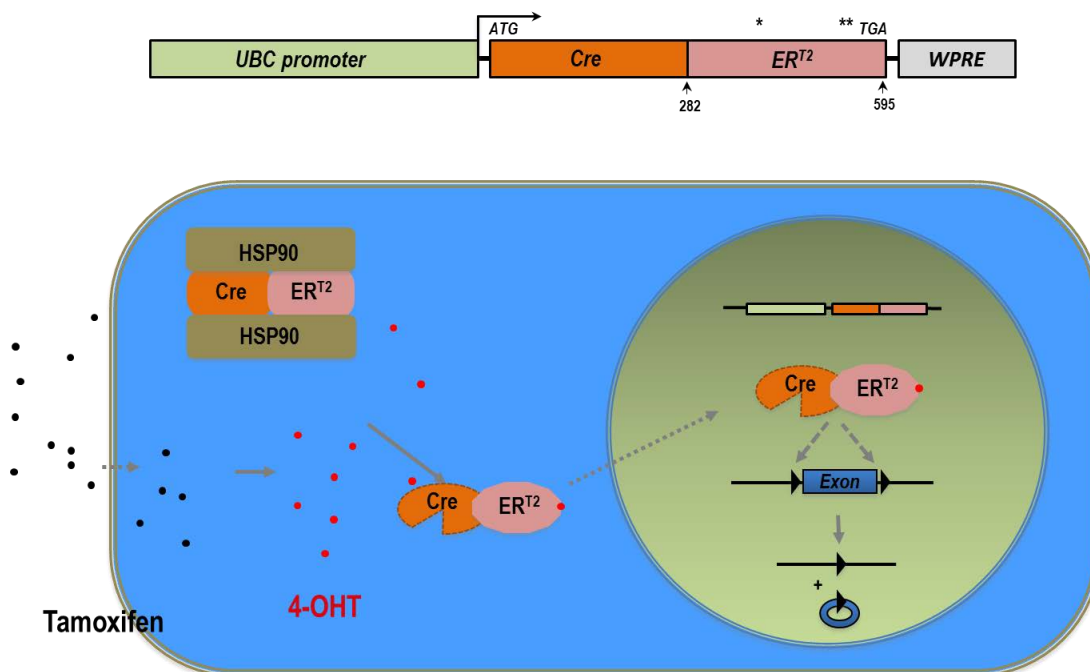
Figure 19. TMX-inducible Cre/lox site-specific recombination system.

1.5.2 Generation of IGF1R-deficient mice (CreERT2)

Igf1r-deficient mice die at birth due to growth retardation and respiratory failure. On this basis, *UBC-CreERT2; Igf1r^{fl/fl}* double transgenic mice with a tamoxifen (TMX)-inducible *Igf1r* gene deletion were generated in order to avoid perinatal mortality and to allow postnatal studies in IGF1R-deficient mice. These mice were generated in two generations by mating *UBC-CreERT2* transgenics (**Figure 20**) [Ruzankina *et al.*, 2007], with *Igf1r^{fl/fl}* mutants that contain loxP sites flanking exon 3 in *Igf1r* gene [Kloting *et al.*, 2008]. TMX administration to prepuberal *UBC-CreERT2; Igf1r^{fl/fl}* mice efficiently deletes *Igf1r* gene floxed sequences generating IGF1R-deficient mice, from now on called **CreERT2** mice.
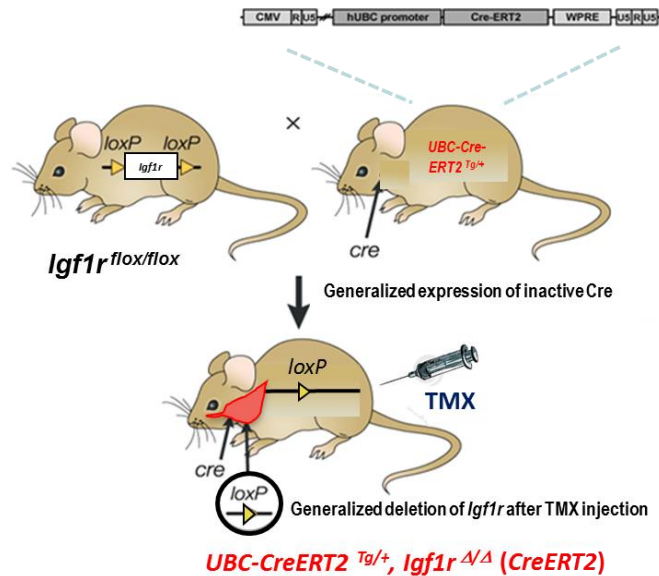
Figure 20. Generation of IGF1R deficient *CreERT2* mice (López et al., 2016).

Igf1r gene deficiency in *CreERT2* mice delays their growth, producing a distinct impact on organ size. Whereas testes are smaller, spleen and heart show an increased organ to body weight ratio. Mosaic *Igf1r* genomic deletions also cause a significant reduction in *Igf1r* mRNA expression in different organs, resulting in diverse phenotypes. While kidneys, spleen and cochlea have unaltered gross morphology, testes exhibit halted spermatogenesis and liver and alveolar lung parenchyma present increased cell proliferation rates without affecting apoptosis [López *et al*., 2015]. Accordingly, increased proliferation was observed in lungs of epithelial-specific *Igf1r*-deficient mice [López *et al*., 2016]. Of note, IGF1R protein deficiency in the lung [Piñeiro-Hermida *et al*., 2017a], brain [Cardoso *et al*., 2021] and other tissues (*unpublished data*) was demonstrated in *CreERT2* mice. In summary, *Igf1r*-deficient mice have advantages over conventional *Igf1r* knockout mice, such as avoiding the perinatal lethality and preventing possible cascades of compensatory responses occurring during early development, which can complicate interpretation of the phenotype, and that IGF1R function is highly dependent on cell, tissue and organ type.

1.6 Role of IGFs in inflammation and allergy

IGFs were reported to play an important role in inflammation as they appear to modify several aspects of inflammation by influencing the actions of cytokines and other inflammatory mediators [Smith 2010]. Notably, both IGF1R and IGF1 could play an important role in the proliferation of alveolar macrophages taking place during inflammation [Rom and Pääkkö 1991]. In this regard, ablation of the macrophage IGF1-IGF1R axis in mice inhibits the NLRP3 inflammasome, which indicates that IGF1R plays an important role in initiation of the inflammatory process [Spadaro *et al*., 2016].

Several lines of evidence and recent experimental data collected by multidisciplinary research groups seem to strengthen the role of the IGF proteins and related proteins in severe allergic asthma, even proposing them as potential therapeutic targets in these pathologies [Vázquez-Mera S *et al*., 2021]. IGF1

signaling has been implicated in activation of different aspects of the asthmatic response, and IGFBP3 was suggested to be involved in allergic airway inflammation [Hoshino et al., 1998; Veraldi *et al.*, 2009; Wang *et al.*, 2018]. On the other hand, the serum biomarker IGF-ALS (IGF Binding Protein Acid Labile Subunit) was recently reported to be capable of differentiating moderate-severe allergic from non-allergic asthma [Nieto-Fontarigo *et al.*, 2020]. In addition, IGF1R was found to be upregulated in eosinophils from bronchoalveolar lavage of mild asthmatic patients [Esnault *et al.*, 2013]. In mice, IGF1 mediates allergic airway inflammation, and IGFBP3 was shown to block the effects of asthma [Yamashita *et al.*, 2005; Lee *et al.*, 2011].

1.6.1 Implication of IGF1R in murine acute lung inflammation and allergy

Noteworthy, the functional implication of IGF1R in acute lung inflammation was previously studied using a bleomycin (BLM) mouse model. In this regard, since IGF1R-deficient mice showed resistance to BLM-mediated acute lung injury by counteracting lung inflammation and alveolar damage, IGF1R may then be considered as an important player in murine acute lung inflammation [Piñeiro-Hermida *et al.*, 2017c]. On the other hand, it was previously studied the implication of IGF1R on airway hyperreactivity and mucus secretion in a chronic HDM model of asthma. In this respect, IGF1R-deficient mice showed reduced allergic airway inflammation and remodeling, mucus production and AHR after chronic HDM exposure [Piñeiro-Hermida *et al.*, 2017a]. Additionally, preventively-induced IGF1R-deficiency was reported to ameliorate typical asthmatic features following acute HDM treatment [Piñeiro-Hermida *et al.*, 2017b]. In conclusion, these results demonstrate that IGF1R plays a key role in murine HDM-induced allergic airway inflammation (**Figure 21**). On this basis, the study of pharmacological blockade of IGF1R upon allergic airway inflammation in mice, would allow the development of future therapeutic approaches for these pathologies.
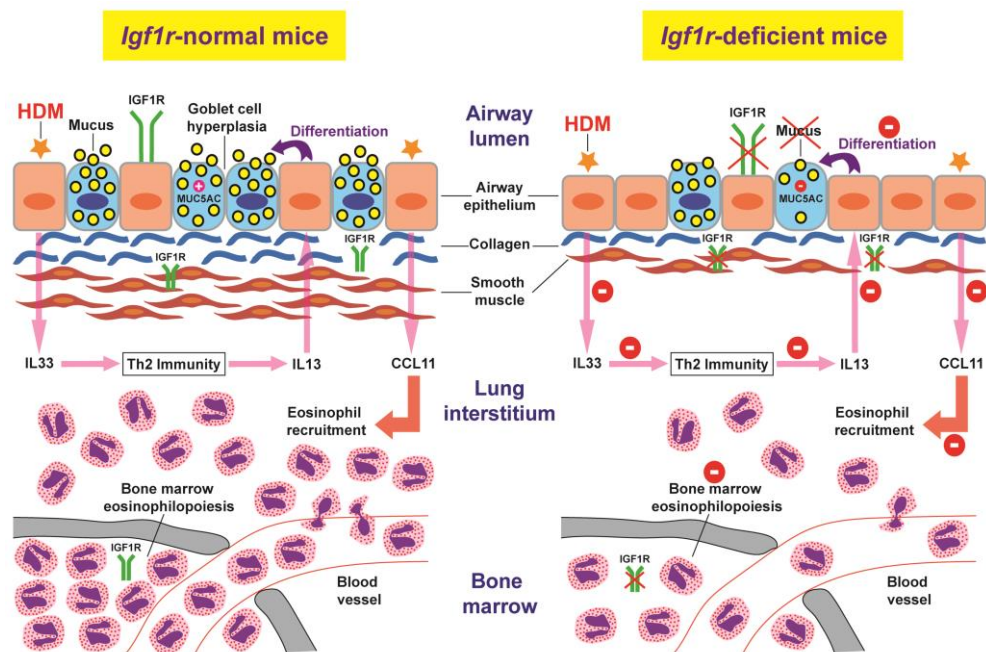
Figure 21. Proposed mechanism for reduced susceptibility to allergic airway inflammation in IGF1R-deficient mice. Following HDM exposure Igf1r deficiency counteracts collagen deposition, smooth muscle thickening and mucus secretion. The airway epithelium is known to be a major source of IL33 and its delayed differentiation by Igf1r deficiency could diminish IL33 levels after HDM treatment, reducing the induction of Th2 immunity and particularly IL13 expression. After HDM exposure, IL13 normally stimulates goblet cell differentiation in the airway epithelium which leads to goblet cell hyperplasia and mucus hyperproduction in addition to triggering the release of CCL11. Delayed differentiation of the airway epithelium caused by Igf1r deficiency together with diminished IL13 levels may inhibit differentiation of goblet cells and CCL11 production, reducing mucus secretion and eosinophil recruitment to the lung. Additionally, decreased eosinophilopoiesis in bone marrow of Igf1r deficient mice can also substantially contribute to reduced eosinophil presence in the lung (Piñeiro-Hermida *et al.*, 2017b).

1.7 Role of IGFs in lung cancer

Deregulation of IGF system was demonstrated at all stages of lung carcinogenesis, ranging from dysplastic lesions of bronchial epithelium to advanced forms of cancer [Weroha and Haluska, 2012]. Specifically, circulating levels of IGFBP3 were found reduced in lung cancer patients [Izycky *et al.*, 2006; Wang *et al.*, 2013; Cao *et al.*, 2012; Tas *et al.*, 2016; Yu *et al.*, 1999]. In accordance, lung tissue expression of IGFBP3 was shown to be lost in 57% of patients with stage I NSCLC, and strongly associated with a poor prognosis in these patients, suggesting that IGFBP3 functions as a tumor suppressor and plays an important role in determining biological aggressiveness in early NSCLC [Chang *et al.*, 2002; Wang *et al.*, 2013]. Moreover, expression of IGFBP7 in serum and lung tissue from NSCLC patients was found significantly lower [Wang *et al.*, 2013]. On the other hand, high levels of circulating IGF1 were associated with the risk of developing lung malignancy. In addition, expression of IGF1 was found significantly incremented in lung tissue from NSCLC patients [Kim *et al.*, 2014; Kim *et al.*, 2011; Vlachostergios *et al.*, 2011; Izycky *et al.*, 2006; Wang *et al.*, 2013; Fu et al., 2016; Zhang *et al.*, 2014; Nurwidya *et al.*, 2016; Yu *et al.*, 1999]. IGF2 was suggested as a potential prognostic factor in lung adenocarcinoma, since patients with increased lung tissue expression of IGF2 exhibited a shorter survival [Takanami *et al.*, 1996a,b]. Furthermore, exogenous addition of IGF1 and IGF2 were reported to stimulate the proliferation of human lung cancer cells in vitro [Nakanishi *et al.*, 1988]. In mice, administration of recombinant human IGFBP3 (rhIGFBP3) was shown to inhibit Lewis lung carcinoma cell growth *in vitro* and *in vivo* [Alami *et al.*, 2008]. Accordingly, lack of IGFBP3 accelerates lung tumorigenesis, and its overexpression inhibits lung cancer survival *in vitro* [Kim *et al.*, 2011; Wang *et al.*, 2017]. Moreover, IGF1 expression by the TME was reported to have a supportive role in tumor initiation and progression, and IGF2 was shown to be an important genetic factor in the development of lung tumorigenesis, since transgenic overexpression of IGF2 induces spontaneous lung tumors in mice [Ajona *et al.*, 2020; Moorehead *et al.*, 2003].

1.7.1 Implication of IGF1R in lung cancer

Notably, circulating levels of IGF1R were found significantly increased in lung cancer patients and IGF1R overexpression was reported to increase cell survival and to supress apoptosis in human lung cancer [Wang *et al.*, 2015] Accordingly, IGF1R was extensively reported to be associated with reduced

survival, poor prognosis and tumor recurrence in NSCLC patients [Nagakawa *et al.,* 2012; Ajona *et al.*, 2020; Zhao *et al.*, 2017; Zhao *et al.*, 2014; Xu *et al.*, 2019; Al-Saad *et al.*, 2017]. Preclinical studies have revealed the implications of IGF1R in lung cancer biology, such as the EMT process, cancer stem cell maintenance, and resistance to cancer therapies. In this sense, IGF1R was shown to play a key role in the development of lung cancer metastasis in animal models [Nurwidya *et al.*, 2016; Gong *et al.*, 2014; Long *et al.*, 1995; Sachdev *et al.*, 2004]. Given that IGF1R has been suggested to play a relevant role in several chronic lung pathologies with an inflammatory component including NSCLC, the study of IGF1R as a cancer-promoting factor in the lung TME of IGF1R deficient mice, would allow to better understand its role in this processes and to improve the development of future therapeutic approaches for NSCLC.

1.7.2 IGF1R inhibitors in cancer therapeutics: preclinical studies and clinical trials

IGF1R and its associated signaling system have provoked considerable interest over recent years as a novel therapeutic target in cancer. In this sense, several IGF/IGF1R inhibitors have been developed: (1) monoclonal antibodies against IGF1R, (2) monoclonal antibodies against IGF1R ligands (IGF1 and IGF2), and (3) IGF1R tyrosine kinase inhibitors (TKIs) (**Table 2**). These IGF1R-targeting agents share common effects on IGF1R signaling but differ in mechanisms of action, spectrum of target inhibition, and pharmacological features. The differing spectrum of target blockade may potentially translate into different toxicity and/or activity profiles. Specifically, particular interest in lung cancer has focused on the development of IGF1R TKIs in view of the known associations of IGF1R and EGFR, the extensive research already performed in lung cancer on the related EGFR TKI family, and the associated problems of overcoming acquired resistance to anti-EGFR therapy. It should be noted that whilst many experimental IGF1R inhibitors have shown preclinical efficacy, only a few have undergone clinical evaluation, and results have been disappointing. Possible reasons for failure include the complexity of the IGF1R/insulin receptor system and parallel growth and survival pathways, as well as a lack of patient selection markers. On this basis, further work is required to ascertain efficacy of IGF1R targeted therapy in the clinical setting, and in addition, to elucidate biomarkers of response to treatment. In spite of this, anti-IGF1R therapies continue to be valid targets for oncologic patients [Hewish *et al.*, 2009; Chen and Sharon 2013; Iams *et al.*, 2015; Osher *et al.*, 2019].

Table 2. Therapeutic targeting of IGF1R (Hewish *et al.*, 2009; Chen and Sharon, 2013, Osher *et al.*, 2019).

TARGET AND COMPOUND	STATUS	TUMOR TYPE
Monoclonal antibodies IGF1-IGF2		
MEDI-573	Phase I	
Monoclonal antibodies IGF1R		
CP-751,871 (Figitumumab)	Discontinued after Phase III	Ewing sarcoma, Adenocortical, Squamous,
AVE1642 (EM164)	Discontinued after Phase III	
IMC-A12 (Cixutumumab)	Phase II	Ewing sarcoma, Hepatocellular, metastatic resistant prostate cancer, thymoma, pancreatic,
AMG-479 (Ganitumab) and 655	Phase III	Ewing sarcoma, Desmoplastic round, pancreatic, breast
R1507 (Teprotumumab)	Phase II	Ewing sarcoma, NSCLC,
MK-0646/h7C10 (Dalotuzumab)	Phase III	Colorectal
BIIBO22	Discontinued after Phase I	
SCH-717454 (19D12 Robatumumab)	Discontinued after Phase II	
MM-141 (Istiratumab)	Phase II	
IGF1R TKIs		
NVP-AEW541	Preclinical	
BMS-536942	Preclinical	
BMS-554417	Preclinical	
BMS-754807	Phase II	
NVP-ADW742	Preclinical	
A-928605	Preclinical	
AG1024	Preclinical	
OSI-906 (Linsitinib)	Phase III	Thymic adrenocortical, colorectal, NSCLC, neck cancer
PQIP	Preclinical	
AXL1717 (PPP Picropodophyllin)	Phase II	
BVP 51004	Phase I	
XL228	Phase I	
INSM-18	Phase II	

2 AIMS OF THE THESIS

The overall aim of this thesis was to investigate IGF1R as a pharmacological target in allergic asthma and cancer-promoting factor in the lung tumor microenvironment.

The following specific aims were proposed:

1. To test if IGF1R TKI NVP-ADW742 ameliorates allergic airway inflammation in mice and to evaluate IGF1R as a candidate biomarker in patients with allergic asthma.

2. To determine the impact of IGF1R deficiency on key components of the lung TME using murine models of tumor heterotopic transplantation and pulmonary metastasis.

3 MATERIALS AND METHODS

3.1 Ethics statement

All experiments and animal procedures were carried out following the guidelines laid down by the European Communities Council Directive (86/609/EEC) and were revised and approved by the CEAA/CIBIR (Gobierno de la Rioja) Bioethics Committee (refs JGP01_v2, JGP02_1, JGP02_7 and JGP02_9). The animals were maintained under specific pathogen-free (SPF) conditions in laminar flow caging at the CIBIR animal facility.

3.2 Establishment of the murine model of allergic asthma

Eight-week-old inbred C57BL/6J female mice were purchased from Charles River Laboratories, Inc. Mice were intranasally (i.n.) challenged either with 40 μg of house dust mite (HDM) extract (Greer Laboratories Inc, Lenoir, NC) in 20 μL PBS (2 mg/mL) or an equal volume of phosphate buffer saline (PBS) under light isoflurane anesthesia five days a week for four weeks. Females were used due to their reported higher susceptibility to allergic airway inflammation [Melgert *et al.*, 2005]. Four different experimental groups were used: 1) PBS + vehicle (PBS i.n. + 2% DMSO in saline intraperitoneal (i.p.) twice daily between D14 and D27); 2) HDM + vehicle (HDM i.n. + 2% DMSO i.p. twice daily between D14 and D27); 3) HDM + NVP-ADW742 (NVP) 1 wk (Selleckchem, Houston, TX) (HDM i.n + 10 mg/kg of NVP-ADW742 in 2% DMSO i.p. twice daily between D21 and D27); and 4) HDM + NVP-ADW742 2 wks (HDM i.n. + 10 mg/kg of NVP-ADW742 in 2% DMSO i.p. twice daily between D14 and D27). Mice were weighed on days (D) D0, D7, D14, D21, D28 of the protocol to assess body weight gain (**Figure 22**). Noteworthy, treatment with the vehicle of NVP (DMSO) did not induce inflammation in lungs of inbred C57BL/6J mice. In accordance, several drugs were previously reported to be dissolved in up to 5% DMSO for their use in preclinical mouse models [Piñeiro-Hermida *et al.*, 2021; Sengupta *et al.*, 2018].
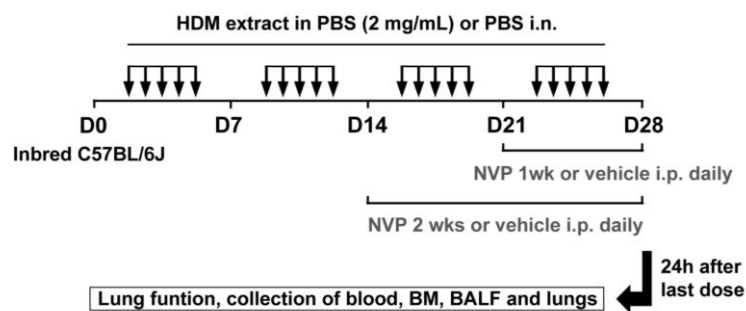
Figure 22. Protocol for HDM exposure and treatment with the IGF1R inhibitor NVP. Mice were challenged by intranasal (i.n.) administration of HDM extract in PBS or equal volume of vehicle, five days a week for four weeks. Mice also received intraperitoneal (i.p.) injections of the IGF1R inhibitor NVP or equal volume of the vehicle (2% DMSO) twice daily during the last one (NVP 1 wk) or two weeks (NVP 2 wks) of the HDM protocol. Lung function assessment and collection of blood, bone marrow (BM), bronchoalveolar lavage fluid (BALF) and lungs were performed 24h after the last exposure on day (D) 28.

3.3 Generation of *UBC-CreERT2; Igf1r*$^{\Delta/\Delta}$ mice (*CreERT2*)

UBC-CreERT2; Igf1r$^{fl/fl}$ mice were created in two generations by mating hemizygous *UBC-CreERT2* transgenics (*Tg(UBC-cre/ERT2)1Ejb*; MGI:3707333) with a 129SvEv/C57BL/6 mixed genetic background [Ruzankina *et al.*, 2007], with homozygous *Igf1r*$^{fl/fl}$ mutants (Igf1^{rtm1Jcbr}; MGI:3818453) that had a C57BL/6 background [Kloting *et al.*, 2008] (F0). *UBC-CreERT2; Igf1r*$^{fl/+}$ heterozygous mice generated in F1 were backcrossed with *Igf1r*$^{fl/fl}$ to yield an F2 with equal proportions of four genotypes, among them mice of the new *UBC-CreERT2; Igf1r*$^{fl/fl}$ double transgenics and the *Igf1r*$^{fl/fl}$ mice, both with a 129SvEv/C57BL/6 mixed genetic background. *UBC-CreERT2; Igf1r*$^{fl/fl}$ double transgenic mice were crossed with *Igf1r*$^{fl/fl}$ mutants to directly generate descendants with equal proportions of both parental genotypes, which were used in experiments to study the impact of IGF1R deficiency on key components of the lung TME (**Figure 23**).
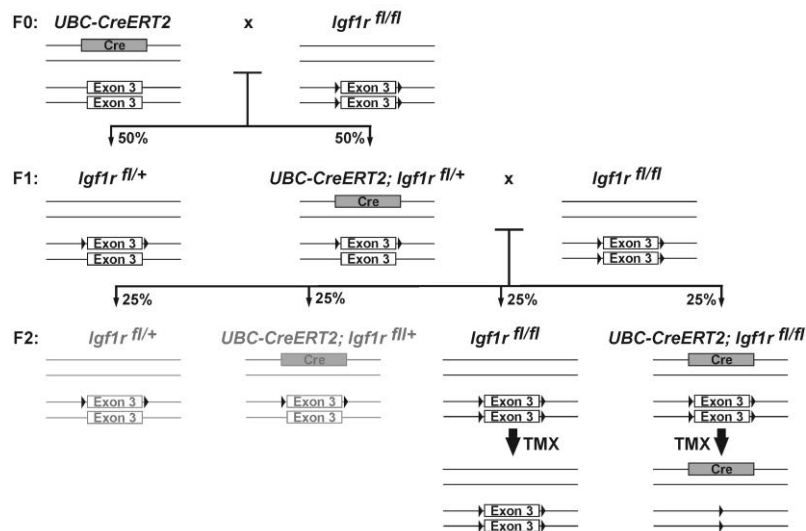
Figure 23. Strategy to achieve TMX-induced *Igf1r* gene deletion in *UBC-CreERT2; Igf1r*$^{fl/fl}$ double mutant mice in two generations (F2), by mating hemizygous *UBC-CreERT2* transgenics with homozygous *Igf1r*$^{fl/fl}$ mutants (F0), followed by a backcross mating in F1. Proportion of genotypes is given in percentages according to Mendelian inheritance. The diagram represents the genomic organization on each locus in the different genotypes. Black arrowheads denote location of loxP sites flanking exon 3 in *Igf1r* gene. Postnatal TMX administration to F2 mice activates Cre recombinase to promote *Igf1r* exon 3 deletion exclusively in *UBC-CreERT2; Igf1r*$^{fl/fl}$ mice, but not in *Igf1r*$^{fl/fl}$ (controls) mice. TMX, tamoxifen.

It should be noted that both *UBC-Cre-ERT2; Igf1r*$^{fl/fl}$ and *Igf1r*$^{fl/fl}$ mice were never employed for breeding purposes. To induce a postnatal *Igf1r* gene conditional deletion in mice, 4 week-old *UBC-CreERT2; Igf1r*$^{fl/fl}$ double transgenics were injected intraperitoneally with tamoxifen (TMX) solution (Sigma-Aldrich, St. Louis, MO) (75 mg/kg) dissolved in corn oil (Sigma-Aldrich) at a concentration of 20 mg/ml for five consecutive days (D0–D4) to obtain the *Igf1r*-deficient *UBC-CreERT2; Igf1r*$^{\Delta/\Delta}$ (**CreERT2**) mice [López *et al.*, 2015]. *Igf1r*$^{fl/fl}$ mice were also injected with TMX as TMX-experimental controls. Animals were monitored for adverse effects, and if these become apparent, treatment was stopped.

3.4 Mouse genotyping

Mice were genotyped by standard PCR analysis of tail DNA obtained as described [Pais *et al.*, 2013], and using specific primers for each gene designed as shown in **Figure 24A,B**. Presence of *UBC-CreERT2* transgene was detected using primers forward (F) (5'-TGAAGCTCCGGTTTTGAACT-3') and reverse (R) (5'-TGGTGTACGGTCAGTAAATTGG-3'), in combination with two additional primers for the IL2 gene, IL2F (5'-CTAGGCCACAGAATTGAAAGATCT-3') and IL2R (5'-GTAGGTGGAAATTCTAGCATCATCC-3'), used as an internal PCR positive control. They rendered 255 and 325 bp-long amplicons, respectively (**Figure 24 A,C**). To identify *Igf1r* wild type (wt) or flox (fl) alleles, both the forward F1 (5'-TCCCTCAGGCTTCATCCGCAA-3') and the reverse R1 (5'-CTTCAGCTTTGCAGGTGCACG-3') primers were used, which generated a 300 and/or 380 bp amplicon for each allele, respectively [Kloting *et al.*, 2008]. *Igf1r* deletion was detected using the following primers: F3 (5'-TTATGCCTCCTCTCTTCATC-3') and R1 (5'-CTTCAGCTTTGCAGGTGCACG-3') which can generate three products of 1300, 1220 and 491 bp (**Figure 24B,C**). The PCR conditions were as follows: (1) For *UBC-CreERT2* and IL2 genes: 94 °C for 3 min; 30 cycles of 94 °C for 30 s, 60 °C for 30 s, and 72 °C for 30 s; finally 72 °C for 7 min. (2) For *Igf1r wt/fl* alleles: 94 °C for 3 min; 35 cycles of 94 °C for 30 s, 56 °C for 30 s, and 72 °C for 30 s; finally 72 °C for 7 min. And lastly (3) for *Igf1r* deletion: 95 °C for 4 min; 30 cycles of 95 °C for 45 s, 58 °C for 45 s, and 72 °C for 80 s, and finally 72 °C for 10 min.
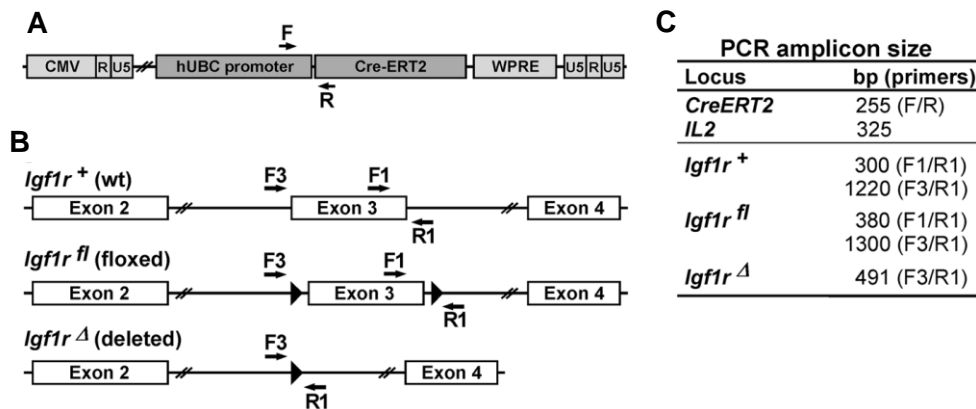
Figure 24. Primers and amplicon sizes to identify presence of the *UBC-CreERT2* transgene and the different *Igf1r* allelic forms by standard PCR analysis. (**A**) *UBC-CreERT2* transgene elements and location of F/R primers for PCR genotyping. (**B**) Genomic DNA organization in alternative allelic forms of the *Igf1r* locus (wt, floxed and deleted), and specific primers (F1, F3 and R1) used for *Igf1r* locus analysis by PCR. (**C**) Expected amplicon sizes in PCR assays to identify presence of the *UBC-CreERT2* transgene and the different *Igf1r* allelic forms. IL2 primers were used as constitutive positive controls when genotyping hemizygous *UBC-CreERT2* mice.

3.5 Generation of the heterotopic syngeneic transplantation mouse model

TMX was administered daily for five consecutive days to four-week-old *UBC-Cre-ERT2; Igf1r^{fl/fl}* and *Igf1r^{fl/fl}* mice to induce a postnatal *Igf1r* gene conditional deletion in *UBC-Cre-ERT2; Igf1r^{fl/fl}* mice [López *et*

al., 2015]. Then, nine- to 10 week-old (W9-10) female mice of both genotypes (*Igf1r^{fl/fl}* and *UBC-Cre-ERT2; Igf1r^{fl/fl}* (CreERT2)) were subcutaneously injected in shaved flanks with 1 x 10^6 Lewis Lung Carcinoma (LLC) cells in PBS (100 µl) or equal volume PBS at day (D) 0, under light isoflurane anesthesia. LLC engraftments were allowed to grow for 14 days (D14). Tumor size was measured with a caliper on alternate days. Tumor volumes were determined using the formula: volume = (width^2 × length) × 0.50 [O´Reilly *et al.*, 1997], and their weight assessed at D14. Mice were euthanized by intraperitoneal injection of 10 µL/g of a ketamine-xylazine anesthetic combination in saline (300:30 mg/kg, respectively). Resected tumors were fixed by inflation with 4% formaldehyde for 8-10h and embedded in paraffin for immunohistochemistry (**Figure 25**).
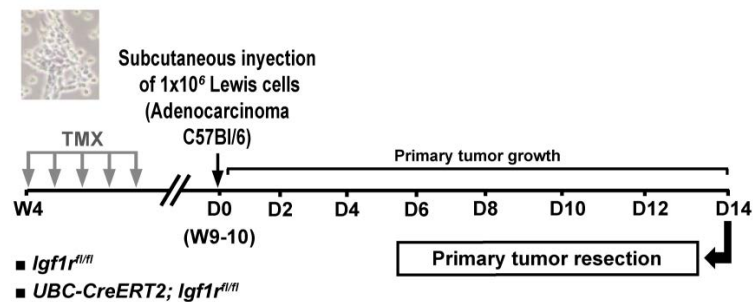
Figure 25. Protocol of the heterotopic syngeneic transplantation. *UBC-CreERT2; Igf1r^{fl/fl}* and *Igf1r^{fl/fl}* (controls) female mice were treated with tamoxifen (TMX) for five consecutive days at four weeks (W) of age to induce Igf1r gene deletion. Then, mice were subcutaneously injected in their right flanks with 1 x 10^6 Lewis lung carcinoma (LLC) cells in PBS or an equal volume of PBS. A follow-up of LLC engraftments was performed for 14 days by measuring tumor size on alternate days; primary tumors were resected on day (D) 14.

3.6 Generation of the experimental pulmonary metastasis mouse model

TMX was administered daily for five consecutive days to four-week-old *UBC-Cre-ERT2; Igf1r^{fl/fl}* and *Igf1r^{fl/fl}* mice to induce a postnatal *Igf1r* gene conditional deletion in *UBC-Cre-ERT2; Igf1r^{fl/fl}* mice [López *et al.*, 2015]. Then, ten- to 12 week-old (W10-12) female mice of both genotypes (*Igf1r^{fl/fl}* and *UBC-Cre-ERT2; Igf1r^{fl/fl}* (CreERT2)) were injected through the lateral tail vein with 1 x 10^6 LLC or B16-F10 cells in PBS (100 µL) or equal volume PBS at D0 under light isoflurane anesthesia (**Figure 26**).
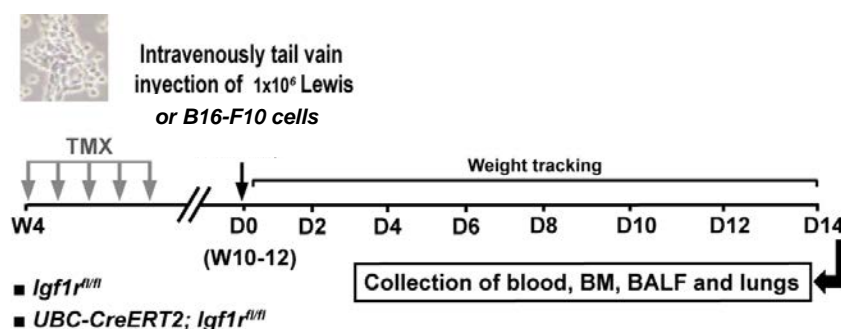
Figure 26. Protocol of experimental pulmonary metastasis. *UBC-CreERT2; Igf1r*$^{fl/fl}$ and *Igf1r*$^{fl/fl}$ female mice were treated with tamoxifen (TMX) for five consecutive days at four weeks (W) of age to induce Igf1r gene deletion (CreERT2). Then, mice were injected through the lateral tail vein with 1×10^6 Lewis Lung Carcinoma (LLC) or B16-F10 cells in PBS or an equal volume of PBS. Collection of blood, bone marrow (BM), BALF and lungs were performed on day (D) 14.

3.7 Cell lines and culture conditions

LLC/1 (Lewis Lung Carcinoma) and B16-F10 (Melanoma) cell lines were cultured following the American Type Culture Collection (http://www.atcc.org) recommendations and standard methods. These cell lines were maintained in DMEM + L-Glutamine (Gibco; Thermo Fisher Scientific, Inc., Waltham, MA) or RPMI 1640 (Lonza; Basel, Switzerland) media, respectively, supplemented with 10% fetal bovine serum (Gibco; Thermo Fisher Scientific) and penicillin (100 U mL−1) and streptomycin (100 μg mL−1). The cultures were maintained under a humidified atmosphere of 95% air / 5% CO2 at 37 °C and subcultured before they became confluent using a 0.25% trypsin/EDTA solution.

3.8 In vivo measurement of lung function

In vivo measurement of lung function was performed 24h after the last HDM exposure (D28). Mice were anesthetized by intraperitoneal injection (2.5 μL/g) with the anaesthetic combination of fentanyl citrate (Fentanest 0.05 mg/mL, KERN PHARMA), medetomidine hydrochloride (Domtor 1 mg/mL, ECUPHAR) and midazolam hydrochloride (Midazolam Accord 5 mg/mL, ACCORD) and intubated with a 24-gauge catheter (BD, Franklin lakes, NJ). Mice received a single intravenous tail injection of 1 mg/kg of methacholine (MCh) (Sigma-Aldrich, St. Louis, MO) [Zoltowska *et al.*, 2018] and lung function was assessed within 5 minutes using a plethysmograph (SCIREQ, Montreal, Canada) to determine LR (Lung resistance) and Cdyn (dynamic compliance), having previously measured basal lung function. Additionally, 0.5 mg/kg of MCh were administrated to HDM-challenged mice treated with NVP-ADW742 for 2 weeks (HDM + NVP 2 wks). A MiniVent (Harvard Apparatus, Holliston, MA) was connected to the plethysmograph and the tracheal cannula for animal ventilation at 10 mL/kg of tidal volume and 150 breaths per minute. Data were measured by 2 pressure transducers that detect pressure variations in the chamber (flow) and in the tracheal cannula (pressure) [Ucero *et al.*, 2019].

3.9 Tissue collection and preparation

Mice were euthanized by intraperitoneal injection of 10 μL/g of a ketamine-xylazine anesthetic combination in saline (300:30 mg/kg, respectively). Blood was collected by cardiac puncture, and then 50 μL were mixed with 1 mL of ACK Lysing Buffer (Thermo Fisher Scientific, Waltham, MA) and centrifuged at 300 xg for 5 min at 4°C after 15 min of incubation. Following aspiration of the supernatants, pellets were washed with 500 μL PBS and centrifuged at 300 xg for 5 min at 4°C, repeating this step once more. The supernatants were discarded and 200 μL of PBS were added to the pellets to prepare the cytospin preparations by centrifugation of the slides at 1500 rpm for 5 min (Cytospin 4, Thermo Fisher Scientific,

Waltham, MA). Serum was obtained by centrifugation at 3000 xg for 10 min at 4°C and stored at -80°C until further use. The animals were bled cutting the cava vein.

Lungs were lavaged twice with 0.8 mL of cold PBS to obtain the bronchoalveolar lavage fluid (BALF) which was centrifuged at 15700 xg for 5 min at 4°C. The BALF supernatants were stored at -80°C to subsequently assess total protein concentration in BALF using the Pierce BCA Protein Assay Kit (Thermo Fisher Scientific). In addition, the BALF pellets were suspended in 500 μL ACK Lysing Buffer (Thermo Fisher Scientific) and centrifuged at 3300 xg for 5 min at 4°C after 10 min of incubation. The supernatants were discarded and 500 μL PBS were added to the pellet to prepare the cytospin preparations as mentioned above. Following lung dissection, right lung lobes were separated, snap-frozen in liquid nitrogen and stored at -80°C for quantitative PCR (qPCR) and ELISA analyses, and the left lung lobe was fixed by inflation with 4% formaldehyde for 8-10h, and subsequently embedded in paraffin and cut into 3 μm sections for histopathology and immunohistochemistry. Notably, a piece of liver was stored at -80º C for regenotiping.

Bone marrow (BM) isolation was carried out following dissection of the femur. After centrifugation at 10000 xg for 15 seconds, BM was suspended in 500 μL PBS and centrifuged at 300 xg for 5 min at 4°C. Following aspiration of the supernatants, BM pellets were resuspended in 500 μL ACK Lysing Buffer (Thermo Fisher Scientific) and centrifuged at 300 xg for 5 min at 4°C after 10 min of incubation. The supernatants were discarded and 1 mL PBS was added to the pellets to prepare the cytospin preparations as mentioned above.

Total cell number was counted and expressed as cells/mL in BALF and BM, and as a percentage in peripheral blood. Differential cell counts were performed on May-Grünwald/Giemsa (Sigma-Aldrich, St. Louis, MO) stained cytospins, counting a minimum of 300 cells per slide in BALF, BM and blood cytospins.

3.10 Histopathological analyses

Paraffin-embedded tissue sections were dewaxed at 70 °C for 30 min, incubated in xylene for 14 min, transferred sequentially into 100% EtOH, 96% EtOH, 70% EtOH and deionized water for 4 minutes.

Hematoxylin/Eosin (H&E): Sections were stained with Harris hematoxylin (Panreac, Barcelona, Spain) for 7 min. After washing with abundant tap water, differentiation was performed by submerging the sections in 1% acid alcohol (1% HCl in 70% EtOH) for 3 sec. Sections were washed again with tap water for 2 min and stained with an alcoholic solution of eosin (Panreac) for 2 min. Finally, after a last wash, sections were dehydrated sequentially in 96% EtOH and 100% EtOH for 1 min, incubated in xylene for 5 min, mounted with Eukitt mounting medium (O. Kindler GmbH & Co, Freiburg, Germany) and photo-documented under a light microscope (Nikon Instruments, Inc, Tokyo, Japan). H&E staining was performed for the quantification of inflamed lung areas and airway thickness, as well as to quantify the number of surface metastases and to evaluate lung tumor areas. Quantification of inflammation and surface metastases were expressed as the percentage of inflamed/metastatic lung area to total section surface, defining "inflamed lung areas" or "lung tumor areas" as darker stained foci. Airway thickness was assessed by means of three different measurements per airway, evaluating 5 different fields per animal.

Fiji open-source image processing software package v1.48r (https://fiji.sc) was used to delimitate inflamed lung areas, but also to quantify airway thickness and epithelium length.

Periodic acid-Schiff (PAS) staining protocol: Lung sections were incubated in alcian blue (pH 2.5) for 20 min, washed with distilled water, incubated in 0.5% periodic acid for 5 min and washed again with distilled water. Then, sections were stained with Schiff reactive for 20 min, washed with distilled water and stained with Harris hematoxylin (Panreac). After a last wash with tap water, sections were dehydrated sequentially in 96% EtOH and 100% EtOH for 1 min, incubated in xylene for 5 min, mounted with Eukitt mounting medium (O. Kindler GmbH & Co) and photo-documented under a light microscope (Nikon Instruments, Inc). PAS protocol served to assess the airway epithelial goblet cell abundance in the murine models of experimental asthma. Quantification of PAS-positive cells was expressed as the number of positive cells per epithelium length (mm), evaluating a minimum of 5 airways per animal.

Masson's trichrome staining protocol: A masson trichrome kit with aniline blue (Bio-Optica, Milan, Italy) was used following the manufacturer's instructions. Finally, after a last wash with tap water, sections were dehydrated, mounted and photo-documented in the same way as in the PAS protocol. Masson's trichrome protocol served to assess the collagen deposition, in the murine models of experimental asthma and lung metastasis. Fiji software was used to quantify the percentage of collagen area as well as for epithelium length measurements, evaluating a minimum of 5 airways per animal.

May-Grünwald/ Giemsa (MGG): BALF, blood and BM cytospin preparations were stained with a solution composed by methanol (EMD Millipore, Billerica, MA) and May-Grünwald (Sigma-Aldrich) (1:5 dilution of methanol in May-Grünwald solution) for 10 min. Then, slides were washed three times with distilled water for 1 min and stained with a solution composed by Giemsa (Sigma-Aldrich) and distilled water (1:10 dilution of Giemsa in distilled water). Finally, after three washes in distilled water for 1 min, slides were allowed to air-dry and mounted with Eukitt mounting medium (O. Kindler GmbH & Co). Differential cell counts were performed counting a minimum of 300 cells per slide or 5 fields per slide in a blinded fashion in BALF, blood and BM cytospins in the murine models of experimental asthma and lung metastasis. Cells were distinguished into macrophages, lymphocytes, neutrophils, and eosinophils by standard morphology criteria and cytospin preparations were photo-documented under a light microscope (Nikon Instruments, Inc).

3.11 Immunostaining analyses

3.11.1 3,3'-Diaminobenzidine (DAB) method

Paraffin-embedded sections were dewaxed at 60 °C for 30 min, incubated in xylene for 14 min, transferred sequentially into 100% EtOH, 96% EtOH, 70% EtOH and deionized water for 4 minutes. Antigen retrieval was performed immersing the slides in a boiling solution of 1 mM EDTA (pH 9.0) or 10 mM Citrate (pH 6.0) for 17 min, and followed by a 30 min cool down in the same buffer. Then, sections were washed in 1X PBS for 5 minutes, three times in PBS-Triton (PBS-T) (0.1%) for 5 min and in MiliQ water for 5 min. Endogenous peroxide was blocked by 0.2% H_2O_2 for 15 min, and sections were washed two times with 1X Tris-buffered saline (TBS) for 5 min and blocked with Protein Block kit (Leica Microsystems) for 1 h at room temperature, and then washed two times with 1X TBS. Hereafter, slides

were incubated at 4°C overnight with primary antibodies diluted in the appropriate blocking solution. The following day the slides were washed two times with 1X TBS for 5 min. Sections were then treated with Novolink Polymer kit (Leica Microsystems) for 1 h at room temperature, washed two times with 1X TBS for 5 min and visualized with DAB cromogen (Leica Microsystems). Finally, sections were stained with Harris haematoxylin (Panreac) for 5 sec, washed with distilled water, differentiated in 1% acid alcohol (1% HCl in 70% EtOH) for 3 sec, washed with distilled water, and dehydrated sequentially in 90% EtOH and 100% EtOH for 2 min, incubated in xylene for 5 min and mounted with Eukitt mounting medium (O. Kindler GmbH & Co). Sections were photo-documented under a light microscope (Nikon Instrumetns, Inc), evaluating at least 5 fields per animal in the murine models of experimental asthma and lung metastasis.

Immunostainings were performed using the following antibodies: IGF1R (1:400, Boster Biological Technology Ltd., USA), C3 (Clone 5A1E 1:200, Abcam, Cambridge, UK), CD45 (Clone D3F8Q 1:900, Cell Signaling Technology, Danvers, MA), CD31 (1:50, Abcam), p-IGF1R (Clone Y1161 1:70, Abcam), p-ERK1/2 (p-42/44) (Clone E10 1:110, Cell Signalling Technology), p21 (Clone M19 1:110, Santa Cruz Biotech. Inc., Dallas, TX), CD34 (Clone RAM34 1:200, Thermo Fisher Scientific, Waltham, MA), Fibronectin (1:100, Dako, Jena, Germany), SOX9 (Clone E9 1:110, Santa Cruz Biotech. Inc.), CD68 (Clone KP1 1:150, Santa Cruz Biotech. Inc.), FOXP3 (Clone 2A11G9 1:150, Santa Cruz Biotech. Inc.), CD4 (Clone D7D2Z 1:80, Cell Signaling Technology) and SOX2 (Clone C70B1 1:100, Cell Signaling Technology). These antibodies were used to evaluate tumor IGF1R, p-IGF1R, p-ERK1/2, CD31 (vacularization), CD34 (differentiated vacularization), Fibronectin (fibroblast diferentiation), and CD68 (tumor associated macrophages) positive areas, as well as to determine the number of p21 (senescence), C3 (apoptosis), SOX9 (epithelial mesenchymal transition), FOXP3 (tumor infiltrating lymphocytes), CD4 (T-cell marker) and SOX2 (differentiation) positive cells per unit area. Fiji software was used to quantify IGF1R, p-IGF1R, p-ERK1/2, CD31, CD34, Fibronectin and CD68 positive areas (percentage of DAB).

3.11.2 Fluorescent immunostaining method

Paraffin-embedded sections were dewaxed at 60 °C for 30 min, incubated in xylene for 14 min, transferred sequentially into 100% EtOH, 96% EtOH, 70% EtOH and deionized water for 4 minutes. Antigen retrieval was performed immersing the slides in a boiling solution of 1 mM EDTA (pH 9.0) or 10 mM Citrate (pH 6.0) for 17 min, and followed by a 30 min cool down in the same buffer. Then, sections were washed in 1X PBS for 5 minutes and three times in PBS-Triton (0.1%)-Glycine (10 mM) for 10 min. Sections were blocked with 10% normal goat serum (Jackson ImmunoResearch Laboratories, Inc., Baltimore, PA) or with 10% normal donkey serum (Jackson ImmunoResearch Laboratories, Inc., Baltimore, PA) in PBS-Triton (0.1%) and Glycine (10 mM) for 1 h at RT. Slides were then incubated at 4 °C overnight with primary antibodies diluted in the appropriate blocking solution. The following day, slides were washed three times with PBS-Triton (0.1%)-Glycine (10 mM) for 5 min, incubated with the appropriate Alexa Fluor® secondary antibodies diluted in 1X PBS for 1 h at RT, washed three times with 1X PBS for 5 min and mounted with ProLong Gold Antifade Reagent with DAPI (Life technologies). Sections were examined under a confocal microscope (Leica Microsystems, Wetzlar, Germany), evaluating at least 5 fields per animal from the murine models of experimental asthma and lung metastasis.

Immunostaining was performed using the following antibodies: 53BP1 (1:500, Novus Biologicals, Centennial, CO), Ki67 (Clone SP6 1:250, Master Diagnostica, Spain), Vimentin (Clone LN-6 1:400, Cell Signaling Technology), Smooth Muscle Actin (SMA) (Clone 1A4 1:400, Sigma-Aldrich, St. Louis, MO), Iba1 (1:800, Wako, Osaka, Japan), Prosurfactant Protein C (SFTPC) (1:200, EMD Millipore, Burlington, MA), CC10 (Clone T18 1:400, Santa Cruz Biotech. Inc., Dallas, TX), and MUC5AC (Clone 45M1 1:50, Thermo Fisher Scientific). These antibodies were used to evaluate tumor Ki67 (proliferation), Vimentin (fibroblast presence) and SMA (fibroblast activation) positive areas, as well as to determine the number of 53BP1 (DNA damage), Iba1 (macrophages), SFTPC (Prosurfactant Protein C), CC10 (SCGB1A1 Club cells) and MUC5AC (goblet cell hyperplasia) positive cells per unit area. Fiji software was used to quantify Ki67, Vimentin and SMA positive areas (percentage of fluorescence), as well as airway and smooth muscle thickness and epithelium length measurements.

3.12 RNA isolation, reverse transcription and qPCR

Mechanical disruption of tissues was performed using a tissue homogenizer T8 Ultra Turrax (IKA Works Inc, Staufen, Germany). Inferior right lung lobes were homogenized at RT in 1 mL of Trizol® (Invitrogen, Carlsbad, CA) using a tissue homogenizer. Then, lung homogenates were incubated at RT for 5 min to allow dissociation of the nucleoprotein complexes, centrifuged at 12000 xg for 10 min at 4 °C and supernatans were transferred to new tubes. Hereafter, 200 µL of chloroform were added to supernatans, tubes were shaken for 15 sec, incubated at RT for 3 min and centrifuged at 12000 xg for 15 min at 4 °C. After centrifugation, the aqueous phases were transferred to new tubes. Then, 500 µL of isopropanol were added to the aqueous phases and shaken for 15 sec. Briefly, the isopropanol supernatants were transferred to the RNeasy columns (Qiagen), following the manufacturer's specifications and treated with 2.72 KU/µl RNase-free DNase (Qiagen). The quantity and quality of total RNA were assessed on a NanoDrop Spectrophotometer (Thermo Fisher Scientific), respectively. Total RNA obtained from individual mice was reverse-transcribed to cDNA using the SuperScript II First-Strand Synthesis System (Invitrogen) following the manufacturer's guidelines. cDNA samples were amplified by qPCR in triplicate reactions for each primer pair assayed (**Table 3**) on a 7300 Real-Time PCR Instrument (Applied Biosystems, Foster City, CA), using SYBR Premix Ex Taq (Takara Bio Inc., Kusatsu, Japan). Results from the murine models of experimental asthma and lung metastasis, were normalized using the 18S rRNA gene (Rn18s) as endogenous control. The qPCR conditions were as follows: 95 °C for 2 min; 40 cycles of 95 °C for 30 s, 60 °C for 30 s and 95 °C for 15 s, 60 °C for 1 min, 95 °C for 15 s, 60 °C for 15 s (Premix Ex Taq).

Table 3. Primer sets used for qPCR.

Gene	Accession No.	Forward primer (5´-3´)	Reverse primer (5´-3´)
Ccl2	NM_011333.3	CACCAGCCAACTCTCACTGA	CGTTAACTGCATCTGGCTGA
Ccl11	NM_011330.3	GAGAGCCTACAGAGCCCAGA	ACCGTGAGCAGCAGGAATAG
Ccl12	NM_011331.3	TCCTCAGGTATTGGCTGGAC	GGCTGCTTGTGATTCTCCTG
Cd4	NM_013488.2	ATGTGGAAGGCAGAGAAGGA	TGGGGTATCTTGAGGGTGAG
Cd8a	NM_001081110.2	GGAGTGGAGAAGCTAAGCCA	TGGAGCTGGAGTTCTGGAAG
Cd68	NM_001291058.1	TGTTCACCTTGACCTGCTCT	TTGCAAGAGAAACATGGCCC
Cd80	NM_001359898.1	TATTGCTGCCTTGCCGTTAC	ACTCGGGCCACACTTTTAGT
Cd86	NM_019388.3	GAAAGAGGAGCAAGCAGACG	TCTCCACGGAAACAGCATCT
Cd163	NM_001170395.1	TCTCCAGTCCAAACAACAAGC	ACCACCTCCACCTACCAAGC
Cd274	NM_021893.3	CATACCGCAAAATCAACCAG	CACTTCTCTTCCCACTCACG
Cxcl1	NM_008176.3	ATCCAGAGCTTGAAGGTGTTG	GTCTGTCTTCTTTCTCCGTTACTT
E-cadherin	NM_009864.3	CCAGCAGTTCGTTGTTGTCA	TGTGGAAGGGACAAGAGACC
Egfr	NM_207655.2	ACAACCCCACCACCTATCAG	GCCATCTTCTTCCACTTCGT
Foxm1	NM_008021.4	CCTGCTTACTGCCCTTTCCT	CACACCCATCTCCCTACACC
Foxp3	NM_001199347.1	CACCCAGGAAAGACAGCAAC	CTGCACCACTTCTCTCTGGA
Hif1α	NM_010431.2	TTGGAACTGGTGGAAAAACTG	ACTTGGAGGGCTTGGAGAAT
Hmox1	NM_010442.2	CACGCATATACCCGCTACCT	CCAGAGTGTTCATTCGAGCA
Ifnγ	NM_008337.4	TTCTTCAGCAACAGCAAGGC	ACTCCTTTTCCGCTTCCTGA
Igf1	NM_010512	CAGAAGCGATGGGGAAAAT	GTGAAGGTGAGCAAGCAGAG
Igf1r	NM_010513	ATGGCTTCGTTATCCACGAC	AATGGCGGATCTTCACGTAG
Igfbp2	NM_008342	GGGAGTGCTGGTGTGTGA	CTGCTGGTGTTCGGGATG
Igfbp3	NM_008343.2	GCCCTCTGCCTTCTTGATTT	TCACTCGGTTATGGGTTTCC
Igfbp4	NM_010517.3	TGTGAGATTGGATTGTGTGTGT	TAGAGATGGCGGGATAGGAG
Igfbp5	NM_010518.2	GATGAGACAGGAATCCGAACAAG	AATCCT TTGCGGTCACAGTTG
Igfbp6	NM_008344	AGGAGAGCAAACCCCAAGGA	TGAACAGGATTGGGCCGTATA
Il1β	NM_008361.3	GCAACTGTTCCTGAACTCAACT	ATCTTTTGGGGTCCGTCAACT
Il4	NM_021283.2	CCTCACAGCAACGAAGAACA	CGAAAAGCCCGAAAGAGTC
Il10	NM_010548.2	GCCTTATCGGAAATGATCCA	TTTTCACAGGGGAGAAATCG
Il13	NM_008355.3	GCCTCCCCGATACCAAAAT	CTTCCTCCTCAACCCTCCTC
Il33	NM_133775.2	GCCTTGCTCTTTCCTTTTCTC	TCGGTTGTTTTCTTGTTTTGC
Insr	NM_010568.2	TCCTGAAGGAGCTGGAGGAGT	CTTTCGGGATGGCCTGG
Mmp2	NM_008610.3	GATGTCGCCCCTAAAACAGA	GGTCTCGATGGTGTTCTGGT
Mmp9	NM_013599.4	CCTGAAAACCTCCAACCTCA	GCTTCTCTCCCATCATCTGG
Mpo	NM_010824.2	TGGTTGCCTGCAGAGTATGA	TCCTTGGTCAGCTGATCGTT
Muc5ac	NM_010844.1	CACACACAACCACTCAACCA	TCTCTCTCCGCTCCTCTCAA
Pdcd1	NM_008798.2	TCAAGGCATGGTCATTGGTA	GCTCCTCCTTCAGAGTGTCG
Rn18s	NR_003278.3	ATGCTCTTAGCTGAGTGTCCCG	ATTCCTAGCTGCGGTATCCAGG
Sftpa1	NM_023134.4	CCATCGCAAGCATTACAAAG	CACAGAAGCCCCATCCAG
Sftpb	NM_147779.2	CTGCTGCTTCCTACCCTCTG	ATCCTCACACTCTTGGCACA
Sftpc	NM_011359	GAAGATGGCTCCAGAGAGCATC	GGACTCGGAACCAGTATCATGC
Sftpd	NM_009160.2	TGAGAATGCTGCCATACAGC	GAATAGACCAGGGGCTCTCC
Sox2	U_31967.1	AACCAAGACGCTCATGAAGAAG	CTGCGAGTAGGACATGCTGTAG
Spdef	NM_013891.4	GGCCAGCCATGAACTATGAT	GGTAGACAAGGCGCTGAGAG
Timp1	NM_011593	ATCTGGCATCCTCTTGTTGC	CTCGTTGATTTCTGGGGAAC
Timp2	NM_011594.3	GCATCACCCAGAAGAAGAGC	GTCCATCCAGAGGCACTCAT
Timp3	NM_011595.2	TAGAAGAGCAGGGCAGGAAG	GTCAGCACAGGGGAAAGATG
Tgfβ	NM_011577.2	CGCAACAACGCCATCTATGA	ACTGCTTCCCGAATGTCTGA
Tnfα	NM_013693.3	GCCTCTTCTCATTCCTGCTTG	CTGATGAGAGGGAGGCCATT

3.13 Mouse ELISAS

Lung tissues were homogenized in a solution composed by a cocktail of protease and phosphatase inhibitors (Roche, Basel, Switzerland) and the tissue protein extraction buffer RIPA (20 mL/g tissue) (Thermo Fisher Scientific), using a tissue homogenizer T8 Ultra Turrax (IKA Works Inc). Lung homogenates were incubated in ice for 30 min and then centrifuged at 14000 xg for 20 min at 4 ºC. Supernatants were then collected and stored at -80°. Total protein concentration was determined using the Pierce BCA Protein Assay Kit (Thermo Fisher Scientific) following manufacturer´s instructions in a POLARstar Omega (Biogen).

IL13, IL33, CCL11, MMP9, IL10, TNFα, PD-1 and p-IGF1R levels were determined in lung lysates from the murine models of experimental asthma and lung metastasis. p-IGF1R levels were quantified with the PathScanphospho-IGF-I receptor β (Tyr1131) sandwich ELISA kit (Cell Signaling Technology), and IL13, IL33, CCL11, MMP9, IL10, TNFα and PD-1 levels were assessed, using mouse IL13 Duoset, and IL33, CCL11, MMP9, IL10, TNFα and PD-1 Quantikine ELISA Kits (R&D systems, Minneapolis, MN) in volumes of lysates normalized to total lung protein levels.

Total serum IgE, IL13, p-IGF1R, IL6 and TNFα levels were assessed with the IgE (Abcam, Cambridge, UK), IL13 Duoset (R&D systems), PathScanphospho-IGF-I receptor β (Tyr1131) sandwich (Cell Signaling Technology), IL6 and TNFα Quantikine (R&D systems) ELISA kits in the murine models of experimental asthma and lung metastasis. ELISAS were performed according to manufacturer´s guidelines and determination of optical density of each well was performed at 450 nm in a POLARstar Omega (Biogen).

3.14 Clinical samples

3.14.1 Moderate-Severe allergic asthma patients

We used the serum samples available from a higher cohort of patients with moderate-severe allergic asthma and matched controls, previously described [Nieto-Fontarigo *et al.*, 2020]. Serum IGF1R and total IgE levels were measured using human IGF1R (Elabscience, Houston, TX) and IgE (Abcam) ELISA kits. A written informed consent was received from participants prior to inclusion in the study. The research protocol was approved by the Ethics Committee of Clinical Research of Galicia (Spain) (ref. 2011/001).

3.14.2 NSCLC patients

Genomic data on amplification frequency, mRNA expression and copy number values of *IGF1R* in tissue samples from NSCLC patients were obtained from the The cBio Cancer Genomics Portal (cBioPortal) (http:// www.cbioportal.org), an online platform which provides visualization, analysis and download of large-scale cancer genomics data sets [Gao *et al.*, 2013].

Formalin-fixed paraffin-embedded lung cancer tissues from 14 NSCLC patients were obtained from the Hospital San Pedro (Logroño, Spain). Serum samples from 24 NSCLC patients and matched

controls were obtained from the Hospital Fundación Jimenez Díaz (Madrid, Spain). All patients gave written informed consent. Study protocols were approved by the Ethics Committee of Clinical Research of La Rioja (CEICLAR, ref. PI-205), and by the Fundación Jiménez Díaz (CEImJGD, ref. ER_EO180-19_FJD-HGV). Serum IGF1R levels were measured using human IGF1R (Elabscience, Houston, TX) ELISA kit.

3.15 Statistical analysis

Following a Shapiro-Wilk normality test, the statistical significance was determined using the Mann-Whitney U test or Student's t-test for comparing 2 groups and the Kruskal-Wallis test or ANOVA multiple comparison test for grouped or multivariate analysis in the murine model of experimental asthma. In the case of murine models of lung metastasis, the statistical significance was determined using the Mann-Whitney U test or Student's t-test for comparing two groups and the Dunn-Sidak test for multiple comparisons. In addition, Pearson's correlation coefficient was used to study the correlation of IGF1R levels with IgE and circulating eosinophils in patients with allergic asthma, as well as in NSCLC patients to assess the correlation of IGF1R mRNA expression with copy number values, and Iba1 and Ki67 expression with p-IGF1R. Statistical analyses were carried out using SPSS Statistics Software v21 for Windows (IBM, Armonk, NY). For all analysis, a p value < 0.05 was considered statistically significant. Data are expressed as mean ± SEM. * $p < 0.05$; ** $p < 0.01$; *** $p < 0.001$.

4 RESULTS

4.1 IGF1R as a potential pharmacological target in allergic asthma (Paper I)

4.1.1 Efficient depletion of IGF1R and IGF system gene expression upon HDM exposure and pharmacological blockade of IGF1R

C57BL/6J mice were challenged with HDM extract and therapeutically treated with NVP as illustrated in **Figure 22**. NVP administration did not induce significant changes in body weight (**Figure 27A**). Noteworthy, treatment with the vehicle of NVP (DMSO) did not induce inflammation in lungs of inbred C57BL/6J mice (**Figure 27B**).
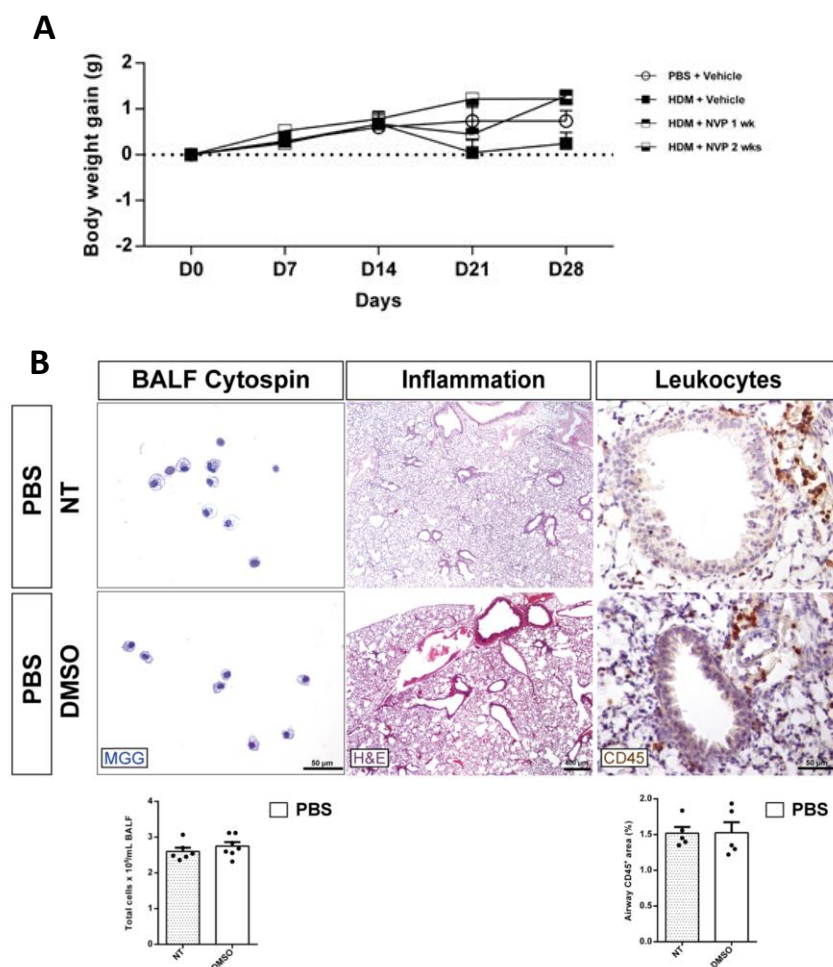
Figure 27. (**A**) Follow-up of the body weight gain upon treatment with the IGF1R inhibitor NVP-ADW742. Weekly follow-up of the body weight gain in HDM-challenged mice treated with the TKI NVP-ADW742 vs. controls (n = 5 mice per group). (**B**) Representative BALF cytospin preparations (May-Grünwald Giemsa (MGG) (left), and images of proximal airways showing H&E (center) and CD45 (brown) stainings (right) and quantification of total BALF cell counts, and CD45+ (leukocytes) area (%) in lung sections from C57BL/6J mice treated with 2% DMSO vs. untreated controls (n = 5-7 mice per group). Data are expressed as mean ± SEM. (Mann-Whitney U test or Student's t-test for comparing 2 groups and Kruskal-Wallis test or ANOVA multiple comparison test for grouped or multivariate analysis).

IGF1R inhibition and assessment of IGF system gene expression were performed on lung extracts of HDM-challenged mice treated with NVP vs. controls (HDM + vehicle and PBS + vehicle) (**Figure 28A-C**). Phospho(p)-IGF1R levels quantified by ELISA were greatly increased in HDM control mice both in serum and lung homogenates. This increment was significantly reduced in NVP-treated mice particularly NVP after 2 weeks of treatment (NVP 2 wks) (**Figure 28A**). mRNA levels of insulin receptor (*Insr*) were significantly decreased in all HDM-challenged groups. In addition, HDM treatment increased *Igf1* mRNA levels that were reverted by NVP treatment (**Figure 28B**). Regarding mRNA expression of IGFBP markers, *Igfbp2* and *Igfbp4* were found to be significantly reduced in NVP-treated mice and *Igfbp3*, *Igfbp5* and *Igfbp6* levels showed a significant depletion upon HDM exposure. Specifically, *Igfbp3* levels were found slightly increased in the NVP 2 wks group (**Figure 28C**). In addition, lung tissue p-ERK1/2 (p42/44) expression evaluated by immunohistochemistry was highly augmented in HDM controls while this increment was significantly reduced in NVP-treated mice particularly after 2 weeks of treatment. Interestingly, expression pattern of p-ERK1/2 was specifically noticed in peribronchiolar smooth muscle cells and inflammatory areas (**Figure 28D**).
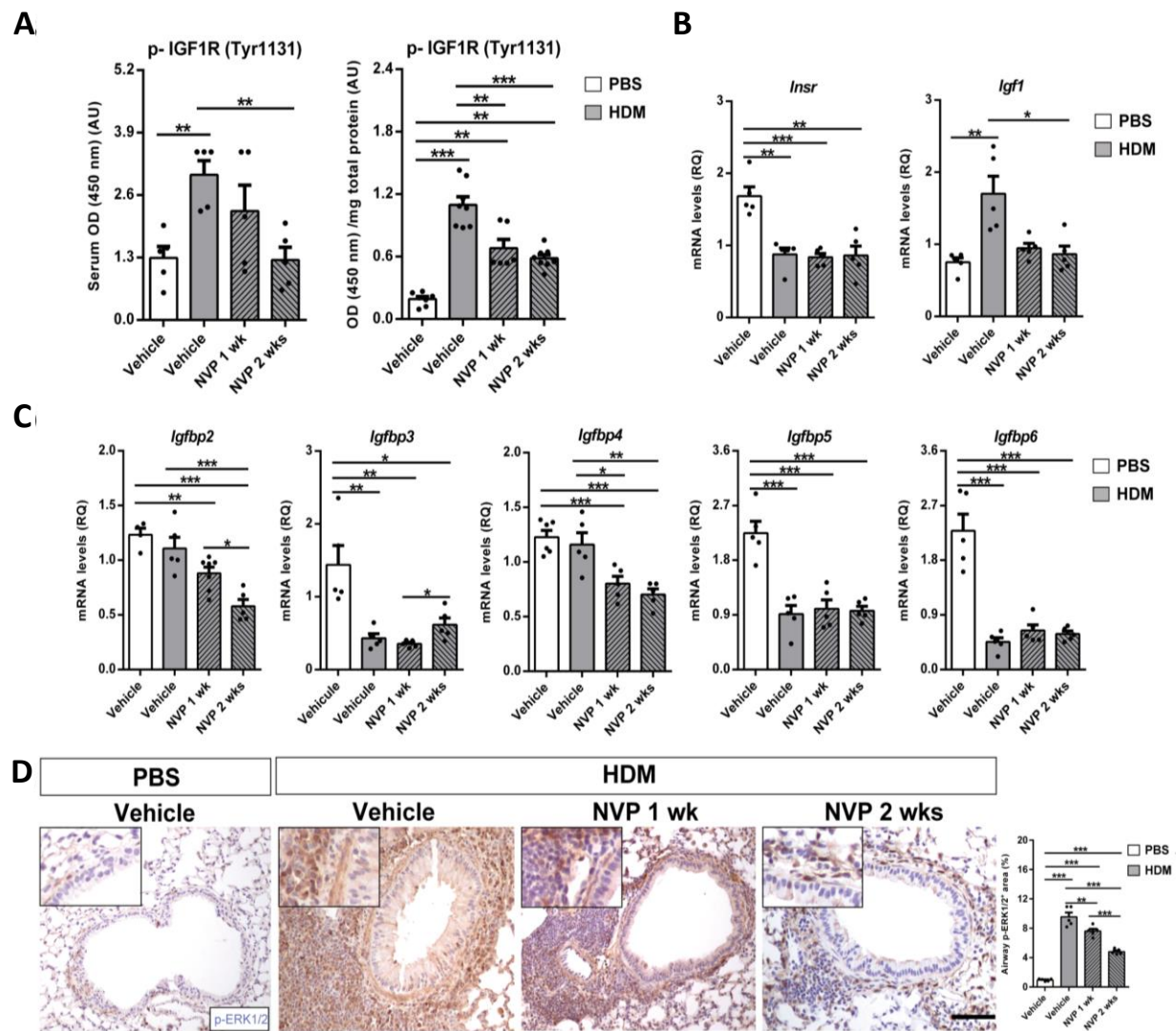
Figure 28. p-IGF1R and IGF system gene expression levels in the lung. (**A**) p-IGF1R protein levels in both serum and lung homogenates from HDM-challenged mice treated with NVP vs. controls (n = 6–8 mice per group). (**B** and **C**) Lung tissue mRNA expression of IGF system-related genes *Insr*, *Igf1* (**B**), and *Igfbp2, Igfbp3, Igfbp4, Igfbp5, Igfbp6* (**C**) normalized to 18S expression in HDM-challenged mice treated with NVP vs. controls (n = 5 mice per group). (**D**) Representative immunostains of proximal airways for p-ERK1/2 (p-42/44) (brown), and quantification of p-ERK1/2+ area (%) in lung sections from HDM-challenged mice treated with NVP vs. controls (n = 5 mice per group; scale bar: 50 μm). Insets illustrate *p-ERK1/2* expression in smooth muscle cells and peribronchiolar areas. Data are expressed as mean ± SEM. * $p < 0.05$; ** $p < 0.01$; *** $p < 0.001$ (Mann–Whitney U test or Student´s *t*-test for comparing two groups, and Kruskal–Wallis test or ANOVA multiple comparison test for grouped or multivariate analysis).

4.1.2 Therapeutic inhibition of IGF1R during HDM exposure attenuates peripheral blood and bone marrow eosinophilia and the increase in serum IL13

We first assessed peripheral blood cellularity and serum IgE and IL13 levels in HDM-challenged mice treated with NVP vs. controls (**Figure 29A,B**). The proportion of eosinophils exhibited a marked increase in HDM control mice. This increase was significantly reduced in NVP-treated mice, reaching basal levels in the NVP 2 wks group. We did not observe changes in the proportion of neutrophils and lymphocytes between experimental groups. In addition, monocyte presence was reduced in HDM-challenged mice compared to PBS controls (**Figure 29A**). We next measured serum IgE and IL13 levels and found that both were clearly induced in HDM control mice. Whereas IgE was not affected by NVP, IL13 levels were significantly reduced upon NVP treatment, reaching basal levels in the NVP 2 wks group (**Figure 29B**). Bone marrow cellularity was also assessed in all experimental groups. A significant increase in total cell numbers, eosinophil and neutrophil counts was observed in HDM controls. Interestingly, eosinophil numbers returned to basal levels after one week of NVP treatment, and neutrophil counts were only normalized in the NVP 2 wks group (**Figure 29C**).
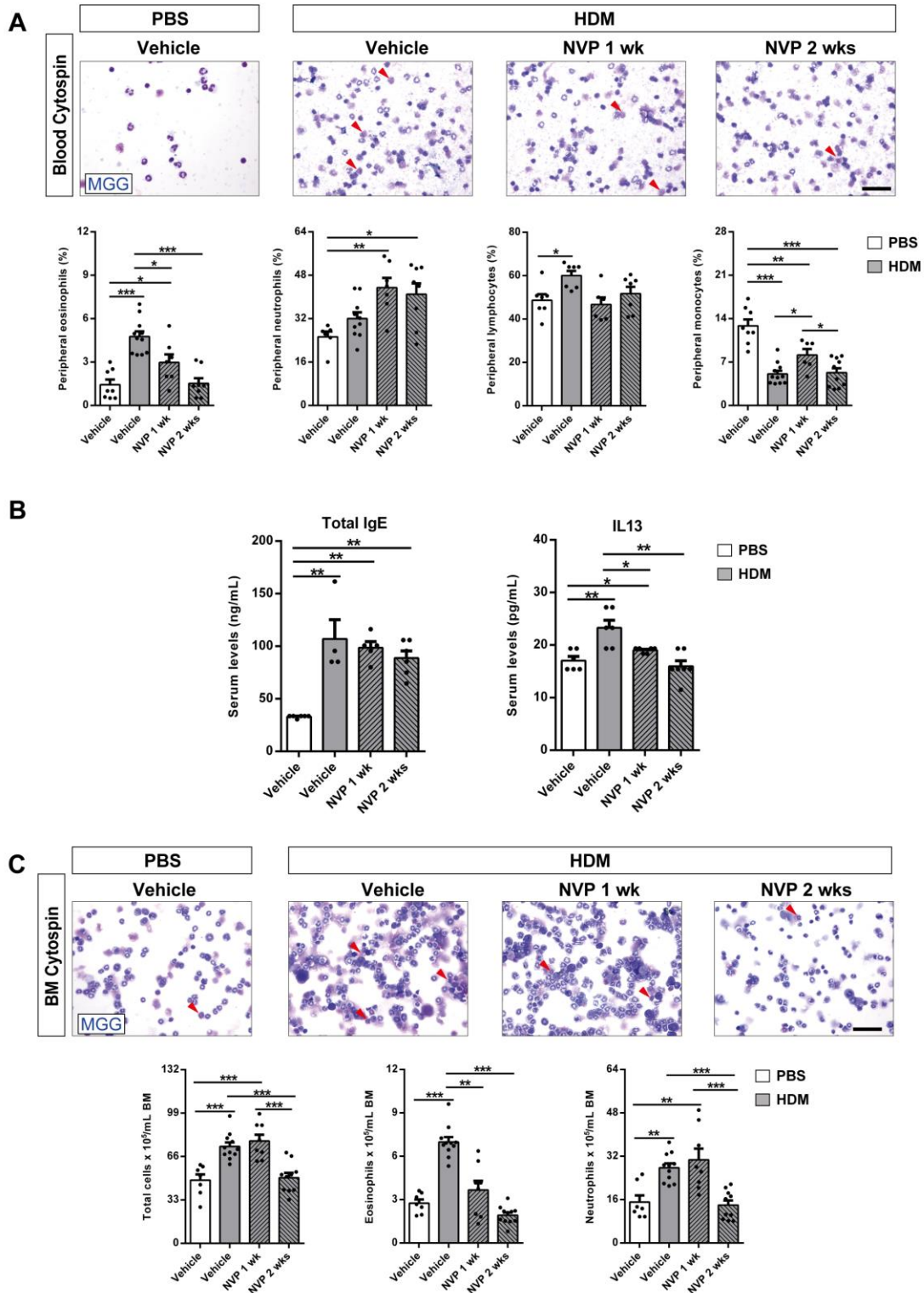
Figure 29. Pharmacological blockade of IGF1R depletes eosinophil presence in peripheral blood and bone marrow and attenuates the increase in serum IL13 levels after HDM exposure. (**A** and **C**) Representative images showing May-Grünwald/Giemsa (MGG) stained peripheral blood and bone marrow cytospin preparations (red arrowheads indicate eosinophils), and differential cell counts for eosinophils, neutrophils, lymphocytes and monocytes in peripheral blood (**A**), and total cells, eosinophils and neutrophils in bone marrow (**C**) from HDM-challenged mice treated with NVP vs. controls (n = 7–10 mice per group; scale bars: 50 µm). (**B**) Total serum IgE and IL13 levels from HDM-challenged mice

treated with NVP vs. controls (n = 5–7 mice per group). Data are expressed as mean ± SEM. * $p < 0.05$; ** $p < 0.01$; *** $p < 0.001$ (Mann–Whitney U test or Student´s t-test for comparing two groups and Kruskal–Wallis test or ANOVA multiple comparison test for grouped or multivariate analysis).

4.1.3 Pharmacological targeting of IGF1R ameliorates pulmonary pathology upon HDM exposure

First, cellularity and total protein levels in bronchoalveolar lavage fluid (BALF) were assessed (**Figure 30A,B**). Total and differential BALF cells counts were found increased in HDM control mice and this increment was strongly reduced in NVP-treated mice (**Figure 30A**). In addition, the increase in total protein content in BALF of HDM control mice remained comparable to unchallenged controls in the NVP 2 wks group (**Figure 30B**).
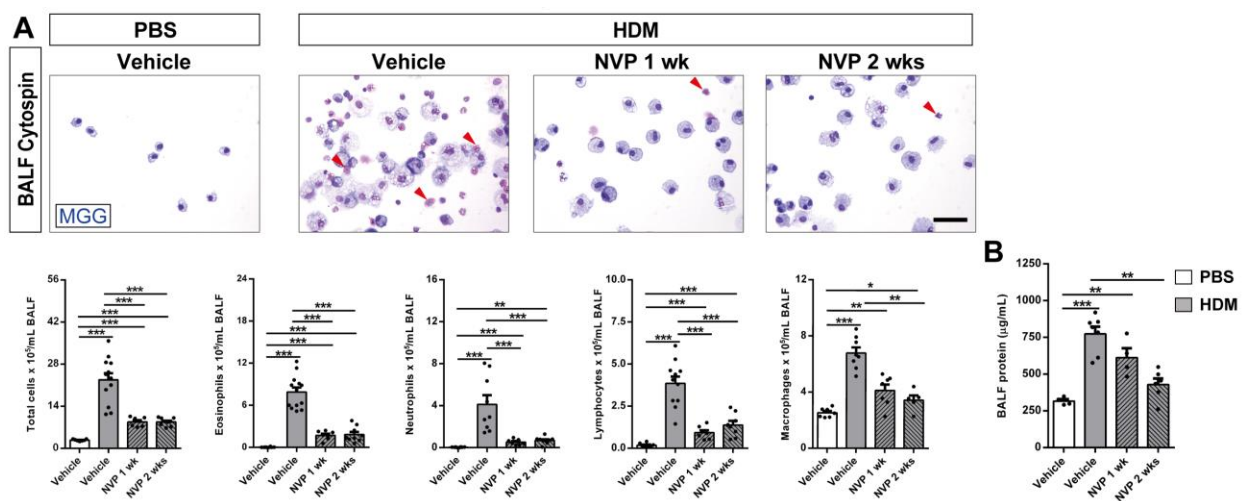
Figure 30. Pharmacological blockade of IGF1R attenuates pulmonary pathology after HDM induced allergy. (**A**) Representative images showing May-Grünwald/Giemsa (MGG) stained BALF cytospin preparations (red arrowheads indicate eosinophils), and total and differential BALF cell counts for eosinophils, neutrophils, lymphocytes and macrophages in HDM-challenged mice treated with NVP vs. controls (n = 7–12 mice per group; scale bar: 50 μm). (**B**) Total protein concentration in BALF of HDM-challenged mice treated with NVP vs. controls (n = 5–8 mice per group). Data are expressed as mean ± SEM. * $p < 0.05$; ** $p < 0.01$; *** $p < 0.001$ (Mann–Whitney U test or Student´s t-test for comparing two groups and Kruskal–Wallis test or ANOVA multiple comparison test for grouped or multivariate analysis).

Next, we evaluated several airway remodeling indicators including inflamed lung area, leukocyte presence, airway thickness, mucus-producing cells, collagen deposition and smooth muscle (SM) thickness (**Figure 31**). Notably, the highly increased values found for all these parameters in HDM-challenged mice were significantly reduced in the NVP 2 wks group. NVP treatment for one week was less effective, counteracting only inflamed lung area and airway thickness (**Figure 31**).
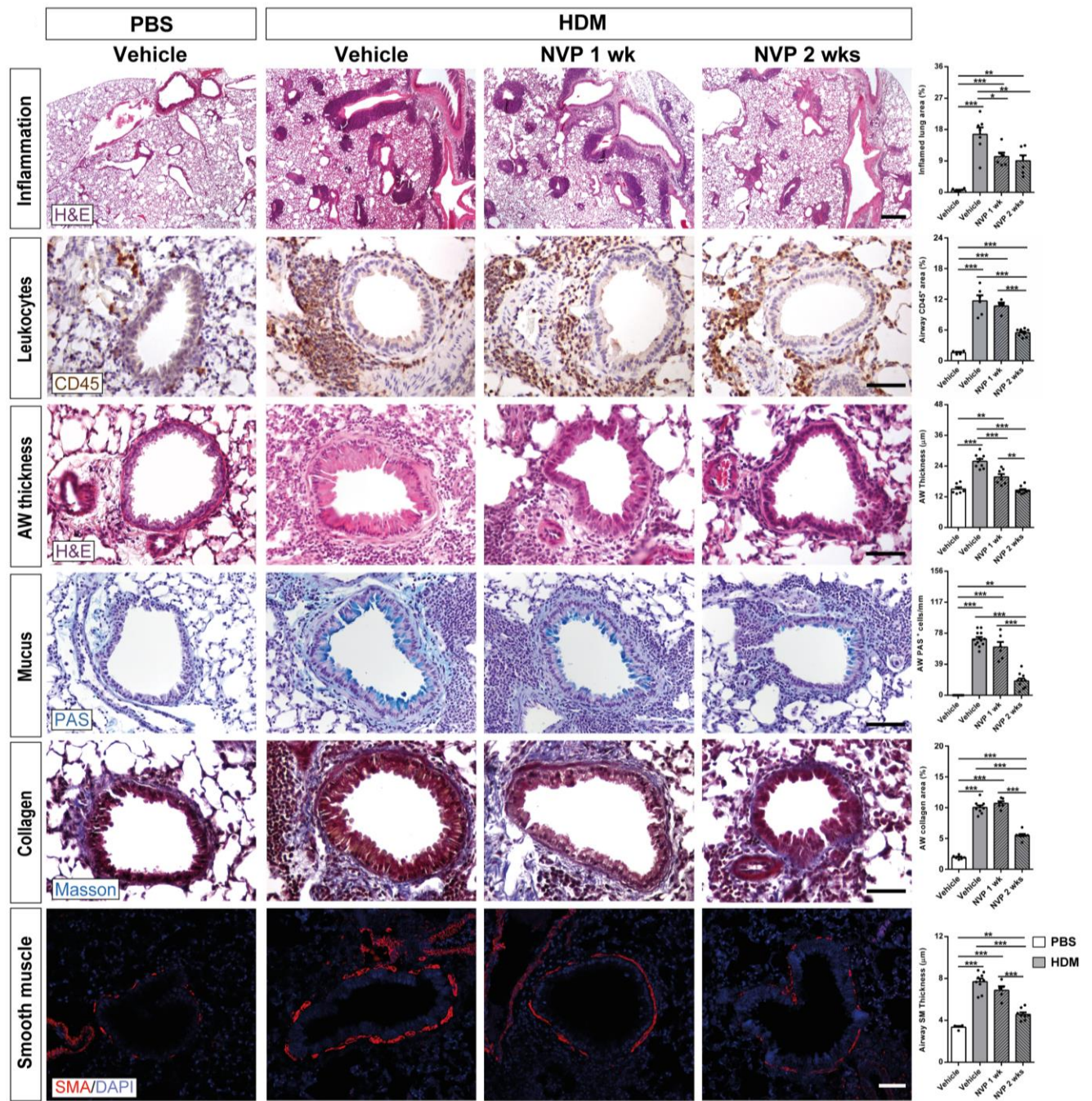
Figure 31. Pharmacological blockade of IGF1R attenuates pulmonary pathology after HDM induced allergy. Representative images of lung inflammation and histopathology of the proximal airways, and respective quantifications of inflamed lung areas (%) (H&E), presence of peribronchiolar CD45+ area (leukocytes) (%) (brown), airway (AW) epithelium thickness (H&E), number of airway PAS+ cells (mucus-producing cells) (blue), peribronchiolar airway collagen content (%) (Masson in blue) and airway smooth muscle (SM) thickness (SMA in red). These parameters were measured in lung sections from HDM-challenged mice treated with NVP vs. controls (n = 6–10 mice per group; scale bars: 50 μm except for the inflammation panel (400 μm)). Quantifications were performed in five different fields in a random way. Data are expressed as mean ± SEM. * $p < 0.05$; ** $p < 0.01$; *** $p < 0.001$ (Mann–Whitney U test or Student´s t-test for comparing two groups and Kruskal–Wallis test or ANOVA multiple comparison test for grouped or multivariate analysis).

44

4.1.4 Pharmacological blockade of IGF1R attenuates AHR and ameliorates surfactant deregulation after HDM challenge

In order to evaluate lung function following HDM-induced allergy, we assessed AHR to methacholine by plethysmography. Methacholine administration induced a marked AHR with increased lung resistance (LR) in HDM controls with respect to PBS challenged mice, whilst mice treated for two weeks with NVP did not show such an increase. However, the dynamic compliance (Cdyn) was reduced in HDM-challenged mice when compared to PBS controls and NVP-treated mice showed a lower reduction in Cdyn (**Figure 32**).

Figure 32. Therapeutic inhibition of IGF1R attenuates AHR upon HDM-induced allergy. Quantification of lung resistance (LR) and dynamic compliance (Cdyn) to methacholine (MCh) evaluated by plethysmography (n = 4–8 mice per group). Data are expressed as mean ± SEM. * $p < 0.05$; ** $p < 0.01$; *** $p < 0.001$; # $p < 0.05$ (comparisons within the same group) (Mann–Whitney U test or Student´s t-test for comparing two groups and Kruskal–Wallis test or ANOVA multiple comparison test for grouped or multivariate analysis).

Gene expression of the surfactant (*Sftp*) markers a1, b, c and d was evaluated to elucidate how the pharmacological blockade of IGF1R modulates their production. Whereas *Sftpa1* and *Sftpd* mRNA expression levels were significantly increased in HDM controls, *Sftpb* and *Sftpc* levels were severely depleted. Interestingly, NVP treatment reversed these changes, especially in the NVP 2 wks group, in which *Sftpa1* and *Sftpd* mRNA levels were normalized (**Figure 33A**). In accordance, immunofluorescence for SFTPC showed that the number of SFTPC+ cells was strongly reduced in HDM control mice, and this decrease was counteracted only in the NVP 2 wks group (**Figure 33B**).
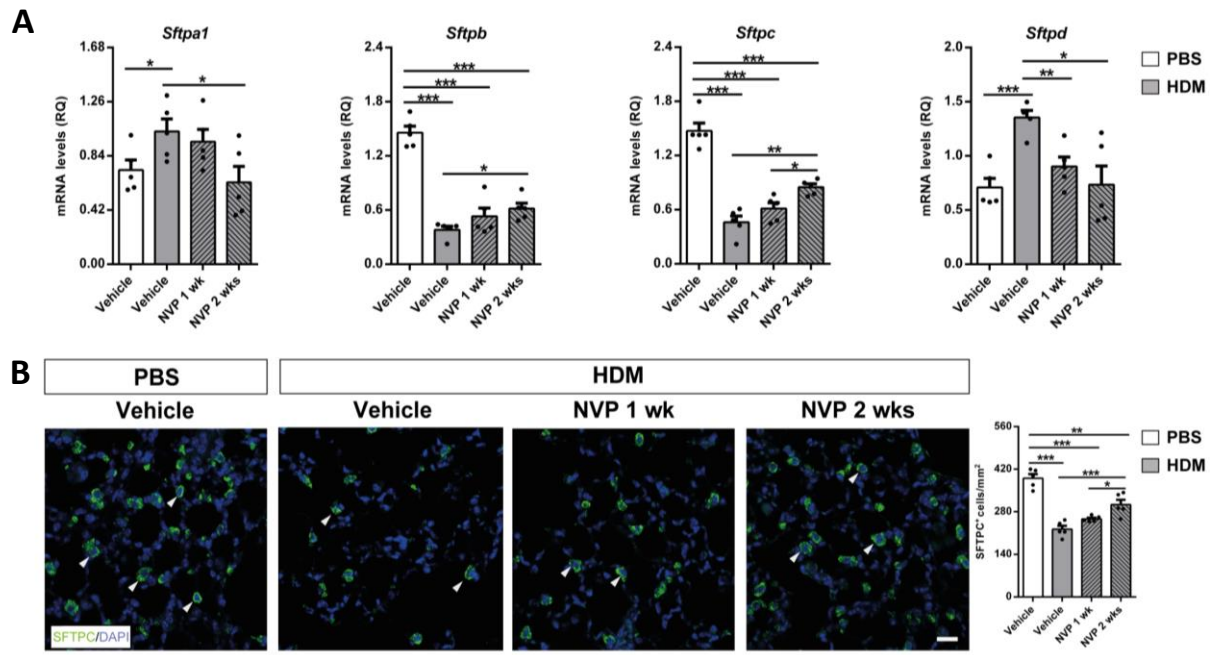
Figure 33. Therapeutic inhibition of IGF1R normalizes pulmonary surfactant expression upon HDM-induced allergy. (**A**) Changes in lung tissue mRNA expression surfactant (*Sftp*) markers *Sftpa1, b, c* and *d*, normalized to 18S expression in HDM-challenged mice treated with NVP vs. controls (*n* = 5 mice per group). (**B**) Representative immunostains for SFTPC (green) (white arrowheads), and quantification of the number of SFTPC+ cells per unit area (mm2) in lung sections from HDM-challenged mice treated with NVP vs. controls (*n* = 5–10 mice per group; scale bar: 50 μm). Data are expressed as mean ± SEM. * *p* < 0.05; ** *p* < 0.01; *** *p* < 0.001; # *p* < 0.05 (comparisons within the same group) (Mann–Whitney U test or Student´s *t*-test for comparing two groups and Kruskal–Wallis test or ANOVA multiple comparison test for grouped or multivariate analysis).

4.1.5 Therapeutic Inhibition of IGF1R halts expression of allergic airway inflammation markers after HDM exposure

Total lung mRNA expression and protein levels of allergic airway inflammation markers were assessed on lung homogenates of HDM-challenged mice treated with NVP vs. controls by qPCR and ELISA, respectively. With the exception of *Il1b*, which did not show any significant difference between groups, mRNA levels of all these markers were strongly induced by HDM (**Figure 34A**). Whereas *Il33*, *Cd274* (PDL-1), *Cd4*, *Il13*, *Tnf*, *Cxcl1* and *Ccl2* mean levels remained around normal after treatment with NVP, *Il4* and *Ccl11* required NVP treatment for two weeks to amend the HDM response. *Pdcd1* (PD-1) showed a compellingly reduced level of mRNA in both NVP-treated groups (**Figure 34A**). In agreement, IL33, IL13 and CCL11 protein levels in lung homogenates were clearly induced in HDM controls and significantly reduced in NVP-treated mice (**Figure 34B**).
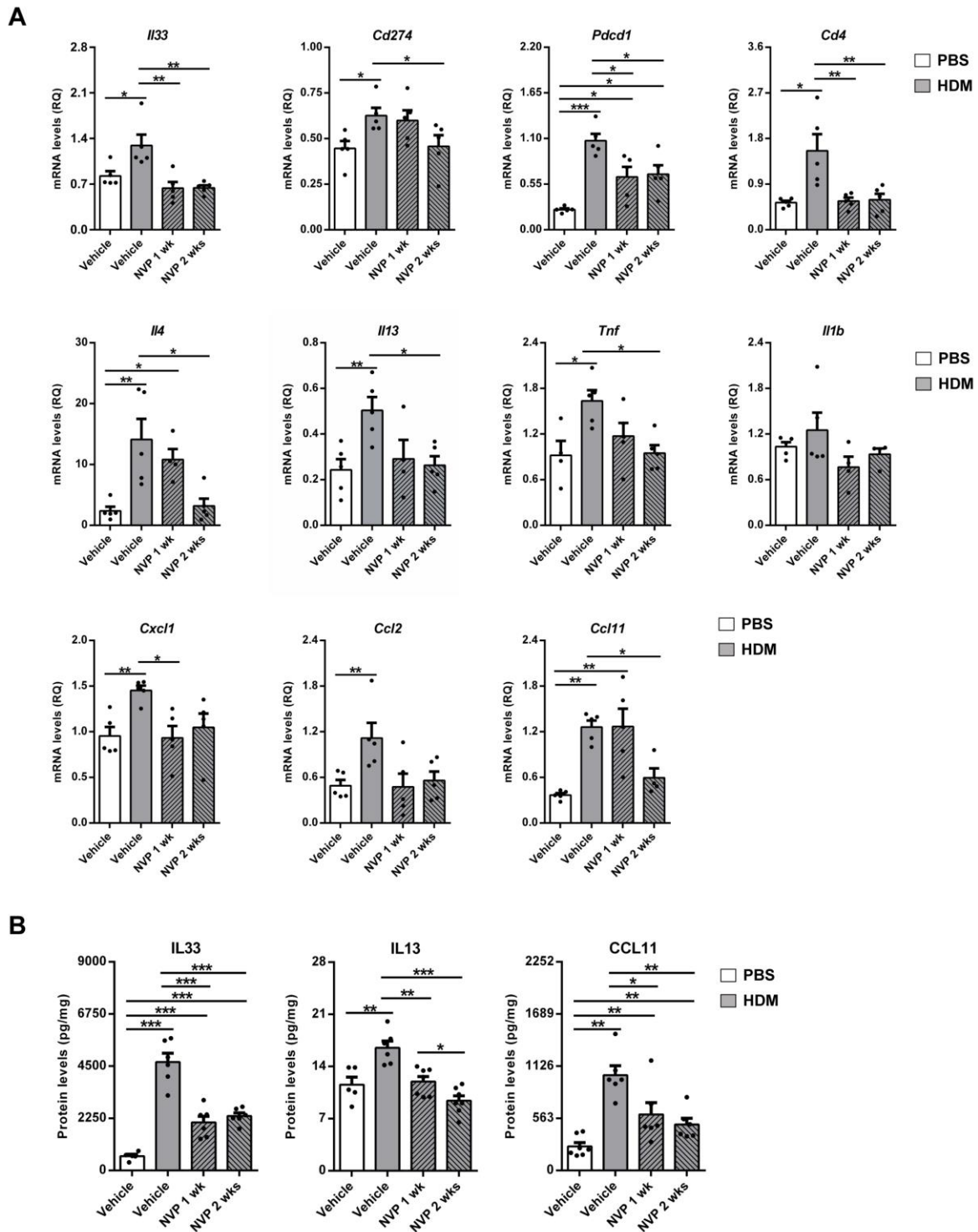
Figure 34. Therapeutic inhibition of IGF1R diminishes expression of allergic airway inflammation markers after HDM exposure. (**A**) Lung tissue mRNA expression levels of *Il33* (dendritic cell activation), *Cd274* (PD-L1) and *Pdcd1* (PD-1) (T cell response), *Cd4* (T cell marker), *Il4* and *Il13* (Th2 cytokines), *Tnf* and *Il1b* (Th1 cytokines), *Cxcl1* (neutrophil chemotaxis), *Ccl2* (macrophage chemotaxis) and *Ccl11* (eosinophil chemotaxis) normalized to 18S expression in HDM-challenged mice treated with NVP vs. controls (*n* = 5 mice per group). (**B**) IL33, IL13 and CCL11 protein levels in lung homogenates from HDM-challenged mice treated with NVP vs. controls (*n* = 5–7 mice per group). Data are expressed as mean ± SEM. * $p < 0.05$; ** $p < 0.01$; *** $p < 0.001$ (Mann–Whitney U test or Student´s *t*-test for comparing two groups and Kruskal–Wallis test or ANOVA multiple comparison test for grouped or multivariate analysis).

4.1.6 IGF1R blockade depleted bronchiolar epithelial differentiation and goblet cell hyperplasia upon HDM-induced allergy

In order to evaluate bronchiolar differentiation and goblet cell hyperplasia, we immunostained SOX2 and MUC5AC, respectively. We observed an increased proportion of SOX2+ cells and double stained SCGB1A1+-MUC5AC+ cells upon HDM challenge, which were significantly reduced in the NVP 2 wks group (**Figure 35A**). To complement these data, we also assessed mRNA expression levels of the goblet cell hyperplasia markers *Sox2*, *Muc5ac*, *Foxm1* and *Spdef*. Results on *Sox2* and *Muc5ac* mirror immunostaining data. *Foxm1* and *Spdef* followed mRNA expression profiles of allergic airway inflammation markers. In all cases, IGF1R inhibition with NVP was able to reverse the increase in mRNA expression triggered by the HDM challenge (**Figure 35B**).
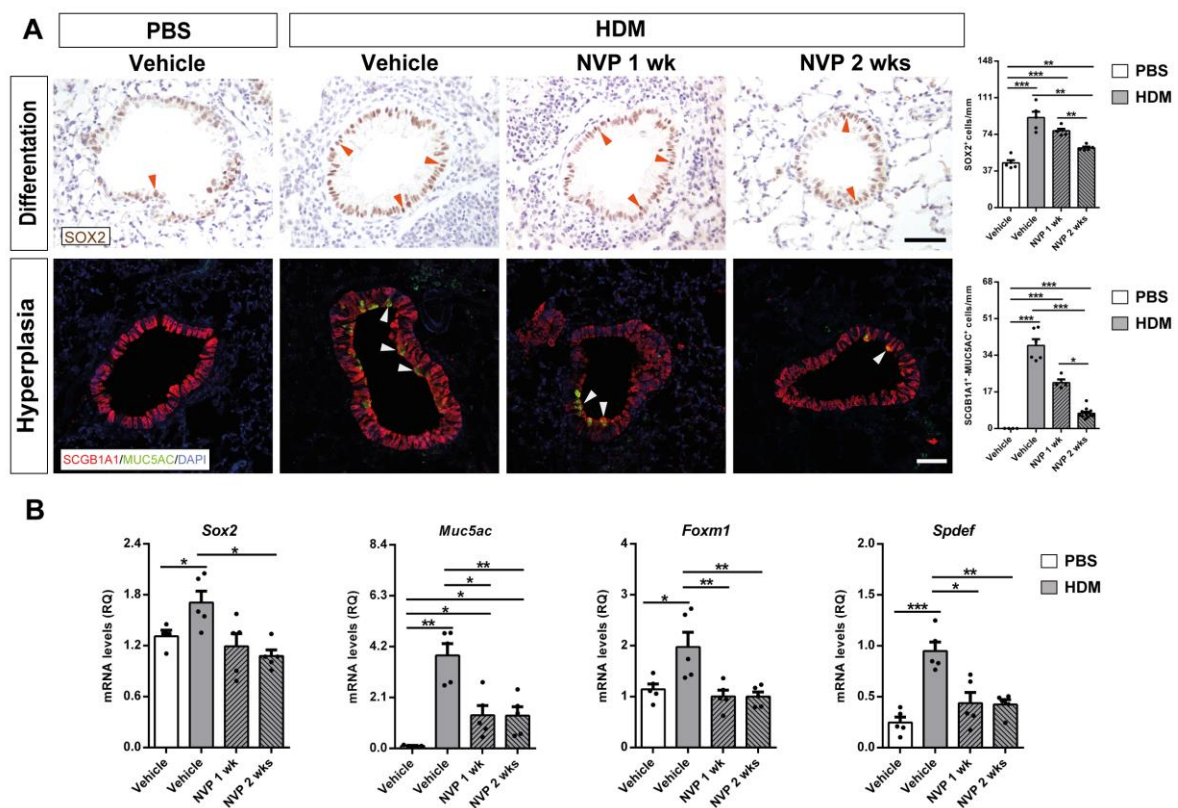
Figure 35. Pharmacological targeting of IGF1R attenuates bronchial differentiation and goblet cell hyperplasia upon HDM-induced allergy. (**A**) Representative immunostains of proximal airways for SOX2 (bronchial differentiation) (brown; orange arrowheads indicate SOX2+ cells), as well as double immunofluorescent stains for SCGB1A1 (red) (club cell marker) and MUC5AC (green) (goblet cell hyperplasia) (white arrowheads indicate double SCGB1A1+-MUC5AC+ cells). Quantification of SOX2+ and double SCGB1A1+-MUC5AC+ cells per epithelium length (mm) in lung sections from HDM-challenged mice treated with NVP vs. controls (n = 5–10 mice per group; scale bars: 50 μm). (**B**) Lung mRNA expression levels of *Sox2* (bronchial differentiation) and *Foxm1, Spdef* and *Muc5ac* markers (goblet cell hyperplasia) normalized to 18S expression in HDM-challenged mice treated with NVP vs. controls (n = 5 mice per group). Quantifications in lung sections were performed in 5 different bronchi in a random manner. Data are expressed as mean ± SEM. * $p < 0.05$; ** $p < 0.01$; *** $p < 0.001$ (Mann–Whitney U test or Student´s *t*-test for comparing two groups and Kruskal–Wallis test or ANOVA multiple comparison test for grouped or multivariate analysis).

4.2 *IGF1R as a candidate biomarker in patients with allergic asthma (Manuscript in preparation)*

4.2.1 Increased serum IGF1R levels from asthmatic patients correlate with IgE levels and circulating eosinophils

Once we had demonstrated that therapeutic inhibition of IGF1R with NVP efficiently attenuates allergic airway inflammation in mice, we decided to explore IGF1R as a candidate biomarker for patients with allergic asthma. Thus, serum IGF1R protein levels evaluated by ELISA revealed a significant increase in patients with allergic asthma compared to healthy controls (**Figure 36**).
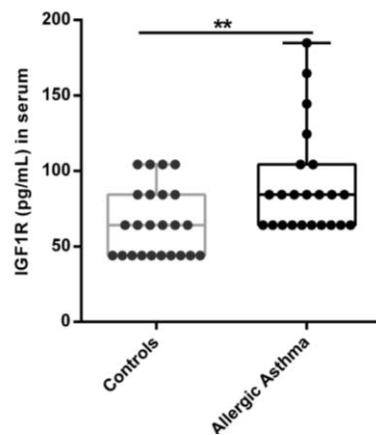
Figure 36. Increased serum IGF1R levels from asthmatic patients. Serum IGF1R levels from patients with allergic asthma and matched controls (n = 24 per group). Data are expressed as mean ±SEM. *p<0.05; **p<0.01; ***p<0.001 (Mann-Whitney U test or Student´s t-test for comparing two groups).

Additional clinical conditions, such as serum IgE levels, peripheral blood cell counts and the FEV1 (forced expiratory volume) /FVC (forced vital capacity) ratio, were evaluated. Serum IgE levels, and total and peripheral blood cell counts with the exception of monocytes, were significantly incremented with respect to controls. Our cohort of asthmatic patients also showed a significant decline to 65% in the FEV1/FVC index, which indicates pulmonary obstruction (**Figure 37A-C**). Finally, we observed that the increase of serum IGF1R levels correlated with IgE levels and circulating eosinophils (Pearson´s correlation coefficient, r = 0.3584, p = 0.0134; and r = 0.3719, p = 0.0100, respectively) (**Figure 37A,B**).
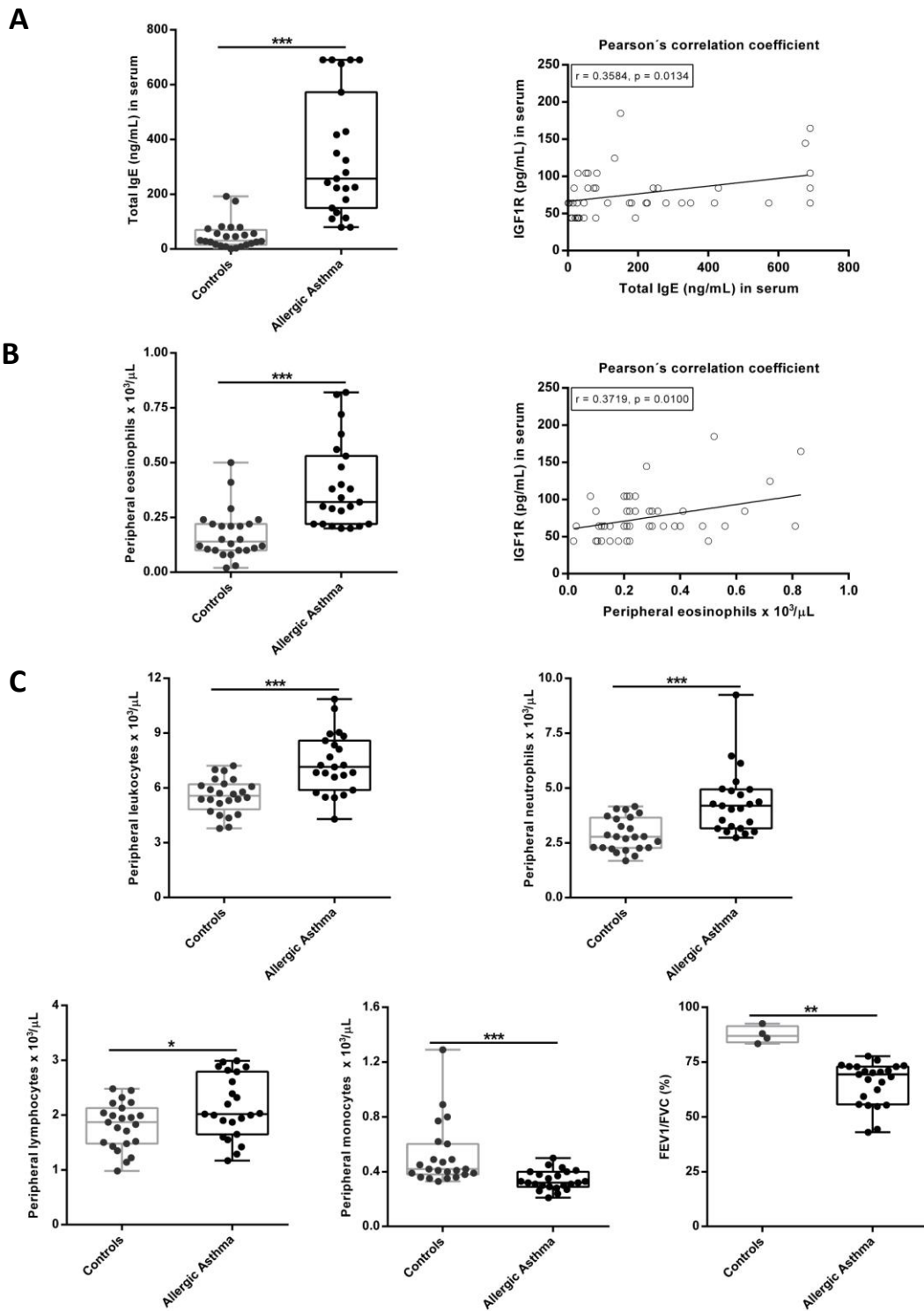
Figure 37. Increased serum IGF1R levels from asthmatic patients correlate with IgE levels and circulating eosinophils. (**A** and **B**) Total serum IgE levels (**A**), peripheral blood eosinophil counts (**B**) and respective Pearson´s correlation with serum IGF1R levels (**A** and **B**). (**C**) Peripheral blood cell counts for total leukocytes, neutrophils, lymphocytes and monocytes, and ratio of the forced expiratory volume in the first second to the forced vital capacity of the lungs (FEV1 (forced expiratory volume) /FVC (forced vital capacity)) from patients with allergic asthma and controls (n = 24 per group). Data are expressed as mean ±SEM. *p<0.05; **p<0.01; ***p<0.001 (Mann-Whitney U test or Student´s t-test for comparing two groups and Pearson´s correlation coefficient).

4.3 *IGF1R acts as a cancer-promoting factor in the tumor microenvironment facilitating lung metastasis implantation and progression* (Manuscript subbmited)

4.3.1 Increased IGF1R amplification and mRNA expression, as well as upregulation of IGF1R protein expression in tumor samples and serum in NSCLC patients

To explore genomic alterations and mRNA expression of *IGF1R* in patients with NSCLC, we used the cBio Cancer Genomics Portal (cBioPortal). Overall, data obtained from different studies included in the cBioPortal cancer database, showed an increased *IGF1R* amplification frequency with an average of 1.385%. In addition, copy number values and mRNA expression were significantly increased in tissue samples from NSCLC patients in which IGF1R was found amplified with respect to diploid tissue. We also observed that the increase of IGF1R mRNA expression correlated with copy number values (Pearson´s correlation coefficient, r = 0.4603, p = 0.0157) (**Figure 38A**). To complement this data IGF1R was assessed in serum and tissue samples from our own NSCLC patient cohort. We show that the increase of p-IGF1R expression in tumoral lung tissues correlated with proliferation (Ki67) and macrophage (Iba1) presence (Pearson´s correlation coefficient, r = 0.5906, p = 0.0013; and r = 0.4012, p = 0.015, respectively) (**Figure 38B**). We also report overexpression of both IGF1R and p-IGF1R, although this increase was more evident in the case of p-IGF1R in peritumoral lung tissue from NSCLC patients, corresponding to accumulations of infiltrated immune cells (**Figure 38C**). Finally, serum IGF1R protein levels evaluated by ELISA revealed a significant increase in NSCLC patients compared to healthy controls (**Figure 38D**).
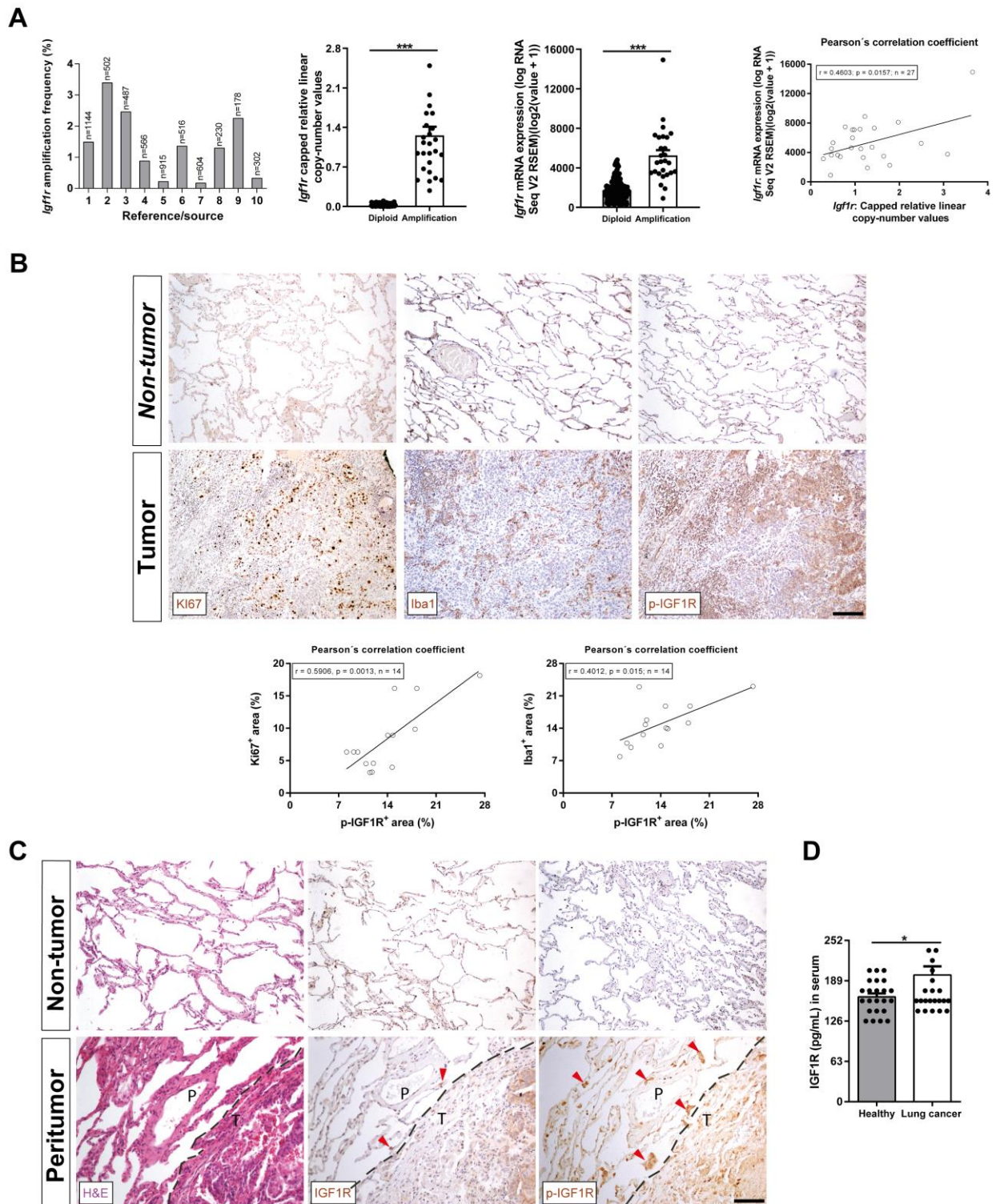
Figure 38. Increased *IGF1R* amplification and mRNA expression as well as upregulation of IGF1R protein expression in NSCLC patient tumor samples and serum. (**A**) *IGF1R* gene amplification frequency, copy number values and mRNA expression levels, as well as Pearson´s correlation of *IGF1R* copy number values with mRNA expression in tumor samples from NSCLC patients. Data were obtained from the cBio Cancer Genomics Portal (cBioPortal). (**B**) Representative immunostains for Ki67 (proliferation), Iba1 (macrophages) and p-IGF1R in tumoral and non-tumoral tissues from NSCLC patients (n = 14; Scale bar: 125 μm), and respective Pearson´s correlations of p-IGF1R+ area with Ki67+ or Iba1+ areas (%). (**C**) Representative stains for H&E and immunostains for IGF1R and p-IGF1R in peritumoral

lung tissues from NSCLC patients (dashed lines indicate limits between peritumoral (P) and tumoral (T) areas. Note accumulations of infiltrated immune cells in P (red arrows). (**D**) Serum IGF1R levels from NSCLC patients and controls (n = 24). In bar graphs, data are expressed as mean ±SEM. *$p<0.05$; ***$p<0.001$ (Mann-Whitney U test for comparing two groups and Pearson´s correlation coefficient).

4.3.2 IGF1R deficiency reduces tumor growth, proliferation, inflammation and vascularization, and increases apoptosis after tumor heterotopic transplantation

Since IGF1R has been implicated in the pathogenesis of lung cancer by facilitating metastasis, tumor associated inflammation and immune checkpoint regulation [Nurwidya *et al.*, 2016; Ajona *et al.*, 2020], we decided to assess whether IGF1R deficiency in the TME delays implantation and progression in a heterotopic LLC mouse model. For that purpose, *UBC-CreERT2; Igf1r*$^{fl/fl}$ and *Igf1r*$^{fl/fl}$ female mice were treated with TMX to induce *Igf1r* gene deletion. Then, mice were subcutaneously injected with LLC cells, and follow-up of LLC engraftments was performed for 14 days to assess the tumor volume as detailed in **Figure 25**. LLC cell tumorigenic capacity was evaluated by measuring the heterotopic tumor volume, which was lower in IGF1R deficient (*CreERT2*) vs. *Igf1r*$^{fl/fl}$ mice (**Figure 39**).
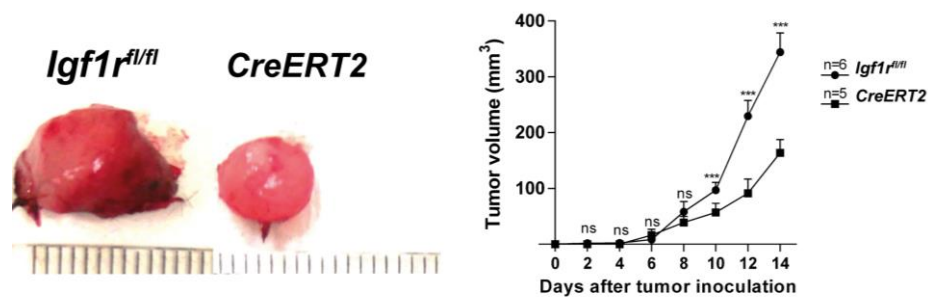
Figure 39. IGF1R deficiency reduces tumor growth after tumor heterotopic transplantation. Macroscopic pictures of subcutaneous resected heterotopic tumors (left) and measurements of tumor volumes on alternate days after inoculation of LLC cells (right) in IGF1R-deficient (*CreERT2*) vs. *Igf1*$^{fl/fl}$ (control) mice (n = 5-6 mice per group; Scale bar: 35 μm). Quantifications were performed randomly in five different fields. Data are expressed as mean ± SEM. *$p<0.05$; **$p<0.01$; ***$p<0.001$ (Mann-Whitney U test or Student´s t-test).

Delayed tumor implantation observed in *CreERT2* mice is supported by reduced proliferation (Ki67$^+$ cells), inflammation (CD45$^+$ area) and vascularization (CD31$^+$ areas), as well as increased apoptosis (C3$^+$ cells) (**Figure 40A**). Overall, these results indicate that IGF1R deficiency has an antitumoral effect on reducing heterotopic tumors growth.
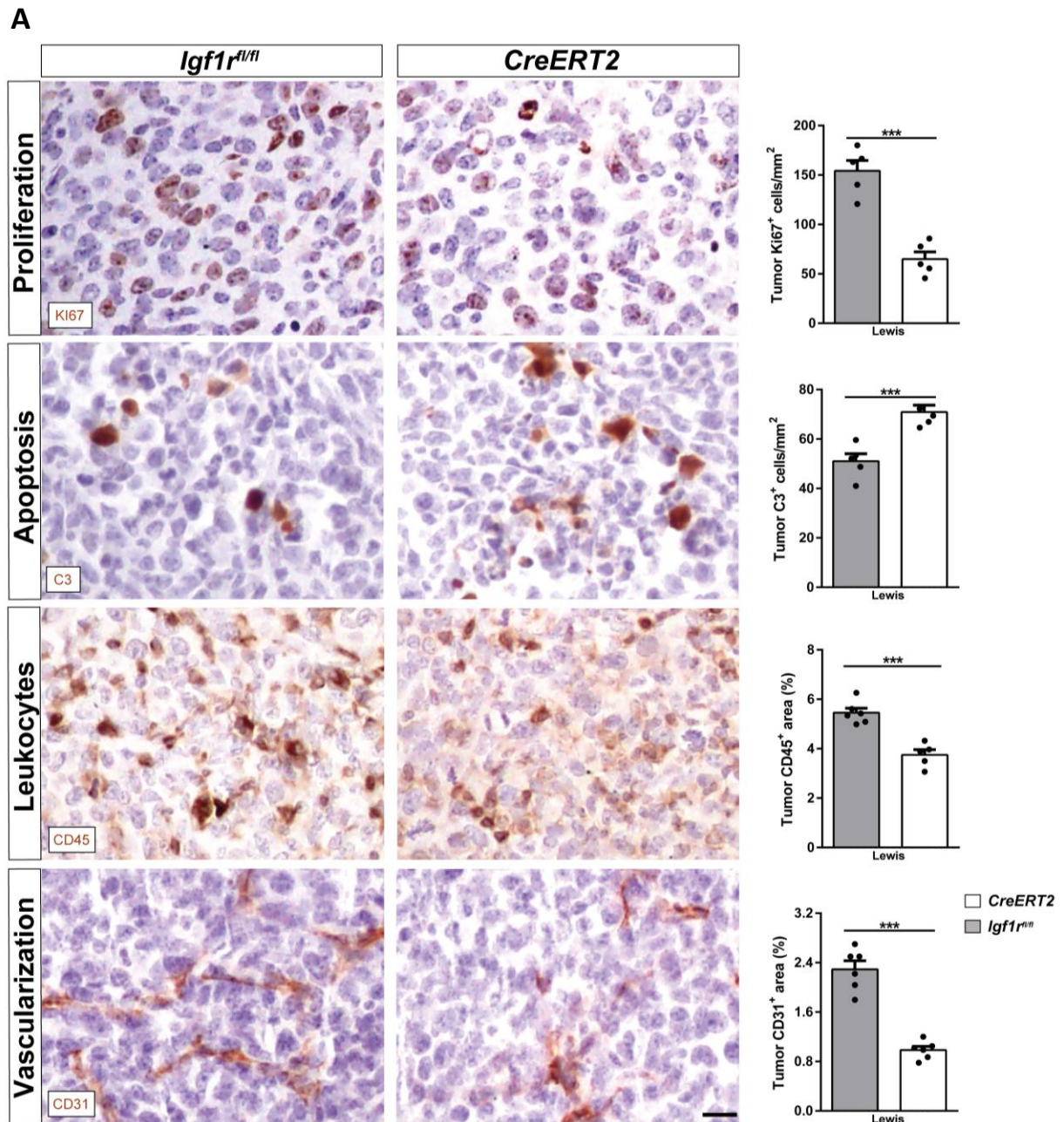
Figure 40. IGF1R deficiency reduces proliferation, inflammation and vascularization, and increases apoptosis after tumor heterotopic transplantation of LLC cells. (**A**) Representative immunostains for Ki67 (proliferation), C3 (apoptosis), CD45 (leukocytes), CD31 (vascularization) in the tumor microenvironment (TME), and respective quantifications of Ki67+ and C3+ cells per unit area (mm^2), and presence of CD45+ and CD31+ areas (%) (brown) in tumor sections from *CreERT2* vs. *Igf1r$^{fl/f}$* mice (n = 5-6 mice per group; Scale bar: 35 μm). Quantifications were performed randomly in five different fields. Data are expressed as mean ± SEM. *$p<0.05$; **$p<0.01$; ***$p<0.001$ (Mann-Whitney U test or Student´s t-test).

4.3.3 IGF1R deficiency depletes peripheral monocytes, bone marrow neutrophils and leukocyte counts in BALF, and attenuates the increase of serum IL6 and TNFα levels after experimental pulmonary metastasis

To determine the effect of IGF1R deficiency on key components of the lung TME, we performed an experimental pulmonary metastasis model. *UBC-CreERT2; Igf1r^{fl/fl}* and *Igf1r^{fl/fl}* female mice were treated with TMX to induce *Igf1r* gene deletion (*CreERT2* mice). Then, mice were intravenously injected with LLC cells in PBS or equal volume of PBS, as illustrated in **Figure 26**. IL6 and TNFα serum levels demonstrated a clear induction in LLC-challenged *Igf1r^{fl/fl}* mice, while both remained unaltered in *CreERT2* mice (**Figure 41**).
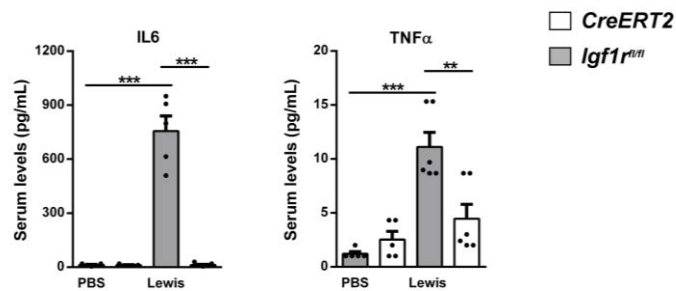
Figure 41. IGF1R deficiency attenuates the increase of serum IL6 and TNFα levels after experimental pulmonary metastasis. Total serum IL6 and TNFα levels from PBS- or LLC-challenged *CreERT2* vs. *Igf1r^{fl/f}* mice (n = 5-6 mice per group). Data are expressed as mean ± SEM. *$p<0.05$; **$p<0.01$; ***$p<0.001$ (Dunn-Sidak test).

The proportion of circulating neutrophils and monocytes exhibited a marked increase in LLC-challenged *Igf1r^{fl/fl}* mice, and while the proportion of neutrophils remained high, monocyte counts did not change in *CreERT2* mice after LLC challenge. In contrast, we observed a significant reduction in the proportion of lymphocytes in LLC-challenged mice, and this reduction was lower in *CreERT2* mice. Circulating levels of eosinophils did not change between experimental groups (**Figure 42A,B**). On the other hand, a significant increase in total cell numbers and neutrophil counts was observed in bone marrow of *Igf1r^{fl/fl}* mice after LLC challenge, an increase that was not significant in LLC-challenged IGF1R-deficient mice (**Figure 42A,C**). Moreover, total and differential BALF cell counts for neutrophils, macrophages and lymphocytes were found elevated in LLC-challenged *Igf1r^{fl/fl}* mice, while this increase was less pronounced in *CreERT2* mice. Total protein concentration in BALF was significantly increased in LLC-challenged *Igf1r^{fl/fl}* mice but remained unaltered in *CreERT2* mice upon LLC challenge (**Figure 42A,D**).

As a complement to the LLC experimental pulmonary metastasis model, we generated an additional mouse model using: B16-F10 (melanoma) cells (**Figure 26**). As noted in the LLC model, TNFα levels in both serum and lung homogenates also demonstrated a clear induction in B16-F10-challenged *Igf1r^{fl/fl}* mice, remaining unaltered in *CreERT2* mice (**Figure 43A**). Accordingly, total and differential BALF cell counts for macrophages and lymphocytes, as well as total protein concentration in BALF were found elevated in B16-F10-challenged *Igf1r^{fl/fl}* mice, but not in *CreERT2* mice as shown in the LLC model.

Neutrophil counts in BALF did not show any significant changes between groups, unlike in the LLC model (**Figure 43B-C**).
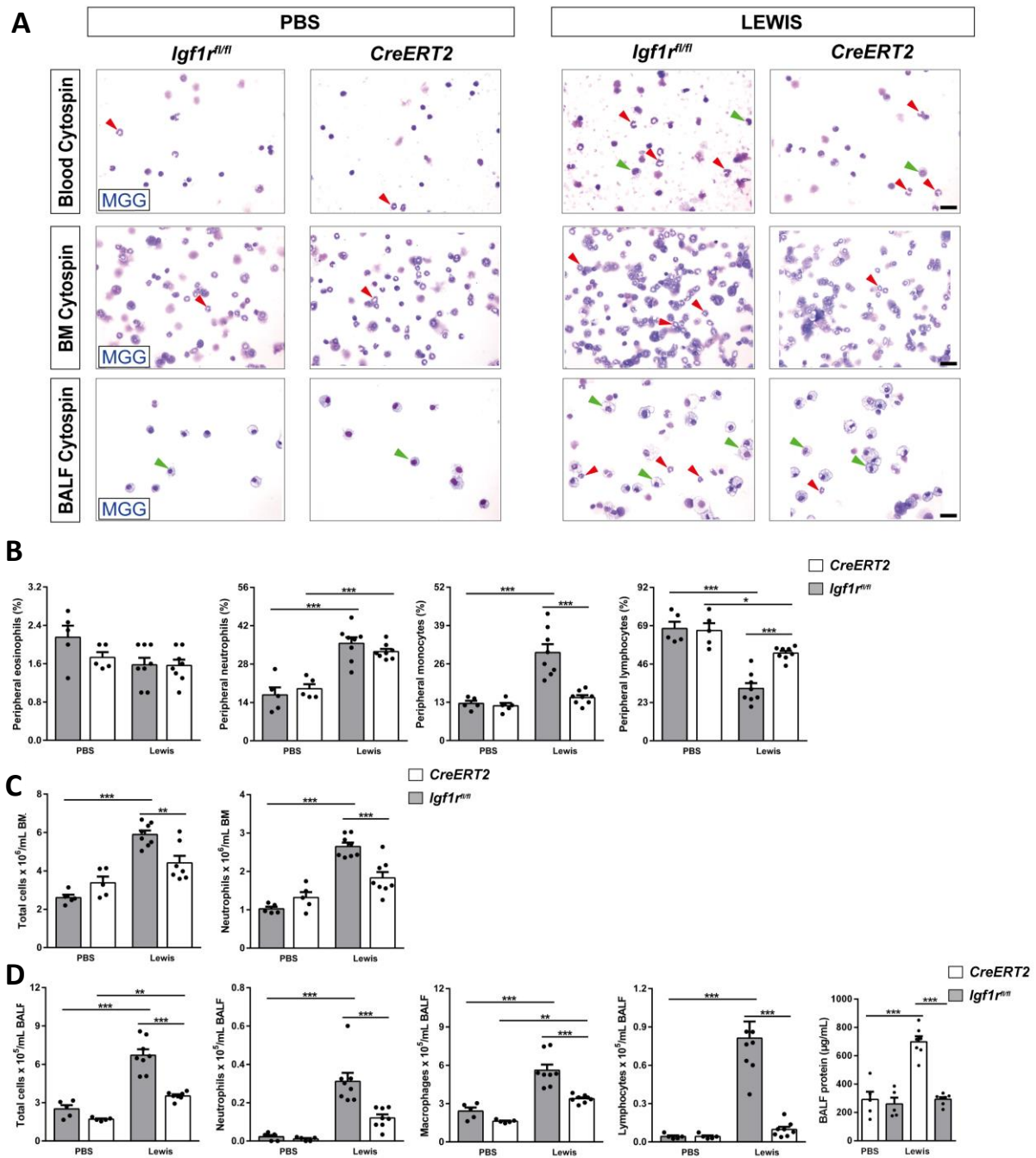
Figure 42. IGF1R deficiency depletes peripheral monocytes, bone marrow neutrophils and leukocyte counts in BALF after experimental pulmonary metastasis with LLC cells. (**A**) Representative images showing May-Grünwald Giemsa (MGG) stained peripheral blood, BM and cytospin preparations (red and green arrowheads indicate neutrophils and macrophages, respectively) (Scale bars: 25 μm). (**B-D**) Differential cell counts for eosinophils, neutrophils, monocytes and lymphocytes in peripheral blood (**B**), total cells and neutrophils in BM (**C**), and total cells, neutrophils, macrophages and lymphocytes, as well as total protein content in BALF (**D**) from PBS- or LLC-challenged *CreERT2* vs. *Igf1r^{fl/fl}* mice (n = 5-8 mice per group). Data are expressed as mean ± SEM. *$p<0.05$; **$p<0.01$; ***$p<0.001$ (Dunn-Sidak test).
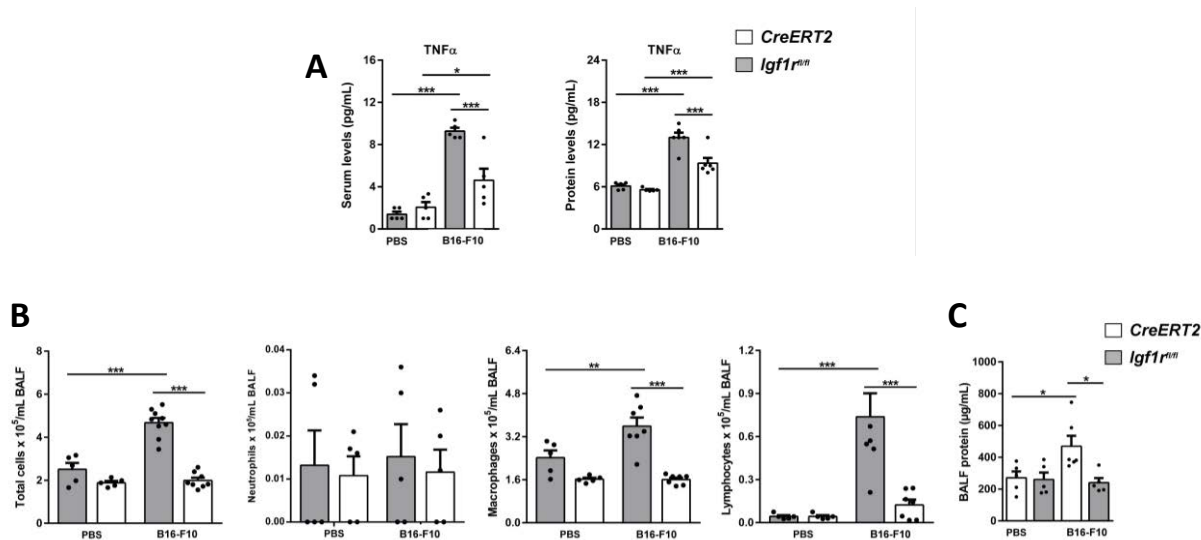
Figure 43. IGF1R deficiency reduces leukocytes in BALF, proliferation, vascularization, fibrosis and macrophage presence in the TME, and attenuates the increase of TNFα levels upon lung melanoma metastasis. (**A**) TNFα levels in both serum and lung homogenates from PBS- or B16-F10-challenged *CreERT2* vs. *Igf1r^fl/fl* mice (n = 5-6 mice per group). (**B-C**) Total cells, neutrophils, macrophages and lymphocytes, as well as, total protein content (**C**) in BALF from PBS- or B16-F10-challenged *CreERT2* vs. *Igf1r^fl/fl* mice (n = 5-7 mice per group). Quantifications were performed in five different fields in a random way. Data are expressed as mean ± SEM. *$p<0.05$; **$p<0.01$; ***$p<0.001$ (Dunn-Sidak test).

4.3.4 Reduced tumor burden and decreased expression of metastasis markers, p-IGF1R and p-ERK1/2, as well as changes in IGF system gene expression in lungs of IGF1R-deficient mice.

To evaluate tumor implantation and metastasis, p-IGF1R, p-ERK1/2 and IGF system gene expression were assessed in lungs of IGF1R-deficient (*CreERT2*) mice vs. controls. After LLC experimental pulmonary metastasis, *CreERT2* mice exhibited decreased lung tumor foci and area with respect to *Igf1r^fl/fl* mice (**Figure 44**). A similar result was found in mice challenged with B16-F10 cells (**Figure 45**).
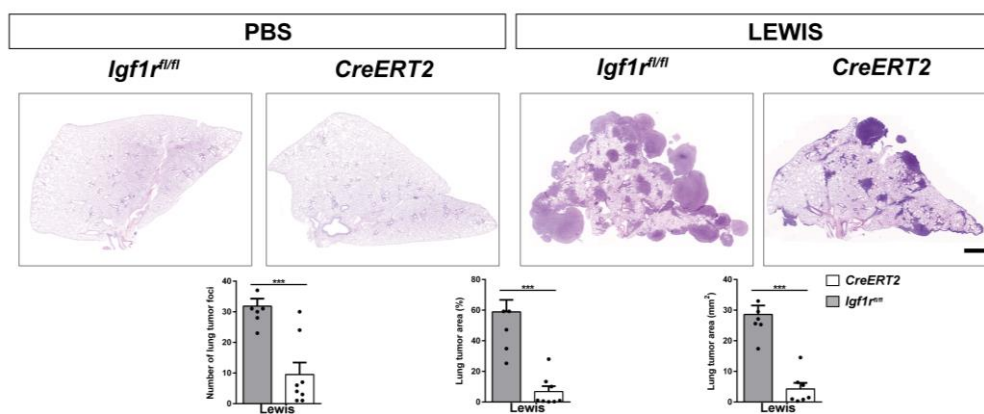
Figure 44. Reduced tumor burden in lungs of IGF1R-deficient mice upon lung Lewis metastasis. Representative histopathology images of lung metastasis (H&E) and respective quantifications of lung foci and lung tumor area (% and mm²) in IGF1R-deficient (*CreERT2*) vs. *Igf1r^fl/f* mice (n = 5-8 mice per group; Scale bar: 100 μm). Data are expressed as mean ± SEM. *$p<0.05$; **$p<0.01$; ***$p<0.001$ (Mann-Whitney U test or Student´s t-test).
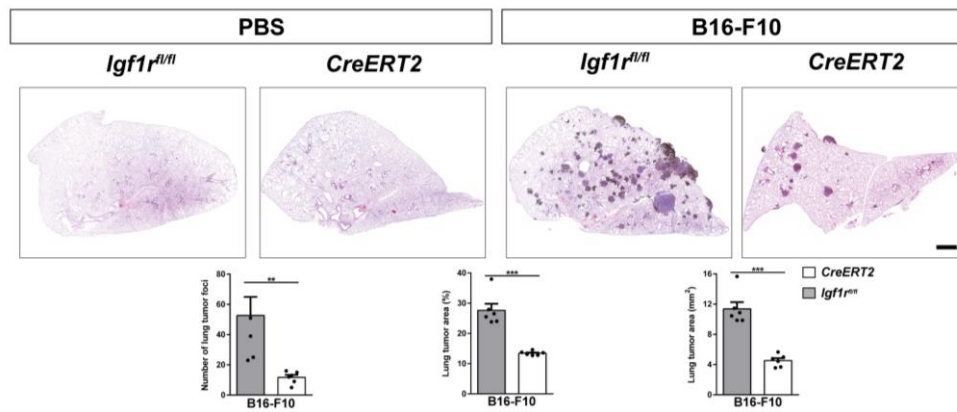
Figure 45. IGF1R deficiency reduces the number of lung tumor foci upon lung melanoma metastasis**.** Representative histopathology images of lung metastasis (H&E) and respective quantifications of number of lung foci and tumor area (% and mm^2) in IGF1R-deficient mice (*CreERT2*) vs. *Igf1r$^{fl/fl}$* mice (n = 5-7 mice per group; Scale bar: 100 μm). Quantifications were performed in five different fields in a random way. Data are expressed as mean ± SEM. *$p<0.05$; **$p<0.01$; ***$p<0.001$ (Mann-Whitney U test or Student´s t-test).

mRNA expression of *Mmp9, Egfr* and *Hmox1* (tumor progression), *Timp1* and *Timp2* (inhibitors of metalloproteinases) and *Hif1α* (hypoxia) evaluated in lung homogenates was significantly augmented in LLC-challenged *Igf1r$^{fl/fl}$* mice, remaining unaltered in *CreERT2* mice. Conversely, *Mmp2* (tumor progression) and *Timp3* (inhibitor of metalloproteinases) mRNA expression was significantly repressed after LLC challenge in *Igf1r$^{fl/fl}$* mice, while this repression was milder in *CreERT2* mice (**Figure 46A**). Accordingly, MMP9 levels quantified by ELISA in lung homogenates mirrored its mRNA expression profile (**Figure 46B**). Regarding IGF system gene expression, *Igf1r* mRNA expression increased significantly in *Igf1r$^{fl/fl}$* mice upon experimental pulmonary metastasis, showing an efficient depletion in PBS- and LLC-challenged CreERT2 mice, as expected due to tamoxifen-mediated *Igr1r* gene depletion. Insulin receptor (*Insr)* mRNA levels did not change between experimental groups. In contrast, *Igf1* mRNA levels showed significantly increased levels in both *CreERT2* experimental groups indicating IGF1 resistance to the IGF1R-defiency condition. Surprisingly, a significant reduction in *Igf1* mRNA levels was noticed in *Igf1r$^{fl/fl}$* mice upon experimental pulmonary metastasis. Notably, mRNA expression of *Igfbp* genes *Igfbp2, Igfbp3* and *Igfbp5* was found significantly depleted, and *Igfbp4* levels significantly increased upon LLC challenge only in *Igf1r$^{fl/fl}$* mice. Specifically*, Igfbp6* expression was slightly increased within LLC experimental groups (**Figure 46C**). p-IGF1R levels assessed by ELISA in lung homogenates showed a significant increase in *Igf1r$^{fl/fl}$* mice after experimental pulmonary metastasis, but were reduced in IGF1R-deficient PBS- and LLC-challenged mice. On the other hand, p-IGF1R and p-ERK1/2, assessed by immunohistochemistry in metastatic tumors, demonstrated smaller stained areas in LLC-challenged *CreERT2* mice (**Figure 46D**).
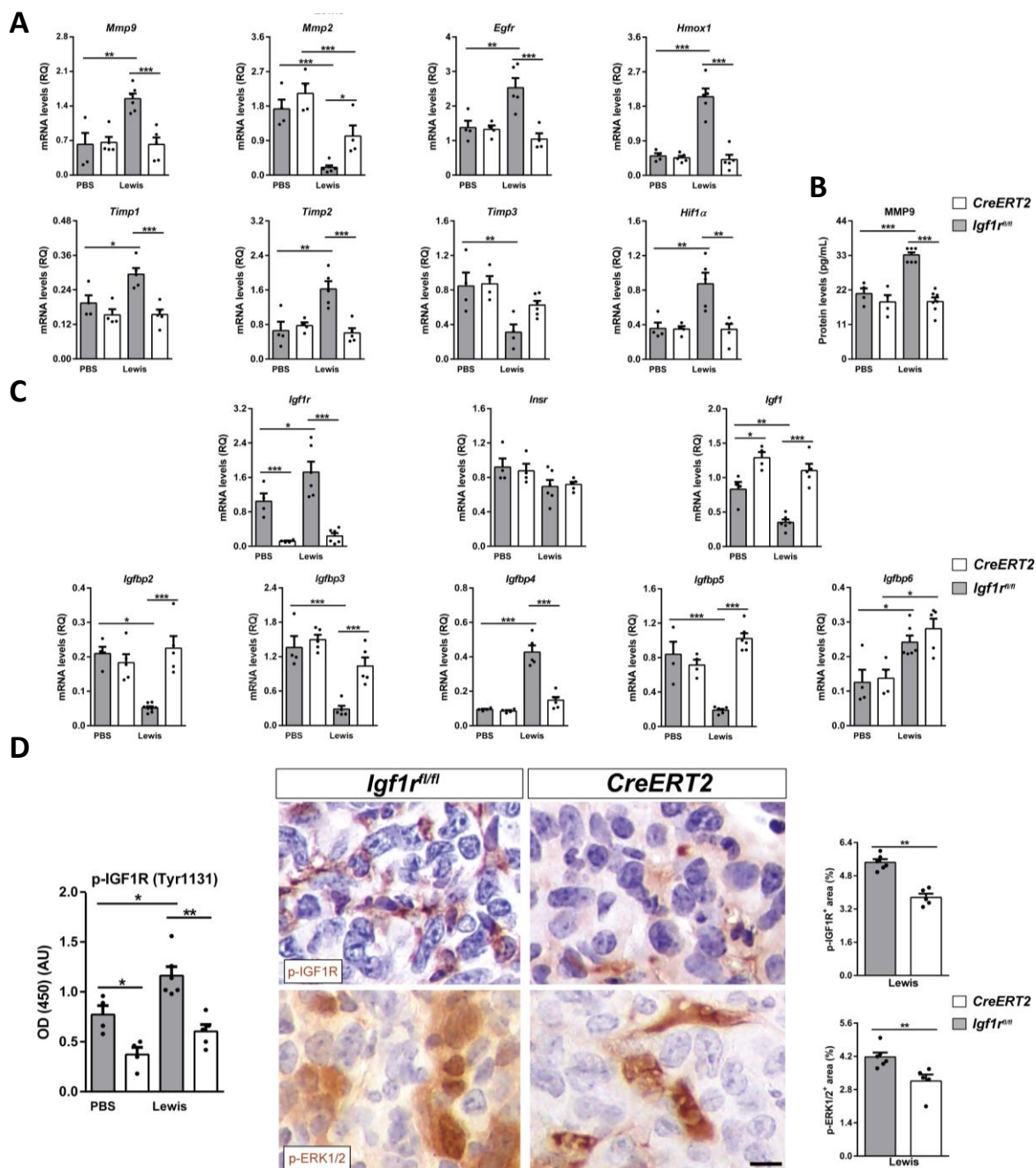
Figure 46. Decreased expression of metastasis markers, p-IGF1R and p-ERK1/2, as well as changes in IGF system gene expression in lungs of IGF1R-deficient mice. (**A**) Lung tissue mRNA expression levels of *Mmp9*, *Mmp2*, *Egfr* and *Hmox1* (tumor progression), *Timp2* and *Timp3* (inhibitors of metalloproteinases), and *Hif1α* (hypoxia) markers, normalized to 18S expression in PBS- or LLC-challenged. (**B**) MMP9 protein levels in lung homogenates of *CreERT2* vs. *Igf1r^fl/fl* mice (n = 4-7 mice per group). (**C**) Lung tissue mRNA expression of IGF system-related genes *Igf1r, Insr, Igf1, Igfbp2, Igfbp3, Igfbp4, Igfbp5* and *Igfbp6* normalized to 18S expression in PBS- or LLC-challenged *CreERT2* vs. *Igf1r^fl/f* mice (n = 5-7 mice per group). (**D**) p-IGF1R protein levels in lung homogenates, as well as representative immunostains for p-IGF1R and p-ERK1/2 (p-42/44) and respective quantifications of p-IGF1R+ and p-ERK1/2+ areas (%) (brown) in lung metastatic tumors of PBS- or LLC-challenged *CreERT2* vs. *Igf1r^fl/fl* mice (n = 4-6 mice per group; Scale bar: 15 μm). Quantifications were performed randomly in five different fields. Data are expressed as mean ± SEM. *$p<0.05$; **$p<0.01$; ***$p<0.001$ (Mann-Whitney U test or Student´s t-test for comparing two groups and the Dunn-Sidak test for multiple comparisons).

4.3.5 IGF1R deficiency decreases proliferation, DNA damage, senescence, and vascularization, attenuates tumor invasion by reduced EMT and fibrosis, and induces apoptosis upon pulmonary metastasis

To determine the effect of IGF1R deficiency in the metastatic TME, we immunostained lung tumors of LLC-challenged mice for the following markers: Ki67 (proliferation), 53BP1 (DNA damage), p21 (senescence), C3 (apoptosis), CD31 and CD34 (vascularization), SOX9 (epithelial-mesenchymal transition, EMT) as well as Vimentin, Fibronectin SMA and Masson (fibrosis). All markers showed decreased expression in LLC-challenged IGF1R-deficient *CreERT2* mice, except for C3 whose expression was found to be significantly increased (**Figure 47A-C**).
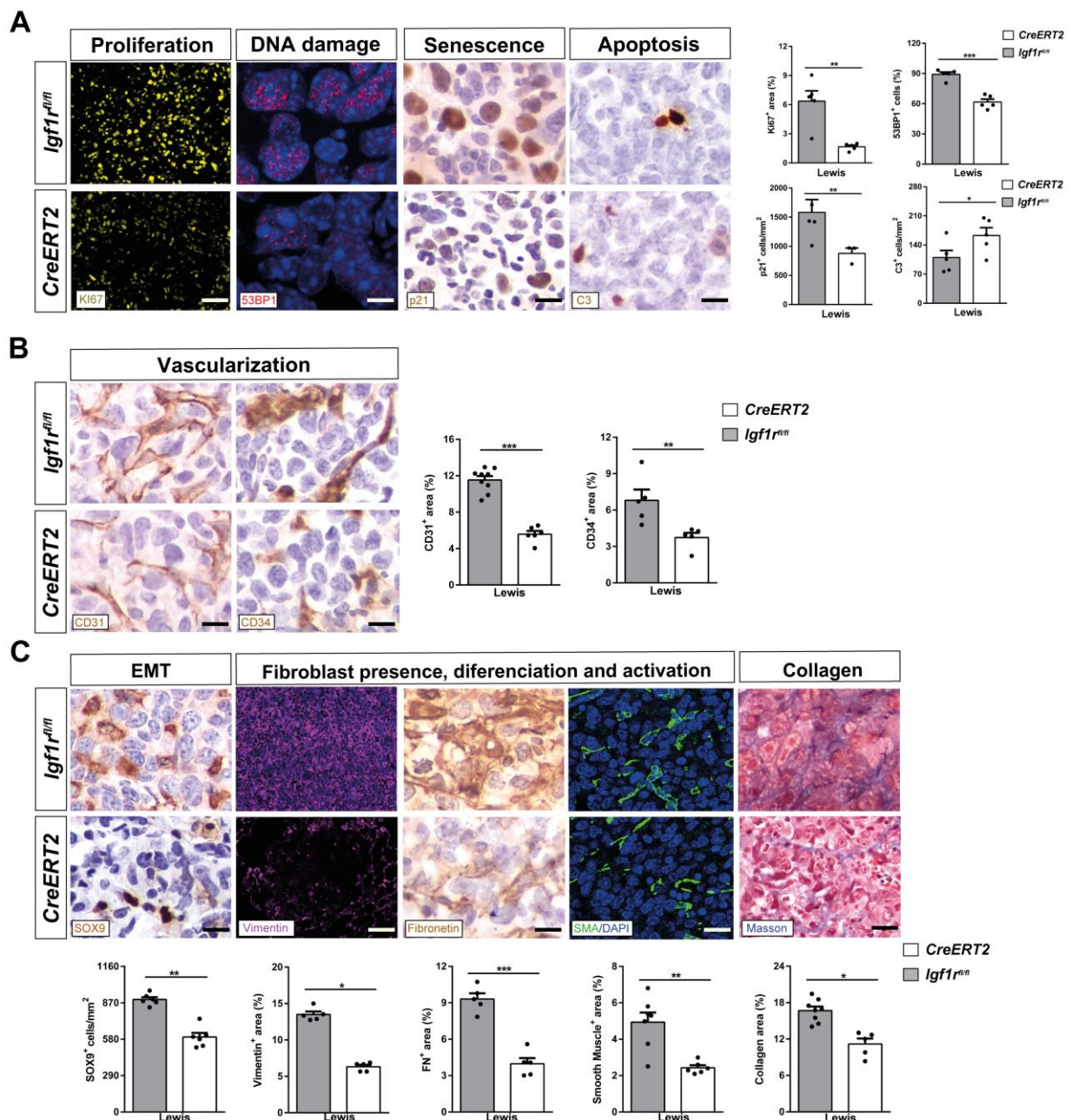
Figure 47. IGF1R deficiency decreases proliferation, DNA damage, senescence and vascularization, attenuates tumor invasion by reduced EMT and fibrosis, and induces apoptosis upon pulmonary metastasis. (**A**) Representative immunostains and quantifications of Ki67+ (proliferation) (yellow), 53BP1+ (DNA damage) (red) area (%), p21+ (senescence) (brown) and C3+ (apoptosis) (brown) cells per unit area (mm^2), as well as (**B**) CD31+ (vascularization) and CD34+ (differentiated vascularization) (brown) areas (%) in the lung TME of LLC-challenged *CreERT2* vs. *Igf1r$^{fl/fl}$* mice (n = 5-7 mice per group; Scale bars: 50 μm in Ki67, and 30 μm rest of immunostains). (**C**) Representative immunostains for SOX9 (EMT) (brown), Vimentin (fibroblast presence) (magenta), Fibronectin (fibroblast differentiation) (brown), and SMA (fibroblast activation) (green), and stains for Masson (collagen content), as well as number of SOX9+ cells per unit area (mm^2) and Vimentin+, Fibronectin+, SMA+ and Masson+ areas (%) in the lung TME of LLC-challenged *CreERT2* vs. *Igf1r$^{fl/f}$* mice (n = 5-6 mice per group; Scale bars: 30, 50, 30, 25, 30 μm, respectively). Quantifications were performed randomly in five different fields. Data are expressed as mean ± SEM. *$p<0.05$; **$p<0.01$; ***$p<0.001$ (Mann-Whitney U test or Student´s t-test).

In accordance, quantification of immunostains for Ki67, CD31, Vimentin and SMA were also found decreased in B16-F10-challenged *CreERT2* mice with respect to *Igf1r$^{fl/fl}$* (**Figure 48**).
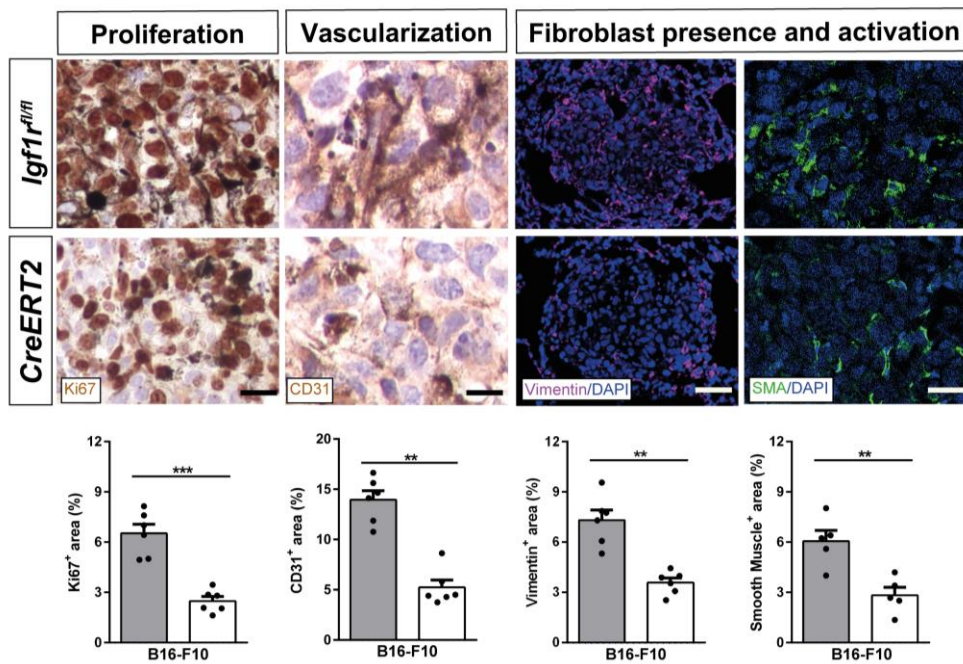
Figure 48. IGF1R deficiency reduces proliferation, vascularization, fibrosis and macrophage presence in the TME upon lung melanoma metastasis**.** Representative immunostains and quantification of Ki67+ (proliferation) (brown), CD31+ (vascularization) (brown), Vimentin+ (fibroblast presence) (magenta) and SMA+ (fibroblast activation) (green) areas (%), in the lung TME of B16-F10-challenged CreERT2 vs. Igf1r$^{fl/fl}$ mice (n = 5-7 mice per group; Scale bars: 50 μm). Quantifications were performed in five different fields in a random way. Data are expressed as mean ± SEM. *$p<0.05$; **$p<0.01$; ***$p<0.001$ (Mann-Whitney U test or Student´s t-test).

To complement these data, we also assessed mRNA expression of *Ccl12* (recruitment of fibrocytes), *Tgfβ* and *E-cadherin* (EMT) markers in lung homogenates. Concerning EMT and fibrosis, lung mRNA levels of *Ccl12* and *Tgfβ* were found significantly increased in LLC-challenged *Igf1r^{fl/fl}* mice, remaining unaltered in *CreERT2* mice. In contrast, *E-cadherin* mRNA expression was highly attenuated in *Igf1r^{fl/fl}* mice upon experimental pulmonary metastasis, while this reduction was milder in *CreERT2* mice (**Figure 49**).
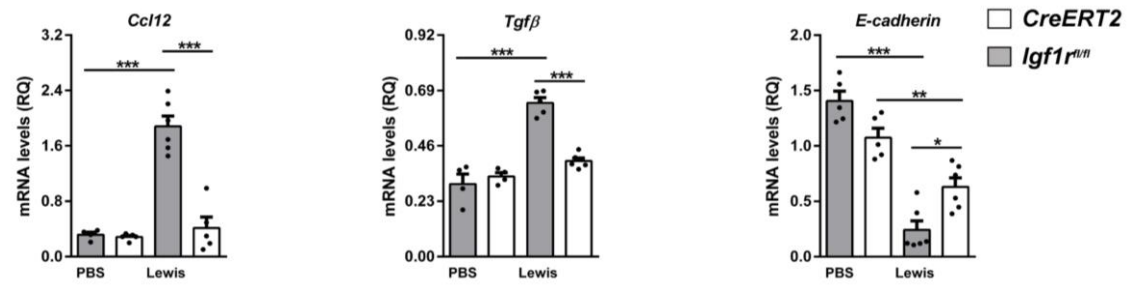
Figure 49. Lung tissue mRNA expression of *Ccl12* (recruitment of fibrocytes), *Tgfβ* and *E-cadherin* (epithelial-mesenchymal transition, EMT) normalized to 18S expression (n = 4-6 mice per group) in lung homogenates from PBS- or LLC-challenged *CreERT2* vs. *Igf1r^{fl/fl}* mice. Quantifications were performed randomly in five different fields. Data are expressed as mean ± SEM. *$p<0.05$; **$p<0.01$; ***$p<0.001$ (Dunn-Sidak test for multiple comparisons).

4.3.6 IGF1R depletion diminishes inflammation and attenuates lung tumor immunosuppression

To evaluate the impact of IGF1R deficiency on lung inflammation and immunosuppression, total mRNA expression and protein levels of related markers were assessed on lung homogenates by qPCR and ELISA, as well as by immunostaining (**Figure 50**). Total lung mRNA expression revealed that with the exception of *Tnfα* and *Foxp3* markers, which were found to be only slightly augmented, and *Cd4* and *Cd8a*, which exhibited a sharp reduction in *Igf1r^{fl/fl}* mice upon LLC challenge. mRNA levels of remaining markers (*Il1β, Ifnγ, Cxcl1, Mpo, Ccl2, Cd68, Cd163, Cd80, Cd86, Pdcd1 and Il10*) were strongly induced after experimental pulmonary metastasis in *Igf1r^{fl/fl}* mice, remaining unaltered in IGF1R-deficient mice (**Figure 50A**). Accordingly, TNFα, PDCD1 (PD-1) and IL10 levels were significantly increased in *Igf1r^{fl/fl}* mice upon LLC challenge, while this increase was milder in *CreERT2* mice (**Figure 50B**). To reinforce these data, we also immunostained for Iba1 (macrophages), CD68 (tumor associated macrophages, TAMs), as well as for FOXP3 and CD4 (tumor infiltrating lymphocytes, TILs) in LLC-challenged mice. We observed a decreased presence of Iba1, CD68 and FOXP3 positive cells, along with an increased number of CD4 positive cells in LLC-challenged *CreERT2* mice (**Figure 50C**). We also consistently found a decreased presence of Iba1+ macrophages in B16-F10 metastatic tumors in *CreERT2* mice (**Figure 51A**).
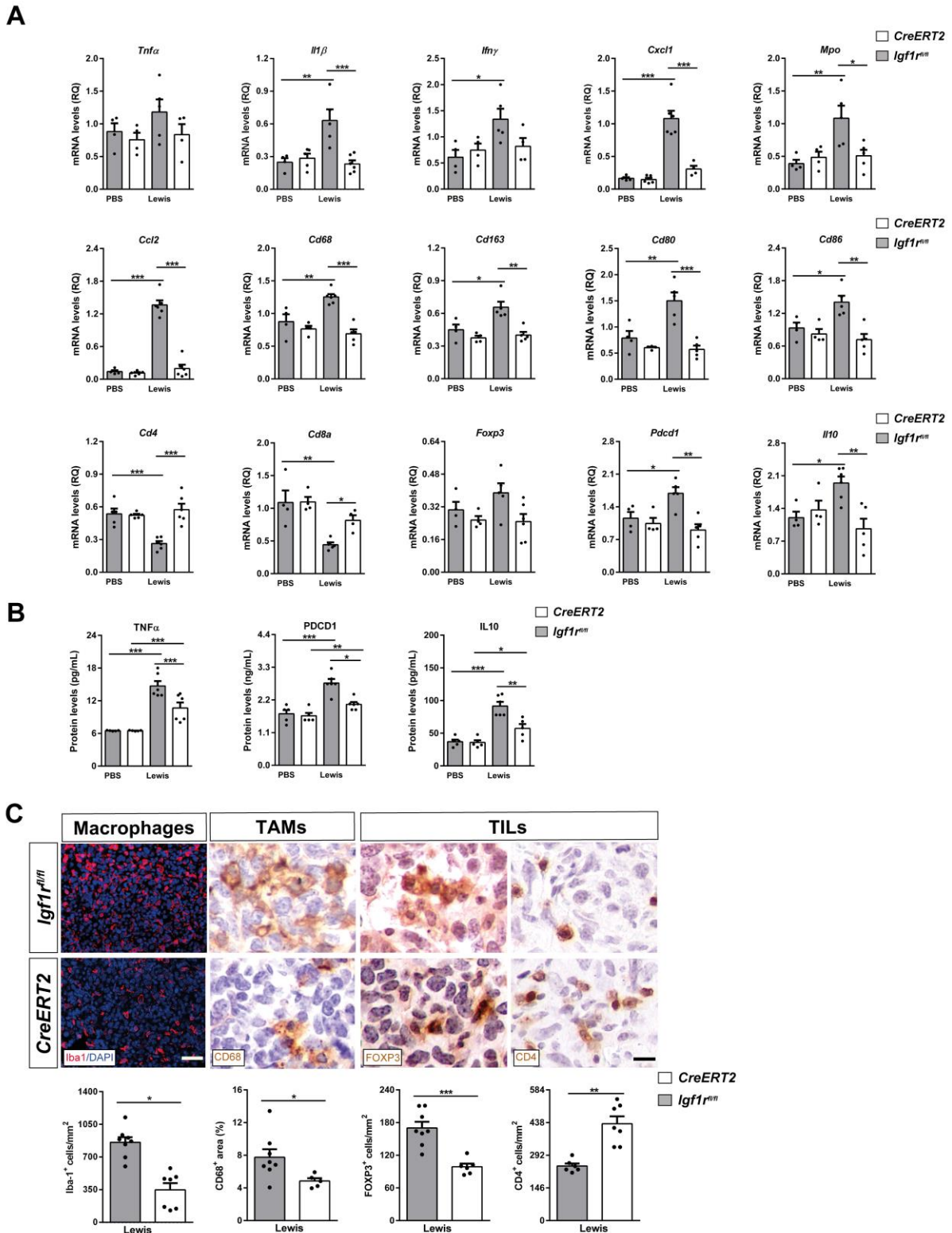
Figure 50. IGF1R depletion diminishes inflammation and attenuates lung tumor immunosuppression. (**A**) Lung tissue mRNA expression levels of *Tnfα* and *Il1β* (Th1 inflammation), *Ifnγ* (T cell exhaustion), *Cxcl1* (neutrophil chemotaxis), *Mpo* (neutrophils), *Ccl2* (macrophage chemotaxis), *Cd68* and *Cd163* (tumor associated macrophages, TAMs), *Cd80* and *Cd86* (dendritic cell activation), *Cd4* and *Cd8a* (T-cells), *Foxp3* (regulatory T cells, Tregs), *Pdcd1* (PD-1) (immunosuppression) and *Il10* (immunosuppression), normalized to *18S* expression in PBS- or LLC-challenged *CreERT2* vs. *Igf1r^fl/f* mice (n = 4-6 mice per group). (**B**) TNFα, PDCD1 (PD-1) and IL10 protein levels in lung

homogenates from PBS- or LLC-challenged *CreERT2* vs. *Igf1r*$^{fl/fl}$ mice (n = 5-7 mice per group). (**C**) Representative immunostains and quantification of CD68$^+$ (TAMs) (brown) area (%), and Iba1$^+$ (macrophages) (red), FOXP3$^+$ (Tregs) (brown) and CD4$^+$ (T-cells) (brown) cells per unit area (mm^2), in the lung TME of LLC-challenged *CreERT2* vs. *Igf1r*$^{fl/fl}$ mice (n = 5-6 mice per group; Scale bar: 50, 40 μm, respectively). Quantifications were performed randomly in five different fields. Data are expressed as mean ± SEM. *p<0.05; **p<0.01; ***p<0.001 (Mann-Whitney U test or Student´s t-test for comparing two groups and the Dunn-Sidak test for multiple comparisons).
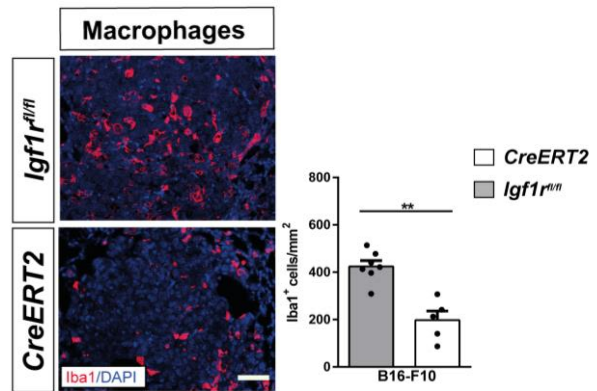
Figure 51. IGF1R deficiency reduces the macrophage presence in the TME upon lung melanoma metastasis**.** Representative immunostains and quantification of Iba1$^+$ (macrophages) (red) cells per unit area (mm^2), in the lung TME of B16-F10-challenged *CreERT2* vs. *Igf1r*$^{fl/fl}$ mice (n = 5-7 mice per group; Scale bars: 50 μm). Quantifications were performed in five different fields in a random way. Data are expressed as mean ± SEM. *p<0.05; **p<0.01; ***p<0.001 (Mann-Whitney U test or Student´s t-test).

5 DISCUSSION

IGF1R plays a relevant role in initiation of the inflammatory response and was identified as a potential therapeutic target in asthma since *Igf1r* gene deletion in mice attenuates allergic airway inflammation, but its pharmacological inhibition has not been investigated yet. For this purpose, it was determined if pharmacological blockade of IGF1R ameliorated allergic airway inflammation in a murine model of asthma. IGF1R was also evaluated as a candidate biomarker in patients with allergic asthma. Lungs of HDM-challenged mice exhibited a significant increase in p-IGF1R levels, incremented AHR, airway remodeling, mucus production, eosinophilia and allergic inflammation, as well as altered pulmonary surfactant expression; being all of these parameters counteracted by NVP treatment. In addition, serum IGF1R levels in patients with allergic asthma were significantly increased as compared to healthy subjects and correlated with IgE levels and circulating eosinophils.

On the other hand, IGF1R was reported to affect the TME; however, the role of IGF1R in the lung TME has not been investigated yet. To this end, it was studied the implication of IGF1R as a cancer-promoting factor in the lung TME by analyzing tumor samples from NSCLC patients, and generating LLC models by performing heterotopic transplantation or pulmonary metastasis in the context of IGF1R deficiency. Notably, incremented amplification and mRNA expression, as well as increased protein expression (IGF1R/p-IGF1R) and IGF1R levels in tumor samples and serum from NSCLC patients, were respectively found. Following induction of lung metastasis, IGF1R-deficient lungs demonstrated a reduced tumor burden, and decreased expression of tumor progression markers, p-IGF1R and p-ERK1/2. Additionally, IGF1R-deficient lungs showed increased apoptosis and diminished proliferation, senescence, vascularization, EMT and fibrosis, along with attenuated inflammation and immunosuppression.

5.1 IGF1R as a potential pharmacological target in allergic asthma (Paper I)

We aimed to determine if therapeutic targeting of IGF1R ameliorates established allergic airway inflammation in a murine model of HDM-induced asthma.

HDM-induced allergy has been successfully proven for the study of asthma pathobiology [Piñeiro-Hermida *et al.*, 2017a,b; Kolmert *et al.*, 2018]. Therefore, we deemed that our asthma model was appropriate for testing the "*in vivo*" anti-asthmatic efficacy of IGF1R inhibition using the IGF1R TKI inhibitor NVP-ADW742 (NVP). NVP was reported to have an inhibitory effect against IGF1R that was >16-fold more potent than towards InsR, the kinase with the highest homology to IGF1R, and exhibited no symptoms of toxicity [Mitsiades *et al.*, 2004]. Even though IGF1R activation levels significantly increased in HDM-exposed mice in serum and lung homogenates, NVP treatment counteracted IGF1R phosphorylation in both compartments. We also assessed expression of p-ERK1/2, which is a major IGF1R MAP kinase signaling mediator [Wang *et al.*, 2018]. In this regard, increased expression of p-ERK1/2 after HDM-induced allergy was attenuated upon treatment with the IGF1R TKI inhibitor NVP. Accordingly, ERK1/2 was reported to stimulate eosinophil chemotaxis, differentiation, cytokine production as well as

eotaxin-induced degranulation [Adachi *et al.*, 2000; Kampen *et al.*, 2000; Sohn *et al.*, 2007]. Furthermore, Bates et al. reported that human airway eosinophils respond to several allergic airway inflammation-related chemoattractants with increased activation of the Ras–ERK cascade [Battes *et al.*, 2010].

We have previously shown that mRNA expression of the IGF system genes *Insr*, *Igfbp3* and *Igfbp5* was repressed upon HDM exposure [Piñeiro-Hermida *et al.*, 2017a]. In particular, increased expression of *Igfbp3* in the NVP 2 wks group corresponds with its protective role in asthma [Lee *et al.*, 2011]. In contrast, *Igfbp2* and *Igfbp4* expression depends solely on IGF1R activation since they were only found diminished by NVP treatment. Increased expression of *Igf1* by HDM, which lowered to basal levels upon treatment with NVP, is in accordance with our previous findings [Piñeiro-Hermida *et al.*, 2017b]. HDM-mediated induction of *Igf1* could be responsible for IGF1R phosphorylation to promote the asthmatic response, and therefore supports why targeting IGF1R with NVP ameliorates HDM-induced asthma. Accordingly, IGF1 was reported to be involved in airway inflammation and remodeling in asthma and increased in serum of asthmatic patients [Wang *et al.*, 2018; Yamashita *et al.*, 2005; Lee *et al.*, 2011; Acat *et al.*, 2017].

On the whole, two weeks of NVP treatment were required to ameliorate the hallmarks of established HDM-induced allergy including AHR and airway remodeling. Notably, many of the typical inflammatory allergic features such as eosinophilia, increased cytokine levels and inflamed lung areas were already normalized after one week of NVP treatment. It should be emphasized that in our mouse model of asthma, the allergic phenotype was reported to be present two weeks after HDM exposure [Piñeiro-Hermida *et al.*, 2017b].

Lung function was improved upon treatment with NVP, which also normalized pulmonary surfactant expression. All these peculiarities were previously reported in *Igf1r*-deficient mice [Piñeiro-Hermida *et al.*, 2017a]. The fact that AHR is considered to be dependent on airway remodeling [Busse, 2010; Evans *et al.*, 2015] is consistent with ameliorated remodeling features upon NVP treatment. Pulmonary surfactant proteins play an essential role in lung function and homeostasis [Whisett *et al.*, 2010]. Whereas SFTPB and SFTPC showed a critical role in the preservation of lung function, SFTPA and SFTPD demonstrated immunomodulatory roles during allergic airway inflammation [Ogawa *et al.*, 2014; Ledford *et al.*, 2012; Ikegami *et al.*, 2005; Glasser *et al.*, 2013]. According to recovered density of SFTPC+ alveolar type II cells following NVP treatment, alveolar type II cells were shown to be major contributors to surfactant synthesis [Glasser *et al.*, 2013].

Lung inflammation in allergic asthma is orchestrated by activation of CD4+ T lymphocytes to stimulate the release of inflammatory mediators and elicit eosinophilia [Coverstone *et al.*, 2020; Jacquet *et al.*, 2011]. Accordingly, HDM exposure caused increased leukocytosis in the bone marrow, blood and BALF, mainly due to eosinophils, and elevated serum IgE and IL13 levels, as we reported [Piñeiro-Hermida *et al.*, 2017a,b]. Of relevance, NVP treatment ameliorated all these features. NVP treatment also decreased the expression of the T cell-related genes *Cd274* (PDL-1), *Pdcd1* (PD-1), *Tnf* and *Cd4*. *Cd274* and *Pdcd1* were reported to be important for the activation of T lymphocytes in asthma and PD-1 expression increased in T-CD4+ lymphocytes of asthmatic patients [McAlees *et al.*, 2015; Akbari *et al.*, 2010;

Mosayebian *et al.*, 2018]. Moreover, TNF was reported to be required for allergen-specific Th2 cell activation and for the development of AHR [Nakae *et al.*, 2007].

NVP treatment also diminished IL13, IL33 and CCL11 levels, reported to be highly induced upon HDM exposure [Piñeiro-Hermida *et al.*, 2017a,b]. IL33 was reported to be a central activator of dendritic cells during HDM allergic sensitization and to exacerbate allergic bronchoconstriction [Chu *et al.*, 2013; Makrinioti *et al.*, 2014; Sjöberg et *al.*, 2015]. IL13 is a central mediator of allergic asthma and its blockade in mice reduces eosinophilia and airway remodeling in response to HDM [Tomlinson *et al.*, 2010]. CCL11 was reported to be released by bronchial epithelial cells in response to cytokines such as IL4, IL13 and TNF, and is essential for lung eosinophilia and AHR development [Conroy *et al.*, 2001; Sonar *et al.*, 2012; Ying *et al.*, 1997]. NVP treatment also reduced the presence of CD45^{+} leucocytes in the lung, which were shown to be involved in allergic airway inflammation [Blaylock *et al.*, 2003; Matsuda *et al.*, 1998].

NVP treatment attenuated bronchial epithelial differentiation and goblet cell hyperplasia. We previously reported that IGF1R is required for proper club cell differentiation in mice [López *et al.*, 2016]. Accordingly, club cells were reported to play a major role in bronchial asthma and SOX2 is required for goblet cell differentiation after allergen sensitization [Sonar *et al.*, 2012; Tompkins *et al.*, 2009]. Upon allergen stimulation, FOXM1 induces differentiation of club cells into goblet cells through transcriptional activation of SPDEF. Then, increased MUC5AC expression by SPDEF in goblet cells contributes to mucus hyperproduction and AHR [Evans *et al.*, 2015; Ren *et al.*, 2013; Rajavelu *et al.*, 2015].

Our results demonstrate that the pharmacological blockade of IGF1R with NVP-ADW742 ameliorates HDM-induced allergy, and places IGF1R as a potential pharmacological target for future therapeutic approaches in asthma.

5.2 IGF1R as a candidate biomarker in patients with allergic asthma (Manuscript in preparation)

Since the implication of IGF1R was not investigated in asthmatic patients, we considered of interest to evaluate serum levels of IGF1R as a candidate biomarker in patients with allergic asthma. We have recently reported that IGF1R activation levels were significantly increased in serum and lung homogenates from HDM-exposed mice [Alfaro-Arnedo *et al.*, 2021], in accordance with incremented serum IGF1R levels observed in our cohort of asthmatic patients. Noteworthy, IGF1R was reported to be upregulated in BALF cells of asthmatic patients [Esnault *et al.*, 2013], and IGF1 was reported to be involved in airway inflammation and remodeling in asthma and increased in serum of asthmatic patients [Wang *et al.*, 2018; Yamashita *et al.*, 2005; Lee *et al.*, 2011; Acat *et al.*, 2017]. Interestingly, IGF1R protein was found in serum and plasma exosomes [Yamaguchi *et al.*, 2015; He *et al.*, 2014] and recently identified as a novel plasma biomarker to predict mortality in COVID-19 patients [Fraser *et al.*, 2020]. In addition, the use of serum protein analysis for biomarker measurements holds multiple advantages compared to alternative methods, because is minimally-invasive, low-cost and has the desirable adaptability for universal applications.

We report for the first time a direct correlation of increased serum IGF1R levels from these patients with the established clinical biomarkers of allergic asthma IgE and eosinophilia [Coverstone *et al.*, 2020; Buhl *et al.*, 2017]. Besides incremented serum IGF1R levels, our cohort of patients with allergic asthma also exhibited a significant decline in the FEV1/FVC index, which indicates pulmonary obstruction, as well as increased neutrophil, lymphocyte and macrophage presence in peripheral blood. Accordingly, a poorer lung function and increased presence of circulating neutrophils and lymphocytes was reported in mice upon allergic airway inflammation, in which IGF1R activation was significantly increased in serum and lung homogenates [Alfaro-Arnedo *et al.*, 2021]. Specifically, lung inflammation in allergic asthma is orchestrated by activation of T lymphocytes to stimulate the release of inflammatory mediators, elicit eosinophilia and increase serum IgE [Coverstone *et al.*, 2020; Jacquet *et al.*, 2011].

Our results demonstrate that increased serum IGF1R levels correlated with established clinical biomarkers of allergic asthma. On this basis, IGF1R can be now considered a promising and valuable candidate biomarker in asthma.

5.3 IGF1R acts as a cancer-promoting factor in the tumor microenvironment facilitating lung metastasis implantation and progression (Manuscript subbmited)

We aimed to determine how IGF1R deficiency acts in the lung tumor microenvironment (TME) conditioning metastatic tumor implantation and progression, by generating LLC models using heterotopic transplantation or pulmonary metastasis in the context of IGF1R deficiency. We also explored genomic alterations of IGF1R in patients with NSCLC, as well as IGF1R protein expression and levels in tissue samples and serum from NSCLC patients.

We found increased serum IGF1R levels in our NSCLC patient cohort. IGF1R was previously found in serum and plasma exosomes [Yamaguchi *et al.*, 2015; He *et al.*, 2014], and recently identified as a novel plasma biomarker to predict mortality in COVID-19 patients [Fraser *et al.*, 2020]. Thus, IGF1R could be a candidate serum biomarker for the NSCLC diagnosis. We also report IGF1R overexpression in NSCLC patient lung tissues, in accordance with previous reports where its upregulation was associated with reduced disease-free survival [Nurwidya *et al.*, 2016; Ajona *et al.*, 2020]. Accordingly, data obtained from cBioPortal cancer database showed increased gene amplification frequency, mRNA expression and copy number values of *IGF1R* in NSCLC patient tissue samples.

Since the Lewis lung carcinoma (LLC) model is the only reproducible syngeneic model for NSCLC [Kellar *et al.*, 2015], we deemed it is appropriate for determining the effect of IGF1R deficiency on key components of the TME, not only using an experimental pulmonary metastasis model but also upon heterotopic syngeneic transplantation. LLC primary tumors generated in IGF1R-deficient mice showed delayed tumor implantation and progression. Overall, these results indicate that IGF1R deficiency could have an antitumoral effect on the lung TME. After experimental pulmonary metastasis, IGF1R-deficient mice exhibited reduced tumor implantation, as similarly observed upon heterotopic syngeneic transplantation. *CreERT2* mice also showed decreased total protein concentration in BALF, an indicator of

reduced vascular permeability, as reported in an additional IGF1R-deficient mouse line [Ahamed *et al.*, 2005], which supports diminished presence of inflammatory cells in the lung. In this regard, *CreERT2* mice were reported to confer resistance to initiation of the inflammatory response [Piñeiro-Hermida *et al.*, 2017a,b,c]. In addition, IGF1/IGF1R signaling in the TME was found to be critical for medulloblastoma growth [Yao *et al.*, 2020]. Furthermore, peripheral IL6 and TNFα levels were found reduced in *CreERT2* mice upon induction of LLC metastasis. Thus, elevated serum IL6 and TNFα levels were found associated with tumor recurrence in NSCLC patients [Shang *et al.*, 2017].

LLC-challenged IGF1R-deficient mice exhibited unchanged lung mRNA expression of *Mmp9*, *Egfr*, *Hmox1*, *Hif1α*, *Timp1, Timp2* and *Timp3*. MMP-9 was reported to promote LLC cell invasiveness and pulmonary metastasis, and was found overexpressed NSCLC patients [Chou *et al.*, 2012; El-Badrawy *et al.*, 2014]. Of relevance, EGFR increased in NSCLC patients, and MMP9 and EGFR co-expression was associated with a poor prognosis [Yang *et al.*, 2015; Cox *et al.*, 2000]. Moreover, HMOX1/HO-1 (heme oxygenase 1) was reported to promote lung metastasis in mice, and its high expression was correlated with tumor invasiveness in NSCLC, as similarly reported for HIF-1α [Lin *et al.*, 2015; Tsai *et al.*, 2012; Yoshema *et al.*, 2009]. In addition, TIMP1 overexpression or TIMP3 silencing have been linked to cancer progression and poor prognosis in NSCLC [Jackson *et al.*, 2017]. The unexpected reduction of *Mmp2* mRNA expression observed in LLC-challenged *Igf1r^{fl/fl}* mice does not correlate with MMP2 overexpression reported in NSCLC patients [Passllick *et al.*, 2000].

As expected, LLC-challenged IGF1R-deficient mice exhibited counteracted IGF1R phosphorylation (p-IGF1R) and diminished p-ERK1/2 levels. Accordingly, IGF1R has been reported to contribute to the pathogenesis of lung cancer, as it is commonly overexpressed in NSCLC patients [Nurwidya *et al.*, 2016; Ajona *et al.*, 2020]. On the other hand, p-ERK1/2 is a major IGF1R MAP kinase signaling mediator that was extensively reported to be activated in NSCLC and associated with tumor cell proliferation [Vicent *et al.*, 2004; López-Malpartida *et al.*, 2009]. Intriguingly, we found unchanged lung mRNA expression of *Insr* in all experimental groups, as well as reduced *Igf1* expression in *Igf1r^{fl/fl}* LLC-challenged mice. Of note, *Insr* expression was found upregulated in mice lungs with compromised IGF1R signaling [Piñeiro-Hermida *et al.*, 2017a,b,c; López *et al.*, 2016], and IGF1 expression by the TME was reported to have a supportive role in tumor initiation and progression [Ajona *et al.*, 2020; Yao *et al.*, 2020]. These discrepancies could be due to differential transcriptional and post-transcriptional regulation of *Insr* and *Igf1* between different mouse models. Even though *Igfbp3* and *Igfbp5* expression was reduced, and in the case of *Igfbp4* increased upon LLC challenge, IGF1R deficiency maintained its levels unchanged. Remarkably, IGFBP3 was reported to inhibit tumorigenesis and cell growth, and IGFBP5 was suggested to function as a tumor suppressor [Wang *et al.*, 2017; Alami *et al.*, 2008; Wang *et al.*, 2015; Le *et al.*, 2021]. Conversely, IGFBP4 overexpression was found adversely associated with the prognosis of lung cancer patients [Xiao *et al.*, 2017].

Interestingly, after LLC-challenge, IGF1R deficient mice showed increased apoptosis. Accordingly, IGF1R signaling was reported to protect tumor cells from apoptosis [Yuan *et al.*, 2018]. Moreover, IGF1R deficiency also reduced proliferation, DNA damage, senescence, vascularization, EMT and fibrosis in the lung TME, most of which are considered cancer hallmarks [Hanahan *et al.*, 2011]. Remarkably, increased

DNA damage was found associated with NSCLC development. Assessment of undifferentiated (CD31^{+}) and differentiated (CD34^{+}) blood vessels are important prognostic factors in advanced NSCLC [Orlow *et al*., 2008; Zhao *et al*., 2012; Bacic *et al*., 2018]. EMT, a key indicator of early stage NSCLC, was reported to promote tumor growth and invasion, and was associated with increased IGF1R expression [Chen *et al*., 2013]. EMT is manifested by the loss of E-cadherin and increased expression of Vimentin and SOX9, thus promoting tumor invasion [Yang *et al*., 2014; Huang *et al*., 2019]. Accordingly, these markers were found counteracted in *CreERT2* mice after LCC challenge. Furthermore, IGF1R deficiency also attenuated TGFβ, an EMT promoter favoring tumor invasion, metastasis, and transdifferentiation of cancer associated fibroblasts (CAFs). SMA, a classical marker of CAFs, was found reduced in *CreERT2* mice, as well as fibronectin that was shown to stimulate NSCLC growth [Kim *et al*., 2020; Calon *et al*., 2014; Schule *et al*., 2020; Han *et al*., 2006].

As expected, LLC-challenged *Igf1r^{fl/fl}* lungs showed augmented levels of the *Il1β, Ifnγ, cd80, cd86,* TNFα and IL10 inflammation markers that were consistently counteracted in IGF1R-deficient mice. TNF-α, IL1B, IFN-γ and IL10 were reported to have immunoevasive and T cell exhaustion functions, and to promote tumorigenesis, drug resistance and poor survival in NSCLC [Shang *et al*., 2017; Mojic *et al*., 2017; Zaidi *et al*., 2019; Sung *et al*., 2013]. Moreover, CD80^{+} and CD86^{+} dendritic cells present in peritumoral tissues of NSCLC patients were associated with an immature phenotype that favors tumor immune escape [Perrot *et al*., 2007]. Within the lung TME many cells modulate the antitumor response including CD68^{+} TAMs, FOXP3^{+} regulatory T cells (Tregs), CD4^{+} helper T cells and CD8^{+} cytotoxic T cells [Nevee *et al*., 2019]. Here we demonstrate that IGF1R deficiency decreased the presence of inflammatory cells (macrophages, TAMs, Tregs and neutrophils) and their respective chemotactic chemokines upon LLC induction (**Figure 52**). The TME of NSCLC contains a large number of TAMs which influence tumor progression and patient prognosis, and specifically, M2 TAMs were shown to induce tumor aggressiveness and proliferation in NSCLC [Sumimoto *et al*., 2019; Li *et al*., 2018]. In this respect, ablation of IGF1R to reduce M2 marker expression in the murine myeloid lineage was reported [Spadaro *et al*., 2017]. Moreover, accumulation of M2 TAMs in solid tumors was associated with hypoxia (HIF1α) as well as IL-10 and TGFβ production [Chen *et al*., 2019; Zheng *et al*., 2020] as well as cytokines that were found counteracted in the TME of IGF1R-deficient mice. Of note, FOXP3 was reported to promote tumor growth and metastasis by inducing EMT in NSCLC, and IGF1R deficient Treg cells were reported to express lower levels of FOXP3 [Yang *et al*., 2017; Bilbao *et al*., 2014]. Conversely, the presence of infiltrating CD8^{+} and CD4^{+} T cells is a favorable prognostic factor in NSCLC, since their activation correlates with a stronger antitumor immune response [Hiraoka *et al*., 2006; Goc *et al*., 2014]. Interestingly, CD4 and CD8 immunity in NSCLC patients was reported to be required for clinical responses to PD-1 [Zuazo *et al*., 2019; Tumeh *et al*., 2014]. PD-1 is a key element within the TME and therefore an important mechanism of tumor-immune resistance, thus PD-1 blockade was proposed as an attractive therapy in NSCLC [Nevee *et al*., 2019; Brahmer *et al*., 2015]. Herein we show that LLC-challenged *CreERT2* mice exhibited reduced inflammation and attenuated tumor immunosuppression by depleted PD-1 levels. Accordingly, Ajona et al. have recently demonstrated that both genetic and pharmacological inhibition of the IGF-1/IGF-1R axis enhance the antitumor activity of anti-PD-1–PD-L1 antibodies against lung cancer [Ajona *et al*., 2020]. Of note, this is

the first report showing that IGF1R acts in the lung TME sustaining inflammation and tumor-associated immunosuppression.

In summary, our results demonstrate that IGF1R deficiency in the lung TME impairs tumor initiation and progression. Our research indicates that IGF1R could be a potential biomarker for early prediction of drug response and clinical evolution of NSCLC patients.
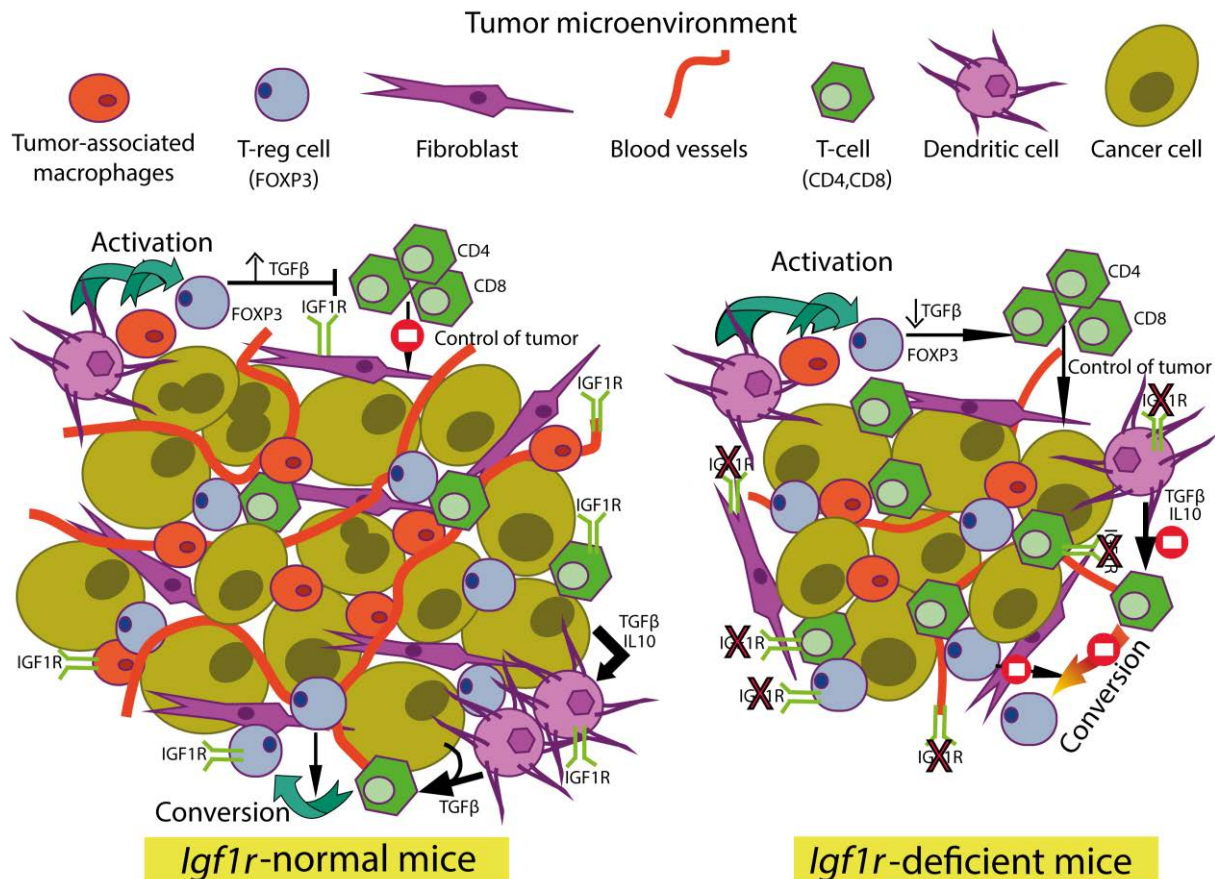
Figure 52. Reduced lung tumor burden in IGF1R-deficient mice and proposed mechanism of regulatory T cell activation and conversion. Following experimental pulmonary metastasis IGF1R-deficient lungs demonstrated reduced tumor foci, proliferation and senescence, and increased apoptosis. Additionally, IGF1R deficiency in the lung tumor microenvironment (TME) caused diminished, vascularization, EMT and fibrosis, along with attenuated inflammation and immunosuppression. Tipically, FOXP3+ regulatory T cells (Tregs), tumor-associated macrophages (TAMs) and dendritic cells (DCs) infiltrate into lung tumor tissue promoting tumor progression. Both TAMs and DCs stimulate FOXP3+ Tregs to release TGFβ, inhibiting the antitumor activity mediated by CD4+ and CD8+ T cells. Infiltrated FOXP3+ Tregs, induce the conversion of antitumor CD4+ T cells into FOXP3+ Tregs. On the other hand, tumor cells, release TGFβ and IL10 stimulating dendritic cells to produce more TGFβ, inducing the conversion of CD4+ T cells into FOXP3+ Tregs, which can be also induced by tumor cells itself. Noteworthy, IGF1R deficiency in the lung TME counteracted the production of TGFβ released by FOXP3+ Tregs, thus stimulating control of tumor. Reduced infiltration of FOXP3+ Tregs in IGF1R-deficient mice could reduce the conversion of CD4+ T cells into FOXP3+ Tregs. In addition, IGF1R deficiency in the lung TME reduced expression of TGFβ and IL10, also contributing to diminish the conversion of CD4+ T cells into FOXP3+ Tregs (Shevach and Davidson 2010; Alfaro-Arnedo *et al.*, under review).

6 CONCLUSIONS

The main conclusions from this thesis are:

1. Considering that pharmacological blockade of IGF1R resolved HDM-driven allergic airway inflammation in mice by attenuating AHR, airway remodeling and mucus secretion, IGF1R can be proposed as a potential pharmacologic target in allergic asthma.

2. IGF1R is suggested to be a candidate serum biomarker in patients with allergic asthma, since IGF1R serum levels were found increased and correlated with IgE levels and circulating eosinophils.

3. IGF1R was demonstrated to play a key role in the lung tumor microenvironment as a cancer promoting factor, since IGF1R deficiency in mice counteracted lung metastasis and tumor burden by reducing tumor proliferation and increasing apoptosis, as a consequence of decreasing tumor vascularization, senescence, immunosuppression, inflammation and invasion.

4. IGF1R is proposed as a potential biomarker in NSCLC due to its increased expression and activation in lung tumors and serum from mice with pulmonary metastasis and NSCLC patients.

5. Altogether, these findings contribute to a better understanding of the relevance of IGF1R as a potential target for therapeutic intervetions in respiratory disesases with an inflammatory component, as well as to postulate IGF1R as a potential diagnostic biomarker for these pathologies.

CONCLUSIONES

Las principales conclusiones de esta tesis son:

1. Considerando que el bloqueo farmacológico de IGF1R en ratones resolvió la inflamación alérgica de las vías respiratorias causada por el ácaro del polvo doméstico al atenuar la hiperreactividad bronquial, el remodelado de las vías respiratorias y la secreción de moco, IGF1R puede considerarse como una diana farmacológica potencial en asma alérgica.

2. Se propone a IGF1R como un candidato a biomarcador sérico en pacientes con asma alérgica, ya que sus niveles en suero se encontraron incrementados y correlancionados con los niveles de IgE y eosinófilos circulantes.

3. Se demostró que IGF1R juega un papel clave en el microambiente tumoral pulmonar como un factor promotor del cáncer, ya que la deficiencia de IGF1R en ratones contrarrestó la metástasis pulmonar y la carga tumoral al reducir la proliferación tumoral y aumentar la apoptosis, como consecuencia de la disminución de la vascularización, senescencia, inmunosupresión, inflamación e invasión tumoral.

4. Se propone a IGF1R como un biomarcador potencial en el cáncer de pulmón de tipo no microcítico (CPNM) debido al incremento de su expresión y activación en tumores y suero de ratones con metástasis pulmonar y en pacientes con CPNM.

5. En conjunto, estos hallazgos contribuyen a una mejor compresión de la relevancia de IGF1R como una diana potencial para futuras intervenciones terapéuticas en enfermedades respiratorias con un componente inflamatorio, así como a postular IGF1R como un biomarcador de diagnóstico para estas patologías.

7 REFERENCES

Abbas A, Imrie H, Viswambharan H, Sukumar P, Rajwani A, Cubbon RM, *et al*. The insulin-like growth factor-1 receptor is a negative regulator of nitric oxide bioavailability and insulin sensitivity in the endothelium. *Diabetes* 2011; 60(8):2169-2178.

Abuzzahab MJ, Schneider A, Goddard A, Grigorescu F, Lautier C, Keller E, *et al*. IGF-I receptor mutations resulting in intrauterine and postnatal growth retardation. *N Engl J Med* 2003; 349(23):2211-2222.

Acat M, Toru EU, Sahim S, Arik O, Ayada C. High Serum Levels of IGF-I and IGFBP3 may Increase Comorbidity Risk for Asthmatic Patients. *Bratisl. Med. J*. 2017; 118(11):691–694.

Adachi T, Choudhury BK, Stafford S, Sur S, Alam R. The Differential Role of Extracellular Signal-Regulated Kinases and p38 Mitogen-Activated Protein Kinase in Eosinophil Functions. *J. Immunol*. 2000; 165(4):2198–2204.

Agulló-Ortuño MT, Díaz-García CV, Agudo-López A, Pérez C, Cortijo A, Paz-Ares L, *et al*. Relevance of insulin-like growth factor 1 receptor gene expression as a prognostic factor in non-small cell lung cancer. *J Cancer Res Clinical Oncol* 2015; 141(1):43-53.

Ahmed N, Zeng M, Sinha I, Polin L, Wei W-Z, Rathinam C, *et al*. The E3 ligase Itch and deubiquitinase Cyld act together to regulate Tak1 and inflammation. *Nat Immunol* 2011; 12(12):1176-83.

Ahamed K, Epaud R, Holzenberger M, Bonora M, Flejou JF, Puard J, *et al*. Deficiency in type 1 insulin-like growth factor receptor in mice protects against oxygen-induced lung injury. *Respir Res* 2005; 6:31-41.

Ahasic AM, Zhao Y, Su L, Sheu CC, Thompson BT, Christiani DC. Adiponectin gene polymorphisms and acute respiratory distress syndrome susceptibility and mortality. *PLoS One* 2014; 9(2):e89170.

Ajona D, et al. Short-term starvation reduces IGF-1 levels to sensitize lung tumors to PD-1 immune checkpoint blockade. *Nat Cancer* 2020; doi.org/10.1038/s43018-019-0007-9.

Akbari O, Stock P, Singh AK, Lombardi V, Lee WL, Freeman GJ, *et al*. PD-L1 and PD-L2 Modulate Airway Inflammation and iNKT-Cell-Dependent Airway Hyperreactivity in Opposing Directions. *Mucosal Immunol*. 2010; 3(1):81–91.

Al-Saad S, Richardsen E, Kilvaer TK, Donnem T, Andersen S, Khanehkenari M, *et al*. The impact of MET, IGF-1, IGF1R expression and EGFR mutations on survival of patients with non-small-cell lung cancer. *PLoS One* 2017; 12(7):e0181527.

Alami N, Page V, Yu Q, Jerome L, Paterson J, Shiry L, *et al*. Recombinant human insulin-like growth factor-binding protein 3 inhibits tumor growth and targets the Akt pathway in lung and colon cancer models. *Growth Horm IGF Res* 2008; 18(6):487-496.

Alfaro-Arnedo E, López IP, Piñeiro-Hermida S, Ucero AC, González-Barcala FJ, Salgado FJ *et al*. IGF1R as a Potential Pharmacological Target in Allergic Asthma *Biomedicines* 2021; 9(8):912.

Alhakamy NA, Ishiguro S, Uppalapati D, Berkland CJ, Tamura M. AT2R Gene Delivered by Condensed Polylysine Complexes Attenuates Lewis Lung Carcinoma after Intravenous Injection or Intratracheal Spray. *Mol Cancer Ther* 2016; 15(1):209-18.

Altorki NK, Markowitz GJ, Gao D, Port JL, Saxena A, Stiles B, *et al*. The lung microenvironment: an important regulator of tumour growth and metastasis. *Nat Rev Cancer* 2019; 19(1):9-31.

American Cancer Society. Cancer Facts and Figures 2021. *A Cancer Journal for Clinicians* 2021.

Anderson IC, Shipp MA, Docherty AJ, Teicher BA. Combination therapy including a gelatinase inhibitor and cytotoxic agent reduces local invasion and metastasis of murine Lewis lung carcinoma. Cancer Res 1996; 56(4):715-8.

Annunziata M, Granata R, Ghigo E. The IGF system. *Acta Diabetol* 2011; 48(1):1-9.

Bacic I, Karlo R, Zadro AŠ, Zadro Z, Skitarelić N, Antabak A. Tumor angiogenesis as an important prognostic factor in advanced non-small cell lung cancer (Stage IIIA). *Oncol Lett* 2018; 15(2):23335-2339.

Battes ME, Sedgwick JB, Zhu Y, Liu LY, Heuser RG, Jarjour NN, *et al.* Human Airway Eosinophils Respond to Chemoattractants with Greater Eosinophil-Derived Neurotoxin Release, Adherence to Fibronectin, and Activation of the Ras-ERK Pathway When Compared with Blood Eosinophils. *J. Immunol.* 2010; 184(12):7125–7133.

Bejarano L, Jordão MJC, Joyce JA. Therapeutic Targeting of the Tumor Microenvironment. *Cancer Discov*. 2021; 11(4):933-959.

Bilbao D, Luciani L, Johannesson B, Piszczek A, Rosenthal N. Insulin-like growth factor-1 stimulates regulatory T cells and suppresses autoimmune disease. *EMBO Mol Med* 2014; 6(11):1423-35.

Blaylock MG, Lipworth BJ, Dempsey OJ, Duncan CJA, Lee DKC, Lawrie A, *et al.* Eosinophils from Patients with Asthma Express Higher Levels of the Pan-Leucocyte Receptor CD45 and the Isoform CD45RO. *Clin. Exp. Allergy* 2003; 33(7):936–941.

Bonnette SG, Hadsell DL. Targeted disruption of the IGF-I receptor gene decreases cellular proliferation in mammary terminal end buds. *Endocrinology* 2001; 142(11):4937-4945.

Brahmer J, Paz-Ares L, Horn L, Spigel DR, Steins M, Neal E Ready, *et al.* Nivolumab versus Docetaxel in Advanced Squamous-Cell Non-Small-Cell Lung Cancer. *N Engl J Med*. 2015; 373(17):123-35.

Buday T, Plevkova J. House dust mite allergy models-reliability for research of airway defensive mechanisms. *Open J Mol Integrative Physiol* 2014; 4(3):27-35.

Bugge TH, Kombrinck KW, Xiao Q, Holmbäck K, Daugherty CC, Witte DP, Degen JL. Growth and dissemination of Lewis lung carcinoma in plasminogen-deficient mice. *Blood* 1997; 90(11):4522-31.

Buhl R, Humbert M, Bjermer L, Chanez P, Heaney LG, Pavord I *et al.* Severe eosinophilic asthma: A roadmap to consensus. *Eur Respir J* 2017; 49(5):1700634.

Busse WW. The relationship of airway hyperresponsiveness and airway inflammation: airway hyperresponsiveness in asthma: its measurement and clinical significance. *Chest* 2010; 138(2 Suppl):4S-10S.

Calderón MA, Linneberg A, Kleine-Tebbe J, De Blay F, Hernandez Fernandez de Rojas D, Virchow JC, *et al.* Respiratory allergy caused by house dust mites: what do we really know? *J Allergy Clin Immunol* 2015; 136(1):38-48.

Calon A, Tauriello DVF, Batle E. TGF-beta in CAF-mediated tumor growth and metastasis. *Semin Cancer Biol* 2014, 25:15-22.

Cao H, Wang G, Meng L, Shen H, Feng Z, Liu Q, Du J. Association between circulating levels of IGF-1 and IGFBP-3 and lung cancer risk: a meta-analysis. *PLoS One* 2012; 7(11):e49884.

Cardoso S, López IP, Piñeiro-Hermida S, Pichel JG, Moreira PI. IGF1R Deficiency Modulates Brain Signaling Pathways and Disturbs Mitochondria and Redox Homeostasis. *Biomedicines* 2021; 9(2):158.

Chaft JE, Rimner A, Weder W, Azzoli CG, Mark GK, Cascone T. Evolution of systemic therapy for stages I–III non- metastatic non- small- cell lung cancer. *Nat Rec Clin Oncol* 2021; 18(9):547-557.

Chang YS, Kong G, Sun S, Liu D, El-Naggar AK, Khuri FR, *et al*. Clinical significance of insulin-like growth factor-binding protein-3 expression in stage I non-small cell lung cancer. *Clin Cancer Res* 2002; 8(12):3796-802.

Chang M. Tamoxifen resistance in breast cancer. *Biomol Ther* (*Seoul*) 2012; 20(3):256-67.

Chen HX and Sharon E. IGF-1R as an anti-cancer target--trials and tribulations. *Chin J Cancer* 2013; 32(5):242-52.

Chen B, Xiao F, Li B, Xie B, Zhou J, Zheng J, Zhang W. The role of epithelial-mesenchymal transition and IGF-1R expression in prediction of gefitinib activity as the second-line treatment for advanced nonsmall-cell lung cancer. *Cancer Invest* 2013; 31(7):454-60.

Chen PC, Chen CC, Ker YB, Chang CH, Chyau CC, Hu ML. Anti-Metastatic Effects of Antrodan with and without Cisplatin on Lewis Lung Carcinomas in a Mouse Xenograft Model. *Int J Mol Sci* 2018; 19(6):1565.

Chen Y, Song Y, Du W, Gong L, Chang H, Zou Z. Tumor-associated macrophages: an accomplice in solid tumor progression. *J Biomed Sci* 2019; 26(1):78.

Chen HX and Sharon E. IGF-1R as an anti-cancer target--trials and tribulations. *Chin J Cancer* 2013; 32(5):242-52.

Chou CH, Teng C-M, Tzen K-Y, Chang Y-C, Chen J-H, Cheng J C-H. MMP-9 from sublethally irradiated tumor promotes Lewis lung carcinoma cell invasiveness and pulmonary metastasis. *Oncogene* 2012; 31(4):458-68.

Chu DK, Llop-Guevara A, Walker TD, Flader K, Goncharova S, Boudreau JE, *et al*. IL-33, but not thymic stromal lymphopoietin or IL-25, is central to mite and peanut allergic sensitization. *J Allergy Clin Immunol* 2013; 131(1):187-200.

Conroy DM, Williams TJ. Eotaxin and the attraction of eosinophils to the asthmatic lung. *Respir Res* 2001; 2(3):150-156.

Coverstone AM, Seibold MA, Peters MC. Diagnosis and Management of T2-High Asthma. *J. Allergy Clin. Immunol. Pract.* 2020; 8(2):442–450.

Corvaia N, Beck A, Caussanel V, Goetsch L. Insulin-like growth factor receptor type I as a target for cancer therapy. *Front Biosci (Schol Ed)* 2013; 5:439-450.

Cox G, Jones JL, O´Byrne. Matrix Metalloproteinase 9 and the Epidermal Growth Factor Signal Pathway in Operable Non-Small Cell Lung Cancer. *Clin Cancer Res* 2000; 6(6):2349-55.

Crudden C, Girnita A, Girnita L. Targeting the IGF-1R: the tale of the tortoise and the hare. *Front Endocrinol (Lausanne)* 2015; 6:64.

El-Badrawy MK, Yousef AM, Shaalan D, Elsamanoudy AZ. Matrix metalloproteinase-9 expression in lung cancer patients and its relation to serum mmp-9 activity, pathologic type, and prognosis. *J Bronchology Interv Pulmonol* 2014; 21(4):327-34.

Engberding N, San Martin A, Martin-Garrido A, Koga M, Pounkova L, Lyons E, *et al*. Insulin-like growth factor-1 receptor expression masks the antiinflammatory and glucose uptake capacity of insulin in vascular smooth muscle cells. *Arterioscler Thromb Vasc Biol* 2009; 29(3):408-415.

Epaud R, Aubey F, Xu J, Chaker Z, Clemessy M, Dautin A, *et al*. Knockout of insulin-like growth factor-1 receptor impairs distal lung morphogenesis. *PLoS One* 2012; 7(11):e48071.

Erle DJ, Sheppard D. The cell biology of asthma. *J Cell Biol* 2014; 205(5):621-631.

Erpenbeck L, Nieswandt B, Schön M, Pozgajova M, Schön MP. Inhibition of platelet GPIb alpha and promotion of melanoma metastasis. *J Invest Dermatol* 2010; 130(2):576-86.

Esnault S, Kelly EA, Schwantes EA, Liu LY, DeLain LP, Hauer JA, *et al*. Identification of genes expressed by human airway eosinophils after an in vivo allergen challenge. *PLoS One* 2013; 8(7):e67560.

Evans CM, Raclawska DS, Ttofali F, Liptzin DR, Fletcher AA, Harper DN, *et al*. The polymeric mucin Muc5ac is required for allergic airway hyperreactivity. *Nat Commun* 2015; 6:6281.

Fahy JV. Type 2 inflammation in asthma-present in most, absent in many. *Nat Rev Immunol* 2015; 15(1):57-65.

Feil R. Conditional somatic mutagenesis in the mouse using site-specific recombinases. *Handb Exp Pharmacol* 2007; 178:3-28.

Feil R, Wagner J, Metzger D, Chambon P. Regulation of Cre recombinase activity by mutated estrogen receptor ligand-binding domains. *Biochem Biophys Res Commun* 1997; 237(3):752-757.

Feil S, Valtcheva N, Feil R. Inducible Cre mice. *Methods Mol Biol* 2009; 530:343-363.

Fidler and Isaiah J. Metastasis, quantitative analysis of distribution and fate of tumor cell emboli labelled with $_1$25 1UdR. *J Natl Cancer Inst* 1970; 45(4):73-82.

Fraser DD, Cepinskas GDVM, Patteron EK, Slessarev M, Martin C, Daley M, *et al*. Novel Outcome Biomarkers Identified With Targeted Proteomic Analyses of Plasma From Critically Ill Coronavirus Disease 2019 Patients. *Crit. Care Explor* 2020; 2(9):e0189.

Fu S, Tang H, Liao Y, Xu Q, Liu C, Deng Y, *et al*. Expression and clinical significance of insulin-like growth factor 1 in lung cancer tissues and perioperative circulation from patients with non-small-cell lung cancer. *Curr Oncol* 2016; 23(1):12-9.

Gao J, Aksoy BA, Dogrusoz U, Dresdner G, Gross B, Sumer SO, Sun Y, Jacobsen A, *et al*. Integrative analysis of complex cancer genomics and clinical profiles using the cBioPortal. *Sci Signal*. 2013; 6(269):pl1. doi: 10.1126/scisignal.2004088.

Gerull WD, Puri V, Kozower BD. The epidemiology and biology of pulmonary metastases. *J Thorac Dis* 2021; 13(4):2585-2589.

Girnita L, Worrall C, Takahashi S, Seregard S, Girnita A. Something old, something new and something borrowed: emerging paradigm of insulin-like growth factor type 1 receptor (IGF-1R) signaling regulation. *Cell Mol Life Sci* 2014; 71(13):2403-2427.

Glasser SW, Maxfield MD, Ruetschilling TL, Akinbi HT, Baatz JE, Kitzmiller JA, *et al*. Persistence of LPS-induced lung inflammation in surfactant protein-C-deficient mice. *Am J Respir Cell Mol Biol* 2013; 49(5):845-854.

Goc J, Germain C, Vo-Bourgais TKD, Lupo A, Klein C, Knockaert S, *et al*. Dendritic cells in tumor-associated tertiary lymphoid structures signal a Th1 cytotoxic immune contexture and license the positive prognostic value of infiltrating CD8+ T cells. *Cancer Res* 2014; 74(3):705-15.

Gong M, Ma J, Guillemette R, Zhou M, Yang Y, Yang Y, *et al*. miR-335 inhibits small cell lung cancer bone metastases via IGF-IR and RANKL pathways. Mol Cancer Res 2014; 12(1):101-10.

Gregory LG, Lloyd CM. Orchestrating house dust mite-associated allergy in the lung. *Trends Immunol* 2011; 32(9):402-411.

Griffiths CD, Bilawchuk LM, McDonough JE, Jamieson KC, Elawar F, Cen Y, *et al*. IGF1R is an entry receptor 1for respiratory syncytial virus. *Nature* 2020; 583(7817):615–619.

Hammad H, Lambrecht BN. Dendritic cells and epithelial cells: linking innate and adaptive immunity in asthma. *Nat Rev Immunol* 2008; 8(3):193-204.

Han SW, Khuri FR, Roman J. Fibronectin stimulates non-small cell lung carcinoma cell growth through activation of Akt/mammalian target of rapamycin/S6 kinase and inactivation of LKB1/AMP-activated protein kinase signal pathways. *Cancer Res* 2006; 66(1):315-23.

Hanahan D, Weinberg RA. Hallmarks of Cancer: The Next Generation. *Cell* 2011; 144(5):646-74.

Hayashi S, McMahon AP. Efficient recombination in diverse tissues by a tamoxifen-inducible form of Cre: a tool for temporally regulated gene activation/inactivation in the mouse. *Dev Biol* 2002; 244(2):305-318.

He M, Crow J, Roth M, Zeng Y, Godwin AK. Integrated immunoisolation and protein analysis of circulating exosomes using microfluidic technology. *Lab Chip* 2014; 14(19):3773-3780.

Herbst RS, Morgensztern D, Boshoff C. The biology and management of non-small cell lung cancer. *Nature* 2018; 553(7689):446-454.

Herriges M, Morrisey EE. Lung development: orchestrating the generation and regeneration of a complex organ. *Development* 2014; 141(3):502-513.

Hewish M, Chau I, Cunningham D. Insulin-Like Growth Factor 1 Receptor Targeted Therapeutics: Novel Compounds and Novel Treatment Strategies for Cancer Medicine. *Recent Pat Anticancer Drug Discov*. 2009; 4(1):54–72.

Hiraoka K, Miyamoto M, Cho Y, Suzuoki M, Oshikiri T, Nakakubo Y, *et al*. Concurrent infiltration by CD8þ T cells and CD4þ T cells is a favourable prognostic factor in non-small-cell lung carcinoma. *Br J Cancer* 2006; 94(2):275-80.

Hogan BL, Barkauskas CE, Chapman HA, Epstein JA, Jain R, Hsia CC, *et al*. Repair and regeneration of the respiratory system: complexity, plasticity, and mechanisms of lung stem cell function. *Cell Stem Cell* 2014; 15(2):123-138.

Holzenberger M, Leneuve P, Hamard G, Ducos B, Perin L, Binoux M, *et al*. A targeted partial invalidation of the insulin-like growth factor I receptor gene in mice causes a postnatal growth deficit. *Endocrinology* 2000; 141(7):2557-2566.

Hoshino M, Nakamura Y, Sim JJ, Yamashiro Y, Uchida K, Hosaka K, *et al*. Inhaled corticosteroid reduced lamina reticularis of the basement membrane by modulation of insulin-like growth factor (IGF)-I expression in bronchial asthma. *Clin Exp Allergy* 1998; 28(5):568-577.

Hsu E, Feghali-Bostwick CA. Insulin-like growth factor-II is increased in systemic sclerosis-associated pulmonary fibrosis and contributes to the fibrotic process via Jun N-terminal kinase- and phosphatidylinositol-3 kinase-dependent pathways. *Am J Pathol* 2008; 172(6):1580-1590.

Huang J-Q, Wei F-W, Xu X-L, Ye S-X, Song J-W, Ding P-K, *et al.* SOX9 drives the epithelial-mesenchymal transition in non-small-cell lung cancer through the Wnt/β-catenin pathway. *J Transl Med* 2019; 17:(1)143.

Humbert M, Bousquet J, Bachert C, Palomares O, Pfister P, Kottakis I, Jaumont *et al.* IgE-Mediated Multimorbidities in Allergic Asthma and the Potential for Omalizumab Therapy. *J Allergy Clin Immunol Pract.* 2019; 7(5):1418-1429.

Iams WT, Lovly CM. Molecular pathways: clinical applications and future direction of insulin-like growth factor-1 receptor pathway blockade. *Clin Cancer Res* 2015; 21(19):4270-4277.

Ikegami M, Whitsett JA, Martis PC, Weaver TE. Reversibility of lung inflammation caused by SP-B deficiency. *Am J Physiol Lung Cell Mol Physiol* 2005; 289(6):L962-L970.

Imyanitov EN, Iyevleva AG, Levchenko EV. Molecular testing and targeted therapy for non-small cell lung cancer: current status and perspectives. *Crit Rev Oncol Hematol* 2021; 157:103194.

Izycky T, Chyczewska E, Naumnik W, Ossolinska M. Serum levels of IGF-I and IGFBP-3 in patients with lung cancer during chemotherapy. *Oncol Res* 2006; 16(1):49-54.

Jackson HW, Defamie V, Waterhouse P, Khokha R. TIMPs: versatile extracellular regulators in cancer. *Nat Rev Cancer* 2017; 17(1):38-53.

Jacquet A. The role of innate immunity activation in house dust mite allergy. *Trends Mol Med* 2011; 17(10):604-611.

Jamil A and Kasi A. Lung Metastasis. *StatPearls* 2021; BookshelfID:NBK553111.

Kampen GT, Stafford S, Adachi T, Jinquan T, Quan S, Grant JA, *et al.* Eotaxin induces degranulation and chemotaxis of eosinophils through the activation of ERK2 and p38 mitogen-activated protein kinases. *Blood* 2000; 95(6):1911-7.

Kellar SP, Restifo NP. Cellular Constituents of Immune Escape within the Tumor Microenvironment. *Cancer Res.* 2012; 72(13):3125-30.

Kellar A, Egan C, Morris D. Preclinical Murine Models for Lung Cancer: Clinical Trial Applications. *Biomed Res Int* 2015; 2015:621324.

Khweek AA, Kim E, Joldrichsen MR, Amer AO, Boyaka PN. Insights Into Mucosal Innate Immune Responses in House Dust Mite-Mediated Allergic Asthma. *Front Immunol* 2020; 11:534501

Kim BN, Ahn DH, Kang N, Yeo CD, Kim YK, Lee KY, *et al.* TGF‑β induced EMT and stemness characteristics are associated with epigenetic regulation in lung cancer. *Sci Rep* 2020; 10(1):10597.

Kim H, Kim M, Im S-K, Fang S. Mouse Cre-LoxP system: general principles to determine tissue-specific roles of target genes. *Lab Anim Res* 2018; 34(4):147-159.

Kim J-S, Kim ES, Liu D, Lee JJ, Luisa Solis L, Behrens C, *et al.* Prognostic Implications of Tumoral Expression of Insulin-like Growth Factor (IGF)-1 and -2 in Patients with Non-small Cell Lung Cancer. *Clin Lung Cancer* 2014; 15(3):213-21

Kim WY, Kim M-J, Moon H, Yuan P, Kim J-S, Woo J-K, *et al*. Differential impacts of insulin-like growth factor-binding protein-3 (IGFBP-3) in epithelial IGF-induced lung cancer development. *Endocrinology* 2011; 152(6):2164-73.

Kloting N, Koch L, Wunderlich T, Kern M, Ruschke K, Krone W, *et al*. Autocrine IGF-1 action in adipocytes controls systemic IGF-1 concentrations and growth. *Diabetes* 2008; 57(8):2074-2082.

Kolmert J, Piñeiro-Hermida S, Hamberg M, Gregory JA, López IP, Fauland, *et al*. Prominent Release of Lipoxygenase Generated Mediators in a Murine House Dust Mite-Induced Asthma Model. *Prostaglandins Other Lipid Mediat* 2018; 137:20–29.

König D, Prince SS, Rothschild SI. Targeted Therapy in Advanced and Metastatic Non-Small Cell Lung Cancer. An Update on Treatment of the Most Important Actionable Oncogenic Driver Alterations. *Cancers (Basel)* 2021; 13(4):804.

Krishnan K, Khanna C, Helman LJ. The molecular biology of pulmonary metastasis. *Thorac Surg Clin* 2006; 16(2):115-24.

Kuo CHS, Pavlidis S, Loza M, Baribaud F, Rowe A, Pandis I, Hoda U, Rossios C, Sousa A, Wilson SJ *et al*. A Transcriptome-Driven Analysis of Epithelial Brushings and Bronchial Biopsies to Define Asthma Phenotypes in U-BIOPRED. *Am.J. Respir. Crit. Care Med*. 2017; 195(4)443–455.

Kuruvilla, M.E.; Lee, F.E.-H.; Lee, G.B. Understanding Asthma Phenotypes, Endotypes and Mechanisms of Disease. *Clin. Rev. Allergy Immunol* 2019; 56(2):219-233.

Lambrecht BN, Hammad H. The airway epithelium in asthma. *Nat Med* 2012; 18(5):684-692.

Lambrecht BN, Hammad H. The immunology of asthma. *Nat Immunol* 2015; 16(1):45-56.

Le HT, Lee HJ, Cho J, Min H-Y, Lee J-S, Lee S-J, *et al*. Insulin-Like Growth Factor Binding Protein-3 Exerts Its Anti-Metastatic Effect in Aerodigestive Tract Cancers by Disrupting the Protein Stability of Vimentin. *Cancers (Basel)* 2021; 13(5):1041.

Le Y, Sauer B. Conditional gene knockout using Cre recombinase. *Mol Biotechnol* 2001; 17(3):269-75.

Ledford JG, Mukherjee S, Kislan MM, Nugent JL, Hollingsworth JW, Wright JR. Surfactant protein-A suppresses eosinophil-mediated killing of Mycoplasma pneumoniae in allergic lungs. *PLoS One* 2012; 7(2):e32436.

Lee YC, Jogie-Brahim S, Lee DY, Han J, Harada A, Murphy LJ, *et al*. Insulin-like growth factor-binding protein-3 (IGFBP-3) blocks the effects of asthma by negatively regulating NF-κB signaling through IGFBP-3R-mediated activation of caspases. *J Biol Chem* 2011; 286(20):17898-17909.

Lemanske RF Jr, Busse WW. Asthma: clinical expression and molecular mechanisms. *J Allergy Clin Immunol* 2010; 125(2 Suppl 2):S95-102.

LeRoith D, Roberts CT Jr. The insulin-like growth factor system and cancer. *Cancer Lett* 2003; 195(2):127-137.

Li Z, Maeda D, Yoshida M, Umakoshi M, Nanjo H, Shiraishi K, *et al*. The intratumoral distribution influences the prognostic impact of CD68- and CD204-positive macrophages in non-small cell lung cancer. *Lung Cancer* 2018; 123:127-135.

Lin H-H, Chiang M-T, Chang P-C, Chau L-Y. Myeloid heme oxygenase-1 promotes metastatic tumor colonization in mice. *Cancer Sci* 2015; 106(3):299-306.

Liu JP, Baker J, Perkins AS, Robertson EJ, Efstratiadis A. Mice carrying null mutations of the genes encoding insulin- like growth factor I (Igf-1) and type 1 IGF receptor (Igf1r). *Cell* 1993; 75(1):59-72.

Long L, Rubin R, Baserga R, Brodt P. Loss of the metastatic phenotype in murine carcinoma cells expressing an antisense RNA to the insulin-like growth factor receptor. *Cancer Res* 1995; 55(5):1006-9.

López IP, Rodriguez-de la Rosa L, Pais RS, Piñeiro-Hermida S, Torrens R, Contreras J, *et al*. Differential organ phenotypes after postnatal *Igf1r* gene conditional deletion induced by tamoxifen in *UBC-CreERT2; Igf1r*^{fl/fl} double transgenic mice. *Transgenic Res* 2015; 24(2):279-294.

López IP, Piñeiro-Hermida S, Pais RS, Torrens R, Hoeflich A, Pichel JG. Involvement of *Igf1r* in bronchiolar epithelial regeneration: role during repair kinetics after selective club cell ablation. *PLoS One* 2016; 11(11):e0166388.

López-Malpartida AV, Ludeña MD, Varela G, Pichel JG. Differential ErbB receptor expression and intracellular signaling activity in lung adenocarcinomas and squamous cell carcinomas. *Lung Cancer* 2009; 65(1):25-33.

Lukacs NW. Role of chemokines in the pathogenesis of asthma. *Nat Rev Immunol* 2001; 1(2):108-116.

Majeed U, Manochakian R, Zhao Y, Lou Y. Targeted therapy in advanced non‑small cell lung cancer: current advances and future trends. *J Hematol Oncol* 2021; 14(1):108.

Makrinioti H, Toussaint M, Jackson DJ, Walton RP, Johnston SL. Role of interleukin 33 in respiratory allergy and asthma. *Lancet Respir Med* 2014; 2(3):226-237.

Maru Y. The lung metastatic niches. *J Mol Med (Berl)* 2015; 93(11):1185-92.

Martín-Granado V, Ortiz-Rivero S, Carmona R, Guitiérrez-Herreo S, Barrera M, San-Segundo L, et al. C3G promotes a selective release of angiogenic factors from activated mouse platelets to regulate angiogenesis and tumor metastasis. *Oncotarget* 201; 8(67):110994-111011.

Masoli M, Fabian D, Holt S, Beasley R; Global Initiative for Asthma (GINA) Program. The global burden of asthma: executive summary of the GINA Dissemination Committee report. *Allergy* 2004; 59(5):469-478.

Matsuda A, Motoya S, Kimura S, McInnis R, Maizel AL. Takeda, A. Disruption of Lymphocyte Function and Signaling in CD45-Associated Protein-Null Mice. *J. Exp. Med*. 1998; 187(11):1863–1870.

Mattioni T, Louvion JF, Picard D. Regulation of protein activities by fusion to steroid binding domains. *Methods Cell Biol* 1994; 43(Pt A):335–352.

McAlees JW, Lajoie S, Dienger K, Sproles AA, Richgels PK, Yang Y, *et al*. Differential Control of CD4+ T Cell Subsets by the PD-1/PD-L1 Axis in Allergic Asthma. *Eur. J. Immunol* 2015; 45(4):1019–1029.

Melgert BN, Postma DS, Kuipers I, Geerlings M, Luinge MA, van der Strate BW, *et al*. Female mice are more susceptible to the development of allergic airway inflammation than male mice. *Clin Exp Allergy* 2005; 35(11):1496-1503.

Metzger D, Chambon P. Site- and time-specific gene targeting in the mouse. *Methods* 2001; 24(1):71-80.

Meyerholz DK, Suarez CJ, Dintzis SM, Frevert CW. Respiratory system. *Comparative Anatomy and Histology* (*volm. 9 Second Edition*) 2018; doi.org/10.1016/B978-0-12-802900-8.00009-9.

Mitsiades CS, Mitsiades NS, McMullan CJ, Poulaki V, Shringarpure R, Akiyama M, *et al*. Inhibition of the Insulin-Like Growth Factor Receptor-1 Tyrosine Kinase Activity as a Therapeutic Strategy for Multiple Myeloma, Other Hematologic Malignancies and Solid Tumors. *Cancer Cell* 2004; 5(3):221–230.

Mojic M, Takeda K, Hayakawa Y. The Dark Side of IFN-Its Role in Promoting Cancer Immunoevasion. *Int J Mol Sci* 2017; 19(1):89.

Moody G, Beltran PJ, Mitchell P, Cajulis E, Chung YA, Hwang D, *et al*. IGF1R blockade with ganitumab results in systemic effects on the GH-IGF axis in mice. *J Endocrinol* 2014; 221(1):145-155.

Moorehead RA, Sanchez OH, Baldwin RM, Khokha R. Transgenic overexpression of IGF-II induces spontaneous lung tumors: a model for human lung adenocarcinoma. *Oncogene* 2003; 22(6):853-7.

Moreno-Barriuso N, López-Malpartida AV, de Pablo F, Pichel JG. Alterations in alveolar epithelium differentiation and vasculogenesis in lungs of LIF/IGF-I double deficient embryos. *Dev Dyn* 2006; 235(8):2040-2050.

Mosayebian A, Koohini Z, Hossein-Nataj H, Abediankenari S, Abedi S, Asgarian-Omran H. Elevated Expression of Tim-3 and PD-1 Immune Checkpoint Receptors on T-CD4 + Lymphocytes of Patients with Asthma. Iran. *J. Allergy Asthma Immunol*. 2018; 17(6):517–525.

Nagakawa M, Uramoto H, Oka S, Chikaishi Y, Iwanami T, Shimokawa H, *et al*. Clinical significance of IGF1R expression in non-small-cell lung cancer. *Clin Lung Cancer* 2012; 13(2):136-42.

Nakae S, Lunderius C, Ho LH, Schafer B, Tsai M, Galli SJ. TNF can contribute to multiple features of ovalbumin-induced allergic inflammation of the airways in mice. *J Allergy Clin Immunol* 2007; 119(3):680-686.

Nakanishi Y, Mulshine JL, Kasprzyk PG, Natale RB, Maneckjee R, Avis I, *et al*. Insulin-like growth factor-I can mediate autocrine proliferation of human small cell lung cancer cell lines in vitro. *J Clin Invest* 1988; 82(1):354-9.

Nef S, Verma-Kurvari S, Merenmies J, Vassalli J-D, Efstratiadis A, Accili D, *et al*. Testis determination requires insulin receptor family function in mice. *Nature* 2003; 426(6964):291-295.

Nevee SC, Robinson BW, Fear VS. The role and therapeutic implications of T cells in cancer of the lung. *Clin Transl Immunology* 2019; 8(8):e1076.

Nieto-Fontarigo JJ, Gonzalez-Barcala FJ, Andrade-Bulos LJ, San-José ME, Cruz MJ, Valdés-Cuadrado L, *et al*. iTRAQ-Based Proteomic Analysis Reveals Potential Serum Biomarkers of Allergic and Nonallergic Asthma. *Allergy* 2020; 75(12):3171–3183.

Nurwidya F, Andarini S, Takahashi F, Syahruddin E, Takahashi K. Implications of Insulin-like Growth Factor 1 Receptor Activation in Lung Cancer. Malays *J Med Sci* 2016; 23(3):9-21.

O´Reilly MS, Boehm T, Shing Y, Fukai N, Vasios G, Lane W S, *et al*. Endostatin: an endogenous inhibitor of angiogenesis and tumor growth. *Cell* 1997; 88(2):277-85.

Ogawa H, Ledford JG, Mukherjee S, Aono Y, Nishioka Y, Lee JJ, *et al*. Surfactant Protein D Attenuates Sub-Epithelial Fibrosis in Allergic Airways Disease through TGF-? *Respir. Res* 2014; 15(1):1–13.

Okano T, Xuan S, Kelley MW. Insulin-like growth factor signaling regulates the timing of sensory cell differentiation in the mouse cochlea. *J Neurosci* 2011; 31(49):18104-18118.

Orlow I, Park BJ, Mujumdar U, Patel H, Siu-Lau P, Clas BA, Downey R, *et al*. DNA damage and repair capacity in patients with lung cancer: prediction of multiple primary tumors. *J Clin Oncol* 2008; 26(21)3560-6.

Osher E, Macaulay VM. Therapeutic Targeting of the IGF Axis. *Cells* 2019; 8(8):895.

Pais RS, Moreno-Barriuso N, Hernández-Porras I, López IP, De Las Rivas J, Pichel JG. Transcriptome analysis in prenatal IGF1-deficient mice identifies molecular pathways and target genes involved in distal lung differentiation. *PLoS One* 2013; 8(12):e83028.

Pala L, Giannini S, Rosi E, Cresci B, Scano G, Mohan S *et al*. Direct measurement of IGF-I and IGFBP-3 in bronchoalveolar lavage fluid from idiopathic pulmonary fibrosis. *J Endocrinol Invest* 2001; 24(11):856-864.

Pan H, Deutsch GH, Wert SE, Ontology Subcommittee NHLBI Molecular Atlas of Lung Development Program Consortium. Comprehensive anatomic ontologies for lung development: A comparison of alveolar formation and maturation within mouse and human lung. *J Biomed Semantics* 2019; 10(1):18.

Passllick B, W Sienel, R Seen-Hibler, W Wöckel, O Thetter, W Mutschler, K Pantel. Overexpression of matrix metalloproteinase 2 predicts unfavorable outcome in early-stage non-small cell lung cancer. *Clin Cancer Res* 2000; 6(10)3944-8.

Peinado H, Zhang H, Matei IR, Costa-Silva B, Hoshino A, Rodrigues G *et al*. Pre-metastatic niches: organ-specific homes for metastases. *Nat Rev Cancer* 2017; 17(5):302-317.

Perrot I, Blanchard D, Freymond N, Isaac S, Guibert B, Pachéco Y, Lebecque S. Dendritic cells infiltrating human non-small cell lung cancer are blocked at immature stage. *J Immunol* 2007; 178(5):2763-9.

Piñeiro-Hermida S, Gregory JA, López IP, Torrens R, Ruiz-Martinez C, Adner M, *et al*. Attenuated airway hyperresponsiveness and mucus secretion in HDM-exposed IGF1R-deficient mice. *Allergy* (2017a); 72(9):1317-1326.

Piñeiro-Hermida S, Alfaro-Arnedo E, Gregory JA, Torrens R, Ruíz-Martínez C, Adner M, López IP, Pichel JG. Characterization of the acute inflammatory profile and resolution of airway inflammation after *Igf1r*-gene targeting in a murine model of HDM-induced asthma. *PLoS One* (2017b); 12(12):e0190159.

Piñeiro-Hermida S, López IP, Alfaro-Arnedo E, Torrens R, Iñiguez M, Alvarez-Erviti L, *et al*. IGF1R deficiency attenuates acute inflammatory response in a bleomycin-induced lung injury mouse model. *Sci Rep* (2017c); 7(1):4290.

Piñeiro-Hermida S, Martínez P, Blasco MA. Short and Dysfunctional Telomeres Protect from Allergen-Induced Airway Inflammation. *Aging Cell* 2021; 20(5):e13352.

Pollak MN, Schernhammer ES, Hankinson SE. Insulin-like growth factors and neoplasia. *Nat Rev Cancer* 2004; 4(7):505-518.

Pollak M. Insulin and insulin-like growth factor signaling in neoplasia. *Nat Rev Cancer* 2008; 8(12):915-928.

Possa SS, Leick EA, Prado CM, Martins MA, Tibério IF. Eosinophilic inflammation in allergic asthma. *Front Pharmacol* 2013; 4:46.

Qiu W and Su GH. Development of orthotopic pancreatic tumor mouse models. *Methods Mol Biol* 2013; 980:215-23.

Raile K, Klammt J, Schneider A, Keller A, Laue S, Smith R, *et al*. Clinical and functional characteristics of the human Arg59Ter insulin-like growth factor I receptor (IGF1R) mutation: implications for a gene dosage effect of the human IGF1R. *J Clin Endocrinol Metab* 2006; 91(6):2264-2271.

Rajavelu P, Chen G, Xu Y, Kitzmiller JA, Korfhagen TR, Whitsett JA. Airway epithelial SPDEF integrates goblet cell differentiation and pulmonary Th2 inflammation. *J Clin Invest* 2015; 125(5):2021-2031.

Rangachari D, Brahmer JR. Targeting the Immune System in the Treatment of Non-Small-Cell Lung Cancer. *Curr Treat Options Oncol* 2013; 14(4):580-94.

Rashidi B, Yang M, Jiang P, Baranov E, An Z, Wang X, Moossa AR, Hoffman RM. A highly metastatic Lewis lung carcinoma orthotopic green fluorescent protein model. *Clin Exp Metastasis* 2000; 18(1):57-60.

Rawlins EL, Hogan BL. Epithelial stem cells of the lung: privileged few or opportunities for many? *Development* 2006; 133(13):2455-2465.

Ren X, Shah TA, Ustiyan V, Zhang Y, Shinn J, Chen G, *et al*. FOXM1 promotes allergen-induced goblet cell metaplasia and pulmonary inflammation. *Mol Cell Biol* 2013; 33(2):371-386.

Rock JR, Randell SH, Hogan BL. Airway basal stem cells: a perspective on their roles in epithelial homeostasis and remodeling. *Dis Model Mech* 2010; 3(9-10):545-556.

Rock JR, Hogan BL. Epithelial progenitor cells in lung development, maintenance, repair, and disease. *Annu Rev Cell Dev Biol* 2011; 27:493-512.

Rom WN1, Pääkkö P. Activated alveolar macrophages express the insulin-like growth factor-I receptor. *Am J Respir Cell Mol Biol* 1991; 4(5):432-439.

Ruan W, Ying K. Abnormal expression of IGF-binding proteins, an initiating event in idiopathic pulmonary fibrosis? *Pathol Res Pract* 2010; 206(8):537-543.

Ruzankina Y, Pinzon-Guzman C, Asare A, Ong T, Pontano L, Cotsarelis G, *et al*. Deletion of the developmentally essential gene ATR in adult mice leads to age-related phenotypes and stem cell loss. *Cell Stem Cell* 2007; 1(1):113-126.

Sachdev D, Hartell JS, Lee AV, Zhang X, Yee D. A dominant negative type I insulin-like growth factor receptor inhibits metastasis of human cancer cells. J Biol Chem 2004; 279(6):5017-24.

Schulze AB, Schmidt LH, Heitkötter B, Huss S, Mohr M, Marra A, *et al*. Prognostic impact of CD34 and SMA in cancer-associated fibroblasts in stage I-III NSCLC. *Thorac Cancer* 2020; 11(1):120-129.

Scolnick JA, Cui K, Duggan CD, Xuan S, Yuan X-B, Efstratiadis A, *et al*. Role of IGF signaling in olfactory sensory map formation and axon guidance. *Neuron* 2008; 57(6):847-857.

Sengupta S, Sobo M, Lee K, Kumar SS, White AR, Mender I, *et al*. Induced Telomere Damage to Treat Telomerase Expressing Therapy-Resistant Pediatric Brain Tumors. *Mol. Cancer Ther* 2018; 17(7):1504–1514.

Shang GS, Liu L, Quin YW. IL-6 and TNF-α promote metastasis of lung cancer by inducing epithelial-mesenchymal transition. *Oncol Lett* 2017; 13(6):4657-4660.

Shevach E and Davidson T. Regulatory T cells. *Nature reviews Immunology* 2010; Available at: http://www.nature.com/nri/posters/tregcells.

Siegel RL, Miller KD, Jemal A. Cancer Statistics. *CA Cancer J Clin* 2021; 71:7-33.

Sjöberg LC, Gregory JA, Dahlén SE, Nilsson GP, Adner M. Interleukin-33 exacerbates allergic bronchoconstriction in the mice via activation of mast cells. *Allergy* 2015; 70(5):514-521.

Smith TJ. Insulin-like growth factor-I regulation of immune function: a potential therapeutic target in autoimmune diseases? *Pharmacol Rev* 2010; 62(2):199-236.

Sohn MH, Lee KE, Kim KW, Kim ES, Park JY, Kim KE. Calcium-Calmodulin Mediates House Dust Mite-Induced ERK Activation and IL-8 Production in Human Respiratory Epithelial Cells. *Respiration* 2007; 74(4):447–453.

Sonar SS, Ehmke M, Marsh LM, Dietze J, Dudda JC, Conrad ML, *et al*. Clara cells drive eosinophil accumulation in allergic asthma. *Eur Respir J* 2012; 39(2):429-438.

Spadaro O, Goldberg EL, Camell CD, Youm YH, Kopchick JJ, Nguyen KY, *et al*. Growth hormone receptor deficiency protects against age-related NLRP3 inflammasome activation and immune senescence. *Cell Rep* 2016; 14(7):1571-1580.

Spadaro O, Camell CD, Bosurgi L, Nguyen KY, Youm Y-H, Rothlin CV, *et al*. IGF1 Shapes Macrophage Activation in Response to Immunometabolic Challenge. *Cell Rep* 2017; 19(2):225-234.

Stella GM, Kolling S, Benvenuti S, Bortolotto C. Lung-Seeking Metastases. *Cancers* (*Basel*) 2019; 19;11(7):1010.

Sullivan JP, Minna JD, Shay JW. Evidence for self-renewing lung cancer stem cells and their implications in tumor initiation, progression, and targeted therapy. *Cancer Metastasis Rev* 2010; 29(1):61-72.

Sumimoto R, Hirai T, Fujita M, Murakami H, Otake Y, Huang C-L. M2 tumor-associated macrophages promote tumor progression in non-small-cell lung cancer. *Exp Ther Med* 2019; 18(6):4490-4498.

Sung W-W, Wang Y-C, Lin P-L, Cheng Y-W, Chen C-Y, Wu T-C, Le H, *et al*. IL-10 promotes tumor aggressiveness via upregulation of CIP2A transcription in lung adenocarcinoma. *Clin Cancer Res* 2013; 19(15):4092-103.

Takanami I, Imamuma T, Hashizume T, Kikuchi K, Yamamoto Y, Yamamoto T, *et al*. Insulin-like growth factor-II as a prognostic factor in pulmonary adenocarcinoma. *J Surg Oncol.* 1996a; 61(3):205-8.

Takanami I, Imamuma T, Hashizume T, Kikuchi K, Yamamoto Y, Yamamoto T, *et al*. Expression of PDGF, IGF-II, bFGF and TGF-beta 1 in pulmonary adenocarcinoma. *Pathol Res Pract* 1996b; 192(11):1113-20.

Tas F, Bilgin E, Tastekin D, Erturk K, Duranyildiz D. Teicher and Beverly. Serum IGF-1 and IGFBP-3 levels as clinical markers for patients with lung cancer *Biomed Rep* 2016; 4(5):609-614.

Teicher and Beverly. Tumor models in cancer research. *Humana Press* 2002.

The Global Asthma Report 2014. Auckland, New Zealand: Global Asthma Network, 2018.

Tomlinson KL, Davies GC, Sutton DJ, Palframan RT. Neutralisation of interleukin-13 in mice prevents airway pathology caused by chronic exposure to house dust mite. *PLoS One* 2010; 5(10):e13136.

Tompkins DH, Besnard V, Lange AW, Wert SE, Keiser AR, Smith AN, *et al*. Sox2 is Required for Maintenance and Differentiation of Bronchiolar Clara, Ciliated and Goblet Cells. *PLoS ONE* 2009; 4(12):e8248.

Tsai J-R, Wang H-M, Liu P-L, Chen Y-H, Yang M-C, Chou S-H *et al.* High expression of heme oxygenase-1 is associated with tumor invasiveness and poor clinical outcome in non-small cell lung cancer patients. *Cell Oncol (Dordr.)* 2012; 35(6):461-71.

Tumeh PC, Harview CL, Yearley JH, Shintaku IP, Taylor EJM, Robert L, *et al.* PD-1 blockade induces responses by inhibiting adaptive immune resistance. *Nature* 2014; 515(7568):568-71.

Ucero AC, Bakiri L, Roediger B, Suzuki M, Jimenez M, Mandal P, *et al.* Fra-2-expressing macrophages promote lung fibrosis. *JClin Invest* 2019; 129(8):3293–3309.

Vandereyken M, Jacques S, Overmeire EV, Amad M, Rocks N, Delierneux C, *et al.* Dusp3 deletion in mice promotes experimental lung tumour metastasis in a macrophage dependent manner. *PloS One* 2017; 12(10):e0185786.

Varela-Nieto I, Murillo-Cuesta S, Rodriguez-de la Rosa L, Lassatetta L, Contreras J. IGF-I deficiency and hearing loss: molecular clues and clinical implications. *Pediatr Endocrinol Rev* 2013; 10(4):460-472.

Vázquez-Mera S, Pichel JG, Salgado FJ. Involvement of IGF Proteins in Severe Allergic Asthma: New Roles for Old Players. *Arch Bronconeumol* (*Engl Ed*) 2021; S0300-2896(21):00094-6.

Veraldi KL, Gibson BT, Yasuoka H, Myerburg MM, Kelly EA, Balzar S, *et al.* Role of insulin-like growth factor binding protein-3 in allergic airway remodeling. *Am J Respir Crit Care Med* 2009; 180(7):611-617.

Vicent S, López-Picazo JM, Toledo G, Lozano MD, Torre W, Garcia-Corchón C, Quero C*, et al.* ERK1/2 is activated in non-small-cell lung cancer and associated with advanced tumours. *Br J Cancer* 2004; 90(5):1047-1052.

Vlachostergios PJ, Gioulbasanis I, Kamposioras K, Georgoulias P, Baracos VE, Ghosh S, *et al.* Baseline insulin-like growth factor-I plasma levels, systemic inflammation, weight loss and clinical outcome in metastatic non-small cell lung cancer patients. *Oncology* 2011; 81(2):113-8.

Volckaert T, De Langhe S. Lung epithelial stem cells and their niches: Fgf10 takes center stage. *Fibrogenesis Tissue Repair* 2014; 7:8.

Walenkamp MJ, Karperien M, Pereira AM, Hilhorst-Hofstee Y, van Doorn J, Chen JW, *et al.* Homozygous and heterozygous expression of a novel insulin-like growth factor-I mutation. *J Clin Endocrinol Metab* 2005; 90(5):2855-2864.

Walenkamp MJ, de Muinck Keizer-Schrama SM, de Mos M, Kalf ME, van Duyvenvoorde HA, Boot AM, *et al.* Successful long-term growth hormone therapy in a girl with haploinsufficiency of the insulin-like growth factor-I receptor due to a terminal 15q26.2-qter deletion detected by multiplex ligation probe amplification. *J Clin Endocrinol Metab* 2008; 93(6):2421-2425.

Wang Z, Wang Z, Liang Z, Liu J, Shi W, Bai P, *et al.* Expression and clinical significance of IGF-1, IGFBP-3, and IGFBP-7 in serum and lung cancer tissues from patients with non-small cell lung cancer. *Onco Targets Ther* 2013; 6:1437-44.

Wang J, Ding N, Li Y, Cheng H, Wang D, Yang Q, *et al.* Insulin-like growth factor binding protein 5 (IGFBP5) functions as a tumor suppressor in human melanoma cells. *Oncotarget* 2015; 6(24):20636-49.

Wang YA, Sun Y, Palmer J, Solomides C, Huang L-C, Shyr Y, *et al.* IGFBP3 Modulates Lung Tumorigenesis and Cell Growth through IGF1 Signaling. *Mol Cancer Res* 2017; 15(7):896-904.

Wang Z, Li W, Guo Q, Wang Y, Ma L, Zhang X. Insulin-Like Growth Factor-1 Signaling in Lung Development and Inflammatory Lung Diseases. *Biomed Res Int* 2018; 2018:6057589.

Werner H, Bruchim I. The insulin-like growth factor-I receptor as an oncogene. *Arch Physiol Biochem* 2009; 115(2):58-71.

Weroha SJ and Haluska P. The insulin-like growth factor system in cancer. *Endocrinol Metab Clin North Am* 2012; 41(2):335-50.

Whitsett JA, Wert SE, Weaver TE. Alveolar Surfactant Homeostasis and Pathogenesis of Pulmonary Disease. *Annu. Rev. Med* 2010; 61:105–119.

Whitsett JA, Alenghat T. Respiratory epithelial cells orchestrate pulmonary innate immunity. *Nat Immunol* 2015; 16(1):27-35.

Withers DJ, Burks DJ, Towery HH, Altamuro SL, Flint CL, White MF. Irs-2 coordinates Igf-1 receptor-mediated beta-cell development and peripheral insulin signalling. *Nat Genet* 1999; 23(1):32-40.

Xiao Y, Zhu S, Yin W, Liu X, Hu Y. IGFBP‑4 expression is adversely associated with lung cancer prognosis. *Oncol Lett* 2017; 14(6):6876-6880.

Xu J, Bie F, Wang Y, Chen X, Yan T, Du J. Prognostic value of IGF-1R in lung cancer: A PRISMA-compliant meta-analysis. *Medicine* (*Baltimore*) 2019; 98(19):e15467.

Yamaguchi T, Izumi Y, Nakamura Y, Yamazaki T, Shiota M, Sano S, *et al*. Repeated remote ischemic conditioning attenuates left ventricular remodeling via exosome-mediated intercellular communication on chronic heart failure after myocardial infarction. *Int J Cardiol* 2015; 178:239-246.

Yamashita N, Tashimo H, Ishida H, Matsuo Y, Arai H, Nagase H, *et al*. Role of insulin-like growth factor-I in allergen-induced airway inflammation and remodeling. *Cell Immunol* 2005; 235(2): 85-91.

Yang Y-L, Chen M-W, Xian L. Prognostic and clinicopathological significance of downregulated E-cadherin expression in patients with non-small cell lung cancer (NSCLC): a metaanalysis. *PLoS One* 2014; 9(6):e99763.

Yang S, Liu Y, Li M-Y, Ng CSH, Yang S-L, Wang S, *et al*. FOXP3 promotes tumor growth and metastasis by activating Wnt/β-catenin signaling pathway and EMT in non-small cell lung cancer. *Mol Cancer* 2017; 16(1):124.

Yang C-H, Chou C-H, Fu Y-N, Yeh C-L, Cheng H-W, Chang I-C *et al*. EGFR over-expression in non-small cell lung cancers harboring EGFR mutations is associated with marked down-regulation of CD82. Biochim Biophys Acta 2015; 1852(7):1540-9.

Yao M, Ventura PB, Jiang Y, Rodriguez FJ, Wang L, Perry JSA, *et al*. Astrocytic trans-Differentiation Completes a Multicellular Paracrine Feedback Loop Required for Medulloblastoma Tumor Growth. Cell 2020; 180(3):502-520.

Ye J, Wen L, Liu DL, Lai GX. ATF3 and extracellular matrix-related genes associated with the process of chronic obstructive pulmonary. *Lung* 2014; 192(6):881-888.

Ye Z, Huang Y, Ke J, Zhu X, Leng S, Luo H. Breakthrough in targeted therapy for non-small cell lung cancer. *Biomed Pharmacother* 2021; 133:111079.

Ying S, Robinson DS, Meng Q, Rottman J, Kennedy R, Ringler DJ, *et al*. Enhanced expression of eotaxin and CCR3 mRNA and protein in atopic asthma. Association with airway hyperresponsiveness and predominant co-localization of eotaxin mRNA to bronchial epithelial and endothelial cells. *Eur J Immunol* 1997; 27(12):3507-3516.

Yoshema T, Yoshino I, Takenaka T, Kameyama T, Ohba T, Kuniyoshi Y, *et al*. Upregulation of hypoxia-inducible factor-1alpha mRNA and its clinical significance in non-small cell lung cancer. *J Thorac Oncol* 2009; 4(3):284-90.

Yu H, Spitz MR, Mistry J, Gu J, Hong WK, Wu X. Plasma levels of insulin-like growth factor-I and lung cancer risk: a case-control analysis. *J Natl Cancer Inst* 1999; 91(2):151-6.

Yuan J, Yin Z, Kaixiong T, Wang G, Gao J. Function of insulin-like growth factor 1 receptor in cancer resistance to chemotherapy. *Oncol Lett* 2018; 15(1):41-47.

Zaidi MR. The Interferon-Gamma Paradox in Cancer. *J Interferon Cytokine Res* 2019; 39(1):30-38.

Zappa C, Mousa SA. Non-small cell lung cancer: current treatment and future advances. *Transl Lung Cancer Res*. 2016; 5(3):288-300.

Zhang M, Li X, Zhang X, Yang Y, Feng Z, Liu X. Association of serum hemoglobin A1c, C-peptide and insulin-like growth factor-1 levels with the occurrence and development of lung cancer. *Mol Clin Oncol* 2014; 2(4):506-508.

Zhao J, Shi X, Wang T, Ying C, He S, Chen Y. The Prognostic and Clinicopathological Significance of IGF-1R in NSCLC: a Meta-Analysis. *Cell Physiol Biochem* 2017; 43(2):697-704.

Zhao S, Qiu Z, He J, Li L, Li W. Insulin-like growth factor receptor 1 (IGF1R) expression and survival in non-small cell lung cancer patients: a meta-analysis. *Int J Clin Exp Pathol* 2014; 7(10):6694-6704.

Zhao Y-Y, Xue C, Jiang W, Zhao H-Y, Huang Y, Feenstra K, *et al*. Predictive Value of Intratumoral Microvascular Density in Patients with Advanced Non-small Cell Lung Cancer Receiving Chemotherapy Plus Bevacizumab. *J Thorac Oncol* 2012; 7(1):71-5.

Zheng X, Weigert A, Reu S, Guenther S, Mansouri S, Bassaly B, *et al*. Spatial Density and Distribution of Tumor-Associated Macrophages Predict Survival in Non-Small-Cell Lung Carcinoma. *Cancer Res* 2020; 80(20):4414-4425.

Zhu T, Bao X, Chen M, Lin R, Zhuyan J, Zhen T. Mechanisms and Future of Non-Small Cell Lung Cancer Metastasis. *Front Oncol* 2020; 10:585284.

Zoltowska Nilsson AM, Lei Y, Adner M, Nilsson GP. Mast cell-dependent IL-33/ST2 signaling is protective against the development of airway hyperresponsiveness in a house dust mite mouse model of asthma. *Am. J. Physiol. Lung Cell. Mol. Physio*. 2018; 314(3):L484–L492.

Zomer A and van Rheenen J. Implications of Extracellular Vesicle Transfer on Cellular Heterogeneity in Cancer: What Are the Potential Clinical Ramifications?. *Cancer Res* 2016; 15;76(8):2071-5.

Zuazo M, Arasanz H, Fernández-Hinojal G, García-Granda MJ, Gato M, Bocanegra A, *et al*. Functional systemic CD4 immunity is required for clinical responses to PD-L1/PD-1 blockade therapy. *EMBO Mol Med* 2019; 11(7):e10293.

Zuo X, Xu W, Xu, M, Tian R, Moussalli MJ, Mao F, et al. Metastasis regulation by PPARD expression in cancer cells. *JCI Insight* 2017; 2(1):e91419.

8 LIST OF PUBLICATIONS

<u>This thesis is based on the following three publications:</u>

Alfaro-Arnedo E, López IP, Piñeiro-Hermida S, Ucero AC, González-Barcala FJ, Salgado FJ, Pichel JG. IGF1R As a Potential Pharmacological Target in Allergic Asthma. *Biomedicines* 2021; 9(8):912.

Alfaro-Arnedo E, López IP, Piñeiro-Hermida S, Canalejo M, Gotera C, Sola JJ, Roncero A, Peces-Barba G, Ruíz-Martínez C, Pichel JG. IGF1R acts as a cancer-promoting factor in the tumor microenvironment facilitating lung metastasis implantation and progression. (Under review)

Alfaro-Arnedo E, *et al*. IGF1R as a candidate biomarker in patients with allergic asthma. (In preparation)

<u>I also contributed to 11 additional publications that were not included within the body of this thesis:</u>

Pérez-Matute P, López IP, Íñiguez M, Recio-Fernández E, Torrens R, Piñeiro-Hermida S, **Alfaro-Arnedo E**, Wirthgen E, Hoeflich A, Oteo JA, Pichel JG. Involvement of IGF1R in metabolic homeostasis: effects of aging and obesity. (In preparation)

Ezquerro C, **Alfaro-Arnedo E**, López IP, Serrano E, Lalinde E, Larráyoz IM, Pichel JG, García-Marínez J, Berenguer JR. Highly Emissive Hybrid Mesoporous Organometallo-Silica Nanoparticles for Bioimaging. (In preparation)

Urtubia A**,** *et al*. Whole transcriptome analysis on lungs of bleomicin or house dust mite-exposed IGF1R-deficient mice provides new insights in acute lung injury and allergic airway inflammation. (In preparation)

Lalinde E, Lara R, Millán G, Moreno MT, **Alfaro-Arnedo E**, López IP, Larráyoz IM, Pichel JG. Investigation on Optical and Biological Properties of 2-(4-Dimethylaminophenyl)benzothiazole Based Cycloplatinated Complexes. *Chemistry* 2021; doi.org/10.1002/chem.202102737.

Martínez-Junquera M, Lalinde E, Moreno MT, **Alfaro-Arnedo E**, López IP, Larráyoz IM, Pichel JG. Luminescent Cyclometalated Platinum(II) Complexes with Acyclic Diaminocarbene Ligands: Structural, Photophysical and Biological Properties. *Dalton Trans* 2021;50(13):4539-4554.

Sevilla-Montero J, Labrousse-Arias D, Fernández-Pérez C, Fernández-Blanco L, Barreira B, Mondéjar-Parreño G, **Alfaro-Arnedo E**, López IP, Pérez-Ria S, Peces-Barba G, Pichel JG, Ivo Peinado V, Cogolludo A, Calzada MJ. Cigarette smoke directly promotes pulmonary arterial remodeling and Kv7.4 channel dysfunction. *AM j Respir Crit Care Med* 2021; 203(10):1290-1305.

Martínez-López D, García-Iriepa C, Piñeiro-Hermida S, López IP, Fernández-Martínez D, **Alfaro-Arnedo E**, Pichel JG, Campos PJ, Sampedro D. Design and synthesis of novel metronidazole-based photoswitches with potential biological appliccations. *ChemPhotoChem* 2019*;* 3:425–430.

Millán G, Giménez N, Lara R, Berenguer JR, Moreno MT, Lalinde E, **Alfaro-Arnedo E**, López IP, Piñeiro-Hermida S, Pichel JG. Luminescent cycloplatinated complexes with biologically relevant phosphine ligands: optical and cytotoxic properties. *Inorg Chem* 2019;58(2):1657-1673

Lalinde E, Lara R, López IP, Moreno MT, **Alfaro-Arnedo E**, Pichel JG, Piñeiro-Hermida S. Benzothiazole based cycloplatinated chromophores: synthetic, optical and biological studies. *Chem Eur J* 2018; 24(10):2440-2456.

Piñeiro-Hermida S, **Alfaro-Arnedo E**, Gregory JA, Torrens R, Ruíz-Martínez C, Adner M, López IP, Pichel JG. Characterization of the acute inflammatory profile and resolution of airway inflammation after *Igf1r*-gene targeting in a murine model of HDM-induced asthma. *PLoS One* 2017; 12(12):e0190159.

Piñeiro-Hermida S, López IP, **Alfaro-Arnedo E**, Torrens R, Iñiguez M, Alvarez-Erviti L, Ruíz-Martínez C, Pichel JG. IGF1R deficiency attenuates acute inflammatory response in a bleomycin-induced lung injury mouse model. *Sci Rep* 2017; 7(1):4290.

9 APPENDICES

Article

IGF1R as a Potential Pharmacological Target in Allergic Asthma

Elvira Alfaro-Arnedo [1], Icíar P. López [1], Sergio Piñeiro-Hermida [2], Álvaro C. Ucero [3,4],
Francisco J. González-Barcala [5,6,7], Francisco J. Salgado [8] and José G. Pichel [1,7,*]

[1] Lung Cancer and Respiratory Diseases Unit, Center for Biomedical Research of La Rioja (CIBIR),
Fundación Rioja Salud, 26006 Logroño, Spain; ealfaro@riojasalud.es (E.A.-A.); iplgarcia@riojasalud.es (I.P.L.)
[2] Telomeres and Telomerase Group, Molecular Oncology Program, Spanish National Cancer Centre (CNIO),
28029 Madrid, Spain; spineiro@cnio.es
[3] Thoracic Oncology, Research Institute Hospital 12 de Octubre, 28041 Madrid, Spain; acuceroh@ucm.es
[4] Department of Physiology, Faculty of Medicine, Complutense University, 28040 Madrid, Spain
[5] Department of Respiratory Medicine, University Hospital of Santiago de Compostela (CHUS),
15706 Santiago de Compostela, Spain; francisco.javier.gonzalez.barcala@sergas.es
[6] Health Research Institute of Santiago de Compostela (FIDIS), 15706 Santiago de Compostela, Spain
[7] Spanish Biomedical Research Networking Centre-CIBERES, 15706 Santiago de Compostela, Spain
[8] Department of Biochemistry and Molecular Biology, Faculty of Biology-Biological Research Centre (CIBUS),
Universidad de Santiago de Compostela, 15706 Santiago de Compostela, Spain;
franciscojavier.salgado@usc.es
* Correspondence: jgpichel@riojasalud.es; Tel.: +34-638-056-014

Abstract: Background: Asthma is a chronic lung disease characterized by reversible airflow obstruction, airway hyperresponsiveness (AHR), mucus overproduction and inflammation. Although Insulin-like growth factor 1 receptor (IGF1R) was found to be involved in asthma, its pharmacological inhibition has not previously been investigated in this pathology. We aimed to determine if therapeutic targeting of IGF1R ameliorates allergic airway inflammation in a murine model of asthma. Methods: C57BL/6J mice were challenged by house dust mite (HDM) extract or PBS for four weeks and therapeutically treated with the IGF1R tyrosine kinase inhibitor (TKI) NVP-ADW742 (NVP) once allergic phenotype was established. Results: Lungs of HDM-challenged mice exhibited a significant increase in phospho-IGF1R levels, incremented AHR, airway remodeling, eosinophilia and allergic inflammation, as well as altered pulmonary surfactant expression, all of being these parameters counteracted by NVP treatment. HDM-challenged lungs also displayed augmented expression of the IGF1R signaling mediator p-ERK1/2, which was greatly reduced upon treatment with NVP. Conclusions: Our results demonstrate that IGF1R could be considered a potential pharmacological target in murine HDM-induced asthma and a candidate biomarker in allergic asthma.

Keywords: asthma; allergy; house dust mite; IGF1R; NVP-ADW742; pharmacological blockade

1. Introduction

Asthma is a chronic inflammatory disease characterized by reversible airflow obstruction, airway hyperresponsiveness (AHR) and inflammation [1]. The house dust mite (HDM) is ubiquitous in human habitats and a significant factor underlying allergic asthma since 65 to 130 million people worldwide are sensitive to HDM [2,3] Most asthmatics are well controlled on inhaled corticosteroids, but some patients, including those with eosinophilic asthma, continue to experience symptoms and exacerbations, with no effective treatments [4]. In this sense, the identification of asthma phenotypes, as well as underling Th2-high (eosinophilic) or Th2-low (noeosinophilic) endotypes, represent a key point for the development of novel therapeutic strategies [5].

The insulin-like growth factor 1 receptor (IGF1R) is a ubiquitously expressed membrane-bound tyrosine kinase receptor that recognizes its two major ligands, IGF1 and IGF2. IGF activity is modulated by six high-affinity IGF binding proteins (IGFBPs) that control multiple essential cellular functions [6]. IGF activity is highly relevant in several chronic lung

pathologies with an inflammatory component [7–9]. Accordingly, IGF1R was recently identified as a novel outcome biomarker in critical COVID-19 patients to predict mortality [10], but it has not been evaluated in asthmatics.

Specifically, IGF1 signaling has been implicated in activation of different aspects of the asthmatic response and IGFBP3 was suggested to be involved in allergic airway inflammation [7]. On the other hand, the serum biomarker IGF-ALS (IGF Binding Protein Acid Labile Subunit) was recently reported to be capable of differentiating moderate-severe allergic from non-allergic asthma [11]. In addition, IGF1R was found to be upregulated in eosinophils from bronchoalveolar lavage of mild asthmatic patients [12]. In mice, IGF1 mediates allergic airway inflammation, and IGFBP3 was shown to block the effects of asthma [13,14]. Notably, we have reported that IGF1R plays a relevant role in initiation of the inflammatory response and that *Igf1r*-gene targeting in mice attenuates allergic airway inflammation [15–17].

Anti-IGF1R therapies, including small tyrosine kinase inhibitors (TKIs), continue to be valid targets for patients with cancer [18,19]. In this sense, the TKI NVP-ADW742 (NVP) was reported to suppress multiple myeloma tumor growth [20]. However, the IGF1R inhibitor NVP has still not been investigated in asthma. Here, we aimed to determine if therapeutic targeting of IGF1R ameliorates allergic airway inflammation in a murine model of asthma. For this purpose, C57BL/6J mice were challenged with HDM extract and therapeutically treated with NVP.

2. Materials and Methods

2.1. HDM Sensitization Protocol and Therapeutic Inhibition of IGF1R

Eight-week-old C57BL/6J mice were intranasally (i.n.) challenged with 40 μg of house dust mite (HDM) extract or PBS for four weeks [15]. Mice were also intraperitoneally (i.p.) injected with 200 μL of IGF1R tyrosine kinase inhibitor (TKI) NVP-ADW742 or vehicle (DMSO) twice a day during the last one or two weeks of the HDM protocol (Figure 1A). The concentration and dose-response of NVP were previously assessed by Mitsiades et al. [20] and Cintron-Colon et al. [21], respectively. For additional details, see Supplementary Materials.

2.2. In Vivo Assessment of Lung Function

Mice were anesthetized, intubated with a 24-gauge catheter and intravenously injected with 1 mg/kg of methacholine (MCh). Lung function was assessed in a plethysmograph to determine LR (lung resistance) and Cdyn (dynamic compliance). For additional details, see Supplementary Materials.

2.3. Sample Collection and Preparation

Animals were euthanized using 10 μL/g of ketamine-xylazine. Blood was then collected and lungs were lavaged with PBS. Right lung lobes were dissected and snap frozen for quantitative PCR (qPCR) and ELISA analyses, and the left lung lobe was harvested for histopathological evaluation or immunohistochemistry. Femurs were dissected to isolate bone marrow. For additional details, see Supplementary Materials.

2.4. Histopathological and Immunostaining Analysis

Hematoxylin and eosin (H&E) staining was performed for the quantification of inflammation and to assess airway thickness. Periodic acid-Schiff (PAS) and Masson's trichrome staining served to evaluate the number of mucus-producing cells and collagen deposition. p-ERK1/2 (p-42/44), CD45 and SMA antibodies were used to evaluate airway p-ERK1/2+ and CD45+ areas, and smooth muscle thickness. SFTPC antibody was used to determine the number of SFTPC+ cells in the lung. SOX2, SCGB1A1 and MUC5AC antibodies served to quantify the degree of bronchial differentiation and for the assessment of goblet cell hyperplasia, respectively. For additional details, see Supplementary Materials.
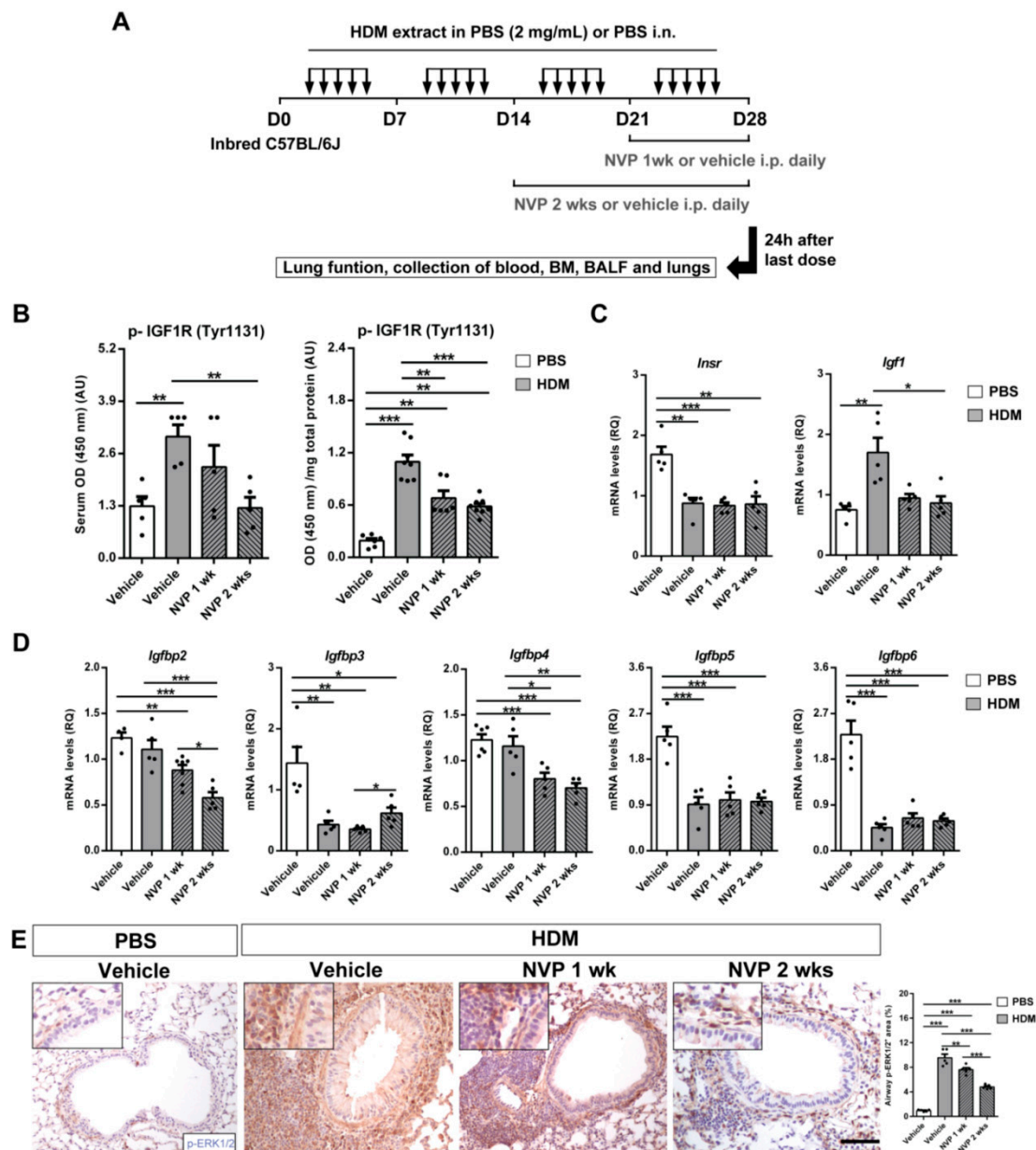
Figure 1. Protocol for HDM exposure and treatment with the IGF1R inhibitor NVP, as well as p-IGF1R and IGF system gene expression levels in the lung. (**A**) Mice were challenged by intranasal (i.n.) administration of HDM extract in phosphate buffer saline (PBS) or equal volume of vehicle, five days a week for four weeks. Mice also received intraperitoneal (i.p.) injections of the IGF1R inhibitor NVP or equal volume of the vehicle (2% DMSO) twice daily during the last one (NVP 1 week) or two weeks (NVP 2 weeks) of the HDM protocol. Lung function assessment and collection of blood, bone marrow (BM), BALF and lungs were performed 24 h after the last exposure on day (**D**) 28. (**B**) p-IGF1R protein levels in both serum and lung homogenates from HDM-challenged mice treated with NVP vs. controls (*n* = 6–8 mice per group). (**C,D**) Lung tissue mRNA expression of IGF system-related genes *Insr*, *Igf1* (**C**), and *Igfbp2, Igfbp3, Igfbp4, Igfbp5, Igfbp6* (**D**) normalized to 18S expression in HDM-challenged mice treated with NVP vs. controls (*n* = 5 mice per group). (**E**) Representative immunostains of proximal airways for p-ERK1/2 (p-42/44) (brown), and quantification of p-ERK1/2$^+$ area (%) in lung sections from HDM-challenged mice treated with NVP vs. controls (*n* = 5 mice per group; scale bar: 50 μm). Insets illustrate *p-ERK1/2* expression in smooth muscle cells and peribronchiolar areas. Data are expressed as mean ± SEM. * *p* < 0.05; ** *p* < 0.01; *** *p* < 0.001 (Mann–Whitney U test or Student´s *t*-test for comparing two groups, and Kruskal–Wallis test or ANOVA multiple comparison test for grouped or multivariate analysis).

2.5. RNA Isolation, Reverse Transcription and qPCR

Inferior right lung lobes were homogenized in TRIzol, and then RNA was isolated and reverse-transcribed to cDNA. cDNA samples were amplified by qPCR for each primer pair assayed (Table S1). Results were normalized using the 18S rRNA gene (*Rn18s*). For additional details, see Supplementary Materials.

2.6. Mouse ELISAS

Serum total IgE, IL13 and p-IGF1R levels were assessed with mouse ELISA kits. Superior right lung lobes were homogenized in RIPA Buffer. IL13, IL33, CCL11 and p-IGF1R levels were evaluated in homogenized lung tissue lysates using mouse ELISA kits, and normalized to total lung protein levels. For additional details, see Supplementary Materials.

2.7. Statistics

Following a Shapiro–Wilk normality test, the statistical significance was determined using the Mann–Whitney U test or Student's *t*-test for comparing 2 groups and the Kruskal–Wallis test or ANOVA multiple comparison test for grouped or multivariate analysis. Statistical analyses were carried out using SPSS Statistics Software v21 for Windows (IBM, Armonk, NY, USA). For all analysis, a *p* value < 0.05 was considered statistically significant.

3. Results

3.1. Efficient Depletion of IGF1R and IGF System Gene Expression upon HDM Exposure and Pharmacological Blockade of IGF1R

C57BL/6J mice were challenged with HDM extract and therapeutically treated with NVP (Figure 1A). NVP administration did not induce significant changes in body weight (Figure S1). Noteworthy, treatment with the vehicle of NVP (DMSO) did not induce inflammation in lungs of inbred C57BL/6J mice (Figure S2). In accordance, several drugs were previously reported to be dissolved in up to 5% DMSO for their use in preclinical mouse models [22,23].

IGF1R inhibition and assessment of IGF system gene expression were performed on lung extracts of HDM-challenged mice treated with NVP vs. controls (HDM + vehicle and PBS + vehicle) (Figure 1B–D). Phospho(p)-IGF1R levels quantified by ELISA were greatly increased in HDM control mice both in serum and lung homogenates. This increment was significantly reduced in NVP-treated mice particularly NVP after 2 weeks of treatment (NVP 2 weeks) (Figure 1B). mRNA levels of insulin receptor (*Insr*) were significantly decreased in all HDM-challenged groups. In addition, HDM treatment increased *Igf1* mRNA levels that were reverted by NVP treatment (Figure 1C). Regarding mRNA expression of IGFBP markers, *Igfbp2* and *Igfbp4* were found to be significantly reduced in NVP-treated mice and *Igfbp3*, *Igfbp5* and *Igfbp6* levels showed a significant depletion upon HDM exposure. Specifically, *Igfbp3* levels were found slightly increased in the NVP 2 weeks group (Figure 1D). In addition, lung tissue p-ERK1/2 (p42/44) expression evaluated by immunohistochemistry was highly augmented in HDM controls while this increment was significantly reduced in NVP-treated mice particularly after 2 weeks of treatment. Interestingly, expression pattern of p-ERK1/2 was specifically noticed in peribronchiolar smooth muscle cells and inflammatory areas (Figure 1E).

3.2. Therapeutic Inhibition of IGF1R during HDM Exposure Attenuates Peripheral Blood and Bone Marrow Eosinophilia and the Increase in Serum IL13

We first assessed peripheral blood cellularity and serum IgE and IL13 levels in HDM-challenged mice treated with NVP vs. controls (Figure 2A,B). The proportion of eosinophils exhibited a marked increase in HDM control mice. This increase was significantly reduced in NVP-treated mice, reaching basal levels in the NVP 2 weeks group. We did not observe changes in the proportion of neutrophils and lymphocytes between experimental groups. In addition, monocyte presence was reduced in HDM-challenged mice compared to PBS controls (Figure 2A). We next measured serum IgE and IL13 levels and found that both

were clearly induced in HDM control mice. Whereas IgE was not affected by NVP, IL13 levels were significantly reduced upon NVP treatment, reaching basal levels in the NVP 2 weeks group (Figure 2B).

Bone marrow cellularity was also assessed in all experimental groups. A significant increase in total cell numbers, eosinophil and neutrophil counts was observed in HDM controls. Interestingly, eosinophil numbers returned to basal levels after one week of NVP treatment, and neutrophil counts were only normalized in the NVP 2 weeks group (Figure 2C).

3.3. Pharmacological Targeting of IGF1R Ameliorates Pulmonary Pathology upon HDM Exposure

First, cellularity and total protein levels in bronchoalveolar lavage fluid (BALF) were assessed (Figure 3A,B). Total and differential BALF cells counts were found increased in HDM control mice and this increment was strongly reduced in NVP-treated mice (Figure 3A). In addition, the increase in total protein content in BALF of HDM control mice remained comparable to unchallenged controls in the NVP 2 weeks group (Figure 3B).

Next, we evaluated several airway remodeling indicators including inflamed lung area, leukocyte presence, airway thickness, mucus-producing cells, collagen deposition and smooth muscle (SM) thickness (Figure 3C). Notably, the highly increased values found for all these parameters in HDM-challenged mice were significantly reduced in the NVP 2 weeks group. NVP treatment for one week was less effective, counteracting only inflamed lung area and airway thickness (Figure 3C).

3.4. Pharmacological Blockade of IGF1R Attenuates AHR and Ameliorates Surfactant Deregulation after HDM Challenge

In order to evaluate lung function following HDM-induced allergy, we assessed AHR to methacholine by plethysmography. Methacholine administration induced a marked AHR with increased lung resistance (LR) in HDM controls with respect to PBS challenged mice, whilst mice treated for two weeks with NVP did not show such an increase. However, the dynamic compliance (Cdyn) was reduced in HDM-challenged mice when compared to PBS controls and NVP-treated mice showed a lower reduction in Cdyn (Figure 4A).

Gene expression of the surfactant (*Sftp*) markers a1, b, c and d was evaluated to elucidate how the pharmacological blockade of IGF1R modulates their production. Whereas *Sftpa1* and *Sftpd* mRNA expression levels were significantly increased in HDM controls, *Sftpb* and *Sftpc* levels were severely depleted. Interestingly, NVP treatment reversed these changes, especially in the NVP 2 weeks group, in which *Sftpa1* and *Sftpd* mRNA levels were normalized (Figure 4B). In accordance, immunofluorescence for SFTPC showed that the number of SFTPC+ cells was strongly reduced in HDM control mice, and this decrease was counteracted only in the NVP 2 weeks group (Figure 4C).

3.5. Therapeutic Inhibition of IGF1R Halts Expression of Allergic Airway Inflammation Markers after HDM Exposure

Total lung mRNA expression and protein levels of allergic airway inflammation markers were assessed on lung homogenates of HDM-challenged mice treated with NVP vs. controls by qPCR and ELISA, respectively. With the exception of *Il1b*, which did not show any significant difference between groups, mRNA levels of all these markers were strongly induced by HDM (Figure 5A). Whereas *Il33*, *Cd274* (PDL-1), *Cd4*, *Il13*, *Tnf*, *Cxcl1* and *Ccl2* mean levels remained around normal after treatment with NVP, *Il4* and *Ccl11* required NVP treatment for two weeks to amend the HDM response. *Pdcd1* (PD-1) showed a compellingly reduced level of mRNA in both NVP-treated groups (Figure 5A). In agreement, IL33, IL13 and CCL11 protein levels in lung homogenates were clearly induced in HDM controls and significantly reduced in NVP-treated mice (Figure 5B).
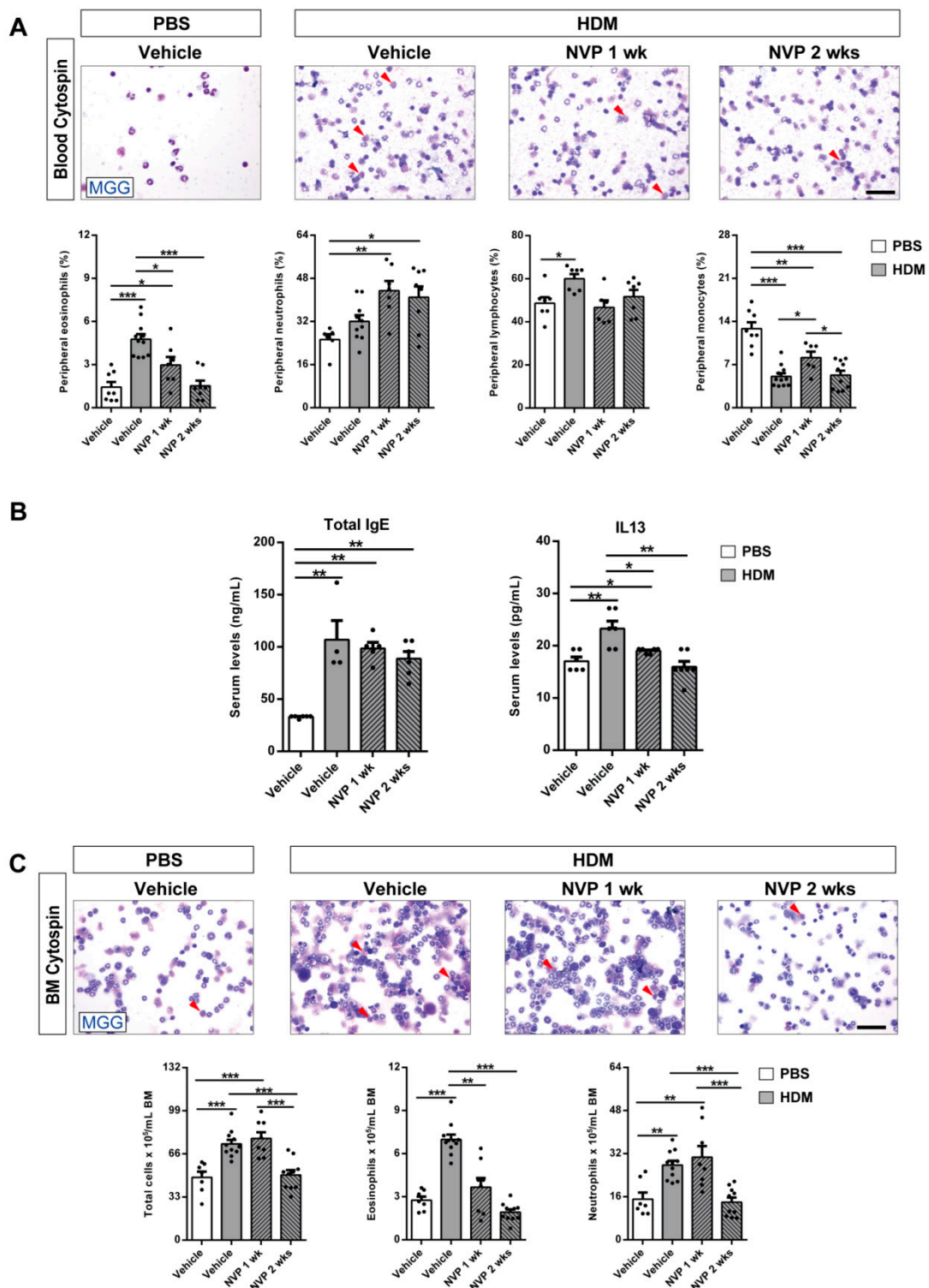
Figure 2. Pharmacological blockade of IGF1R depletes eosinophil presence in peripheral blood and bone marrow and attenuates the increase in serum IL13 levels after HDM exposure. (**A**,**C**) Representative images showing May-Grünwald/Giemsa (MGG) stained peripheral blood and bone marrow cytospin preparations (red arrowheads indicate eosinophils), and differential cell counts for eosinophils, neutrophils, lymphocytes and monocytes in peripheral blood (**A**), and total cells, eosinophils and neutrophils in bone marrow (**C**) from HDM-challenged mice treated with NVP vs. controls (n = 7–10 mice per group; scale bars: 50 μm). (**B**) Total serum IgE and IL13 levels from HDM-challenged mice treated with NVP vs. controls (n = 5–7 mice per group). Data are expressed as mean ± SEM. * p < 0.05; ** p < 0.01; *** p < 0.001 (Mann–Whitney U test or Student´s t-test for comparing two groups and Kruskal–Wallis test or ANOVA multiple comparison test for grouped or multivariate analysis).
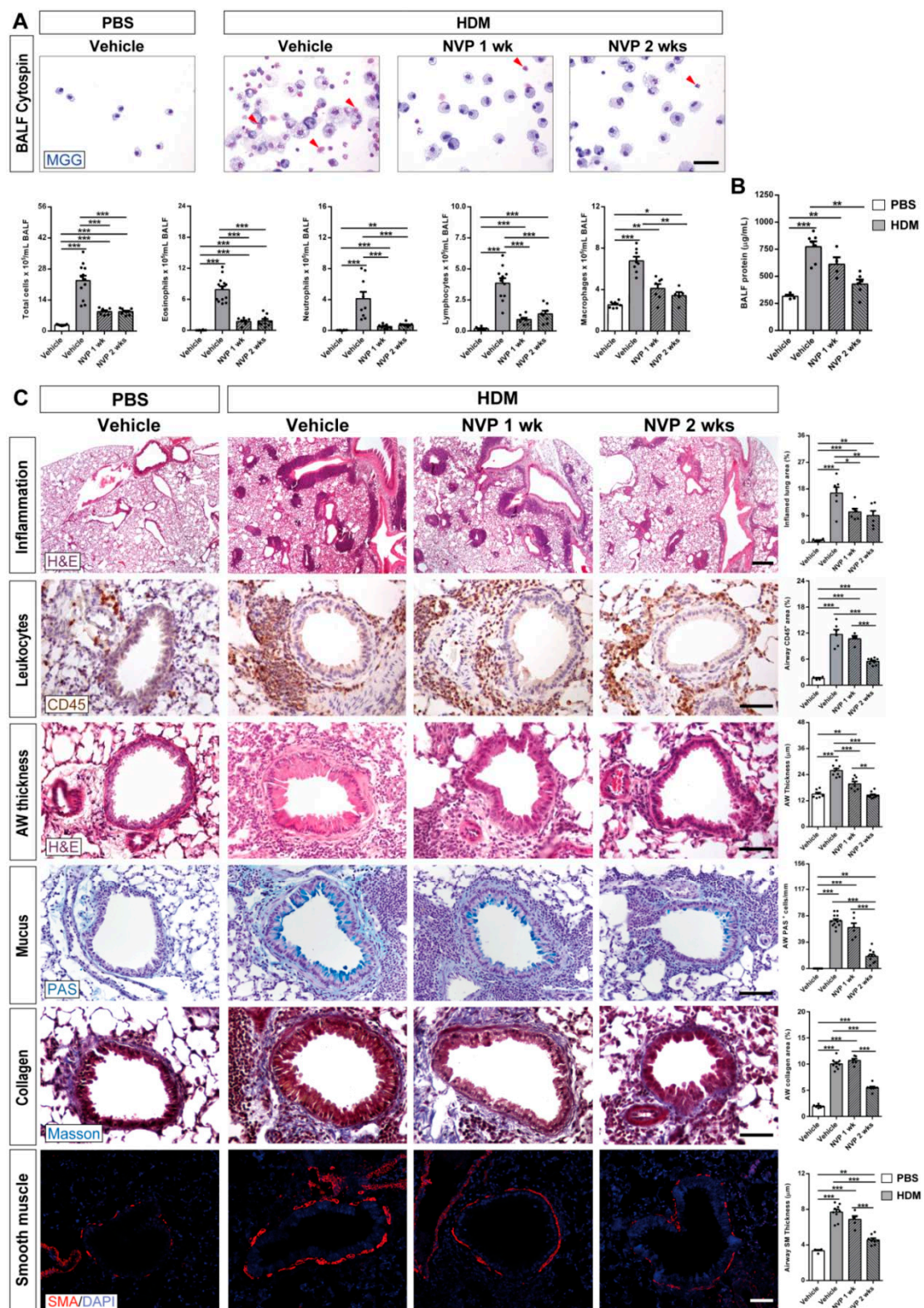
Figure 3. Pharmacological blockade of IGF1R attenuates pulmonary pathology after HDM induced allergy. (**A**) Representative images showing May-Grünwald/Giemsa (MGG) stained BALF cytospin preparations (red arrowheads indicate eosinophils), and total and differential BALF cell counts for eosinophils, neutrophils, lymphocytes and macrophages in HDM-challenged mice treated with NVP vs. controls (*n* = 7–12 mice per group; scale bar: 50 μm). (**B**) Total protein concentration in BALF of HDM-challenged mice treated with NVP vs. controls (*n* = 5–8 mice per group). (**C**) Representative images of lung inflammation and histopathology of the proximal airways, and respective quantifications of inflamed lung areas (%) (H&E), presence of peribronchiolar CD45+ area (leukocytes) (%) (brown), airway (AW) epithelium thickness (H&E),

number of airway PAS+ cells (mucus-producing cells) (blue), peribronchiolar airway collagen content (%) (Masson in blue) and airway smooth muscle (SM) thickness (SMA in red). These parameters were measured in lung sections from HDM-challenged mice treated with NVP vs. controls (n = 6–10 mice per group; scale bars: 50 μm except for the inflammation panel (400 μm)). Quantifications were performed in five different fields in a random way. Data are expressed as mean ± SEM. * $p < 0.05$; ** $p < 0.01$; *** $p < 0.001$ (Mann–Whitney U test or Student´s t-test for comparing two groups and Kruskal–Wallis test or ANOVA multiple comparison test for grouped or multivariate analysis).

Figure 4. Therapeutic inhibition of IGF1R attenuates AHR and normalizes pulmonary surfactant expression upon HDM-induced allergy. (**A**) Quantification of lung resistance (LR) and dynamic compliance (Cdyn) to methacholine (MCh) evaluated by plethysmography (n = 4–8 mice per group) and (**B**) changes in lung tissue mRNA expression surfactant (*Sftp*) markers *Sftpa1, b, c* and *d*, normalized to 18S expression in HDM-challenged mice treated with NVP vs. controls (n = 5 mice per group). (**C**) Representative immunostains for SFTPC (green) (white arrowheads), and quantification of the number of SFTPC+ cells per unit area (mm^2) in lung sections from HDM-challenged mice treated with NVP vs. controls (n = 5–10 mice per group; scale bar: 50 μm). Data are expressed as mean ± SEM. * $p < 0.05$; ** $p < 0.01$; *** $p < 0.001$; # $p < 0.05$ (comparisons within the same group) (Mann–Whitney U test or Student´s t-test for comparing two groups and Kruskal–Wallis test or ANOVA multiple comparison test for grouped or multivariate analysis).
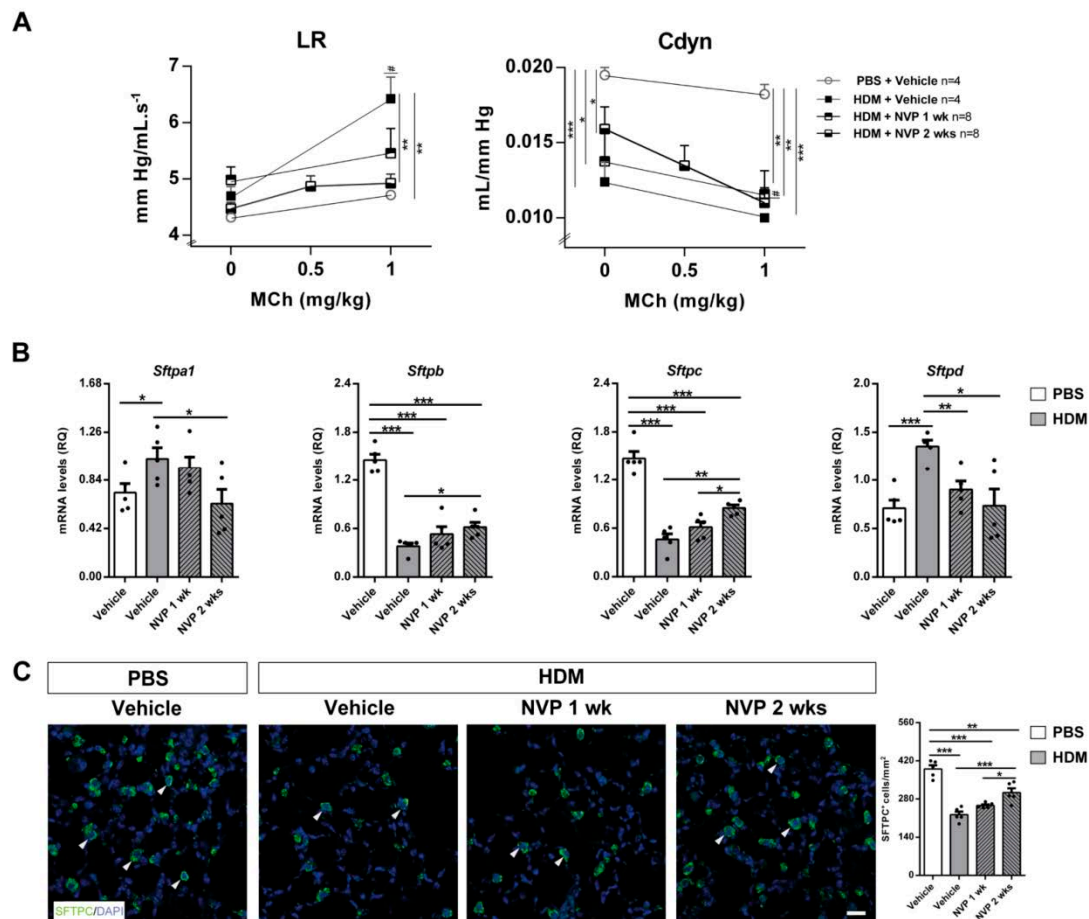
Figure 5. Therapeutic inhibition of IGF1R diminishes expression of allergic airway inflammation markers after HDM exposure. (**A**) Lung tissue mRNA expression levels of *Il33* (dendritic cell activation), *Cd274* (PD-L1) and *Pdcd1* (PD-1) (T cell response), *Cd4* (T cell marker), *Il4* and *Il13* (Th2 cytokines), *Tnf* and *Il1b* (Th1 cytokines), *Cxcl1* (neutrophil chemotaxis), *Ccl2* (macrophage chemotaxis) and *Ccl11* (eosinophil chemotaxis) normalized to 18S expression in HDM-challenged mice treated with NVP vs. controls (*n* = 5 mice per group). (**B**) IL33, IL13 and CCL11 protein levels in lung homogenates from HDM-challenged mice treated with NVP vs. controls (*n* = 5–7 mice per group). Data are expressed as mean ± SEM. * $p < 0.05$; ** $p < 0.01$; *** $p < 0.001$ (Mann–Whitney U test or Student´s *t*-test for comparing two groups and Kruskal–Wallis test or ANOVA multiple comparison test for grouped or multivariate analysis).
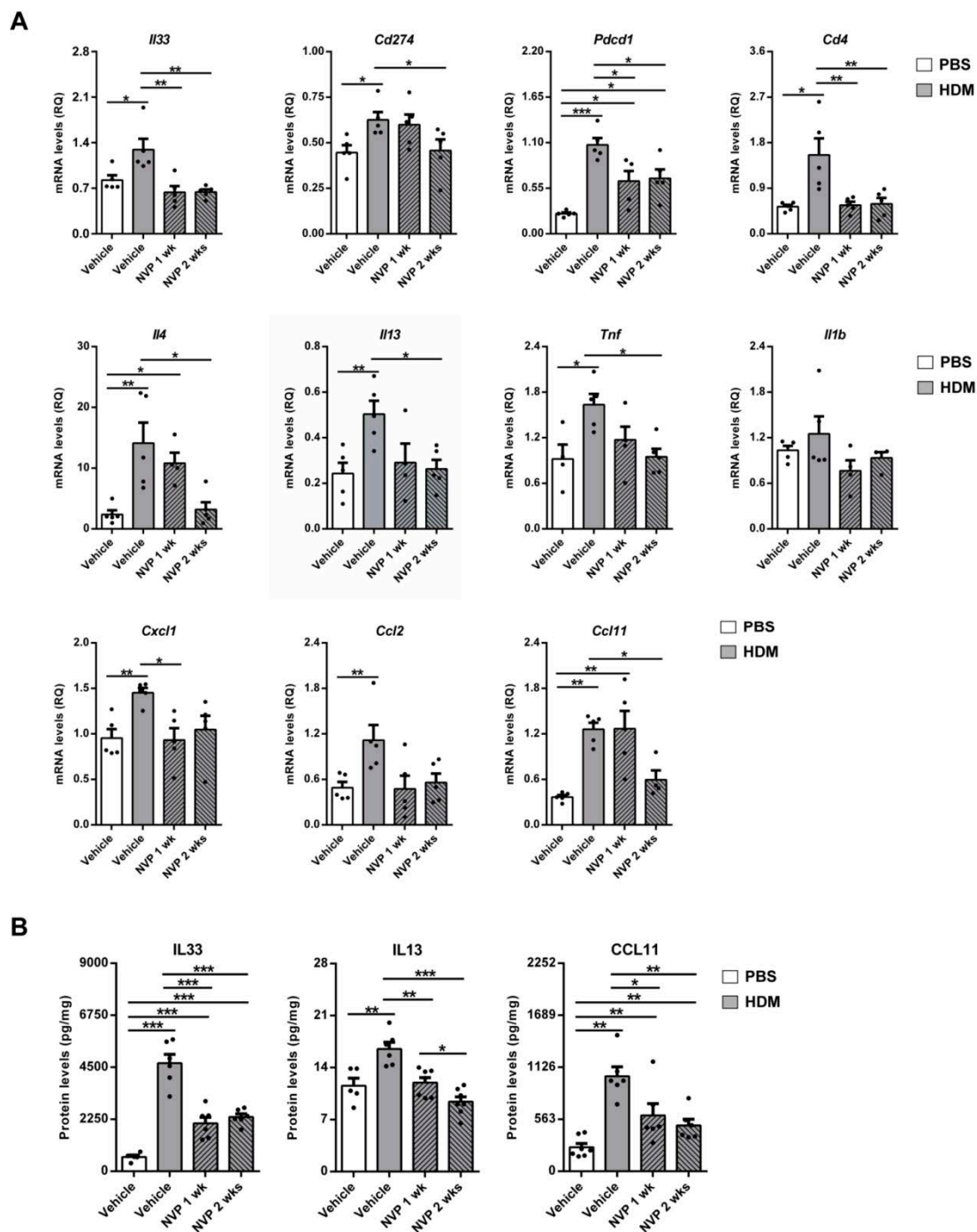
3.6. IGF1R Blockade Depleted Bronchiolar Epithelial Differentiation and Goblet Cell Hyperplasia upon HDM-Induced Allergy

In order to evaluate bronchiolar differentiation and goblet cell hyperplasia, we immunostained SOX2 and MUC5AC, respectively. We observed an increased proportion of SOX2+ cells and double stained SCGB1A1+-MUC5AC+ cells upon HDM challenge, which were significantly reduced in the NVP 2 weeks group (Figure 6A). To complement these data, we also assessed mRNA expression levels of the goblet cell hyperplasia markers *Sox2*, *Muc5ac*, *Foxm1* and *Spdef*. Results on *Sox2* and *Muc5ac* mirror immunostaining data. *Foxm1* and *Spdef* followed mRNA expression profiles of allergic airway inflammation markers. In all cases, IGF1R inhibition with NVP was able to reverse the increase in mRNA expression triggered by the HDM challenge (Figure 6B).
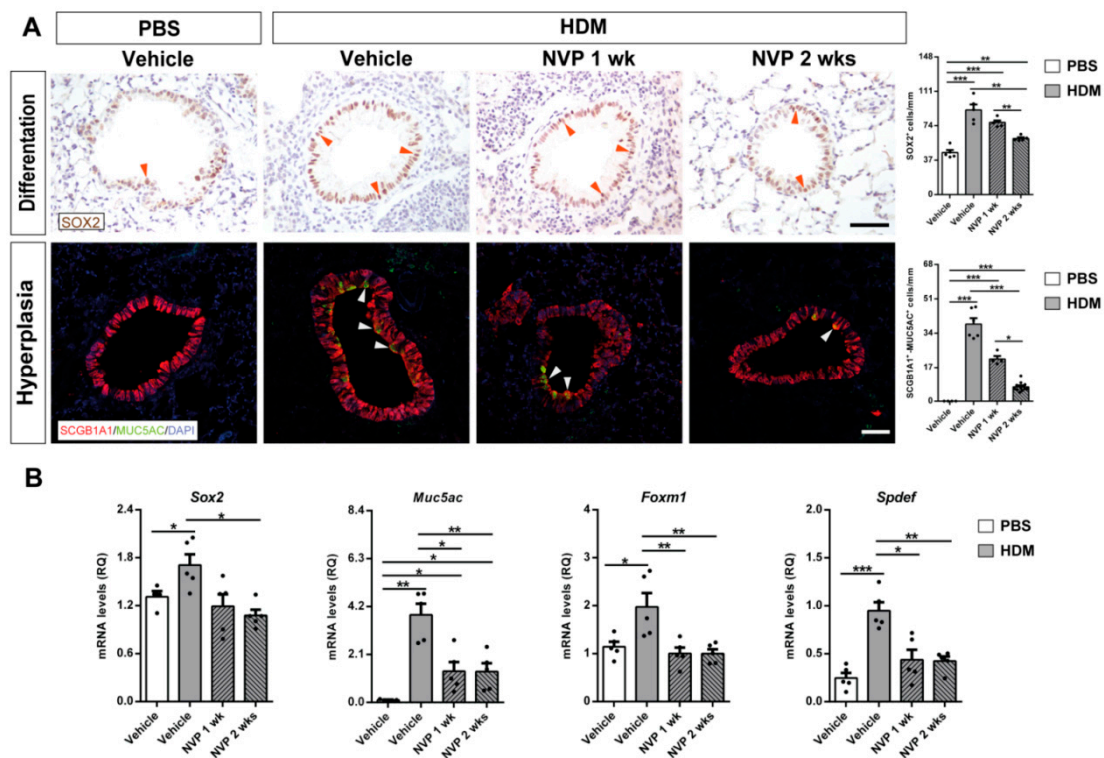

Figure 6. Pharmacological targeting of IGF1R attenuates bronchial differentiation and goblet cell hyperplasia upon HDM-induced allergy. (**A**) Representative immunostains of proximal airways for SOX2 (bronchial differentiation) (brown; orange arrowheads indicate SOX2+ cells), as well as double immunofluorescent stains for SCGB1A1 (red) (club cell marker) and MUC5AC (green) (goblet cell hyperplasia) (white arrowheads indicate double SCGB1A1+-MUC5AC+ cells). Quantification of SOX2+ and double SCGB1A1+-MUC5AC+ cells per epithelium length (mm) in lung sections from HDM-challenged mice treated with NVP vs. controls (*n* = 5–10 mice per group; scale bars: 50 μm). (**B**) Lung mRNA expression levels of *Sox2* (bronchial differentiation) and *Foxm1, Spdef* and *Muc5ac* markers (goblet cell hyperplasia) normalized to 18S expression in HDM-challenged mice treated with NVP vs. controls (*n* = 5 mice per group). Quantifications in lung sections were performed in 5 different bronchi in a random manner. Data are expressed as mean ± SEM. * *p* < 0.05; ** *p* < 0.01; *** *p* < 0.001 (Mann–Whitney U test or Student´s *t*-test for comparing two groups and Kruskal–Wallis test or ANOVA multiple comparison test for grouped or multivariate analysis).

4. Discussion

We aimed to determine if therapeutic targeting of IGF1R ameliorates established allergic airway inflammation in a murine model of HDM-induced asthma.

HDM-induced allergy has been successfully proven for the study of asthma pathobiology [15,16,24]. Therefore, we deemed that our asthma model was appropriate for testing the in vivo anti-asthmatic efficacy of IGF1R inhibition using the IGF1R TKI inhibitor NVP-ADW742 (NVP). NVP was reported to have an inhibitory effect against IGF1R that

was >16-fold more potent than towards InsR, the kinase with the highest homology to IGF1R, and exhibited no symptoms of toxicity [20]. Even though IGF1R activation levels significantly increased in HDM-exposed mice in serum and lung homogenates, NVP treatment counteracted IGF1R phosphorylation in both compartments. We also assessed expression of p-ERK1/2, which is a major IGF1R MAP kinase signaling mediator [7]. In this regard, increased expression of p-ERK1/2 after HDM-induced allergy was attenuated upon treatment with the IGF1R TKI inhibitor NVP. Accordingly, ERK1/2 was reported to stimulate eosinophil chemotaxis, differentiation, cytokine production as well as eotaxin-induced degranulation [25–27]. Furthermore, Bates et al. reported that human airway eosinophils respond to several allergic airway inflammation-related chemoattractants with increased activation of the Ras–ERK cascade [28].

We have previously shown that mRNA expression of the IGF system genes *Insr*, *Igfbp3* and *Igfbp5* was repressed upon HDM exposure [15]. In particular, increased expression of *Igfbp3* in the NVP 2 weeks group corresponds with its protective role in asthma [14]. In contrast, *Igfbp2* and *Igfbp4* expression depends solely on IGF1R activation since they were only found diminished by NVP treatment. Increased expression of *Igf1* by HDM, which lowered to basal levels upon treatment with NVP, is in accordance with our previous findings [16]. HDM-mediated induction of *Igf1* could be responsible for IGF1R phosphorylation to promote the asthmatic response, and therefore supports why targeting IGF1R with NVP ameliorates HDM-induced asthma. Accordingly, IGF1 was reported to be involved in airway inflammation and remodeling in asthma and increased in serum of asthmatic patients [7,13,14,29].

On the whole, two weeks of NVP treatment were required to ameliorate the hallmarks of established HDM-induced allergy including AHR and airway remodeling. Notably, many of the typical inflammatory allergic features such as eosinophilia, increased cytokine levels and inflamed lung areas were already normalized after one week of NVP treatment. It should be emphasized that in our mouse model of asthma, the allergic phenotype was reported to be present two weeks after HDM exposure [16].

Lung function was improved upon treatment with NVP, which also normalized pulmonary surfactant expression. All these peculiarities were previously reported in *Igf1r*-deficient mice [15]. The fact that AHR is considered to be dependent on airway remodeling [30,31] is consistent with ameliorated remodeling features upon NVP treatment. Pulmonary surfactant proteins play an essential role in lung function and homeostasis [32]. Whereas SFTPB and SFTPC showed a critical role in the preservation of lung function, SFTPA and SFTPD demonstrated immunomodulatory roles during allergic airway inflammation [33–36]. According to recovered density of SFTPC+ alveolar type II cells following NVP treatment, alveolar type II cells were shown to be major contributors to surfactant synthesis [37].

Lung inflammation in allergic asthma is orchestrated by activation of CD4+ T lymphocytes to stimulate the release of inflammatory mediators and elicit eosinophilia [38,39]. Accordingly, HDM exposure caused increased leukocytosis in the bone marrow, blood and BALF, mainly due to eosinophils, and elevated serum IgE and IL13 levels, as we reported [15,16]. Of relevance, NVP treatment ameliorated all these features. NVP treatment also decreased the expression of the T cell-related genes *Cd274* (PDL-1), *Pdcd1* (PD-1), *Tnf* and *Cd4*. *Cd274* and *Pdcd1* were reported to be important for the activation of T lymphocytes in asthma and PD-1 expression increased in T-CD4+ lymphocytes of asthmatic patients [40–42]. Moreover, TNF was reported to be required for allergen-specific Th2 cell activation and for the development of AHR [43].

NVP treatment also diminished IL13, IL33 and CCL11 levels, reported to be highly induced upon HDM exposure [15,16]. IL33 was reported to be a central activator of dendritic cells during HDM allergic sensitization and to exacerbate allergic bronchoconstriction [44–46]. IL13 is a central mediator of allergic asthma and its blockade in mice reduces eosinophilia and airway remodeling in response to HDM [47]. CCL11 was reported to be released by bronchial epithelial cells in response to cytokines such as IL4,

IL13 and TNF, and is essential for lung eosinophilia and AHR development [48–50]. NVP treatment also reduced the presence of CD45$^+$ leucocytes in the lung, which were shown to be involved in allergic airway inflammation [51,52].

NVP treatment attenuated bronchial epithelial differentiation and goblet cell hyperplasia. We previously reported that IGF1R is required for proper club cell differentiation in mice [53]. Accordingly, club cells were reported to play a major role in bronchial asthma and SOX2 is required for goblet cell differentiation after allergen sensitization [49,54]. Upon allergen stimulation, FOXM1 induces differentiation of club cells into goblet cells through transcriptional activation of SPDEF. Then, increased MUC5AC expression by SPDEF in goblet cells contributes to mucus hyperproduction and AHR [31,55,56].

5. Conclusions

Our results demonstrate that the pharmacological blockade of IGF1R with NVP-ADW742 ameliorates HDM-induced allergy, and places IGF1R as a potential pharmacological target for future therapeutic approaches in asthma. In addition, IGF1R could be considered a promising candidate biomarker in asthma.

Supplementary Materials: The following are available online at https://www.mdpi.com/article/10.3390/biomedicines9080912/s1. Figure S1: Follow-up of the body weight gain upon treatment with the IGF1R inhibitor NVP-ADW742, Figure S2: Treatment with DMSO does not induce inflammation in the lungs of C57BL/6J mice, Table S1: Primer sets used for qPCR.

Author Contributions: E.A.-A., I.P.L. and J.G.P. designed the experiments, Á.C.U. contributed with experimental support, E.A.-A., S.P.-H. and I.P.L. performed the experiments, E.A.-A. and J.G.P. analyzed the data and E.A.-A., S.P.-H., F.J.G.-B., F.J.S. and J.G.P. wrote the manuscript, with input from all authors. All authors have read and agreed to the published version of the manuscript.

Institutional Review Board Statement: The study was conducted according to the guidelines of the Declaration of Helsinki. All experiments and animal procedures conducted were carried out following the guidelines of the European Communities Council Directive (86/609/EEC), and were revised and approved by the CEAA/CIBIR (Gobierno de La Rioja) Bioethics Committee (ref. JGP01_v2).

Informed Consent Statement: Not applicable.

Data Availability Statement: The data that support the findings of this study are available from the corresponding author upon reasonable request.

Conflicts of Interest: The authors declare no conflict of interest.

References

1. Fahy, J.V. Type 2 Inflammation in Asthma-Present in Most, Absent in Many. *Nat. Rev. Immunol.* **2015**, *15*, 57–65. [CrossRef]
2. Gregory, L.G.; Lloyd, C.M. Orchestrating House Dust Mite-Associated Allergy in the Lung. *Trends Immunol.* **2011**, *32*, 402–411. [CrossRef] [PubMed]
3. Calderón, M.A.; Linneberg, A.; Kleine-Tebbe, J.; De Blay, F.; de Rojas, D.H.F.; Virchow, J.C.; Demoly, P. Respiratory Allergy Caused by House Dust Mites: What do We Really Know? *J. Allergy Clin. Immunol.* **2015**, *136*, 38–48. [CrossRef] [PubMed]
4. Kuo, C.H.S.; Pavlidis, S.; Loza, M.; Baribaud, F.; Rowe, A.; Pandis, I.; Hoda, U.; Rossios, C.; Sousa, A.; Wilson, S.J.; et al. A Transcriptome-Driven Analysis of Epithelial Brushings and Bronchial Biopsies to Define Asthma Phenotypes in U-BIOPRED. *Am. J. Respir. Crit. Care Med.* **2017**, *195*, 443–455. [CrossRef] [PubMed]
5. Kuruvilla, M.E.; Lee, F.E.-H.; Lee, G.B. Understanding Asthma Phenotypes, Endotypes and Mechanisms of Disease. *Clin. Rev. Allergy Immunol.* **2019**, *56*, 219–233. [CrossRef]
6. Girnita, L.; Worrall, C.; Takahashi, S.I.; Seregard, S.; Girnita, A. Something Old, Something New and Something Borrowed: Emerging Paradigm of Insulin-Like Growth Factor Type 1 Receptor (IGF-1R) Signaling Regulation. *Cell Mol. Life Sci.* **2014**, *71*, 2403–2427. [CrossRef]
7. Wang, Z.; Li, W.; Guo, Q.; Wang, Y.; Ma, L.; Zhang, X. Insulin-Like Growth Factor-1 Signaling in Lung Development and Inflammatory Lung Diseases. *BioMed Res. Int.* **2018**, *2018*, 17–19. [CrossRef]

8. Griffiths, C.D.; Bilawchuk, L.M.; McDonough, J.E.; Jamieson, K.C.; Elawar, F.; Cen, Y.; Duan, W.; Lin, C.; Song, H.; Casanova, J.-L.; et al. IGF1R is an Entry Receptor for Respiratory Syncytial Virus. *Nature* **2020**, *583*, 615–619. [CrossRef]

9. Vázquez-Mera, S.; Pichel, J.G.; Salgado, F.J. Involvement of IGF Proteins in Severe Allergic Asthma: New Roles for Old Players. *Arch. Bronconeumol.* **2021**, *S0300-2896*, 94–96. [CrossRef]

10. Fraser, D.D.; Cepinskas, G.D.V.M.; Patteron, E.K.; Slessarev, M.; Martin, C.; Daley, M.; Patel, M.A.; Miller, M.R.; O'Gorman, D.B.; Gill, S.E.; et al. Novel Outcome Biomarkers Identified with Targeted Proteomic Analyses of Plasma From Critically Ill Coronavirus Disease 2019 Patients. *Crit. Care Explor.* **2020**, *2*, e0189. [CrossRef]

11. Nieto-Fontarigo, J.J.; Gonzalez-Barcala, F.J.; Andrade-Bulos, L.J.; San-José, M.E.; Cruz, M.J.; Valdés-Cuadrado, L.; Crujeiras, R.M.; Arias, P.; Salgado, F.J. iTRAQ-Based Proteomic Analysis Reveals Potential Serum Biomarkers of Allergic and Nonallergic Asthma. *Allergy* **2020**, *75*, 3171–3183. [CrossRef]

12. Esnault, S.; Kelly, E.A.; Schwantes, E.A.; Liu, L.Y.; DeLain, L.P.; Hauer, J.A.; Bochkov, Y.A.; Denlinger, L.C.; Malter, J.S.; Mathur, S.K.; et al. Identification of Genes Expressed by Human Airway Eosinophils after an In Vivo Allergen Challenge. *PLoS ONE* **2013**, *8*, e67560. [CrossRef]

13. Yamashita, N.; Tashimo, H.; Ishida, H.; Matsuo, Y.; Arai, H.; Nagase, H.; Adachi, T.; Ohta, K. Role of Insulin-Like Growth Factor-I in Allergen-Induced Airway Inflammation and Remodeling. *Cell. Immunol.* **2005**, *235*, 85–91. [CrossRef]

14. Lee, Y.C.; Jogie-Brahim, S.; Lee, D.Y.; Han, J.; Harada, A.; Murphy, L.J.; Oh, Y. Insulin-Like Growth Factor-Binding Protein-3 (IGFBP-3) Blocks the Effects of Asthma by Negatively Regulating NF-?B Signaling through IGFBP-3R-Mediated Activation of Caspases. *J. Biol. Chem.* **2011**, *286*, 17898–17909. [CrossRef]

15. Piñeiro-Hermida, S.; Gregory, J.A.; López, I.P.; Torrens, R.; Ruíz-Martínez, C.; Adner, M.; Pichel, J.G. Attenuated Airway Hyperresponsiveness and Mucus Secretion in HDM-Exposed Igf1r-Deficient Mice. *Allergy* **2017**, *72*, 1317–1326. [CrossRef]

16. Piñeiro-Hermida, S.; Alfaro-Arnedo, E.; Gregory, J.A.; Torrens, R.; Ruíz-Martínez, C.; Adner, M.; López, I.P.; Pichel, J.G. Characterization of the Acute Inflammatory Profile and Resolution of Airway Inflammation after Igf1r-Gene Targeting in a Murine Model of HDM-Induced Asthma. *PLoS ONE* **2017**, *12*, e0190159. [CrossRef]

17. Piñeiro-Hermida, S.; López, I.P.; Alfaro-Arnedo, E.; Torrens, R.; Iñiguez, M.; Alvarez-Erviti, L.; Ruiz-Martinez, C.; Pichel, J.G. IGF1R Deficiency Attenuates Acute Inflammatory Response in a Bleomycin-Induced Lung Injury Mouse Model. *Sci. Rep.* **2017**, *7*, 1–13. [CrossRef]

18. Hewish, M.; Chau, I.; Cunningham, D. Insulin-Like Growth Factor 1 Receptor Targeted Therapeutics: Novel Compounds and Novel Treatment Strategies for Cancer Medicine. *Recent Pat Anticancer Drug Discov.* **2009**, *4*, 54–72. [CrossRef]

19. Osher, E.; Macaulay, V.M. Therapeutic Targeting of the IGF Axis. *Cells* **2019**, *8*, 895. [CrossRef]

20. Mitsiades, C.S.; Mitsiades, N.S.; McMullan, C.J.; Poulaki, V.; Shringarpure, R.; Akiyama, M.; Hideshima, T.; Chauhan, D.; Joseph, M.; Libermann, T.A.; et al. Inhibition of the Insulin-Like Growth Factor Receptor-1 Tyrosine Kinase Activity as a Therapeutic Strategy for Multiple Myeloma, Other Hematologic Malignancies and Solid Tumors. *Cancer Cell* **2004**, *5*, 221–230. [CrossRef]

21. Cintron-Colon, R.; Sanchez-Alavez, M.; Nguyen, W.; Mori, S.; Gonzalez-Rivera, R.; Lien, T.; Bartfai, T.; Aid, S.; Francois, J.-C.; Holzenberger, M.; et al. Insulin-Like Growth Factor 1 Receptor Regulates Hypothermia During Calorie Restriction. *Proc. Natl. Acad. Sci USA* **2017**, *114*, 9731–9736. [CrossRef] [PubMed]

22. Piñeiro-Hermida, S.; Martínez, P.; Blasco, M.A. Short and Dysfunctional Telomeres Protect from Allergen-Induced Airway Inflammation. *Aging Cell.* **2021**, *20*, e13352. [CrossRef] [PubMed]

23. Sengupta, S.; Sobo, M.; Lee, K.; Kumar, S.S.; White, A.R.; Mender, I.; Fuller, C.; Chow, L.M.L.; Fouladi, M.; Shay, J.W.; et al. Induced Telomere Damage to Treat Telomerase Expressing Therapy-Resistant Pediatric Brain Tumors. *Mol. Cancer Ther.* **2018**, *17*, 1504–1514. [CrossRef] [PubMed]

24. Kolmert, J.; Piñeiro-Hermida, S.; Hamberg, M.; Gregory, J.A.; López, I.P.; Fauland, A.; Wheelock, C.E.; Dahlen, S.-E.; Pichel, J.G.; Adner, M. Prominent Release of Lipoxygenase Generated Mediators in a Murine House Dust Mite-Induced Asthma Model. *Prostaglandins Other Lipid Mediat.* **2018**, *137*, 20–29. [CrossRef]

25. Adachi, T.; Choudhury, B.K.; Stafford, S.; Sur, S.; Alam, R. The Differential Role of Extracellular Signal-Regulated Kinases and p38 Mitogen-Activated Protein Kinase in Eosinophil Functions. *J. Immunol.* **2000**, *165*, 2198–2204. [CrossRef]

26. Kamper, G.T.; Stafford, S.; Adachi, T.; Jinquan, T.; Quan, S.; Grant, J.A.; Skov, P.S.; Poulsen, L.K.; Alam, R. Eotaxin Induces Degranulation and Chemotaxis of Eosinophils through the Activation of ERK2 and p38 Mitogen-Activated Protein Kinases. *Blood* **2000**, *95*, 1911–1917. [CrossRef]

27. Sohn, M.H.; Lee, K.E.; Kim, K.W.; Kim, E.S.; Park, J.Y.; Kim, K.E. Calcium-Calmodulin Mediates House Dust Mite-Induced ERK Activation and IL-8 Production in Human Respiratory Epithelial Cells. *Respiration* **2007**, *74*, 447–453. [CrossRef]

28. Battes, M.E.; Sedgwick, J.B.; Zhu, Y.; Liu, L.Y.; Heuser, R.G.; Jarjour, N.N.; Kita, H.; Bertics, P.J. Human Airway Eosinophils Respond to Chemoattractants with Greater Eosinophil-Derived Neurotoxin Release, Adherence to Fibronectin, and Activation of the Ras-ERK Pathway When Compared with Blood Eosinophils. *J. Immunol.* **2010**, *184*, 7125–7133. [CrossRef]

29. Acat, M.; Toru, E.U.; Sahim, S.; Arik, O.; Ayada, C. High Serum Levels of IGF-I and IGFBP3 may Increase Comorbidity Risk for Asthmatic Patients. *Bratisl. Med. J.* **2017**, *118*, 691–694. [CrossRef]

30. Busse, W.W. The Relationship of Airway Hyperresponsiveness and Airway Inflammation: Airway Hyperresponsiveness in Asthma: Its Measurement and Clinical Significance. *Chest* **2010**, *138*, 4S–10S. [CrossRef]

31. Evans, C.M.; Raclawska, D.S.; Ttofali, F.; Liptzin, D.R.; Fletcher, A.A.; Harper, D.N.; McGing, M.A.; McElwee, M.M.; Williams, O.W.; Sanchez, E.; et al. The Polymeric Mucin Muc5ac is Required for Allergic Airway Hyperreactivity. *Nat. Commun.* **2015**, *17*, 6281. [CrossRef]

32. Whitsett, J.A.; Wert, S.E.; Weaver, T.E. Alveolar Surfactant Homeostasis and Pathogenesis of Pulmonary Disease. *Annu. Rev. Med.* **2010**, *61*, 105–119. [CrossRef]

33. Ogawa, H.; Ledford, J.G.; Mukherjee, S.; Aono, Y.; Nishioka, Y.; Lee, J.J.; Izumi, K.; Hollingsworth, J.W. Surfactant Protein D Attenuates Sub-Epithelial Fibrosis in Allergic Airways Disease through TGF-? *Respir. Res.* **2014**, *15*, 1–13. [CrossRef]

34. Ledford, J.G.; Mukherjee, S.; Kislan, M.M.; Nugent, J.L.; Hollingsworth, J.W.; Wright, J.R. Surfactant Protein-a Suppresses Eosinophil-Mediated Killing of Mycoplasma Pneumoniae in Allergic Lungs. *PLoS ONE* **2012**, *7*, e32436. [CrossRef]

35. Ikegami, M.; Whitsett, J.A.; Martis, P.C.; Weaver, T.E. Reversibility of Lung Inflammation Caused by SP-B Deficiency. *Am. J. Physiol. Lung Cell. Mol. Physiol.* **2005**, *289*, L962–L970. [CrossRef]

36. Glasser, S.W.; Maxfield, M.D.; Ruetschilling, T.L.; Akinbi, H.T.; Baatz, J.E.; Kitzmiller, J.A.; Page, K.; Xu, Y.; Bao, E.L.; Korfhagen, T.R. Persistence of LPS-Induced Lung Inflammation in Surfactant Protein-C-Deficient Mice. *Am. J. Respir Cell Mol. Biol.* **2013**, *49*, 845–854. [CrossRef]

37. Glasser, S.W. Surfactant Protein-C in the Maintenance of Lung Integrity and Function. *J. Allergy Ther.* **2011**, *7*, 001. [CrossRef]

38. Coverstone, A.M.; Seibold, M.A.; Peters, M.C. Diagnosis and Management of T2-High Asthma. *J. Allergy Clin. Immunol. Pract.* **2020**, *8*, 442–450. [CrossRef]

39. Jacquet, A. The Role of Innate Immunity Activation in House Dust Mite Allergy. *Trends Mol. Med.* **2011**, *17*, 604–611. [CrossRef]

40. McAlees, J.W.; Lajoie, S.; Dienger, K.; Sproles, A.A.; Richgels, P.K.; Yang, Y.; Khodoun, M.; Azuma, M.; Yagita, H.; Fulkerson, P.C.; et al. Differential Control of CD4+ T Cell Subsets by the PD-1/PD-L1 Axis in Allergic Asthma. *Eur. J. Immunol.* **2015**, *45*, 1019–1029. [CrossRef]

41. Akbari, O.; Stock, P.; Singh, A.K.; Lombardi, V.; Lee, W.L.; Freeman, G.J.; Sharpe, A.H.; Umetsu, D.T.; DeKruyff, R.H. PD-L1 and PD-L2 Modulate Airway Inflammation and iNKT-Cell-Dependent Airway Hyperreactivity in Opposing Directions. *Mucosal Immunol.* **2010**, *3*, 81–91. [CrossRef]

42. Mosayebian, A.; Koohini, Z.; Hossein-Nataj, H.; Abediankenari, S.; Abedi, S.; Asgarian-Omran, H. Elevated Expression of Tim-3 and PD-1 Immune Checkpoint Receptors on T-CD4 + Lymphocytes of Patients with Asthma. *Iran. J. Allergy Asthma Immunol.* **2018**, *17*, 517–525. [CrossRef]

43. Nakae, S.; Lunderius, C.; Ho, L.H.; Schäfer, B.; Tsai, M.; Galli, S.J. TNF Can Contribute to Multiple Features of Ovalbumin-Induced Allergic Inflammation of the Airways in Mice. *J. Allergy Clin. Immunol.* **2007**, *119*, 680–686. [CrossRef]

44. Chu, D.K.; Llop-Guevara, A.; Walker, T.D.; Flader, K.; Goncharova, S.; Boudreau, J.E.; Moore, C.L.; In, T.S.; Waserman, S.; Coyle, A.J.; et al. IL-33, But not Thymic Stromal Lymphopoietin or IL-25, is Central to Mite and Peanut Allergic Sensitization. *J. Allergy Clin. Immunol.* **2013**, *131*, 187–200. [CrossRef] [PubMed]

45. Makrinioti, H.; Toussaint, M.; Jackson, D.J.; Walton, R.P.; Johnston, S.L. Role of Interleukin 33 in Respiratory Allergy and Asthma. *Lancet. Respir. Med.* **2014**, *2*, 226–237. [CrossRef]

46. Sjöberg, L.C.; Gregory, J.A.; Dahlén, S.E.; Nilsson, G.P.; Adner, M. Interleukin-33 Exacerbates Allergic Bronchoconstriction in the Mice via Activation of Mast Cells. *Allergy Eur. J. Allergy Clin. Immunol.* **2015**, *70*, 514–521. [CrossRef] [PubMed]

47. Tomlinson, K.L.; Davies, G.C.G.; Sutton, D.J.; Palframan, R.T. Neutralisation of Interleukin-13 in Mice Prevents Airway Pathology Caused by Chronic Exposure to House Dust Mite. *PLoS ONE* **2010**, *5*, e13136. [CrossRef] [PubMed]

48. Conroy, D.M.; Williams, T.J. Eotaxin and the Attraction of Eosinophils to the Asthmatic Lung. *Respir. Res.* **2001**, *2*, 150. [CrossRef]

49. Sonar, S.S.; Ehmke, M.; Marsh, L.M.; Dietze, J.; Dudda, J.C.; Conrad, M.L.; Renz, H.; Nockher, W.A. Clara Cells Drive Eosinophil Accumulation in Allergic Asthma. *Eur. Respir. J.* **2012**, *39*, 429–438. [CrossRef]

50. Ying, S.; Robinson, D.S.; Meng, Q.; Rottman, J.; Kennedy, R.; Ringler, D.J.; Mackay, C.R.; Daugherty, B.L.; Springer, M.S.; Durham, S.R.; et al. Enhanced Expression of Eotaxin and CCR3 mRNA and Protein in Atopic Asthma. Association with Airway Hyperresponsiveness and Predominant Co-Localization of Eotaxin mRNA to Bronchial Epithelial and Endothelial Cells. *Eur. J. Immunol.* **1997**, *27*, 3507–3516. [CrossRef]

51. Blaylock, M.G.; Lipworth, B.J.; Dempsey, O.J.; Duncan, C.J.A.; Lee, D.K.C.; Lawrie, A.; Doulas, J.G.; Walsh, G.M. Eosinophils from Patients with Asthma Express Higher Levels of the Pan-Leucocyte Receptor CD45 and the Isoform CD45RO. *Clin. Exp. Allergy* **2003**, *33*, 936–941. [CrossRef]

52. Matsuda, A.; Motoya, S.; Kimura, S.; McInnis, R.; Maizel, A.L.; Takeda, A. Disruption of Lymphocyte Function and Signaling in CD45-Associated Protein-Null Mice. *J. Exp. Med.* **1998**, *187*, 1863–1870. [CrossRef]

53. López, I.P.; Piñeiro-Hermida, S.; Pais, R.S.; Torrens, R.; Hoeflich, A.; Pichel, J.G. Involvement of Igf1r in Bronchiolar Epithelial Regeneration: Role During Repair Kinetics after Selective Club Cell Ablation. *PLoS ONE* **2016**, *11*, e0166388. [CrossRef]

54. Tompkins, D.H.; Besnard, V.; Lange, A.W.; Wert, S.E.; Keiser, A.R.; Smith, A.N.; Lang, R.; Whitsett, J.A. Sox2 is Required for Maintenance and Differentiation of Bronchiolar Clara, Ciliated and Goblet Cells. *PLoS ONE* **2009**, *4*, e8248. [CrossRef]

55. Ren, X.; Shah, T.A.; Ustiyan, V.; Zhang, Y.; Shinn, J.; Chen, G.; Whitsett, J.A.; Kalin, T.V.; Kalinichenko, V.V. FOXM1 Promotes Allergen-Induced Goblet Cell Metaplasia and Pulmonary Inflammation. *Mol. Cell. Biol.* **2013**, *33*, 371–386. [CrossRef]

56. Rajavelu, P.; Chen, G.; Xu, Y.; Kitzmiller, J.A.; Korfhagen, T.R.; Whitsett, J.A. Airway Epithelial SPDEF Integrates Goblet Cell Differentiation and Pulmonary Th2 Inflammation. *J. Clin. Investig.* **2015**, *125*, 2021–2031. [CrossRef]